Selective enzyme inhibition in the prevention of neuronal apoptosis: A molecular modelling study

Claudine Burger

13074105

Dissertation submitted in fulfilment of the requirements for the degree Magister Scientiae in Pharmaceutical Chemistry at the Potchefstroom Campus of the North-West University

Supervisor: Prof. S.F. Malan

Co-supervisor: Prof. D.W. Oliver

NOVEMBER 2009

Table of Content

Abstract

Alzheimer's disease (AD), Parkinson's disease (PD) and Huntington's disease (HD) are neurodegenerative diseases which may be caused by neuronal apoptosis and there are currently no treatments to delay the progression of these diseases. Finding a cure or delaying the progression of these diseases, will improve the quality of life of the patients and relieve the burden on the caregivers and loved ones of the patients.

Many enzymes are involved in the apoptotic processes that contribute to neurodegenerative diseases. These enzymes include CDK5/p25 (Cyclin dependent kinase 5 in complex with activator protein p25), calpain I, caspase 3 and GSK3β (Glycogen synthase kinase 3β). *Inhibition* of these enzymes will have the potential to counteract the neurodegeneration caused by various apoptotic processes.

In this study, computational pharmacophore hypotheses for CDK5/p25, calpain I, caspase 3 and GSK3β were formulated to predict the geometry of the chemical features necessary to exhibit inhibitory activity against these enzymes. The generated hypotheses were validated using published structures with known activity and an in-house library of compounds was screened to determine which compounds comply with the hypotheses for the respective enzymes. Docking studies were subsequently performed using the in-house library to determine which compounds have the ability to fit into the respective enzyme cavities, thus having potential as inhibitors for the specific enzymes. Using a combination of docking results and hypothesis compliance, the compounds with the most promising combined results were selected for biological screening in enzyme assays.

The 'pharmacophore hypothesis in combination with docking studies' model had the best predictive capabilities for calpain I and GSK3β (60% and 85% respectively) and these enzymes were therefore selected for the biological assays to serve as *in vitro* proof of concept. The most potent inhibitor identified for calpain I, which was a hypothesis hit as well as having a better dock score than the co-crystallised ligand, had an IC_{50} value of 95.42 μM. The most potent inhibitor identified for GSK3β, which was a hypothesis hit as well as having a better dock score than that of the co-crystallised ligand, had an IC_{50} value of 0.6819 μM.

Molecular dynamics were subsequently performed on selected compounds from the biological assays to determine binding modes and active conformations. Critical interactions necessary for enzyme inhibition was identified for both enzymes from the molecular modelling studies.

In this study, hypothesis generation, combined with docking studies, were found to be valuable to identify scaffolds and can be effectively applied during drug design of kinase and related enzyme inhibitors. The identified scaffolds could be further optimised as drug leads to design potent inhibitors during future studies.

Opsomming

Alzheimer's siekte, Parkinson's siekte en Huntington's siekte is neurodegeneratiewe siektes wat deur neuronale apoptose veroorsaak mag word en daar is tans geen behandelings om die siektes stadiger te laat verloop nie. Deur 'n genesing vir die siektes te vind, of selfs 'n behandeling wat die verloop van die siektes kan vertraag, kan die lewenskwaliteit van die pasiënte verbeter en die las op die gesondheidspersoneel en geliefdes verminder word.

'n Verskeidenheid ensieme is betrokke by die apoptotiese prosesse wat verantwoordelik is vir neurodegeneratiewe siektes. Hierdie ensieme sluit CDK5/p25 (Cyclin afhanklike kinase 5 in kompleks met aktiverende protein p25), calpain I, caspase 3 and GSK3β (Glikogeen sintetase kinase 3β) in. Inhibisie van hierdie ensieme het die potensiaal om die neurodegenerasie wat deur die verskeie apoptotiese prosesse veroorsaak word, teen te werk.

In hierdie studie is rekenaargebaseerde farmakofoorhipoteses vir CDK5/p25, calpain I, caspase 3 en GSK3β opgestel om die geometrie van die chemiese funksionaliteite wat benodig word om hierdie ensieme te inhibeer, te illustreer. Die hipoteses is gevalideer deur gebruik te maak van gepubliseerde strukture met bekende aktiwiteit en 'n biblioteek verbindings is ondersoek om te bepaal watter verbindings aan die hipoteses vir die onderskeie ensieme voldoen. Passingstudies is daarna met die biblioteek verbindings gedoen om te bepaal watter verbindings die vermoë het om in die onderskeie ensieme se aktiewe setels in te pas en dus die potensiaal besit om as inhibeerders vir die spesifieke ensieme op te tree. Deur die kombinasie van passingsresultate en voldoening aan die hipotese te gebruik, is die verbindings met die belowendste gekombineerde resultate gekies vir biologiese siftingstoetse.

Die 'hipotese voldoening in kombinasie met passingsresultate' model het die beste voorspelbaarheid getoon vir calpain I en GSK3β (60% en 85% onderskeidelik) en hierdie ensieme is dus gekies vir biologiese siftingstoetse. Die mees potente inhibeerder wat vir calpain I geïdentifiseer is, is 'n verbinding wat voldoen aan die hipotese en het 'n passingstelling gehad wat beter is as die van die mede-gekristalliseerde ligand, met 'n IC_{50}-waarde van 95.42 μM. Die mees potente inhibeerder wat vir GSK3β geïdentifiseer is, is 'n

verbinding wat voldoen aan die hipotese en het 'n passingstelling gehad wat beter is as die van die mede-gekristalliseerde ligand, met 'n IC_{50}-waarde van 0.6819 µM.

Molekulêre dinamika is vervolgens gedoen op geselekteerde verbindings uit die biologiese evaluering om hulle bindingswyses en aktiewe konformasies vas te stel. Kritiese interaksies vir inhibisie is vir beide ensieme identifiseer vanuit die molekulêre modellering.

In hierdie studie is hipoteses in kombinasie met passingstudies waardevol gevind om kernstrukture te identifiseer en dit kan dus effektief aangewend word gedurende geneesmiddelontwerp van kinase- en soortgelyke ensieminhibeerders. Die geïdentifiseerde kernstrukture kan verder geoptimiseer word as geneesmiddelleidrade om potente inhibeerders te ontwerp in toekomstige studies.

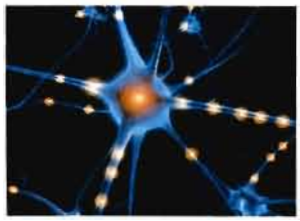

Abbreviations

Aβ	β-amyloid
AD	Alzheimer's disease
ALS	Amyotrophic lateral sclerosis
AP1	Activator protein 1
APP	Amyloid precursor protein
BAD	Bcl-2-associated death promotor
BDNF	Brain-derived neurotrophic factor
CAG	Cytosine-adenosine-guanosine
CaMK	Calcium calmodulin dependent kinase
CaMKIβ2	Calcium calmodulin dependent kinase Iβ2
CaMKII	Calcium calmodulin dependent kinase II
CaMKIV	Calcium calmodulin dependent kinase IV
CDK	Cyclin dependent kinase
CDK1	Cyclin dependent kinase 1
CDK2	Cyclin dependent kinase 2
CDK4	Cyclin dependent kinase 4
CDK5	Cyclin dependent kinase 5
CDK6	Cyclin dependent kinase 6
CDKI	Cyclin dependent kinase inhibitor
c-FLIP	Cellular-FLICE inhibitory protein
CGR	Calpain-Glo Reagent
CREB	cAMP-responsive element binding protein
DARPP32	Dopamine and cAMP-regulated phosphoprotein of 32kDA
EGFR	Epidermal growth factor receptor
eIF2B	Eukaryotic initiation factor 2 B

ERK1	Extracellular signal regulated kinase 1
ERK2	Extracellular signal regulated kinase 2
FADD/MORT1	Fas-associating protein with death domain
FAK	Focal adhesion kinase
GSK3	Glycogen synthase kinase 3
GSK3α	Glycogen synthase kinase 3α
GSK3β	Glycogen synthase kinase 3β
Htt	Huntingtin
JNK1	C-Jun N-terminal kinase 1
JNK2	C-Jun N-terminal kinase 2
JNK3	C-Jun N-terminal kinase 3
JNKK	JNK kinase
LRRK2	Leucine-rich repeat kinase 2
MAP	Mitogen activated protein
MAP2	Microtubule-associated protein 2
MAPK	MAP kinase
MAPKK	MAP kinase kinase
MAPKKK	MAP kinase kinase kinase
MEF	Myocyte enhancer factor
MEK1	MAPK/ERK kinase 1
MEK2	MAPK/ERK kinase 2
MEKK	MEK kinase
MEKK1	MEK kinase 1
MKK3	MAPK kinase 3
MKK4	MAPK kinase 4
MKK6	MAPK kinase 6
MKK7	MAPK kinase 7
MOE	Molecular operating environment
MPTP	1-Methyl-4-phenyl-1,2,3,6-tetrahydropyridine
NF	Neurofilament
NFT	Neurofibrillary tangle

NGF	Nerve growth factor
NMDA	N-methyl-D-aspartic acid
PAK	p21cdc42/rac1-activated serine/threonine kinase
PAK1	p21cdc42/rac1-activated serine/threonine kinase 1
PAK3	p21cdc42/rac1-activated serine/threonine kinase 3
PARP	Poly (ADP-ribose) polymerase
PD	Parkinson's disease
PI3K	Phosphoinositol 3-kinase
PINK	PTEN-induced kinase-1
PKA	Protein kinase A
PKB	Protein kinase B
PKC	Protein kinase C
PKCα	Protein kinase Cα
PLA_2	Phospholipase A_2
PLD	Phospholipase D
PP2A	Protein phosphatase 2A
RFU	Relative fluorescence unit
RLU	Relative luminescence unit
ROS	Reactive oxygen species
SAPK	Stress-activated protein kinase
SOD1	Cu/Zn superoxide dismutase 1
Sos	Son of sevenless
TNFR-1	Tumor necrosis factor receptor 1
TRADD	TNFR-1-associated death domain protein
UCHL1	Ubiquitin carboxy terminal hydrolase L1
UPS	Ubiquitin-proteasome system

1 Introduction, Aims and Objectives

Alzheimer's disease (AD) is the most common cause of dementia in Western civilisation and currently there are no treatment regimes that slow the progression of the disease (Cavalli *et al.*, 2008). It is also the most prevalent neurodegerative disease (Lev *et al.*, 2003). Most AD patients will suffer for 7-10 years (Adlard & Cummings, 2004) and this results in a great burden on the caregivers and loved ones of the patients.

The second most common progressive neurodegenerative disorder is Parkinson's disease (PD). Every year, about 50 000 patients in the USA are diagnosed with PD (Shastry, 2001). It is currenty an incurable disease and like in AD, there are no drugs that slow the progression of the disease (Wood-Kaczmar *et al.*, 2006).

Huntington's disease (HD) is another progressive and debilitating neurodegenerative disease affecting 4 to 8 persons per 100 000, with an average disease onset between the ages 35 and 45 (Goodman *et al.*, 2008). The current treatments for HD are not able to delay the progression and onset of the disease (Myers, 2004).

From the above it is clear that finding an effective treatment to cure or delay the progression of these neurodegenerative disorders, will improve the quality of life of the patients and relieve the burden on the caregivers and loved ones of the patients.

As neurodegenerative diseases progress, they eventually lead to neuronal death or apoptosis (Adlard & Cummings, 2004). Many enzymes are involved in different stages of this process (Heiner *et al.*, 2004), the most important being cyclin dependent kinase 5 (CDK5), calpains and caspases (Cheung & Ip, 2004), and inhibition of these enzymes in the compromised neuronal cells can avoid the undesirable high rate of neuronal cell death (Concha & Abdel-Meguid, 2002).

In the treatment of cancer, kinases and more specifically cyclin dependant kinases (CDKs), can be altered to inhibit the increased rate of cell proliferation (Knockaert *et al.*, 2002). In the treatment of neurodegeneration, the apoptotic processes however needs to be stopped or reversed and an increased rate of cell proliferation is needed. The rational of this study was

thus to determine targets that play a role in apoptosis and which can be inhibited to atenuate apoptosis.

The aim of this study was to determine which small molecules have the potential to act as inhibitors of specific enzymes - CDK5, caspase 3, calpain and GSK3β - that participate in neuronal apoptosis.

To reach this aim, the following steps were followed for each of the four enzymes:

1) Small molecule pharmacophore hypotheses were formulated based on inhibitors described in the literature.
2) In-house libraries were investigated for molecules that are in compliance with the hypotheses and can potentially be used as inhibitors.
3) Docking studies were performed using these molecules and the selected enzyme.
4) Proof of concept was performed by biological assay testing.
5) The dynamics and binding energy of the enzyme-inhibitor complexes were investigated by using molecular modelling. The molecular operating environment (MOE) software was used.

2 Literature Study

2.1 Neurodegenerative diseases

Neurodegenerative diseases are complex because they involve selective degeneration of several types of neurons. The onset of the clinical symptoms of these neurodegenerative diseases vary in time. (Shastry, 2001). Although each of these diseases exhibits its own uniqueness, there are also specific similarities. These similarities become clear when the symptoms, disease causing factors and molecular changes of the most prevalent diseases, Alzheimer's disease (AD), Parkinson's disease (PD), Huntington's disease (HD) and Amyotrophic lateral sclerosis (ALS) are studied.

2.1.1 Alzheimer's disease (AD)

Alzheimer's disease is the primary cause of dementia in western civilisation (Cavalli *et al.*, 2008). The currently used drugs do not slow the progression of AD but only alleviate the symptoms (Cavalli *et al.*, 2008). Most AD patients suffer for the last 7-10 years of their lives from the onset of the disease (Adlard & Cummings, 2004). The prevalence of AD is 3% in persons between the ages of 65 and 74, 19% for persons between the ages of 75 and 84 and 47% for those older than 85 (Hölscher, 1998).

2.1.1.1 Clinical symptoms and disease classification

The primary symptoms of AD include memory loss, beginning with the loss of memory of *recent* events and escalating to almost complete memory loss. During the initial phase there is also interference in other cognitive domains affecting mood, reasoning ability, judgemental skills and language usage. Eventually the patients are not able to perform daily life functions and become completely dependent upon others (Laferla & Oddo, 2005).

Two types of AD are distinguished namely:

1. **Sporadic (idiopathic) AD**, that occur most frequent, with disease onset at age 65-70.
2. **Familial AD** only contributes to a small number of cases with symptoms appearing before the age of 65 and in patients where gene mutations occur (Laferla & Oddo, 2005).

2.1.1.2 Disease causing factors

Aging is the key risk factor and after the age of 65 the risk to develop AD doubles every 5 years (Laferla & Oddo, 2005). AD is caused by a multitude of other factors, including environmental, genetic and endogenous factors (Cavalli *et al.*, 2008). Included in these factors are excessive protein misfolding and aggregation that can often be related to the ubiquitin-proteasome system (UPS), free radical formation associated with oxidative stress, neuroinflammatory processes and mitochondrial abnormalities (Cavalli *et al.*, 2008).

Genetic mutations that lead to AD include:

- Mutations in the amyloid precursor protein (APP) (chromosome 21) that have an effect on the production and metabolism of β-amyloid (Aβ).
- Mutations in presenilin 1 (chromosome 14) and presenilin 2 (chromosome 1) resulting in changes in intracellular trafficking of Aβ.

Presence of the ε4 variant gene of apolipoprotein E (chromosome 19) and the presence of the Down's syndrome genes also lead to the onset of AD (Adlard & Cummings, 2004).

Head injury or brain trauma may also lead to the development of AD, resulting in 2 to 20% of AD cases (Adlard & Cummings, 2004). AD may have an earlier onset in persons with repetitive head injury as has been found in boxers and individuals demonstrating self abuse behaviour. In these cases AD is caused due to the formation of neurofibrillary tangles (NFT) (Vickers *et al.*, 2000).

2.1.1.3 Molecular changes

The deposit of aggregated Aβ peptide and NFT consisting of hyperphosphorylated tau protein are two of the distinct molecular features of AD (Churcher, 2006). Other pathological features in AD include the formation of neuropil threads, alteration in microtubule architecture and loss of microtubules and synapses (Adlard & Cummings, 2004). The disease is progressive, inevitably leading to neuronal death (Adlard & Cummings, 2004; Cavalli *et al.*, 2008). During neuronal cell death, cholinergic neurons and synapses of the basal forebrain are the targeted cells, thus leading to cognitive impairments (Cavalli *et al.*, 2008) and acetylcholine depletion (Laferla & Oddo, 2005). Lewy bodies have also been seen in some of the AD cases (Laferla & Oddo, 2005) and its formation in the amygdala has been shown to increase the risk for major depression in patients with AD (Lopez *et al.*, 2006).

Aβ increases the intracellular Ca^{2+} levels by several different mechanisms. In one of these mechanisms, Aβ creates leaks in membranes by appearing to act as Ca^{2+} channels and increasing membrane permeability for K^+, Ca^{2+}, Na^+ and organic molecules. Ca^{2+} increase is cytotoxic and leads to the production of free radicals via activation of enzymes, for example

phospholipase A_2 (PLA_2), that produce free radicals. Another enzyme, nitric oxide synthase, is also activated by Ca^{2+} to produce nitric oxide, which is neurotoxic (Hölscher, 1998). The neurotoxicity in this case is due to the fact that nitric oxide leads to the release of cytochrome-c from the mitochondria and eventually activates caspase 3, causing apoptosis (Singh & Dikshit, 2007).

Increased levels of iron, aluminium and mercury were also found in the brain tissue of persons with AD and could also lead to free radical formation (Hölscher, 1998).

2.1.1.4 Aβ, NFT and tau in Alzheimer's disease

Aβ peptide is produced by proteolysis of the amyloid precursor protein (APP) (Laferla & Oddo, 2005; Vickers *et al.*, 2000) and cleavage of APP by α-secretase at amino acids 16 and 17 prevents formation of Aβ (Hölscher, 1998). In another pathway, β-secretase cleaves APP at an extracellular site while gamma-secretase cleaves APP in the intramembrane domain which leads to the production of Aβ (Hölscher, 1998). Aβ is neurotoxic, that results in nerve cell death and its presence has been shown to correlate well with a decline in cognitive function (Adlard & Cummings, 2004). Amyloid plaques are extracellular deposits usually found in the limbic brain regions, for example hippocampus and amygdala, and in specific cortical and subcortical areas (Laferla & Oddo, 2005; Shastry, 2001). Evidence shows that the soluble part of Aβ rather than the insoluble deposits, are toxic (Adlard & Cummings, 2004), but the pathogenic form contributing to AD has not yet been established (Laferla & Oddo, 2005). The deposition of Aβ into plaques is also implicated in the development of inflammation. This in turn leads to an increase in cytokine levels and other substances that can cause or contribute in the degeneration of nerve cells (Vickers *et al.*, 2000).

Normal tau is a soluble protein contributing to microtubule assembly and stabilisation (Laferla & Oddo, 2005). In the early stages of AD, hyperphosphorylated tau (which has a lower affinity for microtubules than normal tau (Laferla & Oddo, 2005)) is deposited in a granular form which becomes increasingly more fibrillar (Adlard & Cummings, 2004). As the disease progresses, this possibly leads to filamentous intracellular inclusions that eventually fills the neurons with compact, hyperphosphorylated tau bundles (Adlard & Cummings, 2004). Alteration in the levels of protein kinases and phosphatases has the ability to induce this hyperphosphorylation. This formation of NFT is associated with widespread gliosis and prominent degeneration of neurons. In AD, NFTs contribute to 2.2 to 17% of neuronal loss (Adlard & Cummings, 2004). Calpain has also been associated with molecular events that lead to hyperphosphorylated tau (Saez *et al.*, 2006). More specifically, calpain is activated by Aβ-induced neurotoxicity and has the ability to disorganise axonal and dendritic cytoskeletal

components such as tau, neurofilaments, microtubule-associated protein 2 (MAP2) and actin (Higuchi *et al.*, 2005).

2.1.2 Parkinson's disease (PD)

Parkinson's disease (PD) is a severe and progressive movement disorder and is the second most common neurodegenerative disease (Corti *et al.*, 2006) and involves the degeneration of nigrostriatal dopaminergic neurons (Barzilai & Melamed, 2003). Every year, about 50 000 patients in the USA are diagnosed with PD (Shastry, 2001) and approximately 5% of patients with PD has the familial form of the disease (Lev *et al.*, 2003). In the population over the age of 65, nearly 2% of individuals have PD (Corti *et al.*, 2005). Current treatment regimes focus on the symptomatic treatment and understanding the apoptotic process is essential in developing treatments that could alter the course of the disease (Lev *et al.*, 2003).

2.1.2.1 Clinical symptoms

The onset of symptoms of PD is triggered by the loss of 50-70% of nigrostriatal dopaminergic neurons (Barzilai & Melamed, 2003) and symptoms include resting tremors, bradykinesia and postural instability (Lev *et al.*, 2003). Hand tremors are more common than resting foot tremors and difficulty with fine motor tasks are the first signs of bradikinesia. Postural instability, or impaired balance, leads to increased risk of falls and rigidity of movement is increased during the performance of mental tasks. Autonomic symptoms include constipation, urinary urgency and frequency, orthostatic hypotension, cognitive and psychiatric changes, like depression and dementia, and sleep disturbances. Dementia was reported in 80% of end-stage PD patients (Samii *et al.*, 2004).

2.1.2.2 Disease causing factors

PD is a disease caused by a multitude of factors including genetic and environmental factors. Environmental factors include amongst others exposure to household pesticides, containing rotenone, and to toxins such as the neurotoxin MPTP (1-methyl-4-phenyl-1,2,3,6-tetrahydropyridine). The use of certain drugs and specific diet may also be contributing factors (Shastry, 2001). Interestingly, it has been shown that smoking and high intake of coffee and caffeine contribute to lowering the risk to develop PD (Samii *et al.*, 2004).

Genetic forms of PD include mutations of the genes that encode for the following proteins:

1. *α-Synuclein*

   This gene is located on chromosome 4q and α-synuclein is usually strongly expressed in the brain (Barzilai & Melamed, 2003). Mutations of this gene cause autosomal dominant PD (Wood-Kaczmar *et al.*, 2006).

2. *Ubiquitin carboxy terminal hydrolase L1 (UCHL1)*

   This gene is located on chromosome 4p and regulates ubiquitin release. An inadequate release can lead to the accumulation of essential components in the formation of neurotoxic fibrils (Barzilai & Melamed, 2003).

3. *An ubiquitin protein ligase known as parkin*

   This gene is located on chromosome 6 (Barzilai & Melamed, 2003) and mutations cause autosomal recessive PD which is the most common cause of early onset and juvenile parkinsonism (Wood-Kaczmar *et al.*, 2006). Mutations in the parkin gene causes earlier onset of the disease and accumulation of certain proteins could possibly lead to selective neuronal death in the absence of Lewy bodies (Shastry, 2001).

4. *DJ-1*

   This gene is located on chromosome 1p36 (Barzilai & Melamed, 2003) and mutations cause autosomal recessive PD (Wood-Kaczmar *et al.*, 2006).

5. *Leucine-rich repeat kinase 2 (LRRK2)*

   These mutations cause autosomal dominant PD and a specific mutation of this gene cause 5% of familial PD and 1.5% of sporadic PD. In some populations the mutation that causes sporadic PD is observed in 41% of the population and this specific mutation also enhanced kinase activity (Wood-Kaczmar *et al.*, 2006).

6. *PTEN-induced kinase-1 (PINK1)*

   Mutations in this gene cause autosomal recessive PD (Wood-Kaczmar *et al.*, 2006).

Oxidative stress, reactive oxygen species (ROS), abnormal Ca^{2+} homeostasis, exogenous and endogenous toxins, and mitochondrial dysfunction (especially mitochondrial complex I) also lead to degeneration of the nigrostriatal dopaminergic neurons and cause PD (Lev *et al.*, 2003). Neuromelanin and iron possibly have roles in the etiology of PD (Barzilai & Melamed, 2003). It has been shown that dopamine has the ability to cause apoptosis (Lev *et al.*, 2003) and that the oxidation of cytosolic dopamine generates damaging free radicals (Surmeier, 2007). Trophic-factor deprivation also has the ability to promote apoptosis of immature neurons (Barzilai & Melamed, 2003).

2.1.2.3 Molecular changes

The distinct neurological features of PD include amongst others the following: the presence of Lewy bodies, cytoplasmic accumulation of fibrous proteins in brain cells, and the degeneration of nigrostriatal dopaminergic neurons (Samii *et al.*, 2004). α-Synuclein is an abundant brain protein that is localised in the nerve terminals. It is a key component of Lewy bodies and neurites (Barzilai & Melamed, 2003) and mutation of the α-synuclein gene may

promote aggregation of α-synuclein or interference in its degradation pathway (Shastry, 2001). This then leads to the aggregation and fibrillisation of α-synuclein observed in Lewy bodies and Lewy neurites (Wood-Kaczmar *et al.*, 2006), and ultimately neurodegeneration (Corti *et al.*, 2005). It is also possible that α-synuclein sequesters 14-3-3 protein, which is an anti-apoptotic protein, thus counteracting its anti-apoptotic function (Barzilai & Melamed, 2003). α-Synuclein overproduction also leads to increased vulnerability to mitochondrial toxins (Corti *et al.*, 2005).

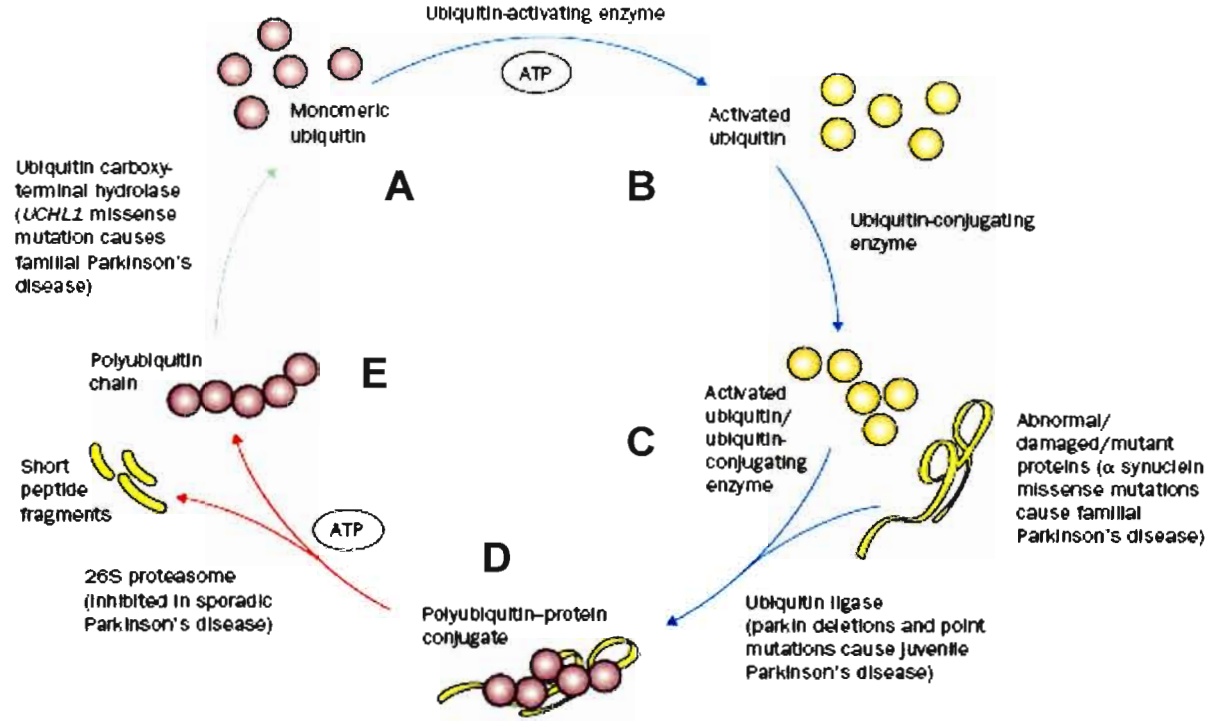

Figure 2.1: Degradation of abnormal proteins by the ubiquitin-proteasome system (Samii *et al.*, 2004). The blue sections shows ATP-dependent identification and labelling of abnormal proteins with ubiquitin molecules (ubiquination) as a signal for degradation by the 26S proteasome complex (red section shows the proteolysis). The green section shows the recovery and recycling of the ubiquitin molecules from the polyubiquitin chain. (Samii *et al.*, 2004).

Another pathological characteristic of PD is the intracellular deposition of aggregated and ubiquinated proteins (Barzilai & Melamed, 2003). This cycle consists of five major steps as shown in figure 2.1. Ubiquitin molecules attach to damaged proteins, thereby sending a degradation signal (section **C** of figure 2.1). This ubiquitin-protein complex (section **D** of figure 2.1) is degraded by the 26S protease. Mutant α-synuclein protein misfolds, aggregates and resists degradation by the ubiquitin-proteasome system. Parkin catalyses the ligation of ubiquitin to degradation targeted proteins. The degraded proteins release polyubiquitin chains (section **E** of figure 2.1) that are transformed back into ubiquitin monomers (section **A**

of figure 2.1) by UCHL1 and re-enter the cycle. Mutations in parkin and UCHL1 are likely to interfere with this pathway (Samii *et al.*, 2004).

2.1.3 Huntington's disease (HD)

HD is a progressive and debilitating neurodegenerative disease affecting 4 to 8 persons per 100 000, with an average disease onset between the ages 35 and 45 (Goodman *et al.*, 2008). The current treatments for HD are not able to delay the progression and onset of the disease (Myers, 2004).

2.1.3.1 Clinical symptoms

Symptoms of HD include the following: involuntary movements including chorea, subcortical dementia, psychiatric symptoms (Li *et al.*, 2003), mood disorders, behavioural changes (Myers, 2004) and weight loss (Goodman *et al.*, 2008). The hyperkinetic movements could account for the observed weight loss (Goodman *et al.*, 2008).

2.1.3.2 Disease causing factors

HD is a hereditary disease, caused by the abnormal cytosine-adenosine-guanosine (CAG) expansion in the exon 1 of the huntingtin gene (on the 4p16 chromosome (Myers, 2004)), leading to the formation of mutant huntingtin (htt) (Goodman *et al.*, 2008). When the number of CAG expansions surpasses 39, HD is generally present. When there is 36-39 repeats, some individuals may develop HD (Myers, 2004). CAG repeats between 40 and 50 leads to onset in mid-life, whereas a repeat of more than 70, leads to the juvenile form (Li *et al.*, 2003). In disease onset occurring before age 21, the HD gene is normally inherited from the father (Myers, 2004). Physiological huntingtin plays a roll in cytoplasmic membrane trafficking and microtubule based axonal transport (Li *et al.*, 2003).

2.1.3.3 Molecular changes

Mutant huntingtin (htt) form amyloid-like intracellular aggregates, leading to saturation or structural inhibition of the ubiquitin-proteasome system, which is the major pathway normally processing misfolded proteins (Li *et al.*, 2003). Proteins normally involved in synaptic function such as α-synuclein, are recruited by the htt aggregates, leading to exhaustion of vital components, such as complexin II, that are needed in synapse functioning. Htt also decreases the number of N-methyl-D-aspartic acid (NMDA) receptors at presymptomatic stages of the disease (Li *et al.*, 2003). Presymptomatically, there are also decreases in dopamine and cAMP-regulated phosphoprotein (DARPP-32) (Li *et al.*, 2003). Calpain cleaves htt at multiple sites generating toxic protein fragments leading to apoptosis (Saez *et al.*, 2006).

Selective neuronal loss has been found in the tuberal and lateral hypothalamus (Goodman *et al.*, 2008) and loss of neurons in the striatum and cerebellar cortex is associated with intranuclear inclusions (Shastry, 2001). The dopamine D_2 receptors in the striatal and cortical regions are also dysfunctional in HD individuals (Li *et al.*, 2003).

2.1.4 Amyotrophic lateral sclerosis (ALS)

ALS is a neurodegenerative disease that develops during adulthood and is characterised by the selective loss of motor neurons in the spinal cord, brainstem and cerebral cortex ultimately resulting in paralysis and death within 5 years (Patzke & Tsai, 2002). The prevalence of ALS is about 6 per 100 000 individuals (Mitchell & Borasio, 2007) and about 10% of ALS cases are genetically related (Simpson & Al-Chalabi, 2006). An autosomal-dominant type of inheritance is usually seen and 10-20% of this type is due to the mutation of the Cu/Zn superoxide dismutase 1 (SOD1) gene on chromosome 21 (Mitchell & Borasio, 2007). Between 2 and 7% of sporadic cases are due to mutations of SOD1 (Simpson & Al-Chalabi, 2006).

2.1.4.1 Clinical symptoms and disease classification

There are 3 neurological regions where ALS can have an onset namely bulbar, cervical and lumbar. Bulbar onset presents with difficulty swallowing and slurring of speech and cervical onset presents with upper limb symptoms like shoulder abduction, with difficulty lifting arms and trouble performing activities needing pincer grip. Lumbar onset presents with difficulty climbing stairs and a tendency to trip, thus impairment of the lower motor neurons (Mitchell & Borasio, 2007).

Mild cognitive impairment, with associated impaired verbal fluency and attention deficits are common amongst ALS patients. 5% of ALS patients develop frontotemporal dementia, a type of frontotemporal lobar degeneration (FTLD), where patients can have impaired social cognition and impaired recognition of emotions (Phukan *et al.*, 2007). 63% of ALS patients are indifferent, inflexible, restless and disinhibited (Phukan *et al.*, 2007). Indirect symptoms of ALS include sleep disturbances, constipation, drooling, thick mucous secretions, pain and symptoms of chronic hypoventilation (Mitchell & Borasio, 2007).

2.1.4.2 Disease causing factors

Risk factors for ALS include old age, male sex, family history of dementia, low forced vital capacity, pseudobulbar palsy, bulbar site of onset (Phukan *et al.*, 2007) and environmental factors (Mitchell & Borasio, 2007). ALS is also caused due to a mutation of the Cu/Zn superoxide dismutase 1 (SOD1) gene on chromosome 21 (Mitchell & Borasio, 2007). SOD1

is a protein ubiquitously expressed in the cytosol and it is involved in the reduction of superoxide radicals to hydrogen peroxide, which can be inactivated by catalase, preventing oxidative damage (Simpson & Al-Chalabi, 2006).

2.1.4.3 Molecular changes

Mechanisms for the motor neuron loss include oxidative damage, excitotoxicity from impaired clearing of glutamate, intracellular aggregates of mutant SOD1 that causes toxicity, neurofilament disorganisation that leads to the disruption of axonal transport and changes in Ca^{2+} homeostasis that results in CDK5 deregulation (figure 2.2) (Patzke & Tsai, 2002). Some evidence suggest that not only motor neurons are affected, but other neurons as well, predominantly those along the thalamofrontal association pathway (Phukan *et al.*, 2007). Excitotoxicity occurs when neuromodulators like glutamate become toxic at supraphysiological concentrations, leading to excessive calcium influx resulting in the stimulation of the intraneuronal cascade and ultimately resulting in neuronal death (Mitchell & Borasio, 2007).

It has been proposed that compounds that inhibit CDK5 could possibly be beneficial for the survival of motor neurons in mutant SOD1-mediated disease (Patzke & Tsai, 2002), because CDK5/p25 phosphorylates neurofilament protein NF-H, leading to its accumulation (Knockaert *et al.*, 2002).

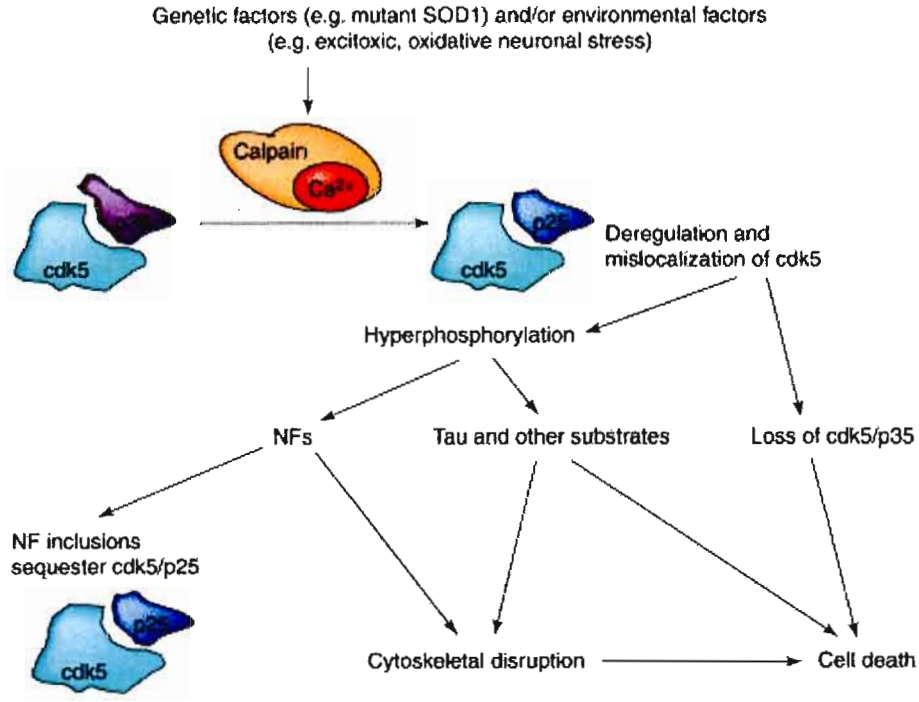

Figure 2.2: CDK5 deregulation in the pathogenesis of ALS (Patzke & Tsai, 2002).

2.2 Apoptosis

Programmed cell death, or apoptosis, is of critical importance in the developmental process to maintain the correct number of cells and preventing an excessive quantity of cells (Weishaupt *et al.*, 2003). The excessive, unwanted or harmful cells are selectively removed, for example by phagocytes (Concha & Abdel-Meguid, 2002). Apoptotic pathways can also be activated during adulthood thus contributing to the neuronal loss, which leads to neurodegenerative diseases (Weishaupt *et al.*, 2003). Apoptotic neuronal death sometimes occur during head injury, spinal cord injury and cerebral ischemia (Stoica *et al.*, 2003). Cell death is characterised by the condensation of chromatin, shrinking of the nucleus, DNA fragmentation and cytoplasm condensation and disintegration (Woodhouse *et al.*, 2006). Apoptotic pathways are very complex and there are a variety of models that depict these pathways (Heiner *et al.*, 2004).

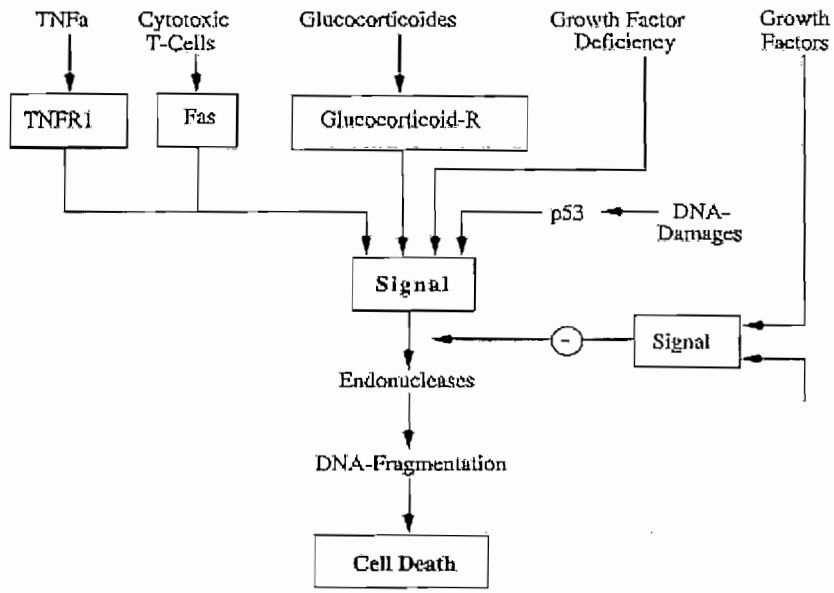

Figure 2.3: Schematic presentation of several apoptosis inducers (Heiner *et al.*, 2004). TNFR-1, Fas and glucocorticoid-R represent the extrinsic pathway and growth factor deficiency and DNA damaging signals represent the intrinsic pathway (Heiner *et al.*, 2004).

Two major pathways are involved during apoptosis, namely: the extrinsic (extracellular) pathway, mediated by death receptors and the intrinsic (intracellular) pathway, also known as the mitochondrial pathway (Olney, 2003). The death receptors include tumor necrosis factor receptor 1 (TNFR-1), glucocorticoid receptor and Fas (figure 2.3) (Heiner *et al.*, 2004). Cytokines bind to the death receptors, caspase 8 is activated leading to the cleavage and

activation of caspases 3, 6 and 7 (Olney, 2003). This pathway is discussed later in more detail (section 2.3.2.1).

P53 is also a key factor during apoptosis, specifically in cancer, by activating certain genes that encode for apoptosis (Shah & Schwartz, 2006). Exposure to hydrogen peroxide (H_2O_2) has the ability to cause apoptosis in neurons by damaging DNA and oxidative stress due to H_2O_2 can increase intracellular free Ca^{2+}, leading to activation of calcium dependent enzymes and eventually apoptosis (Ray *et al.*, 2000).

There are also anti-apoptotic pathways, the phosphoinositol 3-kinase (PI3K) pathway in which Akt (also known as protein kinase B (PKB)) depends on PI3K for its activation. Akt phosphorylates and inactivates pro-apoptotic factors like Bcl-2-associated death promotor (BAD), forkhead family transcription factors, and signalling entities like glycogen synthase kinase 3β (GSK3β) (Stoica *et al.*, 2003).

2.3 Protein kinases

Protein kinases are enzymes that phosphorylate protein substrates (Gurwitz & Eldar-Finkelman, 2001) and are essential components of several signalling pathways (Gerits *et al.*, 2006). Proliferation, differentiation and apoptosis are regulated by protein kinases and they also transduce signals detected on the cell's surface into changes in gene expression (Hagemann & Blank, 2001). Protein kinases are favourable drug targets due to the fact that phosphorylation of serine, threonine and tyrosine residues plays a fundamental role in molecular facets of cell life (Knockaert *et al.*, 2002).

2.3.1 Protein kinases in cancer

There are a variety of protein kinases that play a role in the development of cancer. These include the mitogen activated protein kinase (MAPK) cascade, GSK3β, cyclin dependent kinases (CDKs) and the protein kinase C (PKC) family (Koivunen *et al.*, 2006).

The MAPK cascade stimulates the production of D-type cyclin that can lead to the development of cancer. In cancer, the cell cycle is not regulated in a normal manner. Cells with an abnormally high expression of cyclins or impaired expression in naturally occurring cyclin dependent kinase inhibitors (CDKI), continue to undergo cell growth leading to an aberrant number of cells (Shah & Schwartz, 2006).

PKC's role in tumor promotion has not yet been fully elucidated. PKCα has been shown to act as an anti-apoptotic kinase and it can be activated by tobacco smoke and certain food types, leading to the promotion of tumor formation (Koivunen *et al.*, 2006).

2.3.1.1 Cyclin dependent kinases (CDKs)

CDKs are serine/threonine kinases that are activated by cyclins or other proteins such as p35 and p39 (Dai & Grant, 2003). They exhibit a variety of functions which include regulation of the cell cycle, apoptosis, transcription, differentiation, and other neuronal functions such as regulation of Golgi membrane traffic, insulin exocytosis by pancreatic β-cells and retinal phosphodiesterase regulation (Knockaert *et al.*, 2002). Deregulation of CDKs can lead to various diseases including cancer, alopecia, neurodegenerative disorders (AD, ALS and stroke), cardiovascular disorders (atherosclerosis and restenosis), glomerulonephritis, viral infections (HCMV, HIV and HSV) and parasitic protozoa (*Plasmodium* sp. and *Leishmania* sp.) (Knockaert *et al.*, 2002).

The CDK structure consists of a small N-terminal lobe, containing mostly β-sheets and a large C-terminal lobe consisting mostly of α-helices, while the ATP-binding pocket is situated between the two lobes. Binding of activators to the CDK structure lead to conformation changes of the CDK structure into the active form (Knockaert *et al.*, 2002).

CDKs are the key entities regulating the cell cycle and abnormal regulation of the cell cycle is one of the main features of neoplastic cells (Dai & Grant, 2003). CDK1, CDK2, CDK4 and CDK6 have been found to predominantly regulate the progression through G1, S, G2 and M phase of the cell cycle (Dai & Grant, 2003). Inhibitors of these CDKs will therefore be useful in the treatment of cancer (Shah & Schwartz, 2006). CDK inhibitors have the potential to be used in the treatment of cancer in view of the following:

- They are potent anti-proliferative entities because they arrest cells in G1 and G2/M;
- They can contribute to cell differentiation;
- They cause apoptosis (Knockaert *et al.*, 2002).

CDK inhibitors with the potential to be used in cancer therapy share the following properties:

- Low molecular weight;
- Flat, hydrophobic heterocycles;
- Act by competing with ATP for binding in the kinase ATP-binding site;
- Bind mostly by hydrophobic interactions and hydrogen bonds with the kinase;
- The backbone carbonyl and amino side-chains of Leu83 act, respectively, as an H-bond acceptor and an H-bond donor to the inhibitors, whereas the backbone carbonyl of Glu81 often acts as an H-bond acceptor (Knockaert *et al.*, 2002).

2.3.2 Protein kinases in apoptosis

One approach to develop therapies for neurodegenerative diseases focus on the inhibition of apoptosis. On the other hand, stimulation of apoptosis in the treatment of cancer cells is an approach in the treament of tumors (Tsai *et al.*, 2004; Koh *et al.*, 2006).

2.3.2.1 Cyclin dependent kinase 5 (CDK5)

Cyclin dependent kinase 5 (CDK5) is a proline-directed protein kinase (Tsai *et al.*, 2004), originally identified as a member of the cyclin dependent kinase family of serine/threonine kinases (Wang *et al.*, 2006). CDK5 does not regulate the cell cycle but its activity is mainly observed in postmitotic neurons (Wang *et al.*, 2006). This neuron specific expression is observed because CDK5 has to be activated and the CDK5 activators, p35 and p39, are expressed almost exclusively in the nervous system (Tsai *et al.*, 2004; Weishaupt *et al.*, 2003).

CDK5 substrates

A structural requirement for a CDK5 substrate is a proline residue in the +1 position (Dhavan & Tsai, 2001). CDK5 also prefers a basic residue at the +3 position and phosphorylates the consensus sequence (S/T)PX(K/H/R), where S or T are the phosphorylatable serine or threonine, X is any amino acid and P is the proline residue in the +1 position (Dhavan & Tsai, 2001). Several structural diverse substrates of CDK5 have been identified, including p35, p39, PAK1, Src, Cables, β-catenin, Tau, MAP1B, Nudel, NFH/NFM, Synapsin 1, MUNC18 (phosphorylation alters synaptic vesicle exocytosis (Patrick *et al.*, 1999)), Amphyphysin 1, β-APP, DARPP32 (becomes an inhibitor of protein kinase A after phosphorylation (Patrick *et al.*, 1999)), PP1-inhibitor, Pgamma (PDE regulator), ERBB and pRb (Dhavan & Tsai, 2001).

CDK5 activity

CDK5 activity is involved amongst others in axon guidance, synaptic function (Patzke & Tsai, 2002), the regulation of the cytoskeleton, membrane transport, dopamine signalling and drug addiction (Dhavan & Tsai, 2001).

Role of CDK5 in neuronal cell survival and death

CDK5 plays an important role in both neuronal cell survival and death as illustrated in figure 2.4 (Cheung & Ip, 2004). In response to apoptotic stimuli such as UV irradiation, the activation of c-Jun N-terminal kinase 3 (JNK3) occurs and c-jun is subsequently phosphorylated (Li *et al.*, 2002). Phosphorylated c-jun in turn leads to an increase in activator protein 1 (AP-1) transcription, resulting in apoptosis. CDK5 phosphorylates JNK3, thereby prevents its activation and subsequently prevents apoptosis (Cheung & Ip, 2004). It also inhibits apoptosis by phosphorylating the ErbB receptor, also known as epidermal growth

factor receptor (EGFR). Neuregulin can then bind to the ErbB receptor, activating it and leading to increased PI3K. This subsequently leads to increased Akt (also a known as protein kinase B) and thus the prevention of apoptosis (Cheung & Ip, 2004).

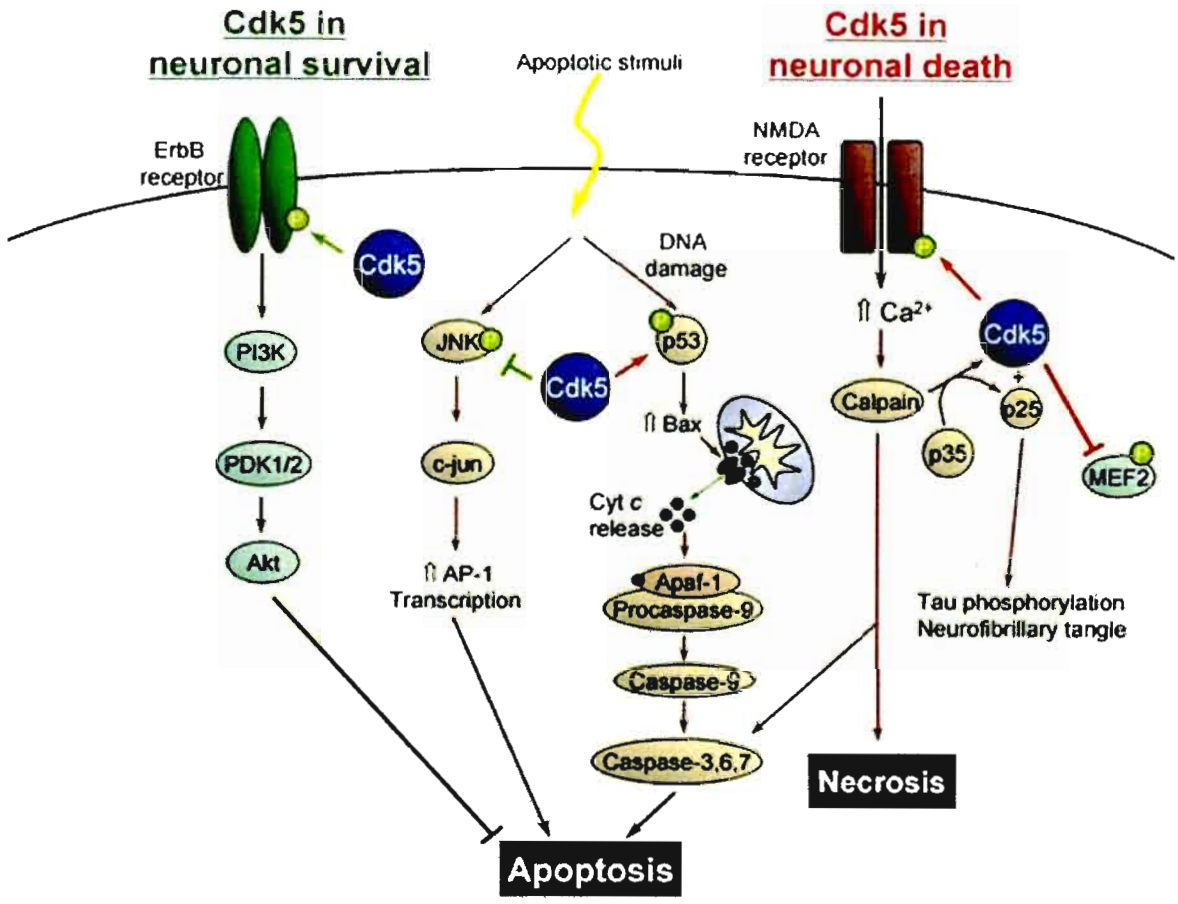

Figure 2.4: Role of CDK5 in neuronal death and survival (Cheung & Ip, 2004).

Phosphorylation of NMDA receptors is also mediated by CDK5, increasing calcium flux into the cells (Cheung & Ip, 2004). Calpain is subsequently activated by the increased calcium concentration (Cheung & Ip, 2004) and other neurotoxic conditions, including the formation of Aβ (Lee *et al.*, 2000), which leads to calpain mediated p35 cleavage and p25 production (Sharma *et al.*, 2007). P25 interacts with CDK5 and causes prolonged activation of CDK5 and the deregulated CDK5/p25 complex phosphorylates tau, is neurotoxic and causes apoptosis (Tsai *et al.*, 2004). The CDK5/p25 complex also causes NFT (Cheung & Ip, 2004). P25 on its own is neurotoxic and causes apoptotic neuronal death (Wang *et al.*, 2006) and was shown to be increased in the brain tissue of persons with AD (Patrick *et al.*, 1999). Increased p25 and over activation of CDK5 were found in a transgenic mouse model for ALS and cultured cortical neurons exposed to Aβ. CDK5 has also been found to be co-localized with Lewy bodies (Weishaupt *et al.*, 2003).

CDK5 also causes apoptosis through the mitochondrial pathway (Cheung & Ip, 2004). CDK5/p25 has been shown to upregulate the expression of p53, which increases the expression of Bax, a pro-apoptotic member of the Bcl-2 family (Zhang *et al.*, 2002). Bax stimulates the release of cytochrome *c* from the mitochondria (Olney, 2003). Other members of the Bcl-2 family also regulate cytochrome *c*; Bak stimulates its release and Bcl-2 and Bcl-X_L both inhibit its release (Wang *et al.*, 2006). Hypoxia, DNA damage and withdrawal of growth factors, including nerve growth factor (NGF) and brain-derived neurotrophic factor (BDNF), also stimulate the release of cytochrome *c* (Wang *et al.*, 2006). Cytochrome *c* binds to Apaf-1 and procaspase-9, resulting in the activation of caspase 9. Caspase 9 then activates other members in the family like caspase 3, 6 and 7, resulting in apoptosis (Cheung & Ip, 2004).

CDK5/p25 has been shown to inhibit the transcription factor MEF2 (myocyte enhancer factor), which has pro-survival actions, by means of phosphorylating it at Ser^{444}. Excitotoxicity and oxidative stress can now damage the cortical neurons without difficulty (Cheung & Ip, 2004).

It has been shown that CDK5 activity levels have to be optimal to prevent neuronal loss. Abnormally high levels inhibit MAPK and abnormally low levels induce sustained activation of MAPK, both causing apoptosis (Sharma *et al.*, 2007).

2.3.2.2 Mitogen activated protein kinase (MAPK) cascade

MAPKs are primarily involved in pathways caused by mitogens or stress stimuli and regulate processes like cell division, differentiation, apoptosis, gene expression, motility and metabolism (Gerits *et al.*, 2006). MAPK represents a family of serine/threonine kinases that can phosphorylate other proteins and translocate to the nucleus where the activity of transcription factors controlling gene expression can be controlled (Hagemann & Blank, 2001). In this cascade, a mitogen activated protein kinase kinase kinase (MAPKKK), phosphorylates and activates a MAP kinase kinase (MAPKK), which in turn phosphorylates and activates the MAP kinase (MAPK) (Hagemann & Blank, 2001). Some MAPKs also have the ability to phosphorylate tau protein *in vitro* leading to neurodegeneration (Holzer *et al.*, 2001).

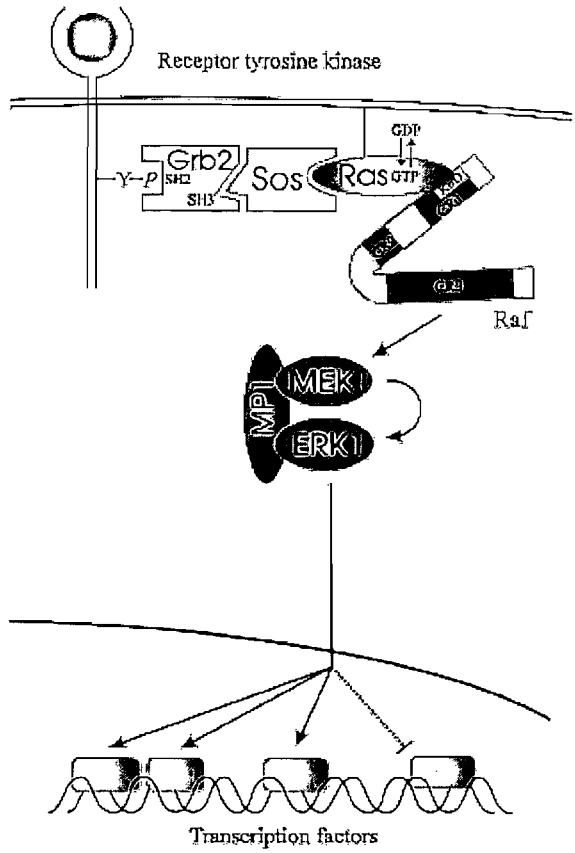

Figure 2.5: The Ras/Raf/MEK/ERK pathway (Hagemann & Blank, 2001).

The pathway shown in figure 2.5 is the MAPK pathway that occurs most frequent (Hagemann & Blank, 2001). In this pathway the MAPKKKs are Raf-1, A-Raf and B-Raf, the MAPKKs are MAPK/ERK kinase 1 (MEK1) and MAPK/ERK kinase 2 (MEK2) and the MAPKs are extracellular signal regulated kinase 1 (ERK1) and extracellular signal regulated kinase 2 (ERK2) (Gerits *et al.*, 2006). In this pathway signals such as growth factors cause activation of receptor tyrosine kinases by phosphorylation. The phosphorylated residues on the receptors serve as docking sites for the adaptor protein Grb2, which is complexed with a guanine nucleotide exchange factor, namely the son of sevenless (Sos) (Hagemann & Blank, 2001). Sos activates the G-protein Ras, from the inactive GDP-bound form to the active GTP-bound form (Holzer *et al.*, 2001). Ras can then either bind to Raf, in the plasma membrane, to activate it or produce indirect regulatory signals (Kolch, 2000). These signals include one provided by PI3K through its phospholipid product that activates Rac, a small G-protein, which binds to and activates p21cdc42/rac1-activated serine/threonine kinase (PAK). PAK3 subsequently phosphorylates and activates Raf-1 (Kolch, 2000). Raf kinase then phosphorylates and activates MAPK kinase, which then activates MAPK (Holzer *et al.*,

2001). MEK1 and MEK2 phosphorylate the Thr-Glu-Tyr motif in the activation loop of the ERKs (Gerits *et al.*, 2006).

Abnormally low levels of B-Raf or the complete loss thereof can lead to spontaneous apoptosis in the brain (Gerits *et al.*, 2006).

MEK kinases (MEKKs) regulate the MAPK pathways that occur as a result of cellular stress and lead to the activation of c-Jun NH_2-terminal kinase (JNK) and p38, which regulates growth arrest, apoptosis and proliferation (Hagemann & Blank, 2001). SAPK/ERK kinase, also known as JNK kinase (JNKK) or MAPK kinase 4 (MKK4), as well as MKK7 phosphorylates and activates JNK and in another instance MKK3 and MKK6 activates p38 (Hagemann & Blank, 2001). Activation of JNK and p38 can be acquired by stimuli such as radiation and conventional chemotherapeutic agents, leading to apoptosis (Senderowicz, 2004). JNK1 and JNK2 play a key role in the morphogenesis of the mammalian brain (Gerits *et al.*, 2006).

MEKK1 is a substrate of caspase and is cleaved to release a 91 kDa C-terminal catalytically active portion of MEKK1 into the cytoplasm from the membrane where it then promotes caspase activation and stimulates apoptosis. MEKK1 has also been shown to be anti-apoptotic, thus cleavage by caspase may be important to convert the function of MEKK1 from a pro-survival agent to a pro-apoptotic agent (Hagemann & Blank, 2001).

2.3.2.3 Glycogen synthase kinase 3 (GSK3)

GSK3 is a serine/threonine protein kinase that is widely expressed and was initially discovered as a regulatory enzyme of glycogen synthesis in response to insulin (Pap & Cooper, 1998). After insulin binds to the insulin cell surface receptor, protein kinase B (PKB) is activated and phosphorylates GSK3 to inactivate it. GSK3 also regulates Wnt signalling as well as the scheme of cell fate during embryonic development (Gurwitz & Eldar-Finkelman, 2001). There are two types of GSK3 namely GSK3α and GSK3β (Moreno *et al.*, 1995).

Existing evidence indicate that overexpression of GSK3 results in neurodegeneration and that the deregulation of GSK3 plays a role in AD (Mattson, 2001). An increased level of active GSK3 was found in the frontal cortex of AD patients (Leroy *et al.*, 2007) and GSK3β accumulates in the cytoplasm of pre-tangle neurons and is thus associated with NFT (Engel *et al.*, 2006; Koh *et al.*, 2006). GSK3β has the ability to generate several phosphorylation sites on tau *in vitro* (Leroy *et al.*, 2007). Hyperphosphorylated tau promotes neuronal apoptosis upon over expression of GSK3 (Churcher, 2006). This phosphorylation of tau, especially by GSK3β at Thr231 (Churcher, 2006), decreases its affinity for microtubules

(Engel *et al.*, 2006). GSK3 can also phosphorylate tau at Ser262 under certain circumstances (Moreno *et al.*, 1995). GSK3 can phosphorylate other factors important in apoptosis such as the initiation factor eIF2B and the transcription factors cAMP-responsive element binding protein (CREB), c-myc, c-jun and β-catenin as well (Stoica *et al.*, 2003).

GSK3 activity is inhibited by Akt (PKB) via the PI3K survival pathway (Pap & Cooper, 1998) and in neuronal cells mainly this pathway is active (Gómez-Ramos *et al.*, 2006). Other pathways and enzymes that inactivate GSK3 includes extracellular signal regulating kinase (ERK), protein kinase A (PKA), protein kinase C (PKC) and MAPK activated proteins (Lin *et al.*, 2007). Protein phosphatase 2A (PP2A) can indirectly activate GSK3β (Lin *et al.*, 2007).

GSK3 appears to be a potential target for the treatment of AD and affective disorders based on the inhibition of GSK3 by lithium ions resulting in reduced Aβ. Lithium is used in the treatment of affective disorders (Gurwitz & Eldar-Finkelman, 2001; Cohen & Goedert, 2004). Phosphorylation of Ser21 inactivates GSK3α and phosphorylation of Ser9 inactivates GSK3β (Chin *et al.*, 2005). Increased GSK3 activation can activate caspase 3, leading to apoptosis; this effect is blocked by the lithium ions (Gurwitz & Eldar-Finkelman, 2001). GSK3β can also regulate activation of caspase 2 and caspase 8 (Lin *et al.*, 2007).

Substrates of GSK3 include presenilin-1, amyloid precursor protein, axin, eukaryotic initiation factor 2 B, heat-shock transcription factor-1, cyclin D1 and pyruvate dehydrogenase (Mattson, 2001).

Several GSK3 inhibitors exhibiting *in vitro* neuroprotection against apoptotic cell death have been patented (Gurwitz & Eldar-Finkelman, 2001).

2.3.2.4 Calcium calmodulin dependent kinases (CaMK)

Intracellular Ca^{2+} regulates a wide variety of neuronal functions and these functions are inhibited by the Ca^{2+}-binding protein calmodulin (Jusuf *et al.*, 2002). The Ca^{2+}-calmodulin complex can activate other enzymes including the calcium calmodulin dependent kinases (CaMKs) and CaMKIβ2 that has been implicated in neurogenesis (Jusuf *et al.*, 2002).

Calcium calmodulin dependent kinase II (CaMKII)

CaMKII is the most prevalent CaMK in mesangial and other smooth muscle cells and is activated by Ca^{2+}-containing calmodulin (Lui & Templeton, 2007). CaMKII is ubiquitously expressed in brain tissue and can phosphorylate tau at Ser262 and Ser356, thus contributing to apoptosis (Churcher, 2006). Other studies have also shown that CaMKII contribute to apoptotic cell death. However, CaMKII phosphorylates cellular-FLICE inhibitory protein (c-

FLIP) and supply Fas-sensitive glioma cells with protection against apoptosis (Lui & Templeton, 2007).

Calcium calmodulin dependent kinase IV (CaMKIV)

CaMKIV is mainly expressed in the brain, thymus and testes. CaMKIV localises in the nuclei of neurons and possibly regulates important processes altered in neurons undergoing apoptosis (McGinnist *et al.*, 1998). CaMKIV is cleaved by caspase 3 to promote neuronal apoptosis. However, in neurons deprived of K^+, CaMKIV can also act in an anti-apoptotic manner (Lui & Templeton, 2007).

2.4 Other enzymes contributing to apoptosis

2.4.1 Calpain

Calpain is a calcium-dependent cysteine protease (Lee *et al.*, 2000) requiring intracellular free Ca^{2+} for activation (Ray *et al.*, 2000) and is found mainly in the plasma membrane (Perrin & Huttenlocher, 2002). Calpastatin, a specific endogenous inhibitor, controls its activity (Ray *et al.*, 2000). There are two isoforms of calpain found in the neuronal tissue namely m-calpain and μ-calpain and they differ in the concentration of calcium needed for activation. 3-50 μM calcium is needed for half-maximal activity for μ-calpain and 0.2-1 mM calcium for m-calpain (Lee *et al.*, 2000). Each isoform is a heterodimer consisting of identical 30 kDa regulatory subunits and similar but not identical 80 kDa catalytic subunits (Ray *et al.*, 2000). m-Calpain is increased following exposure to oxidative stress conditions and Ca^{2+} influx and is also increased in AD brains (Ray *et al.*, 2000). Both isoforms are upregulated in patients with ALS (Ray *et al.*, 2000), PD and Duchenne muscular dystrophy (Saez *et al.*, 2006).

In brain ischemia (Saez *et al.*, 2006), elevated glutamate triggers calcium influx, calpain is activated and cleaves regulatory proteins such as αII-spectrin, βII-spectrin and calpastatin leading to neuronal death (Kawamura *et al.*, 2005). Calpain activity regulates a wide variety of cellular functions including apoptosis, proliferation and cell migration (Perrin & Huttenlocher, 2002). It also participates in the regulation of kinases, transcription factors and receptors (Kawamura *et al.*, 2005). Upregulated calpain may possibly degrade cytoskeletal proteins causing cell death (Ray *et al.*, 2000). Calpain cleaves p35 to form p25 (figure 2.2) following calcium activation (Kusakawa *et al.*, 2000) and p25 activates and deregulates CDK5 leading to apoptosis (Tsai *et al.*, 2004). Apoptosis can also occur via the activation of caspase 3 and 12 by calpain (Saez *et al.*, 2006). Treatment of mice with AD by a calpain inhibitor showed improved synaptic and cognitive function (Kawamura *et al.*, 2005).

Calpain contains two papain-like domains namely domain I and II, with the proteolytic active site located at the interface between the two domains, together forming the proteolytic core of calpain. These domains contain two calcium binding sites and occupation of these sites are essential for the rearrangement of the catalytic triad and the substrate binding site into an active conformation. There are highly flexible gating loops that flank either side of the active site binding pocket and consists of residues 69-82 in domain I and residues 251-261 in domain II (Cuerrier *et al.*, 2006). Domain II has the catalytic sequence CHR (Saez *et al.*, 2006).

2.4.2 Caspases (cysteinyl-aspartate-specific proteinases)

Caspases are members of the cysteine proteases that exist as inactive zymogens activated by proteolytic cleavage (Heiner *et al.*, 2004). Caspases play a critical role in neuronal apoptosis (Stoica *et al.*, 2003). Caspase involvement has also been implicated in differentiation and growth stimulation in certain cell types (Ussat *et al.*, 2002). Fourteen different caspases have been identified and they can be classified into three broad classes of caspases namely; initiator caspases, pro-inflammatory caspases and effector caspases (Wei *et al.*, 2008). Caspase 8, 9 and 10 are initiator caspases and their activation can lead to cleavage and activation of the effector caspases such as caspase 2, 3 and 6, which then cleaves poly (ADP-ribose) polymerase (PARP) (Koh *et al.*, 2006). Cleavage of PARP is one of the known markers for apoptosis (Koh *et al.*, 2006). Pro-caspases consists of a N-terminal, p20, a linker and a C-terminal which is p10. The N-terminal peptide and the linker are cleaved off during activation to produce the p20/p10 active heterodimer caspases (Concha & Abdel-Meguid, 2002).

There are two key receptor activations which lead to caspase mediated apoptosis namely Fas and TNFR-1 (figure 2.6). The Fas ligand binds to the Fas receptor and this triggers the adaptor protein FADD/MORT1 (Fas-associating protein with death domain) to bind to the death receptor domain either directly or via TRADD (TNFR-1-associated death domain protein). Pro-caspase 8 binds to FADD/MORT1 via the death effector domain and is activated. TNF binds to the TNFR-1 and pro-caspase 8 is activated in the same manner. Caspase 9 is activated by the mitochondrial pathway via the "apoptosome" complex consisting of apaf-1 and cytochrome *c* in the presence of dATP. Caspase 8 and caspase 9 subsequently activate caspase 3, leading to apoptosis (Concha & Abdel-Meguid, 2002).

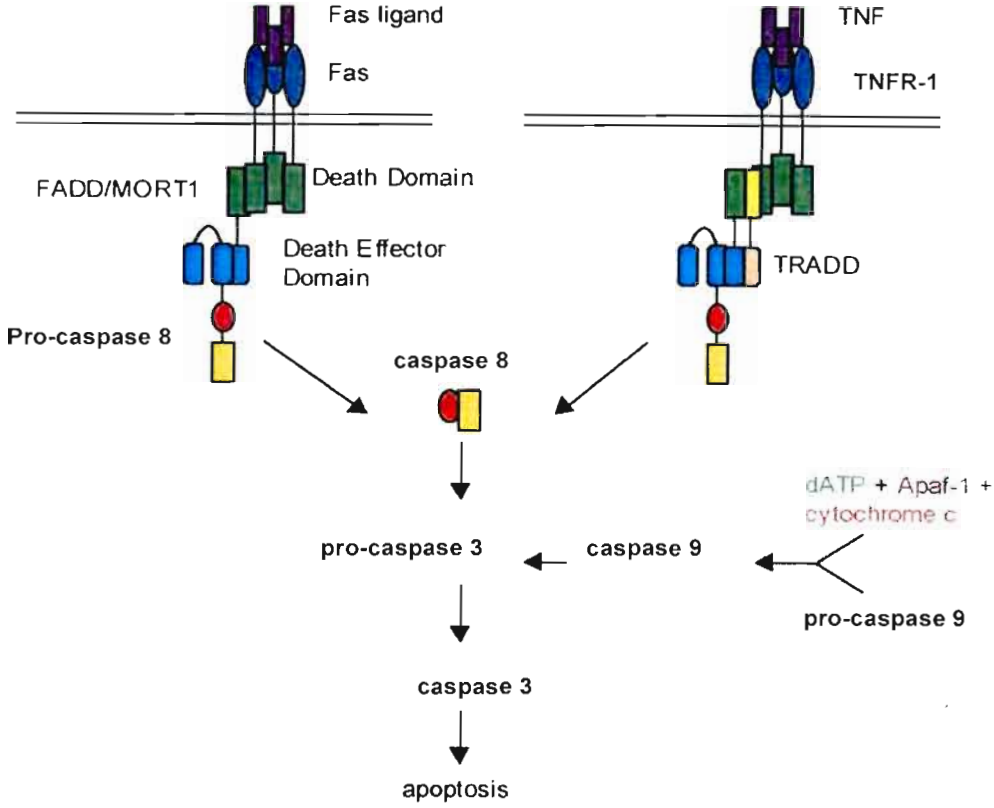

Figure 2.6: Apoptosis signalling through Fas and TNFR-1 receptor (Concha & Abdel-Meguid, 2002).

Caspase 3 plays a key role in the execution phase of apoptosis in neurodegeneration (Wei *et al.*, 2008). All the caspase 3 substrates have a DXXD recognition site, where D is aspartic acid and X is any other amino acid (McGinnist *et al.*, 1998). Caspase 3 cleaves its substrates after the DEVD sites (Becker *et al.*, 2004).

Caspase substrates include cell adhesion molecules such as cadherins, cytoskeletal proteins like actin and gelsolin, lamins, cyclin A, cyclin E, PARP, phospholipase D (PLD) (Wright *et al.*, 2008), p21, PKC, focal adhesion kinase (FAK), PLA_2 and calpastatin (Ussat *et al.*, 2002). All caspases have a QACXG pentapeptide active site in common where X can be R, Q or G and they require an Asp residue in the P_1 position (McGinnist *et al.*, 1998). Caspase 12 is found mostly as a proenzyme in the endoplasmic reticulum (ER) and calpain may be needed for procaspase-12 activation (Koh *et al.*, 2006). An *in vitro* study indicated that Aβ peptide can also activate caspases (Wei *et al.*, 2008).

The S1' binding site of caspase 3 is a large, bowl-shaped predominantly hydrophobic site and is a C-terminal extension of the surface groove that contains S4-S1 (Becker *et al.*, 2004). The S4 subsite has a more open and uncharged stucture than the highly constricted and cationic subsite (Becker *et al.*, 2004).

2.5 Enzyme inhibitors

2.5.1 CDK5/p25 inhibitors

CDK5/p25 can hyperphosphorylate tau, leading to the formation of paired helical filaments and NFT. CDK5/p25 is viewed as a potential target for the treatment of AD as the inhibition of CDK5/p25 would lead to the prevention of NFT (Helal *et al.*, 2004).

Various CDK5/p25 inhibitors (figure 2.7) have been described in the literature (Helal *et al.*, 2004; Alvira *et al.*, 2006; Mapelli *et al.*, 2005; Shiradkar *et al.*, 2007).

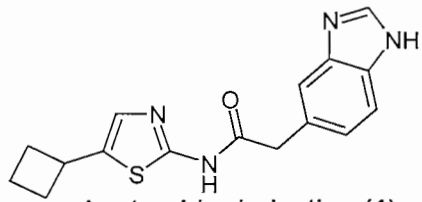

Acetamide derivative (**1**)

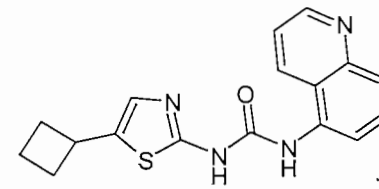

Urea derivative (**2**)

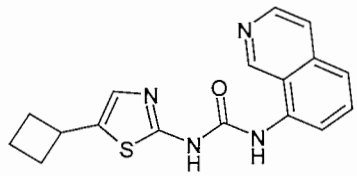

Urea derivative (**3**)

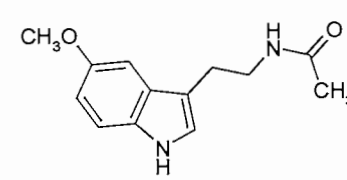

Melatonin (**4**)

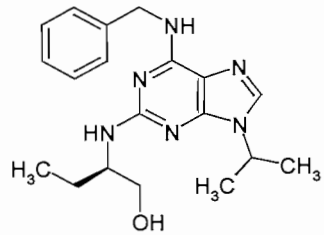

(R)-roscovitine (**5**)

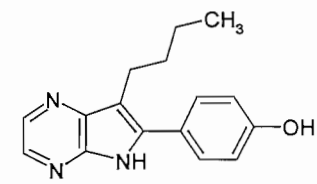

Aloisine-A (**6**)

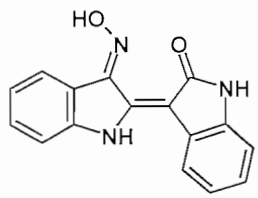

Indirubin-3'-oxime (**7**)

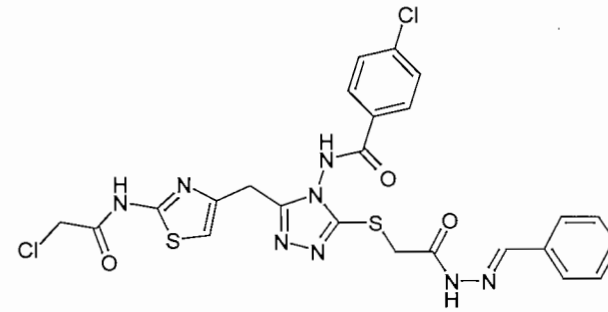

Triazolyl thiazole derivative (**8**)

Figure 2.7: CDK5/p25 inhibitors (Helal *et al.*, 2004; Alvira *et al.*, 2006; Mapelli *et al.*, 2005; Shiradkar *et al.*, 2007).

Molecular modelling studies of structures **1-3** (figure 2.7) in the ATP binding region of CDK5/p25 idicated that hydrogen bonds form between the aminothiazole N-H and the heterocyclic N with the carbonyl and N-H of Cys83, respectively. They may also interact with IleA10 of CDK5/p25. The IC_{50} values for structures **1-3** inhibiting CDK5/p25 were found to be 7, 8 and 5 nM respectively (Helal *et al.*, 2004).

Melatonin (**4**, figure 2.7) has been shown to prevent the association of CDK5 with p25 but a specific mechanism has not been determined (Alvira *et al.*, 2006).

X-ray diffraction studies suggested that (R)-roscovitine (**5**, figure 2.7) forms a hydrogen bond between the oxygen of its chiral hydroxyethyl substituent and the main chain carbonyl oxygen of Gln130 and its ethyl group is engaged in hydrophobic interactions with Ile10 and Val18. There are also hydrophobic interactions between the Ile10, Gly11 and Glu12 in the glycine-rich loop and the structure. The benzyl substituent protrudes into a hydrophobic pocket, which is lined by Ile10 and Phe82. This compound has entered phase II clinical trials against cancer and phase I against glomerulonephritis. (R)-roscovitine (**5**, figure 2.7) is shown in yellow in the ribbon diagram of the CDK5/p25 complex (figures 2.8 and 2.9A) (Mapelli *et al.*, 2005).

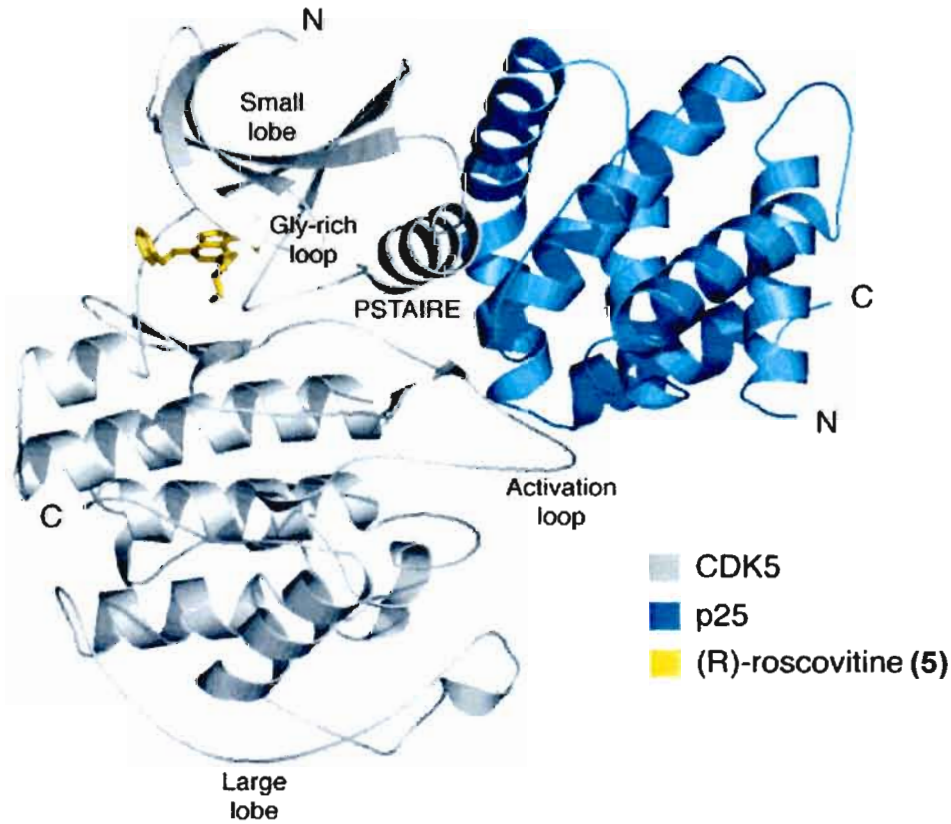

Figure 2.8: Ribbon diagram of the CDK5/p25 complex with the inhibitor, (R)-roscovitine (Mapelli *et al.*, 2005).

Aloisine-A (**6**, figure 2.7) forms hydrogen bonds with the N4 and N5 nitrogen atoms and the backbone amide and oxygen atoms of Cys83 respectively. N1 is involved in a nitrogen bonding network with the side chains of Lys33, Glu51 and Asn144 as well as with two water molecules. The above mentioned bonding pattern targets the active state of the kinase. In this state Lys33 and Glu51 are able to interact after the p25 induced rearrangement of the PSSALRE helix (Mapelli *et al.*, 2005). The structure has been found to be anti-proliferative and non-specific for CDK's and can possibly be of value in cancer treatment (Mettey *et al.*, 2003). Aloisine-A (**6**, figure 2.7) is shown in yellow in the ribbon diagram of the CDK5/p25 complex (figure 2.9B).

In x-ray diffraction studies, indirubin-3'-oxime (**7**, figure 2.7) was shown to form three hydrogen bonds: The NH group of Cys83 donates a hydrogen to the lactam amide oxygen, the cyclic nitrogen acts as a hydrogen bond donor to the backbone oxygen of Cys83 and the lactam amide nitrogen acts as a hydrogen bond donor to the peptide oxygen of Glu81. The hydroxyl group forms a hydrogen bond, using a bridging water molecule, with the Asp86 side chain and there are stacking interactions observed with Phe80 (Mapelli *et al.*, 2005). This compound is a component of the traditional Chinese medicine Danggui Longhui Wan, which is used in the treatment of leukaemia (Wagman *et al.*, 2004). Indirubin-3'-oxime (**7**, figure 2.7) is shown in yellow in the ribbon diagram of the CDK5/p25 complex (figure 2.9C).

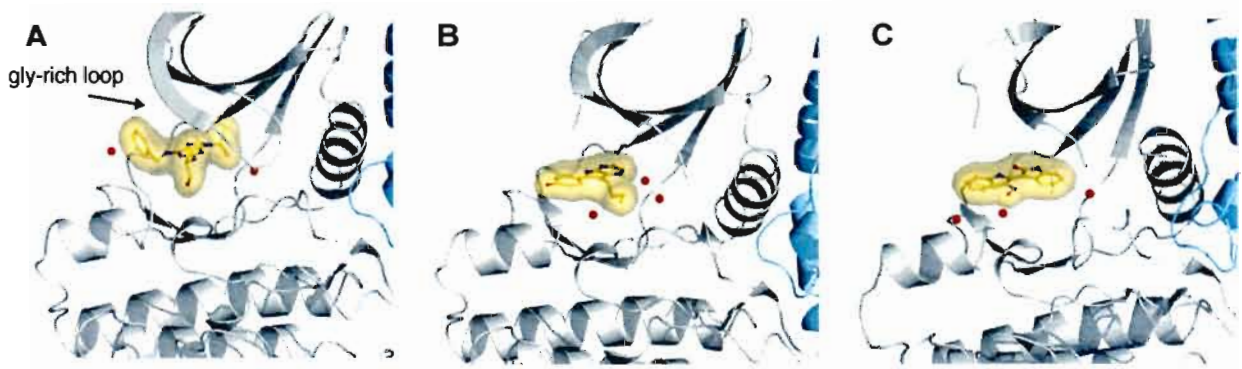

Figure 2.9: Ribbon model of CDK5/p25 with the waters in the nucleotide binding pocket indicated as red spheres (Mapelli *et al.*, 2005). From left to right the inhibitors in yellow are (R)-roscovitine (A), aloisine-A (B) and indirubin-3'-oxime (C) (Mapelli *et al.*, 2005).

2.5.2 Calpain inhibitors

Calpain has the ability to cleave p35 to p25, leading to deregulated CDK5/p25, which in turn hyperphosphorylates tau and leads to apoptosis. Inhibition of calpain thus has the potential to be used in the treatment of AD. Increased calpain has also been seen in the neuronal tissue of patients with ALS and PD and it is therefore a potential target for these diseases. Four classes of calpain inhibitors are known, namely peptidyl epoxides, peptidyl aldehydes, peptidyl α-ketoamides and non-peptide inhibitors (Carragher, 2006). This dissertation will focus on the non-peptide inhibitors (figure 2.12, structures **11-14**), mainly because peptide inhibitors have low oral availability, lack the necessary pharmacokinetic properties (Lubisch & Möller, 2002) and have difficulty crossing the blood-brain barrier in view of their systemic metabolism (Kawamura *et al.*, 2005). The site where peptide inhibitors such as leupeptin bind (figure 2.10 and 2.11), can however be valuable to predict the binding region of other small molecule inhibitors.

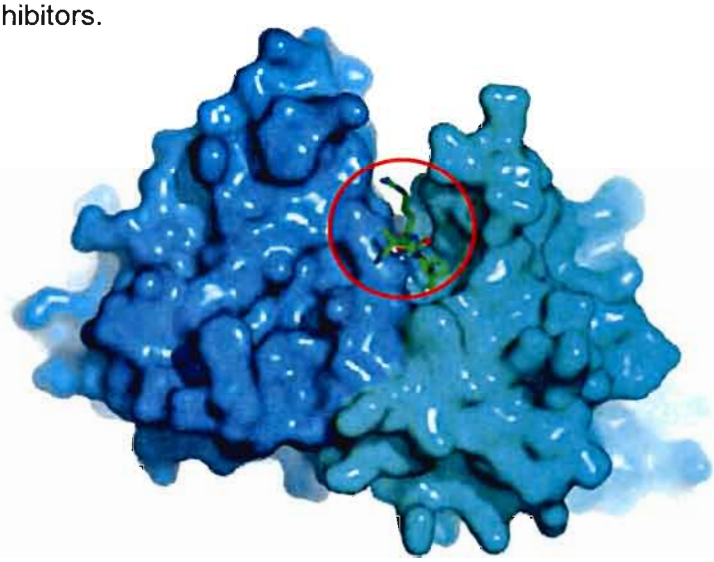

Figure 2.10: Calpain with peptide inhibitor leupeptin, circled in red (Moldoveanu *et al.*, 2004).

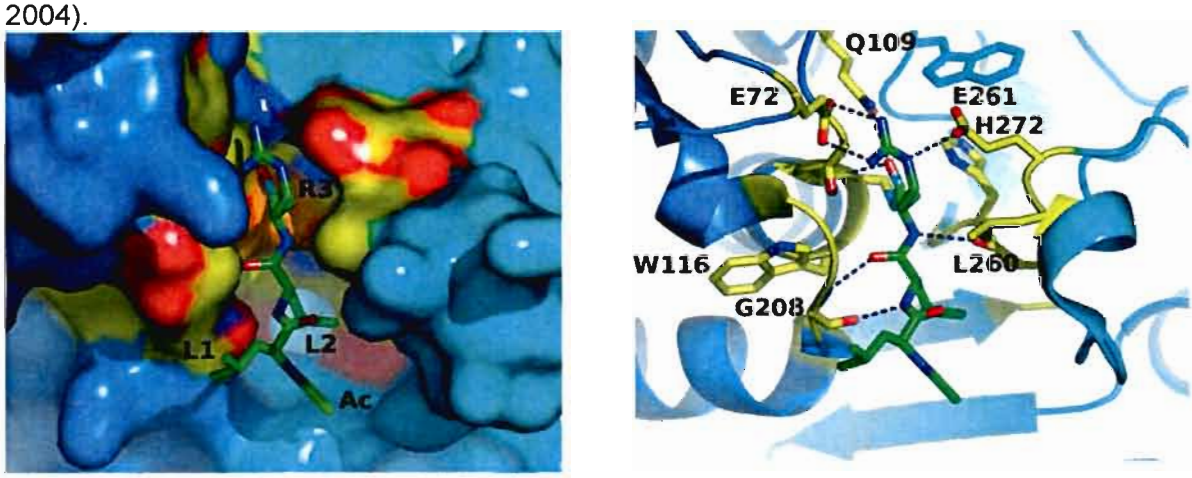

Figure 2.11: Leupeptin in calpain's active site, with hydrogen bonds represented by dotted lines (Moldoveanu *et al.*, 2004).

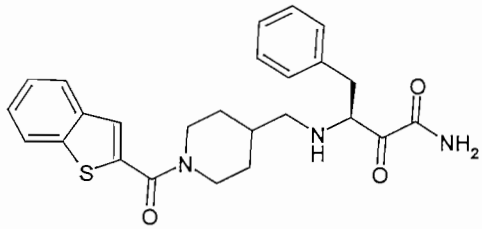

Ketoamide analogue (**9**)

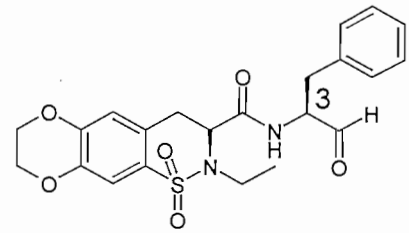

Aldehyde analogue (**10**)

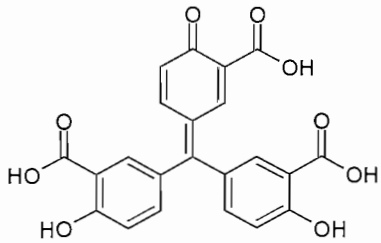

Aurintricarboxylic acid (ATA) (**11**)

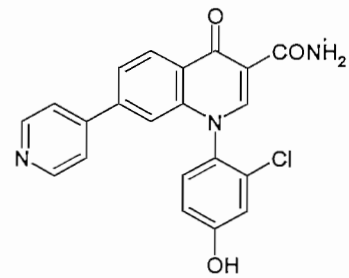

Quinolinecarboxamide derivative (**12**)

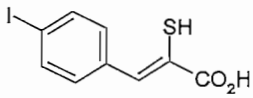

PD 150606 (**13**)

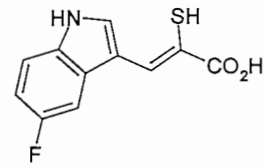

PD 151746 (**14**)

Figure 2.12: Calpain inhibitors (Hernandez & Roush, 2002; Carragher, 2006).

Compounds **9** and **10** (figure 2.12) are reversible inhibitors of calpain with IC_{50} values of 9 nM and 7 nM respectively (Hernandez & Roush, 2002). The ketone and aldehyde functional groups form reversible covalent bonds with the thiol of the cysteine at the active site (Wells *et al.*, 2001). The S configuration at the C-3 position presents the more potent diasteromer of compound **10** (Wells *et al.*, 2001).

ATA (**11**, figure 2.12) is a polymeric dye with the ability to inhibit both m-calpain and μ-calpain (Carragher, 2006). Compound **12** (figure 2.12) is a quinolinecarboxamide derivative and some of its derivatives have been shown to exhibit anticonvulsive properties (Lubisch *et al.*, 2000). No binding modes or mechanisms for these activities have been described (Carragher, 2006; Lubisch *et al.*, 2000).

Compounds **13** and **14** (figure 2.12) are α-mercaptoacrylic acid derivatives (Carragher, 2006) and compound **13** has the ability to alleviate hypoxic/hypoglycemic injury and excitotoxic injury in neuronal cultures. Sulfhydryl and carboxylic acid groups are essential to inhibit

calpain, suggesting that these structures chelate the bound calcium ion. The presence of an aromatic ring suggests a hydrophobic interaction. It is most likely that the binding of **13** to the calcium-binding site can interfere with the conformational changes needed for activation of the catalytic domain (Wang *et al.*, 1996).

2.5.3 Caspase inhibitors

Caspases act downstream of other enzymes on several of the apoptotic pathways including the mitochondrial pathway and the inhibition of caspases 3, 6, 7, 8 and 9, that cleaves a number of proteins leading to apoptosis, can counteract apoptosis (Wang *et al.*, 2007) and prevent or impair disease progression (Nedev *et al.*, 2005). Current known caspase inhibitors are from natural (for example p35, a protein isolated from baculovirus) or synthetic origen. The synthetic inhibitors are peptide based (Z-DEVD-cmk) or non-peptidic (isatin sulfonamides) (Concha & Abdel-Meguid, 2002).

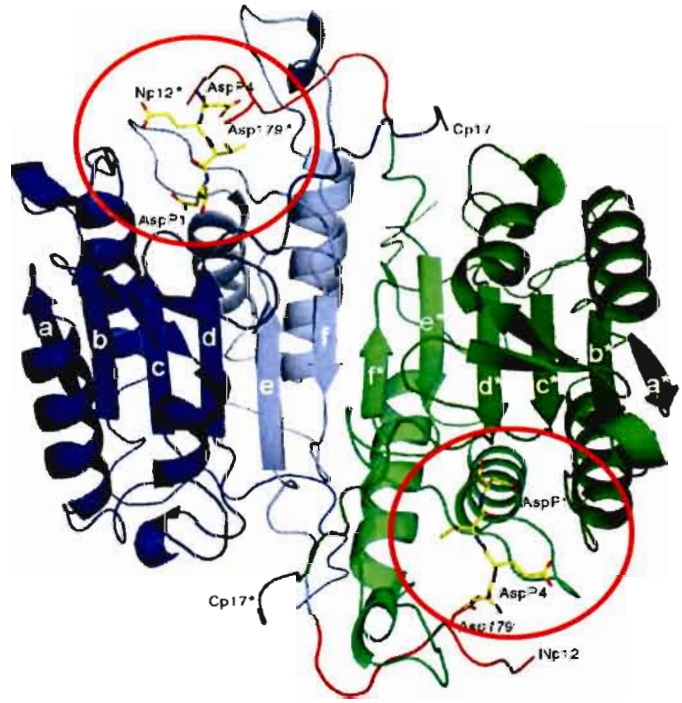

Figure 2.13: Caspase 3 and peptide inhibitor Z-DEVD-cmk, circled in red (Ganesan *et al.*, 2006). The p20 and p10 subunits are shown in light and dark colours respectively and the p20 N-terminal chain is shown in red. The β-sheet strands are labelled (Ganesan *et al.*, 2006).

The structure of caspase 3 (figure 2.13) has been studied by means of x-ray diffraction. Ser29 to Thr174 form the p10 subunit and Ser176 to His277 form the p20 subunit. Residues 1 to 29 form the N terminus of the p10 subunit. The p20 and p10 subunits fold into a six-stranded mixed β-sheet with five α-helices on both sides (Ganesan *et al.*, 2006).

2.5.3.1 Caspase 3 inhibitors

Caspase 3 is a key mediator in the apoptotic cascade and mediates apoptosis from not only the intrinsic pathway but also the extrinsic pathway. The inhibition of caspase 3 is therefore a potential approach in the treatment of diseases with neuronal apoptosis (Allen *et al.*, 2003). Various non-peptide caspase 3 inhibitors have been described in the literature (figure 2.14).

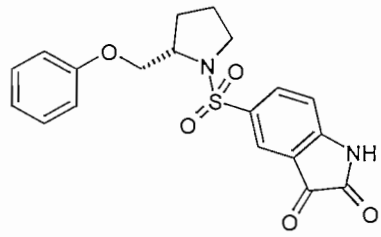

Isatin sulfonamide (**15**)

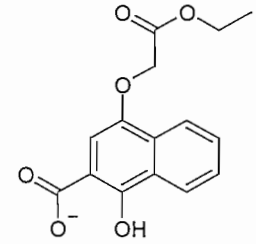

CS4566
(4-(ethoxycarbonylmethoxy)-1-hydroxy-2-naphthoic acid) (**16**)

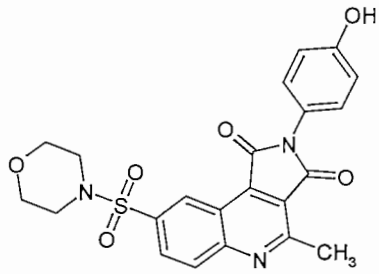

Quinoline derivative (**17**)

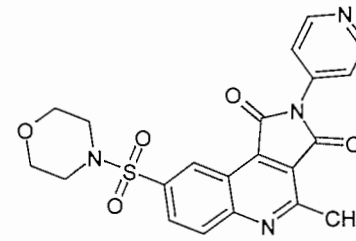

Quinoline derivative (**18**)

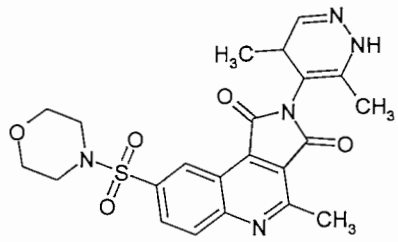

Quinoline derivative (**19**)

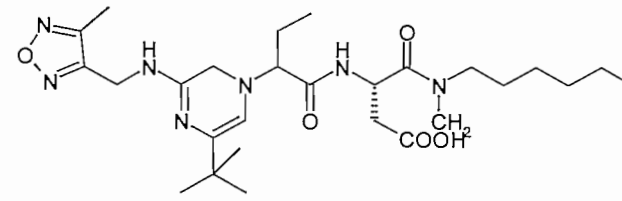

M826 (pyrazinone mono-amide) (**20**)

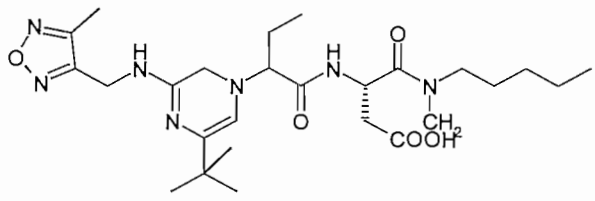

M827 (pyrazinone mono-amide) (**21**)

Figure 2.14: Caspase 3 inhibitors (Concha & Abdel-Meguid, 2002; Sakai *et al.*, 2008; Kravchenco *et al.*, 2005; Han *et al.*, 2005).

The active site of caspase 3 is located at the edge of the β-sheet and is formed by residues from the p10 and p20 subunit. In most cases, peptide inhibitors interact with the S1-S4 subsites while non-peptide inhibitors do not interact with all four sites. Inhibitory activity is however observed when the inhibitor interacts with only one subunit (Concha & Abdel-Meguid, 2002).

Concha and Abdel-Meguid (2002) reported, from x-ray diffraction studies with the isatin sulfonamide (**15**, figure 2.14), that the 5-member pyrrolidine ring fits into the S2 binding pocket (figure 2.15). The sulfur atom of Cys279 is covalently linked to the C3 atom of the isatin and the carbonyl oxygen of the isatin occupies the "oxyanion hole" interacting with the main chain atoms of Gly238 and Cys279. The phenoxy ring interacts with the guanidinium group of Arg341 and the sulfonyl oxygens interact with Ser339 and Arg341 (Concha & Abdel-Meguid, 2002).

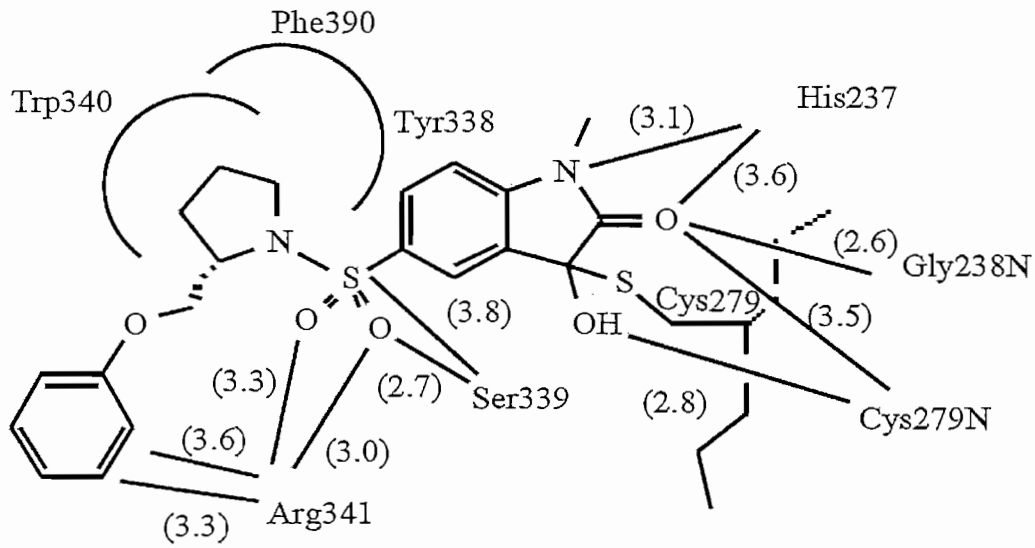

Figure 2.15: Interaction between caspase 3 and the isatin sulfonamide (**15**) (Concha & Abdel-Meguid, 2002). Curved lines indicate hydrophobic interactions and broken lines indicate polar interactions with the interatomic distances in parenthesis (Concha & Abdel-Meguid, 2002).

As seen in a docking simulation of caspase 3 and compound **16** (figure 2.16), there is an important hydrophobic interaction between the ester group and the S_2 subsite of caspase 3 as well as five hydrogen bonds (figure 2.16). The anti-apoptotic effect of **16** is not very promising, possibly due to low cell membrane permeability but could be addressed by esterification of the carboxyl group (Sakai *et al.*, 2008).

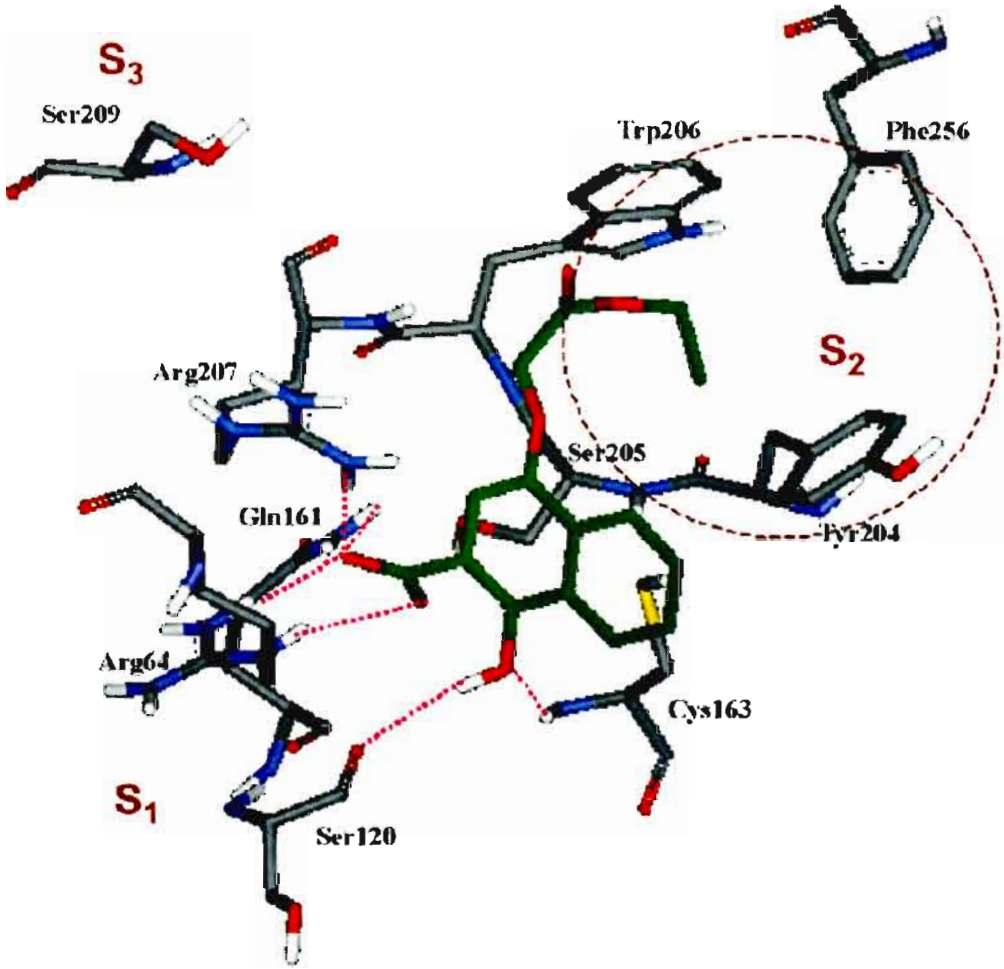

Figure 2.16: Binding mode of compound **16** (illustrated in green) to caspase 3 (Sakai *et al.*, 2008). Nitrogen, oxygen and carbon atoms are illustrated in blue, red and grey, respectively. The pink dashed lines indicate hydrogen bonds and the red dashed circle indicates a hydrophobic interaction. S1, S2 and S3 indicate binding pockets of the active site of caspase 3 (Sakai *et al.*, 2008).

The IC_{50} values of the quinoline derivatives (**17-19**, figure 2.14) are 8 nM, 3 nM and 3 nM respectively and the affinity for caspase 3 might be increased by noncovalent binding between the additional polar functional groups of the heterocyclic moieties of the inhibitor and the enzyme (Kravchenco *et al.*, 2005).

Both M826 and M827 (**20-21,** figure 2.14) exhibit IC_{50} values of 0.7 nM and show protection against cell death and specifically neuroprotection (Han *et al.*, 2005).

2.5.4 GSK3 inhibitors

Neuronal apoptosis can be induced by the over expression of GSK3 and small molecule inhibitors of GSK3 may potentially protect nerve cells from apoptosis (Cohen & Goedert, 2004). More specifically it has been shown that GSK3 can increase Aβ and inhibiting GSK3 would thus decrease Aβ (Cohen & Goedert, 2004). GSK3 also has the ability to hyperphosphorylate tau (Wagman *et al.*, 2004). GSK3 inhibitors further show potential in the development of a treatment for diabetes type II due to their ability to mimic the insulin induced conversion of glucose to glycogen, consequently overcoming the resistance to insulin (Cohen & Goedert, 2004).

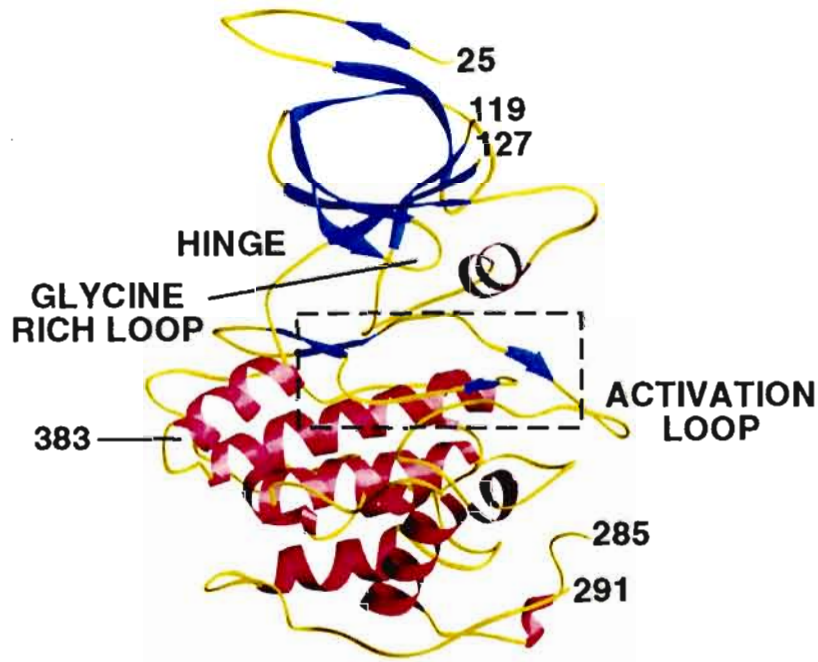

Figure 2.17: Crystal structure of GSK3 (Ter Haar *et al.*, 2001). The N-terminal domain (blue) corresponds to the β-strand domain and exists of residues 25–138. The α-helical domain (magenta) exists of residues 139–349. The hinge, glycine-rich loop and activation loop are indicated and are key features of the kinase fold (Ter Haar *et al.*, 2001).

GSK3 consists of an N-terminal β-sheet lobe and a C-terminal α-helical domain (figure 2.17). The active site is situated between the two domains and measures approximately 22 Å by 13 Å by 15 Å (Wagman *et al.*, 2004).

GSK3 inhibitory activity has been seen in six classes of compounds: hymenialdisine, paullones, indirubines, maleimides, muscarinic agonists and thiadiazolidinones (figure 2.18) (Chin *et al.*, 2005).

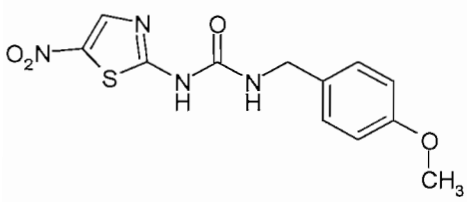

AR A014418 (**22**)

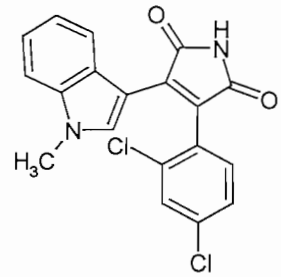

SB 216763 (**23**)

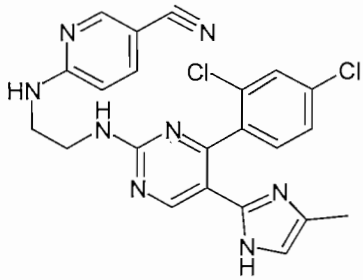

CHIR 99021 (**24**)

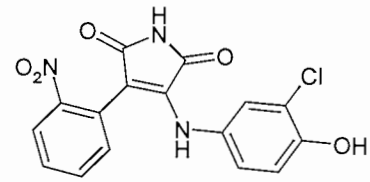

SB 415286 (**25**)

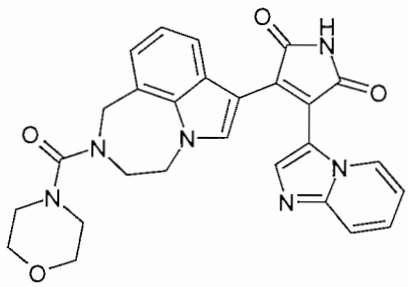

Maleimide derivative (**26**)

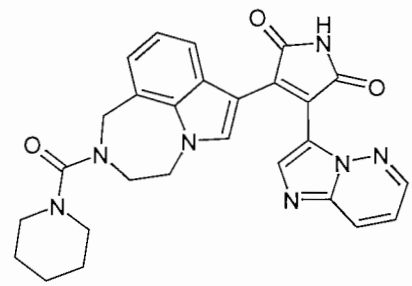

Maleimide derivative (**27**)

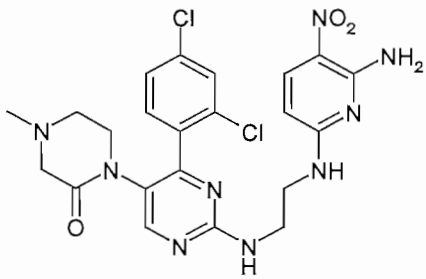

CT 20026 (**28**)

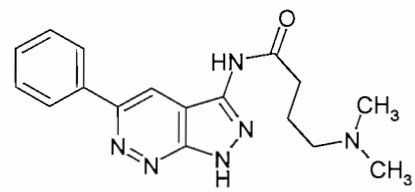

Pyridazine derivative (**29**)

Figure 2.18: GSK3 inhibitors (Cohen & Goedert, 2004; Chin *et al.*, 2005; Engler *et al.*, 2005; Wagman *et al.*, 2004).

Compound **22** (figure 2.18) has been shown to reduce the phosphorylation of tau (Cohen & Goedert, 2004) and compound **23** (figure 2.18) to protect cells against apoptotic cell death (Cohen & Goedert, 2004; Gurwitz & Eldar-Finkelman, 2001) with an IC_{50} value of 34 nM (Wagman *et al.*, 2004). Compound **24** (figure 2.18) promotes the activation of glycogen synthase and stimulates the deposit of glycogen in the liver, lowers glucose and insulin levels, lowers fasting levels of blood glucose and can ultimately be effective in the treatment of type 2 diabetes (Cohen & Goedert, 2004). Compound **25** (figure 2.18) was shown to prevent neuronal cell death (Chin *et al.*, 2005) in both the central and peripheral nervous system and the IC_{50} value is 78 nM (Wagman *et al.*, 2004).

Compounds **26** and **27** (figure 2.18) are maleimide derivatives that inhibit tau phosphorylation, lower plasma glucose and have the potential to treat diabetes and AD (Engler *et al.*, 2005). The IC_{50} of compound **26** for GSK3 inhibition is 1.3 nM and for tau phosphorylation it is 2.6 nM. The IC_{50} for compound **27** for GSK3 inhibition is 0.7 nM and for tau phosphorylation it is 0.3 nM (Engler *et al.*, 2005). Compound **28** (figure 2.18) has an IC_{50} of 4 nM for GSK3 inhibition and can reduce glucose levels in rats and compound **29** (Figure 2.18) has an IC_{50} value of 22 nM for GSK3 inhibition (Wagman *et al.*, 2004).

2.6 Conclusion

Inhibition of specific enzymes, such as CDK5/p25, caspase, calpain and GSK3, can potentially reduce the neuronal cell death observed in neurodegenerative diseases and therefore be of value in the management of diseases such as AD and PD (Concha & Abdel-Meguid, 2002). CDK5/p25 inhibitors have the potential to prevent Aβ phosphorylation and Aβ-induced cytotoxicity, thus presenting opportunities for drug design for the treatment of AD (Knockaert *et al.*, 2002). Several GSK3 inhibitors that protect cultured neurons from apoptotic cell death have been patented and show promise in neuroprotection (Gurwitz & Eldar-Finkelman, 2001). Calpain inhibitors have also been shown to be effective in the reduction of apoptosis (Koh *et al.*, 2006), specifically in neurodegenerative diseases (Ray *et al.*, 2000). Inhibition of caspase activity was shown to prevent cell death and preserve neurological function (Concha & Abdel-Meguid, 2002).

It is therefore clear that exciting opportunities exist for the design and development of drugs that act as inhibitors of the enzymes implicated in neurodegeneration via various apoptotic cascades in diseases such as AD, PD, ALS and HD.

3 Molecular Modelling

3.1 Introduction

The most prominent advantage of using computerised molecular modelling methods is reduction in cost. This is due to the fact that only the most promising compounds are evaluated experimentally. Databases can thus be screened for promising compounds at a rate and cost not achievable when utilising only biological assays (Langer & Wolber, 2004). A schematic representation of the process that was followed in this study is shown in figure 3.1.

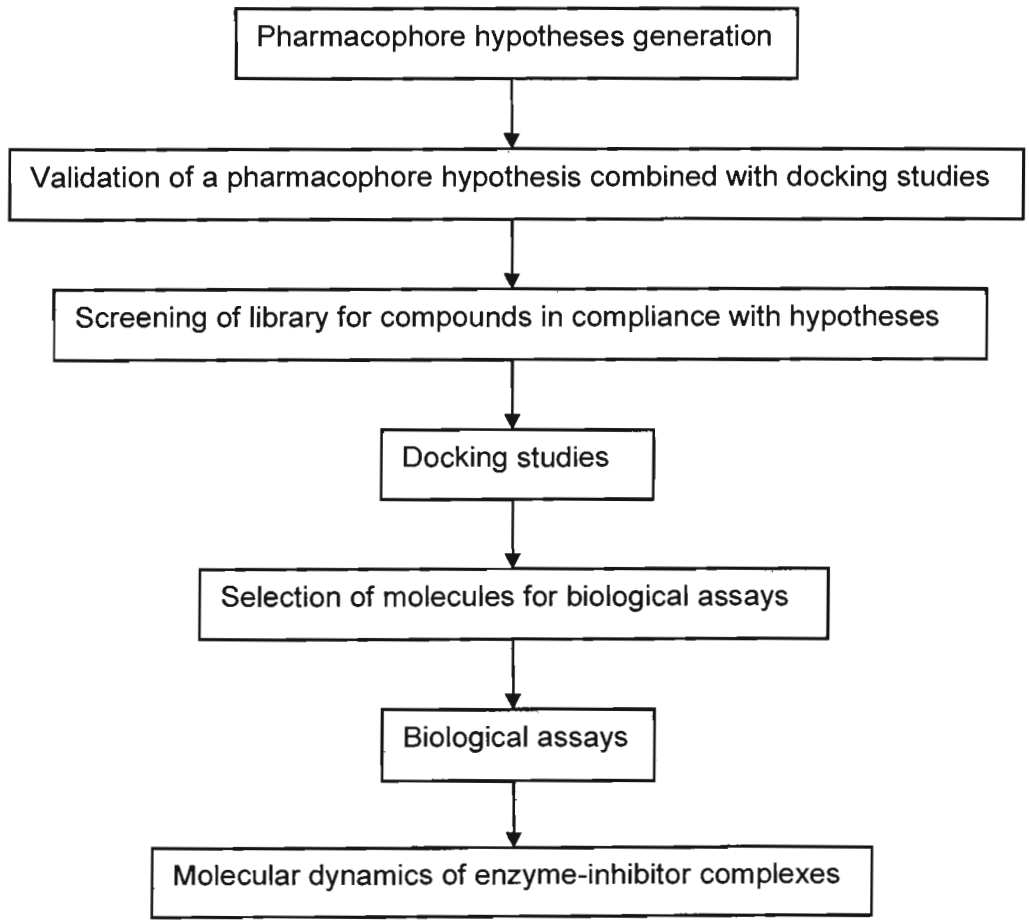

Figure 3.1: Scheme of the process that was followed in this study.

3.2 Pharmacophore hypotheses generation

3.2.1 Background

A pharmacophore hypothesis is a combination of electrostatic and steric features of different compounds which are critical to ensure optimum supramolecular interactions with a specific enzyme or receptor (Langer & Wolber, 2004). When using pharmacophore hypotheses to screen databases, the rate of identifying active compounds through *in vitro* testing of the most promising compounds, is higher than in cases where only *in vitro* testing is utilised (Chang *et al.*, 2006).

3.2.2 Method

Pharmacophore queries (hypotheses) were generated for CDK5/p25, calpain, caspase 3 and GSK3β in the Molecular Operating Environment MOE (Chemical Computing Group, http://www.chemcomp.com/) version 2007.09 using the pharmacophore elucidation function. A stochastic search process was selected to perform the hypothesis generation. The query cluster and query spacing parameters were altered for each hypothesis generation to obtain the optimal setting for each of the enzymes. The hypotheses could contain a combination of the following hypothesis points: Aromatic regions, hydrophobic regions, areas where hydrogen bond donors can possibly be, areas where hydrogen bond acceptors can possibly be, cations and anions. For the remaining parameters, the default settings were used.

For each of these enzymes, the most potent inhibitors described in the literature were carefully selected for the training set. Structural diversity was considered in the selection process, ensuring inclusion of a variety of chemical structures in the training sets. The use of identical biological assays to determine the biological activities of all the inhibitors included in a specific training set was a further prerequisite. Different energy minimised conformations were generated for the structures in the training sets utilising the conformation import function of MOE. Default values were used for all the parameters and the obtained conformers were used to generate the hypotheses.

Potent inhibitors as well as weak inhibitors were used to validate the hypotheses. These potent inhibitors differ structurally from the inhibitors in the training sets, except for GSK3β where some of the chemical classes overlapped. The weak inhibitors were in some cases structurally similar to the inhibitors used in the training set. Various conformations for the compounds used were also generated using the conformation import function of MOE. These conformers were then used to validate the hypotheses. This was performed using the pharmacophore search function of the pharmacophore query editor of MOE. Default values were once again used for all the parameters. Hypothesis hits were defined as compounds

that comply with the requirements of a specific hypothesis. The potent inhibitors had to be hits and the weak inhibitors non-hits for the hypotheses to be validated.

The hypotheses were then refined slightly to ensure that only the potent inhibitors were identified as hypothesis hits.

3.2.3 Compounds used to generate hypotheses

The CDK5/p25 training set consisted of triazolyl-thienyl derivates (Shiradkar *et al.*, 2007), triazolyl thiazole derivatives (Shiradkar *et al.*, 2007) and 2-aminothiazole derivatives (Helal *et al.*, 2004). The complete training set can be found in table 1 of the appendix.

Compounds **xi**, **xiii**, **xiv**, **xvi**, **xvii**, **xix**, **xxiii**, **xxiv**, **xxv** and **xxviii** of table 1 of the appendix are triazolyl-thienyl derivatives. Compounds **xii**, **xv**, **xx** and **xxvi** are triazolyl thiazole derivates. The remaining compounds are 2-aminothiazole derivatives. Examples of these inhibitors are depicted in figure 3.2.

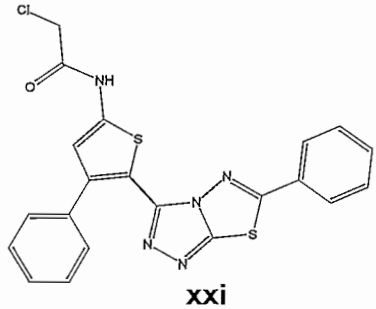

xxi

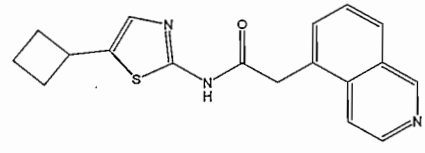

vi

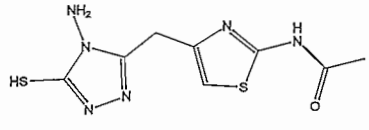

xxvi

Figure 3.2: Compounds **xxi**, **vi** and **xxvi** of table 1 of the appendix.

Chemical structures for the calpain training set included 1,2-benzothiazine 1,1-dioxide α-ketoamide analogues (Bihovsky *et al.*, 2004), 6-hydroxy-3-morpholinones (Nakamura *et al.*, 2003), peptide α-ketohydroxamates (Josef *et al.*, 2001), proline derivatives (Tripathy *et al.*, 1998) and peptidomimetic aldehydes (Wells *et al.*, 2001). The training set is listed in table 3 of the appendix.

Compound **xvii** of table 3 of the appendix can be classified as an α-ketoamide analogue and compound **xx** as a 6-hydroxy-3-morpholinone. Compounds **iii**, **v**, **vi**, **xxiv** and **xxv** are proline derivatives and compounds **xi** – **xvi** and **xxi** are peptidomimetic aldehydes. The remaining

compounds in table 3 of the appendix are peptide α-ketohydroxamates. Examples of these inhibitors are depicted in figure 3.3.

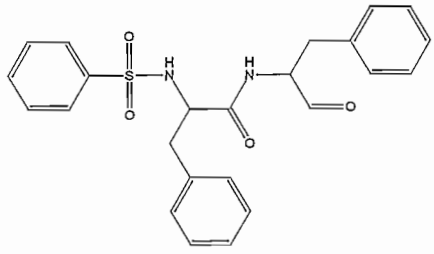

xvii

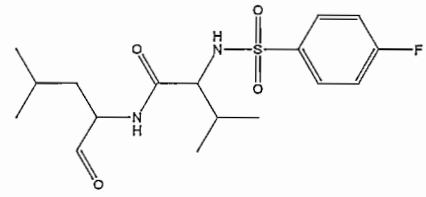

xx

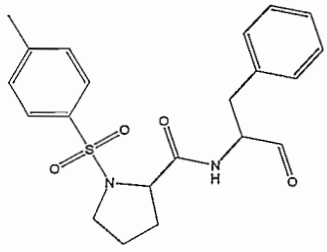

vi

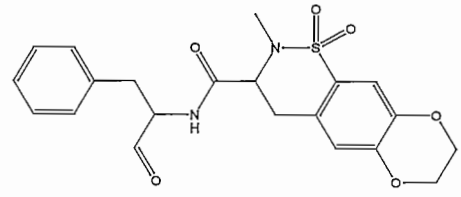

xxii

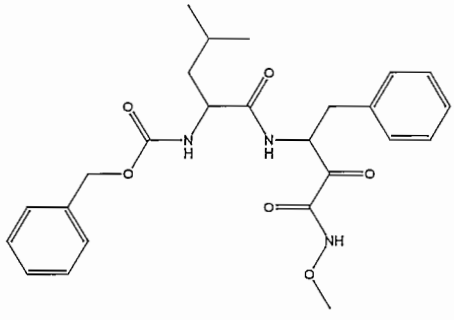

ii

Figure 3.3: Compounds **xvii**, **xx**, **vi**, **xxii** and **ii** of table 3 of the appendix.

The chemical structures for the caspase 3 training set consisted of quinoline derivatives (compounds **i**, **iv-vi**, **ix**, **xiii**, **xiv**, **xvi-xviii** and **xx-xxv**) (Kravchenko *et al.*, 2005; Kravchenko *et al.*; 2006; Chen *et al.*, 2006) and sulfonamide analogues (remaining compounds of table 5 of the appendix) (Chu *et al.*, 2005). The complete training set is listed in table 5 of the appendix and examples of these inhibitors are depicted in figure 3.4.

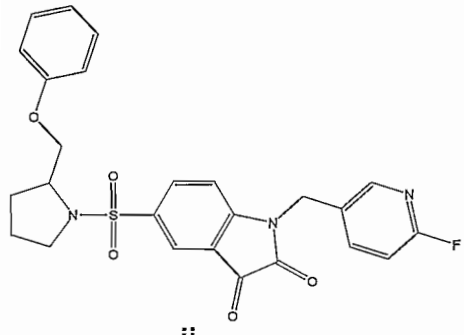

ii

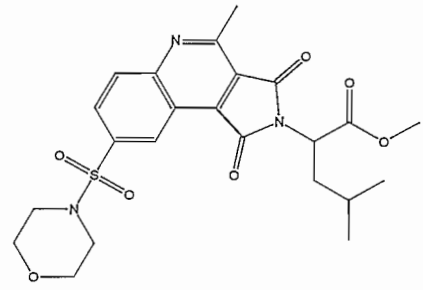

v

Figure 3.4: Compounds **ii** and **v** of table 5 of the appendix.

The GSK3β training set included pyridine analogues (Witherington *et al.*[a,b,c], 2003), indirubin derivatives (Meijer *et al.*, 2003), maleimide derivatives (Smith *et al.*, 2001, Coghlan *et al.*, 2000) and hydrazide derivatives (Olesen *et al.*, 2003). The complete training set is given in table 7 of the appendix.

Compounds **i – vi**, **viii – xxiii**, **xxv**, **xxvi**, **xxviii**, **xxxi – xxxvii**, **xl** and **xlii** of table 7 in the appendix are pyridine analogues, compound **vii** is an indirubin derivative and compounds **xxiv**, **xxvii**, **xxix**, **xxx**, **xxxviii**, **xxxix** and **xli** are maleimide derivatives. Compounds **xliii** and **xliv** are hydrazide derivatives. Examples of these inhibitors are depicted in figure 3.5.

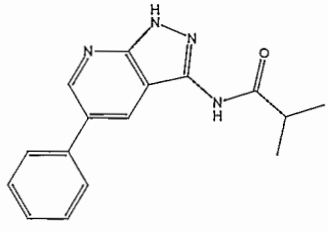

xxii

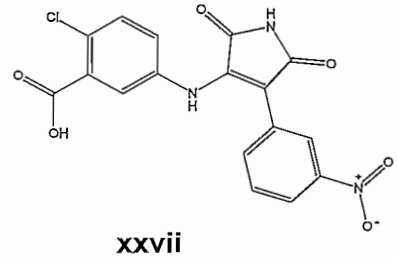

xxvii

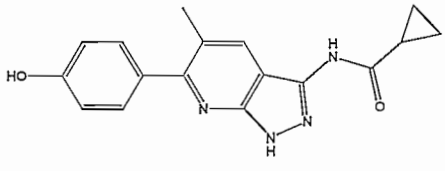

vii

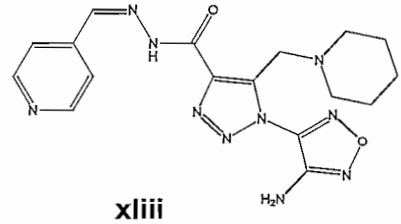

xliii

Figure 3.5: Compound **xxii**, **vii**, **xxvii** and **xliii** of table 7 of the appendix.

3.2.4 Compounds used to validate hypotheses

For CDK5/p25, the validation database consisted of a quinazolin-2-one derivative (Rzasa *et al.*, 2007), quinolin-2(1*H*)-one derivatives (Zhong *et al.*, 2007), triazolyl-thienyl derivates (Shiradkar *et al.*, 2007) and 2-aminothiazoles (Helal *et al.*, 2004). The complete list of compounds used to validate the hypothesis is included in table 2 of the appendix. Examples of the compounds are shown in figure 3.6.

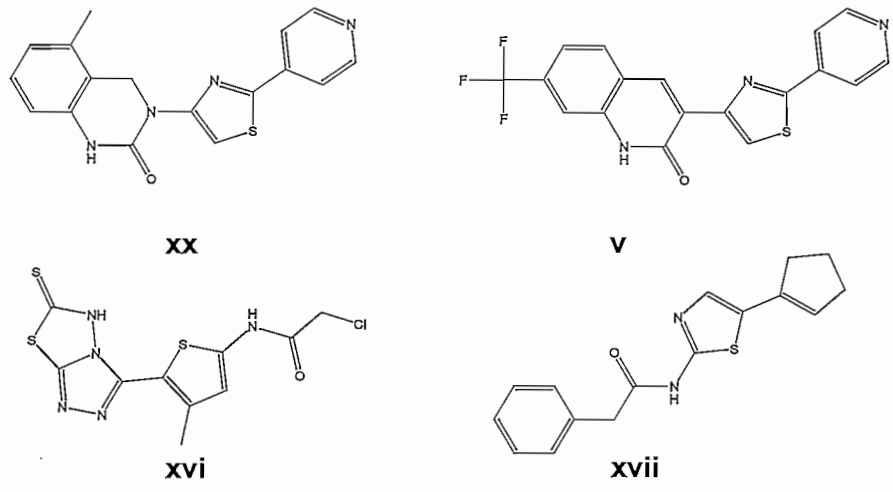

Figure 3.6: Compounds **xx**, **v**, **xxvi** and **xxvii** of table 2 of the appendix. Compound **xx** is an example of a quinazolin-2-one derivative, compound **v** is a quinolin-2(1*H*)-one derivative, compound **xvi** a triazolyl-thienyl derivate and compound **xvii** is an 2-aminothiazole derivative.

The validation database for calpain consisted of α-keto-amide derivatives (Lescop *et al.*, 2005), peptide-biphenyl hybrids (Montero *et al.*, 2004), peptidyl hydrazones (Nakamura & Inoue, 2002), 6-pyridone 2-carboxamide (Lee *et al.*, 2008), 4-quinolonone 2-carboxamides (Nam *et al.*, 2008), 1,2-benzothiazine 1,1-dioxide α-ketoamide analogues (Bihovsky *et al.*, 2004), 6-hydroxy-3-morpholinones (Nakamura *et al.*, 2003), peptidomimetic aldehyde derivatives (Wells *et al.*, 2001) and chromone carboxamides (Lee *et al.*, 2005). The complete list of compounds is depicted in table 4 of the appendix. Examples of the compounds are shown in figure 3.7.

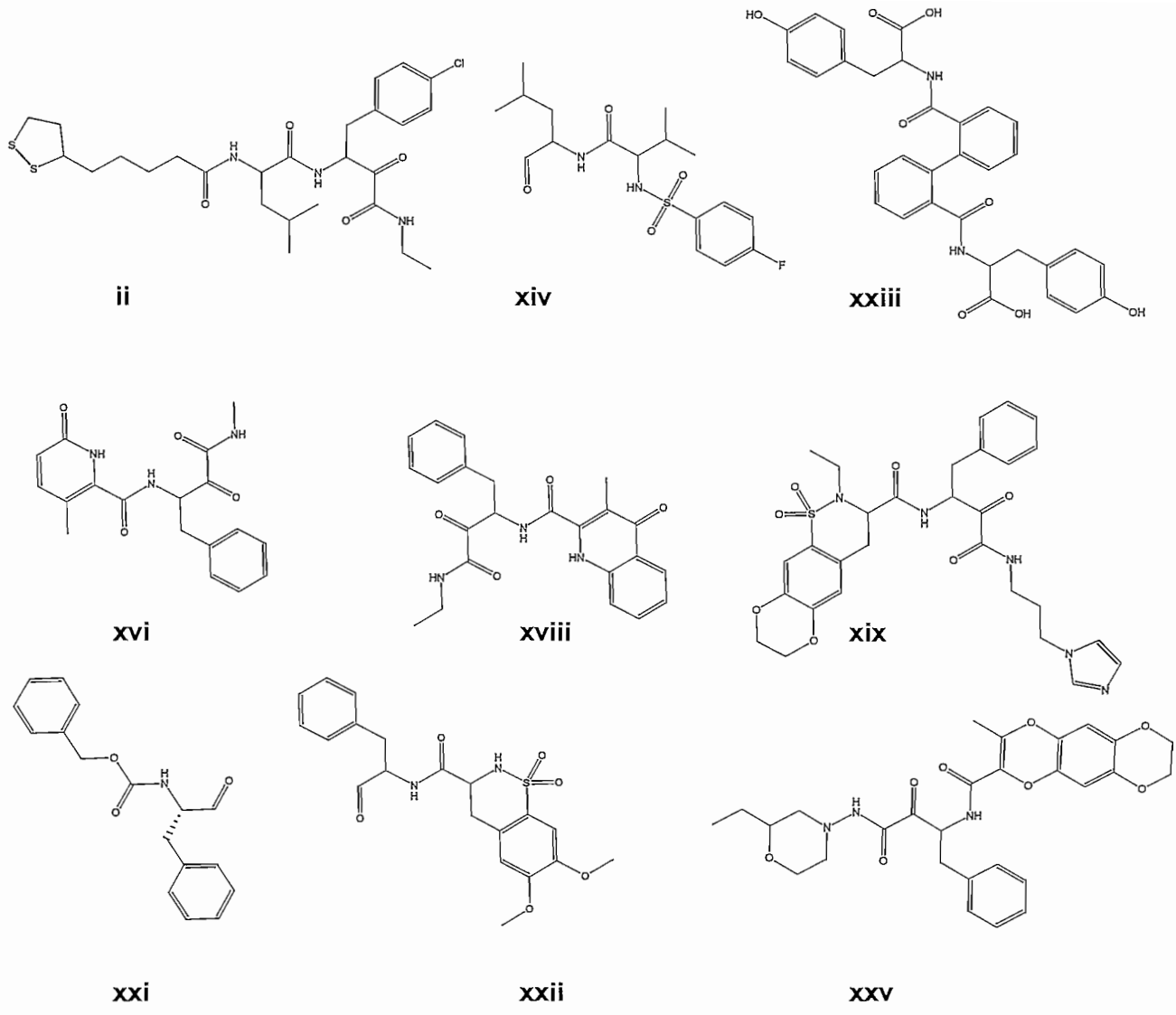

Figure 3.7: Compounds **ii**, **xiv**, **xxiii**, **xvi**, **xviii**, **xix**, **xxi**, **xxii** and **xxv** of table 4 of the appendix. Compound **ii** is an α-ketoamide derivative and compound **xxiii** is a peptide-biphenyl hybrid. Compound **xiv** is a peptidyl hydrazone and compound **xvi** is a 6-pyridone 2-carboxamide. Compound **xviii** is a 4-quinolonone 2-carboxamide and compound **xix** is a 1,2-benzothiazine 1,1-dioxide α-ketoamide analogue. Compound **xxi** is a 6-hydroxy-3-morpholinone and compound **xxii** is a peptidomimetic aldehyde. Compound **xxv** is a chromone carboxamide.

Different chemical classes of inhibitors were also included in the validation database for caspase 3. It consisted of pyrazinone mono-amides (Han *et al.*, 2005), 3-bromopyrazinones (Isabel *et al.*, 2007), tetrapeptide aspartic acid ketone derivatives (Grimm *at al.*, 2004), aspartyl ketone dipeptides (Han *et al.*, 2004), valine aspartyl ketones (Mellon *et al.*, 2005), *N*-benzylisatin sulfonamides (Chu *et al.*, 2005), quinoline derivatives (Kravchenko *et al.*[a,b],

2005) and isoquinoline-1,3,4-trione derivatives (Chen *et al.*, 2006). The compounds are listed in table 6 of the appendix.

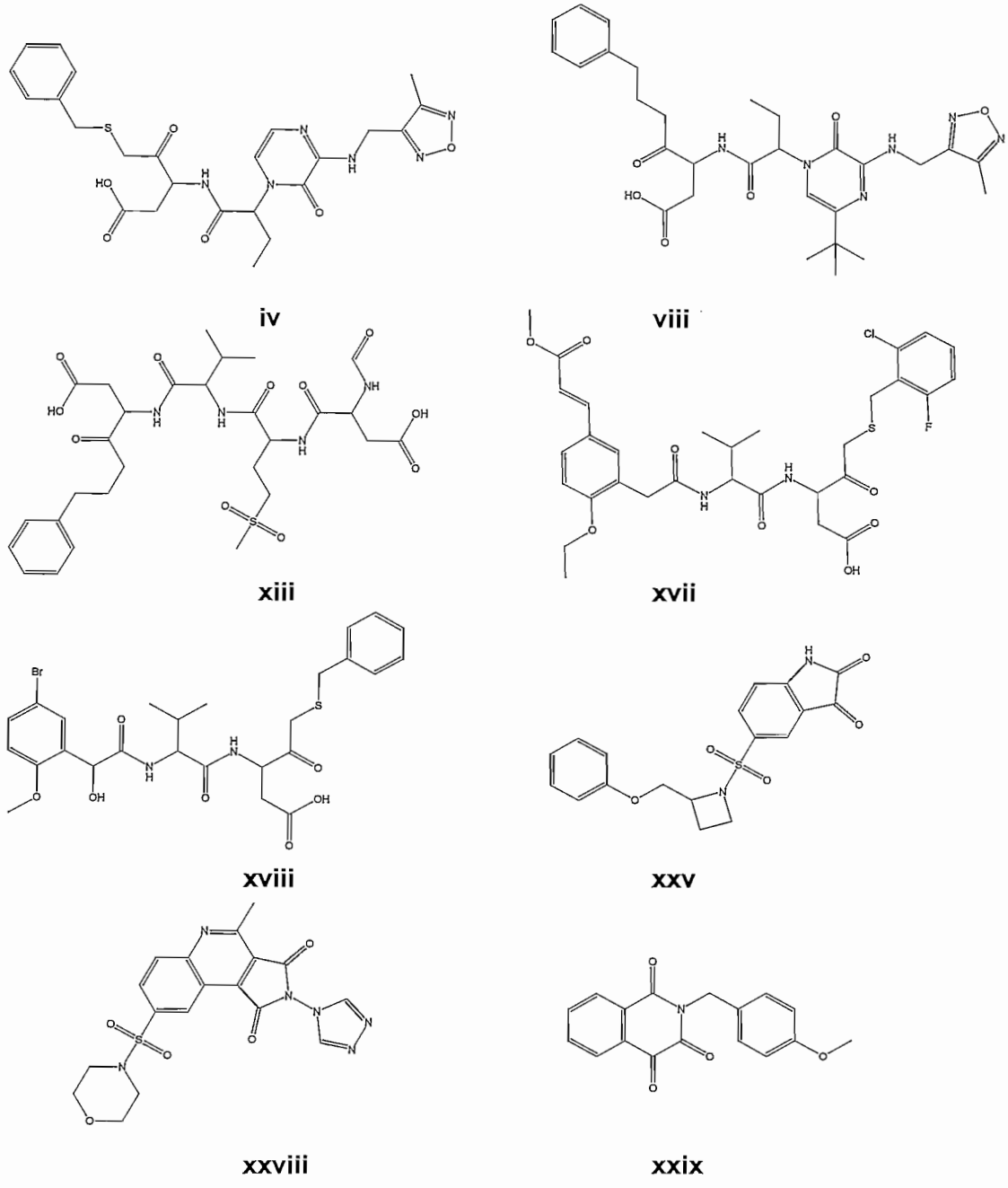

Figure 3.8: Compounds **iv**, **viii**, **xiii**, **xvii**, **xviii**, **xxv**, **xxviii** and **xxix** of table 6 of the appendix. Compound **iv** is a pyrazinone mono-amide and compound **viii** is a 3-bromopyrazinones. Compound **xiii** is a tetrapeptide aspartic acid ketone derivative and compound **xvii** is an aspartyl ketone dipeptide. Compound **xviii** is a valine aspartyl ketone and compound **xxv** is a *N*-benzylisatin sulfonamide. Compound **xxviii** is a quinoline derivative and compound **xxix** is an isoquinoline-1,3,4-trione derivative.

The validation database for GSK3β consisted of pyridazine derivatives (Witherington *et al.*, 2003, Patel & Bharatam, 2008), indirubin derivatives (Meijer *et al.*, 2003), maleimide derivatives (Engler e*t al.*, 2005), pyrrole-2,5-diones (Engler *et al.*, 2005), pyridine derivatives (Witherington *et al.*, 2003), triazole derivatives (Olesen *et al.*, 2003), thiadiazolidinones (Martinez *et al.*, 2002, Castro *et al.*, 2008) and a thiazolidine derivative (Kim *et al.*, 2008). The complete list of compounds used to validate this hypothesis can be located in table 8 of the appendix. Examples of the compounds are shown in figure 3.9.

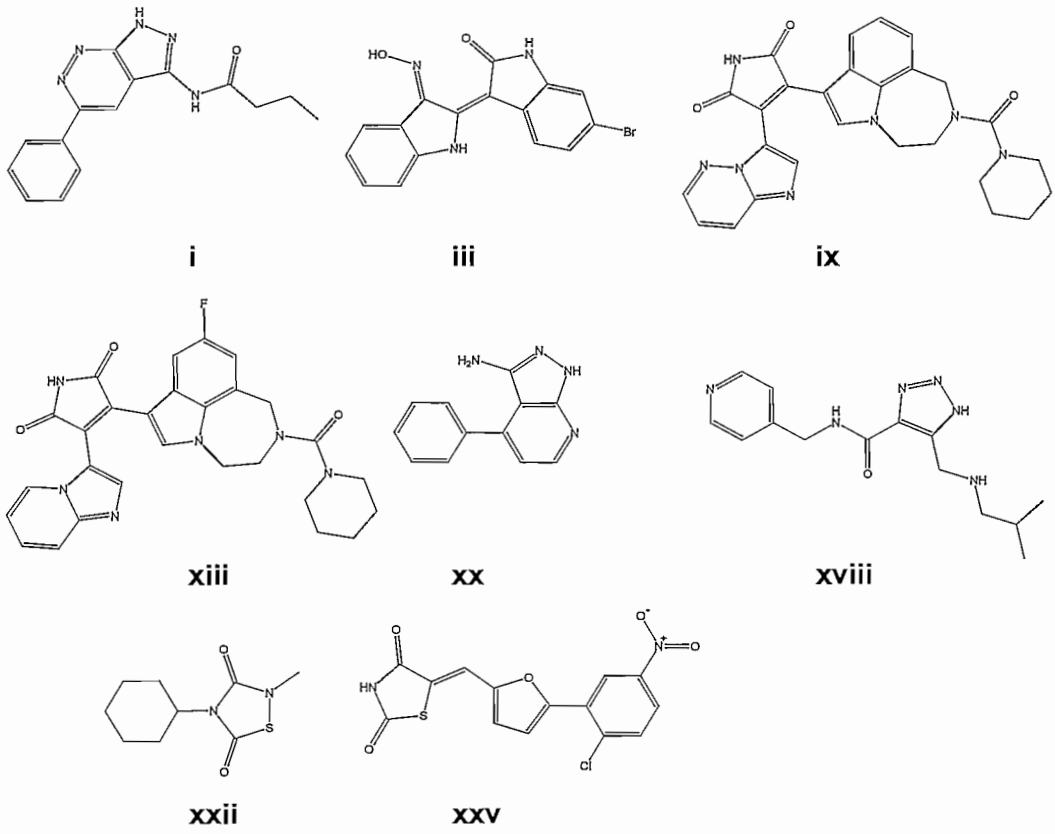

Figure 3.9: Compounds **i**, **iii**, **ix**, **xiii**, **xx**, **xviii**, **xxii** and **xxv** of table 8 of the appendix. Compound **i** is an example of a pyridazine derivative; compound **iii** is an example of an indirubin derivative; compound **ix** is an example of a maleimide derivative; compound **xiii** is an example of a pyrrole-2,5-dione; compound **xx** is an example of a pyridine derivative; compound **xviii** is an example of a triazole derivative; compound **xxii** is an example of a thiadiazolidinone and compound **xxv** is an example of a thiazolidine derivative.

3.2.5 Results and discussion

3.2.5.1 CDK5/p25

The pharmacophore hypothesis generated for CDK5/p25 contains an aromatic area (F1), two hydrophobic areas (F2 and F3), locations of potential H-bond donors (F4) and an aromatic area (F5). F5 has a radius of 2.3 Å and the remaining areas have radii of 1.4 Å, as shown in figure 3.10.

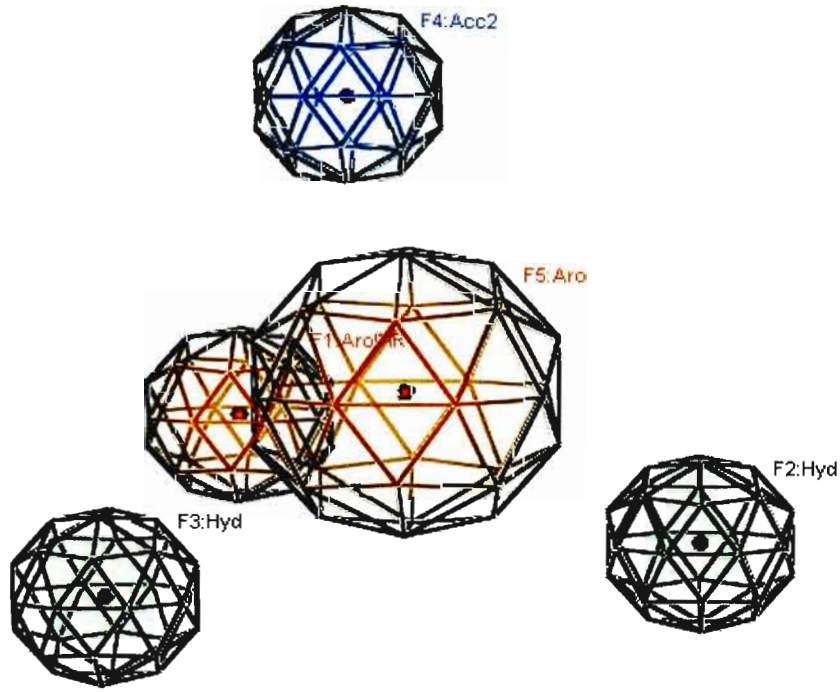

Figure 3.10: CDK5/p25 pharmacophore hypothesis. Acc2 annotates projected locations of potential H-bond donors, Aro annotates centroids used for aromatic and pseudo aromatic rings, PiR annotates centroids used for other π-system rings and Hyd annotates hydrophobic centroids.

From the CDK5/p25 pharmacophore hypothesis it can be deduced that compounds that comply with the pharmacophore hypothesis will consist of an aromatic ring system and have the ability to form hydrogen bonds with CDK5/p25.

In figure 3.11, compound **v** of the validation database for CDK5/p25 is depicted in the CDK5/p25 pharmacophore hypothesis. Both aromatic areas (F1 and F5) of the hypothesis overlap with aromatic rings of compound **v**. F4 is in an area where a hydrogen bond donor can possibly be and either interacts with the lactam nitrogen or the carbonyl oxygen. F2 and F3 depict hydrophobic regions.

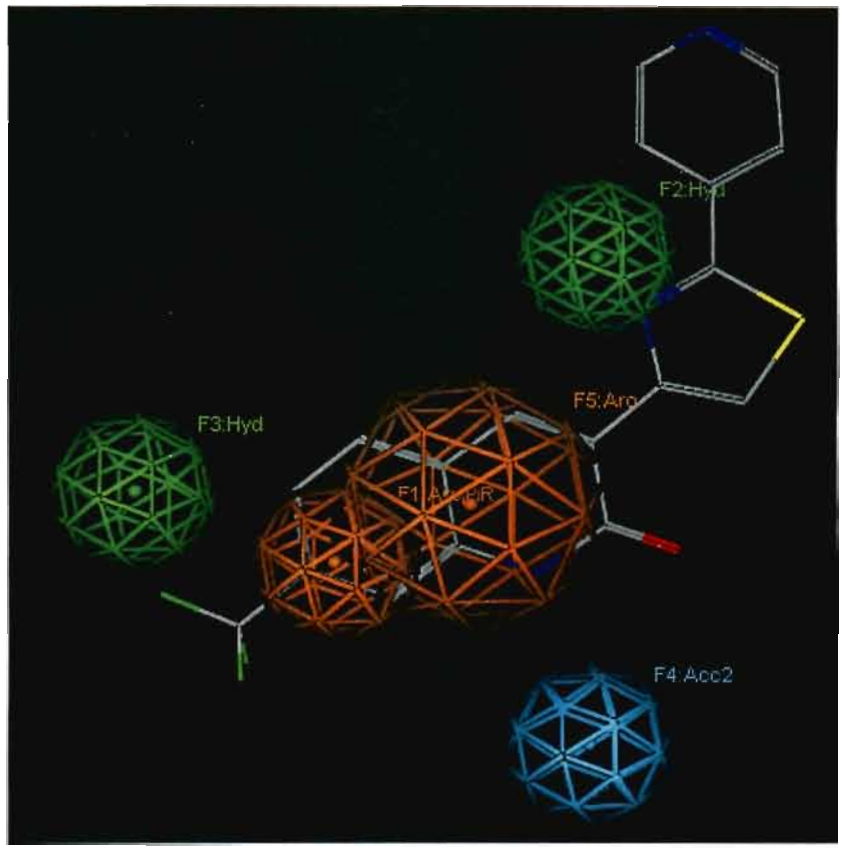

Figure 3.11: Compound **v** of the validation database for CDK5/p25 fitted in the CDK5/p25 pharmacophore hypothesis.

3.2.5.2 Calpain

The pharmacophore hypothesis generated for calpain contains three hydrophobic areas with 1.4 Å radii (F1, F2 and F5) and two locations of potential H-bond donors (F3 and F4) with radii of 1.0 Å, as shown in figure 3.12.

The pharmacophore hypothesis for calpain shows that compounds that comply with the hypothesis will be mainly hydrophobic molecules, with the ability to form hydrogen bonds with calpain.

In figure 3.13, compound **xii** of the training set for calpain is depicted in the calpain hypothesis. F3 is in an area where a hydrogen bond donor can possibly be and either interacts with the amide carbonyl oxygen or the amide nitrogen. F4 is also in an area where another hydrogen bond donor can possibly be and interact with the endocyclic ether oxygen. The hydrophobic areas (F1, F2 and F5) of the hypothesis correlate to the ring system of the compound.

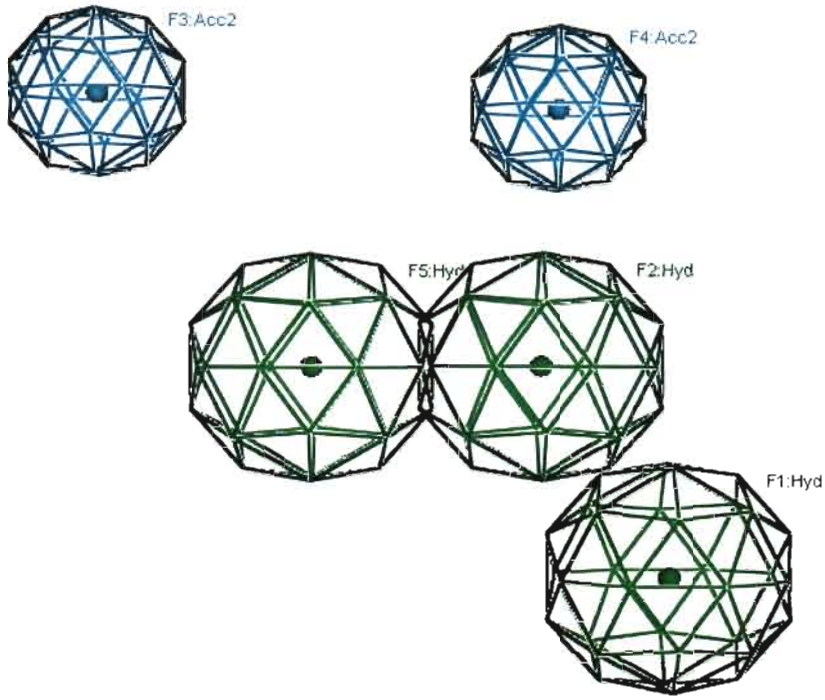

Figure 3.12: Calpain hypothesis.

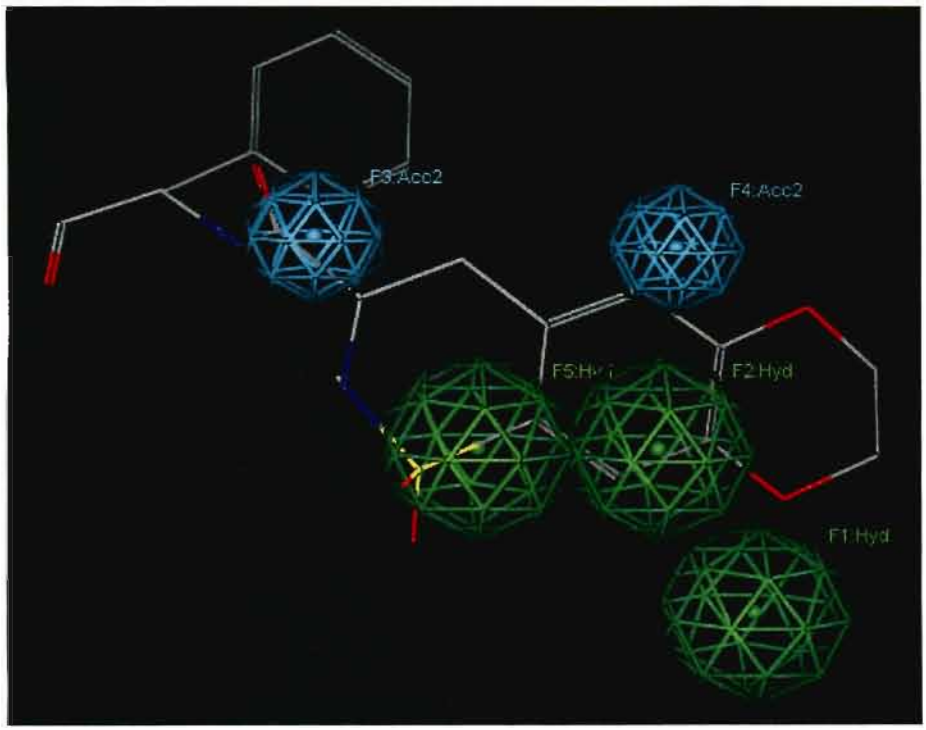

Figure 3.13: Compound **xii** of the training set for calpain fitted in the calpain hypothesis.

3.2.5.3 Caspase 3

The pharmacophore hypothesis generated for caspase 3 contains three hydrophobic areas with 1.4 Å radii (F1, F2 and F3) and three locations of potential H-bond donors (F4, F5 and F6) with radii of 1.0 Å, 2.0 Å and 1.4 Å respectively and is depicted in figure 3.14.

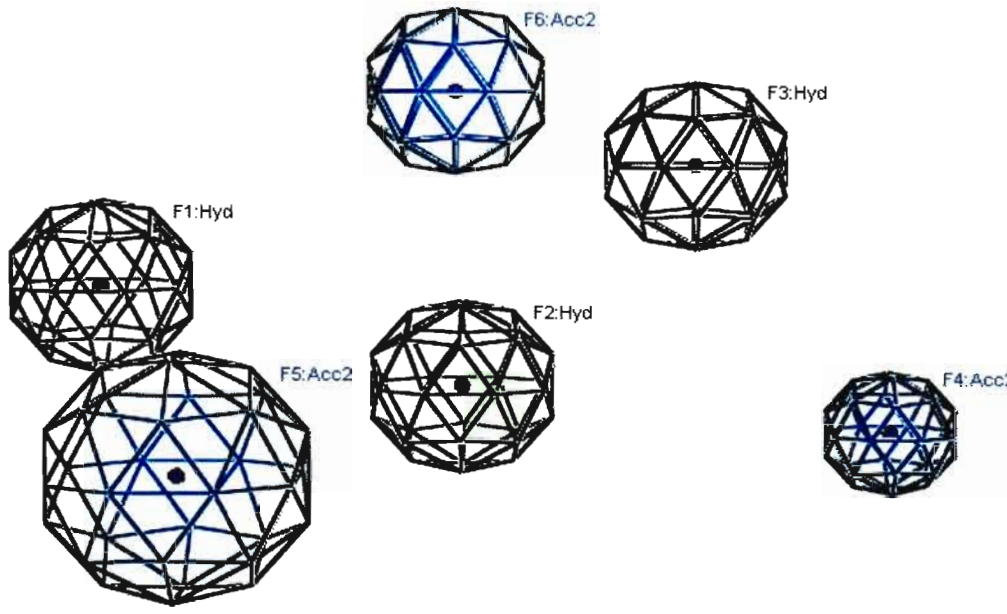

Figure 3.14: Caspase 3 hypothesis.

Compounds that comply with the caspase 3 pharmacophore hypothesis will predominantly consist of moieties that have the ability to form hydrogen bonds with caspase 3 as well as hydrophobic areas.

In figure 3.15, compound **ii** of the training set for caspase 3 is depicted in the caspase 3 hypothesis. F4 is in an area where a hydrogen bond donor can possibly be and interacts with the pyridine nitrogen. F5 and F6 are also areas where hydrogen bond donors can be expected. At F5, the hydrogen bond donor has the ability to interact with the ether oxygen and at F6 the hydrogen bond donor can interact with either one of the carbonyl oxygens of the isatin ring. F1, F2 and F3 depict hydrophobic regions.

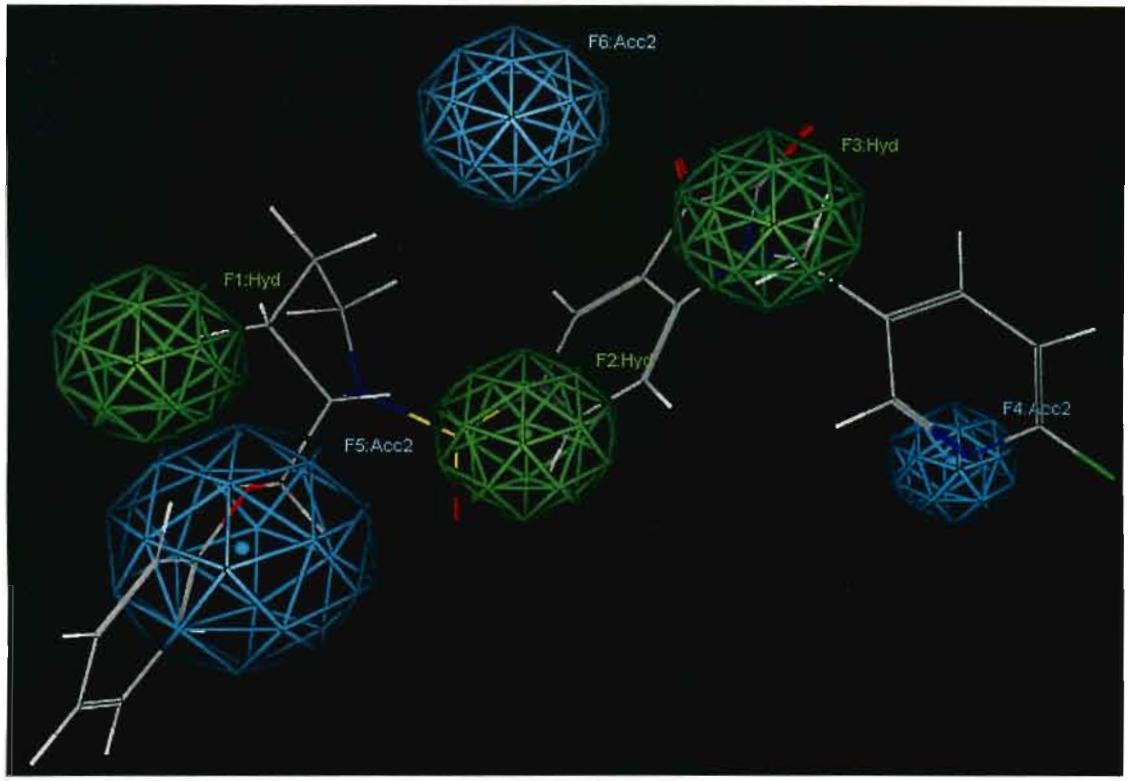

Figure 3.15: Compound **ii** of the training set for caspase 3 fitted in the caspase 3 hypothesis.

3.2.5.4 GSK3β

The pharmacophore hypothesis generated for GSK3β contains an aromatic area (F1), a hydrophobic area (F2), locations of potential H-bond acceptors (F3) and locations of potential H-bond donors (F4). All of the areas have radii of 1.1 Å as illustrated in figure 3.16.

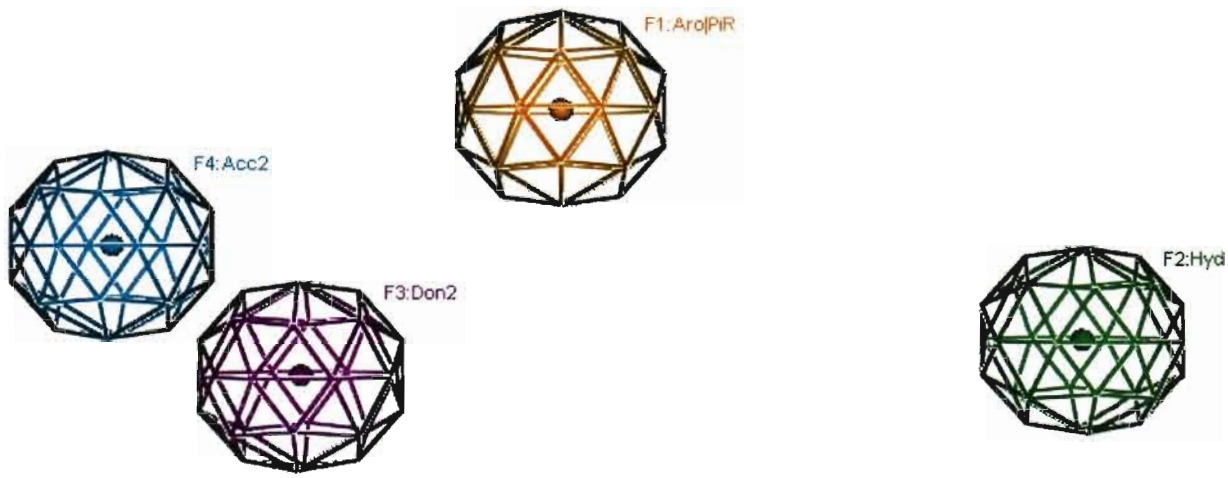

Figure 3.16: GSK3β hypothesis.

From the pharmacophore hypothesis it is clear that compounds that comply with the hypothesis will contain aromatic rings as well as other hydrophobic areas. The compounds will also have the ability to form hydrogen bonds with GSK3β.

In figure 3.17, compound **xxii** of the training set for GSK3β is depicted in the GSK3β hypothesis. The aromatic area (F1) of the hypothesis overlap with an aromatic ring of compound **xxii**. F2 depicts a hydrophobic region and F3 is the area where a hydrogen bond acceptor can possibly be found. F4 is in an area where a hydrogen bond donor can possibly be and interacts with a nitrogen atom adjacent to F4.

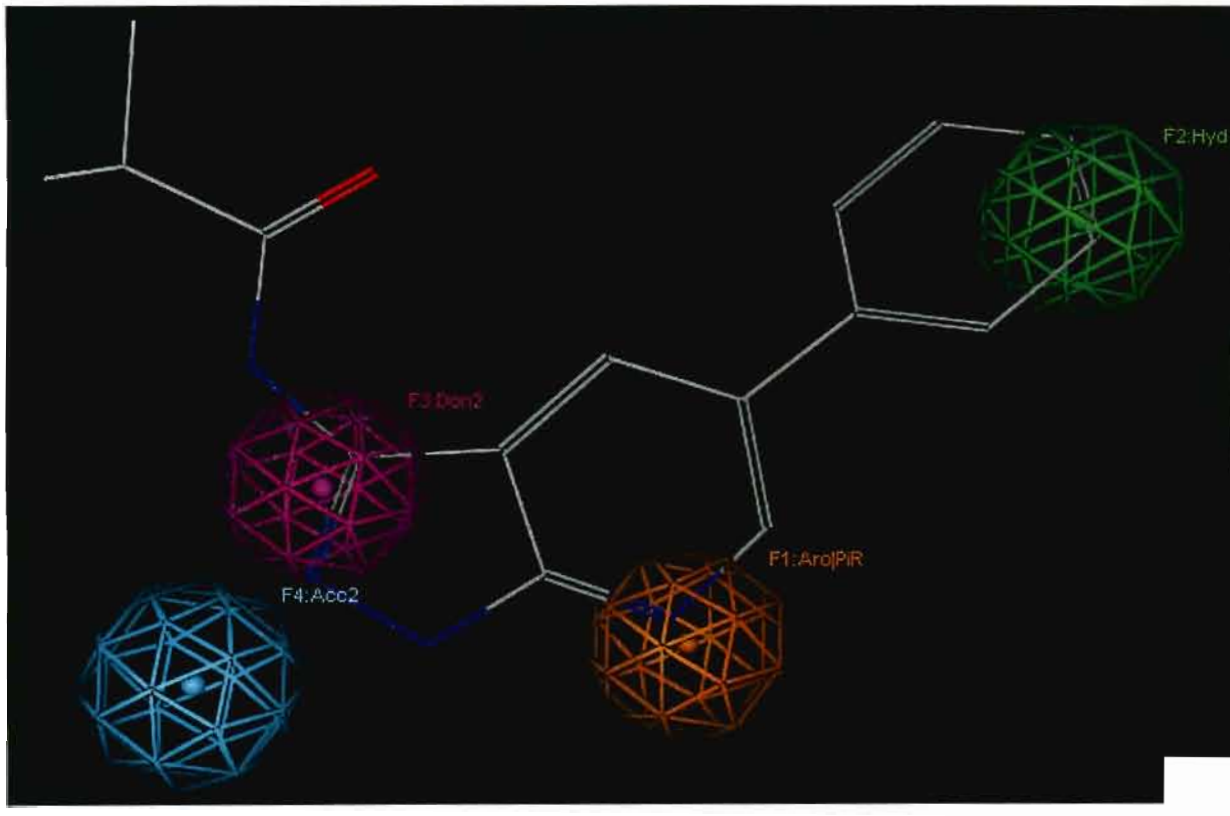

Figure 3.17: Compound **xxii** of the training set for GSK3β fitted on the GSK3β hypothesis.

3.2.6 Conclusion

The pharmacophore hypotheses that were generated for the respective enzymes gave some indication of the characteristics of the pharmacophore needed in a compound for it to have inhibitory potential for a specific enzyme. The pharmacophore hypotheses for CDK5/p25, calpain, caspase 3 and GSK3β all include features representing hydrogen bond donors and/or acceptors. This shows that hydrogen bond interactions are crucial for inhibitory activity for each of the enzymes. All four of the pharmacophore hypotheses include

hydrophobic regions. The pharmacophore hypotheses for both of the kinases, CDK5/p25 and GSK3β, also include aromatic areas.

The obtained hypotheses were validated using an alternative series of structures and were shown to effectively discriminate between active and inactive compounds. It was subsequently used to screen an in-house library to determine if any of the available compounds have potential as small molecule enzyme inhibitors. Compounds with geometric features that correspond to the pharmacophore hypotheses may however, still be inactive due to reasons not related to its geometry.

3.3 Validation of hypotheses and docking studies

3.3.1 Compounds used

To validate the pharmacophore hypotheses used in combination with docking studies, 5 potent inhibitors and 5 weak inhibitors were selected for calpain, caspase 3 and GSK3β respectively. For CDK5/p25, 3 inhibitors and 3 weak inhibitors were selected. These compounds differ from those used in the hypothesis generation. The list of compounds used for the validation process is depicted in table 15 – 18 of the appendix.

The calpain validation database (table 15 of the appendix) consisted of different structural classes. Compounds **i** and **ii** are 1-chloroisoquinolines (Chicharro *et al.*, 2008), compounds **iii** and **iv** are diketopiperazines (Zeng *et al.*, 2005), compound **v** is an aldehyde derivative (Chatterjee *et al.*, 1997), compounds **vi** and **vii** are amide derivatives (Zhang *et al.*, 2009), compound **viii** is a *N*-heterocyclic dipeptide aldehyde (Jones *et al.*, 2008) and compounds **ix** and **x** are peptide mimetic aldehyde derivatives (Wells *et al.*, 2001).

For caspase 3, compounds **i** – **iv** of table 16 of the appendix are peptidyl-aldehydes (Colantonio *et al.*, 2008), compounds **v** and **vi** are dipeptidyl benzoyloxymethyl ketones (Nedev *et al.*, 2005) and compounds **vii** – **x** are nicotinyl aspartyl ketones (Isabel *et al.*, 2003).

In the GSK3β validation database (table 17 of the appendix), compounds **i** and **ii** are azapurine derivatives (Lum *et al.*, 2008), compounds **iii** and **iv** are manzamine alkaloids (Hamann *et al.*, 2007), compounds **v** and **vi** are carboxamide derivatives (Koryakova *et al.*, 2007), compounds **vii** and **viii** are thiadiazolidinones (Martinez *et al.*, 2002) and compounds **ix** and **x** are maleimide derivatives (Kuo *et al.*, 2003).

For CDK5/p25, compounds **i – iii** of table 18 of the appendix are 4-acylamino-1,3-thiazoles (Larsen *et al.*, 2003) and compounds **iv – vi** are pyrazinone derivatives (Rochais *et al.*, 2009).

3.3.2 Molecular modelling method

To perform the validation process, the inhibitors mentioned above were used to validate the hypotheses for CDK5/p25, calpain, caspase 3 and GSK3β respectively. Various conformations for the compounds were generated using the conformation import function of MOE. These conformers were then used to validate the hypotheses. This was performed using the pharmacophore search function of the pharmacophore query editor of MOE. Default values were used for all the parameters. Hypothesis hits were defined as compounds that comply with the requirements of a specific hypothesis.

The compounds described above (paragraph 3.3.1) were also docked into the crystal structures for CDK5/p25, calpain, caspase 3 and GSK3β respectively, using the same methodology as described in paragraph 3.5.

The 'pharmocophore hypothesis in combination with docking studies' method has a 100% prediction potential if all the potent inhibitors are hypothesis hits and the weak inhibitors non hits. The potent inhibitors also need to have better (lower) or similar dock scores than the co-crystallised ligand and the weak inhibitors should have dock scores higher and not close to the dock score of the co-crystallised ligand. A prediction potential of 50% or less is of no value and a prediction potential of 80% or higher is considered useful.

3.3.3 Results

For calpain, only compound **viii** of table 15 (figure 3.18) of the appendix was a hypothesis hit with an IC_{50} value of 150 nM. When docking into the crystal structure of calpain, none of the compounds had a better dock score than the co-crystallised ligand. However, compounds **vi** and **x** had dock scores in close proximity to the dock score of the co-crystallised ligand.

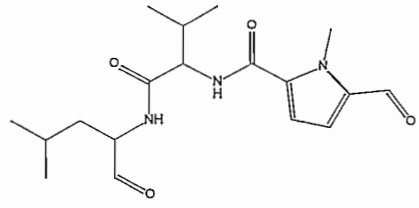

Figure 3.18: Compound **viii** of table 15 of the appendix was a calpain hypothesis hit.

Only compound **i** of table 16 of the appendix (figure 3.19) was a caspase 3 hypothesis hit, and the compound has an IC_{50} value of 3.5 nM. When docked into the crystal structure, none of the compounds had a better dock score than the co-crystallised ligand. However, compound **i**, which was also a hypothesis hit, had a dock score in the same region than the ligand.

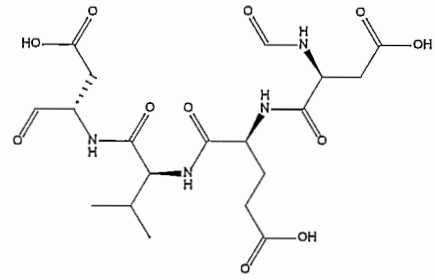

Figure 3.19: Compound **i** of table 16 of the appendix was a caspase 3 hypothesis hit.

Compounds **ix** and **x** of table 17 of the appendix (figure 3.20) were GSK3β hypothesis hits with IC_{50} values of 22 nM and 17 nM respectively. When docking into the crystal structure, all of the slightly active compounds (compounds **i**, **iii**, **iv**, **vii** and **viii** of table 17 of the appendix) had a weaker dock score than the co-crystallised ligand, and four of the five active compounds (compounds **ii**, **v**, **vi** and **x** of table 17 of the appendix) had better dock scores than the co-crystallised ligand.

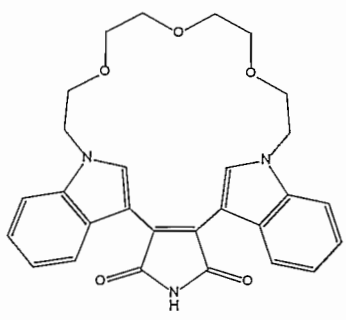

ix

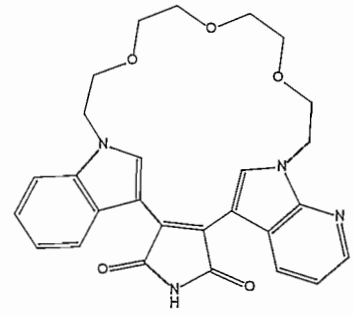

x

Figure 3.20: Compounds **ix** – **x** of table 17 of the appendix were GSK3β hypothesis hits.

None of the compounds were CDK5/p25 hypothesis hits. All of the compounds however had better dock scores than the ligand.

3.3.4 Discussion and conclusion

Not all of the potent inhibitors were hypothesis hits for calpain, caspase 3 and GSK3β. None of the weak inhibitors were however found to be hypothesis hits for calpain, caspase 3 and GSK3β. Although these results indicated that the different hypotheses are able to

differentiate between potent and weak inhibitors to a certain extent, it lacked the ability to select all the potent inhibitors. This could be due to the different structural classes used for each of the enzymes, which may not be able to fully address the unique but different binding modes of the structurally diverse potent compounds.

For calpain and caspase 3, there were no compounds with better dock scores than the co-crystallised ligand. However, there were compounds that had dock scores close to that of the co-crystallised ligand. The prediction potential calculated is thus 65% for calpain and 60% for caspase 3.

The docking results of GSK3β appear to be the most promising and gave the most accurate prediction of the activities of the compounds under investigation. When combining the GSK3β pharmacophore hypothesis with docking studies, the prediction potential is 80%.

As far as CDK5/p25 is concerned, neither the hypothesis nor docking studies could differentiate between potent and weak inhibitors. This is probably because the compounds used to validate the hypothesis were not in the same chemical class as the compounds used to generate the hypothesis. There are only a few CDK5/p25 inhibitors described in the literature, therefore only six inhibitors were used for the validation. The power of the study is very much based on the number of compounds included.

From the results it is clear that a pharmacophore hypothesis combined with docking studies were not sufficient to predict caspase 3 and CDK5/p25 activity. The prediction potential for GSK3β and calpain were the best and were thus used for the biological screening process.

Using a combination of hypotheses and docking studies, the activity of compounds could be predicted more accurately than using a hypothesis or docking studies alone.

3.4 Screening of library for compliance with hypotheses

3.4.1 Method

An in-house library of 301 compounds (table 9 – 14 of the appendix) was evaluated for compliance with the pharmacophore hypotheses for CDK5/p25, calpain, caspase 3 and GSK3β respectively. Different conformations of the compounds were generated using the conformation import function of MOE. Default values were used for all the parameters and the conformers generated were evaluated to determine which compounds comply with the requirements of a specific hypothesis. The screening was performed using the default parameters in the pharmacophore search function of the pharmacophore query editor of

MOE. The structures that showed compliance with a specific hypothesis were defined as hypothesis hits.

3.4.2 Results and discussion

3.4.2.1 CDK5/p25

All the compounds in table 9 – 14 of the appendix were tested on the CDK5/p25 hypothesis. The hypothesis hits are shown in table 3.1.

Table 3.1: Hypothesis hits of CDK5/p25 hypothesis

Nr	Compound	Nr	Compound
JP 11	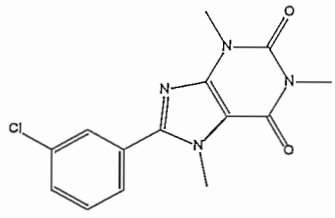	JP 12	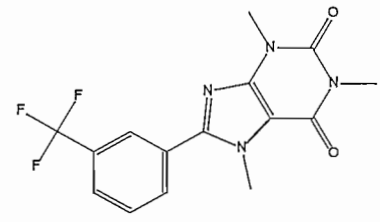
JP 13	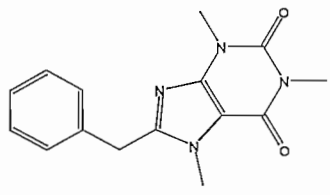	JP 14	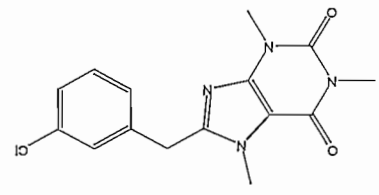
JP 15	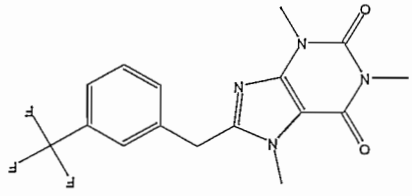	JP 22	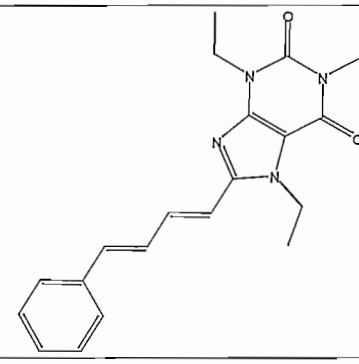
JP 42	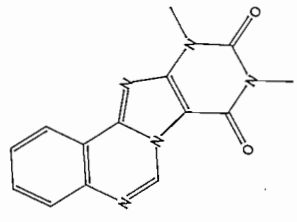	JP 43	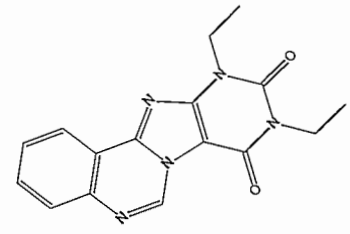

Table 3.1 (Continued): Hypothesis hits of CDK5/p25 hypothesis

JJ 13	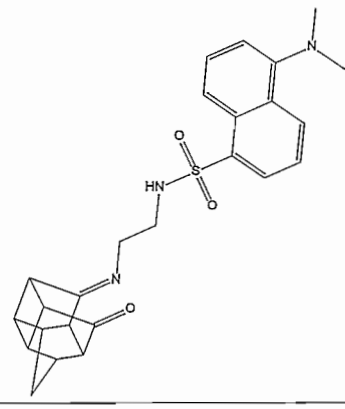	**JJ 14**	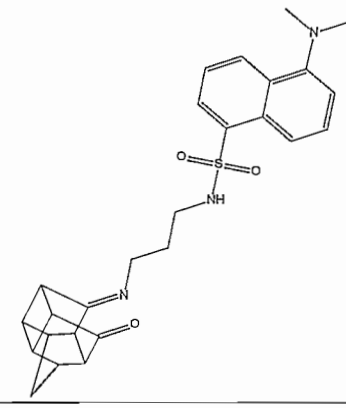
JJ 15	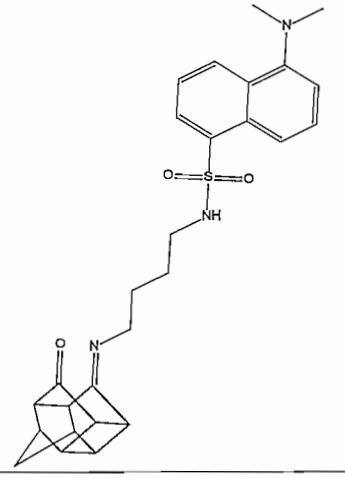	**JJ 18**	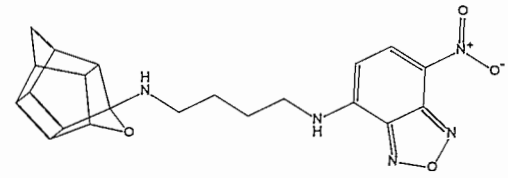
JJ 22	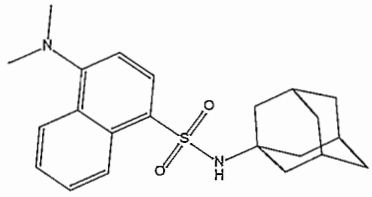	**JJ 23**	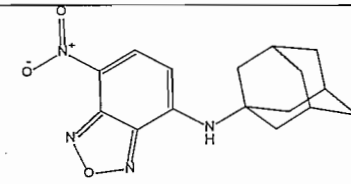
LP 10	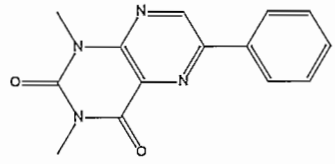	**LP 11**	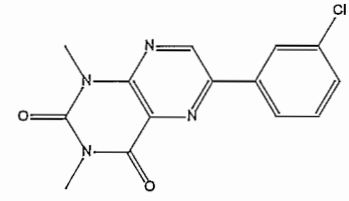
LP 12	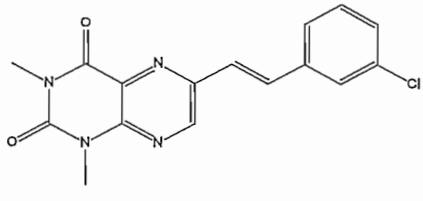	**BR 2**	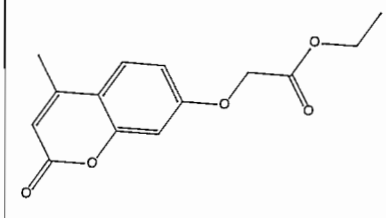

Table 3.1 (Continued): Hypothesis hits of CDK5/p25 hypothesis

BR 3	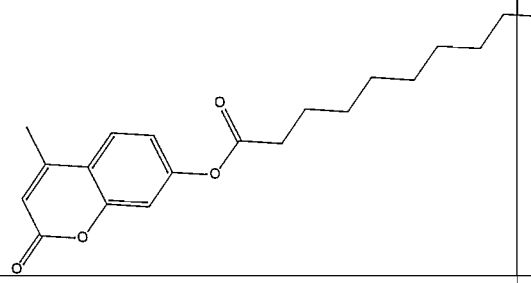	**BR 4**	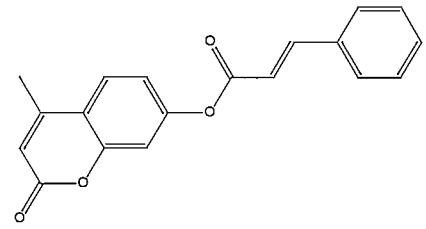
BR 5	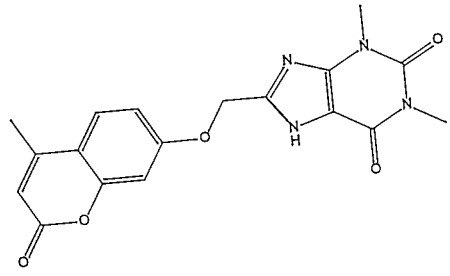	**BR 7**	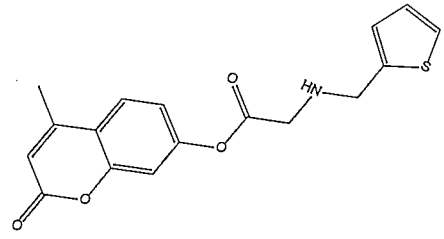
BR 8	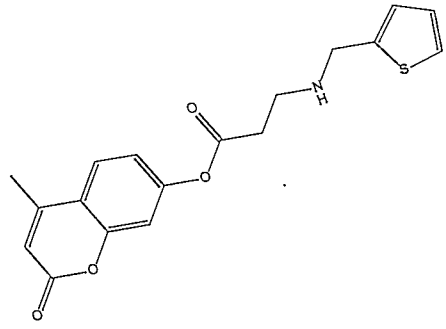	**BR 9**	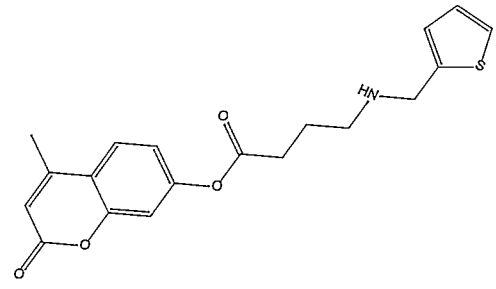
BR 10	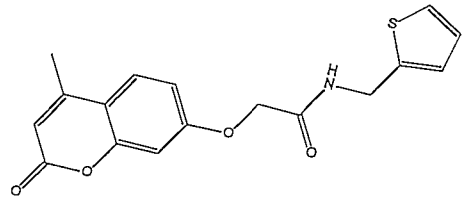	**BR 13**	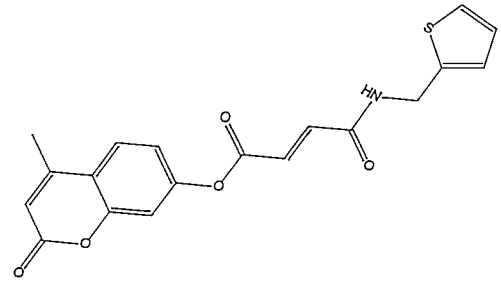

Table 3.1 (Continued): Hypothesis hits of CDK5/p25 hypothesis

BR 14	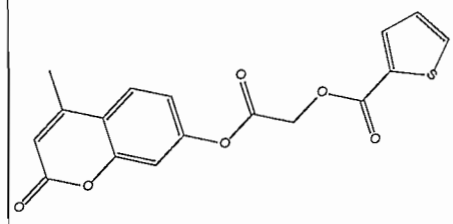	**BR 15**	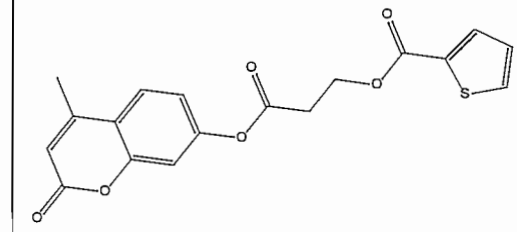
BR 16	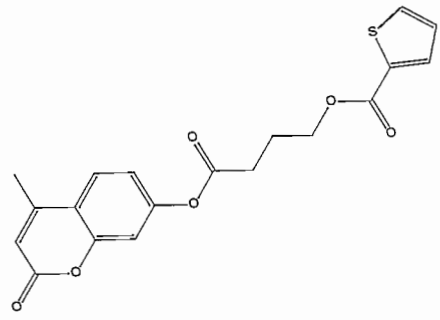	**BR 17**	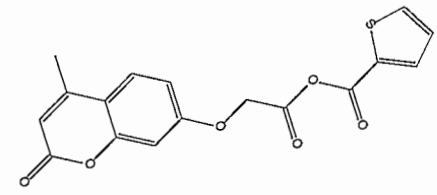
BR 18	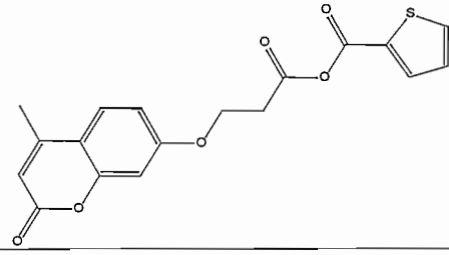	**BR 19**	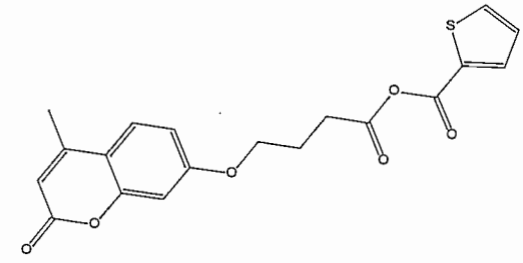
BR 20	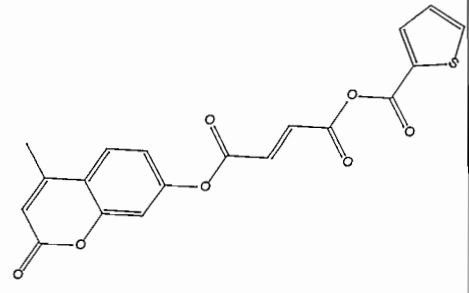	**JB 33**	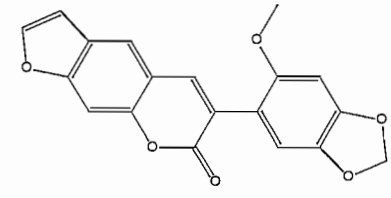

Table 3.1 (Continued): Hypothesis hits of CDK5/p25 hypothesis

JB 35	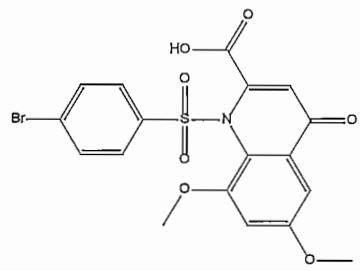	**JB 38**	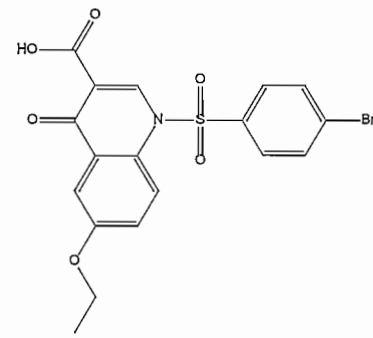
JB 47	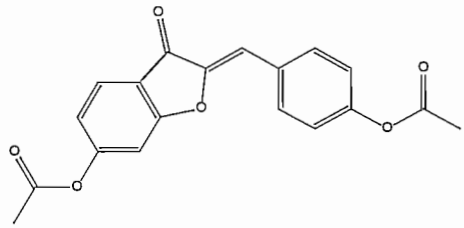	**BR 6**	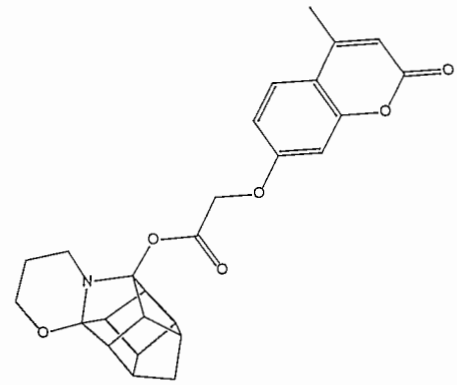
SD 13	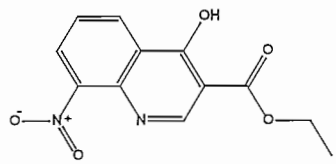		

The compounds that were CDK5/p25 hypothesis hits, contained at least two conjugated ring systems as well as hydrogen bond acceptors which seemed key to their activity. The hit compounds comprised of 10 distinctive chemical classes.

3.4.2.2 Calpain

All the compounds in table 9 – 14 of the appendix were tested on the calpain hypothesis. The hypothesis hits are shown in table 3.2.

Table 3.2: Hypothesis hits of calpain hypothesis

Nr	Compound	Nr	Compound
JP 42	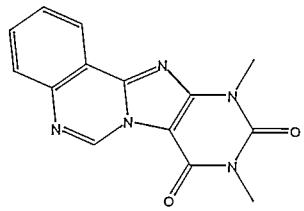	JP 43	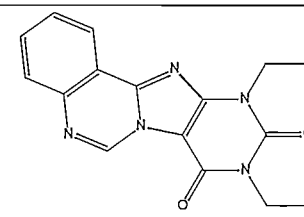
JJ 13	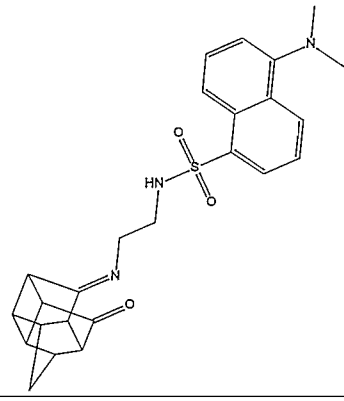	JJ 27	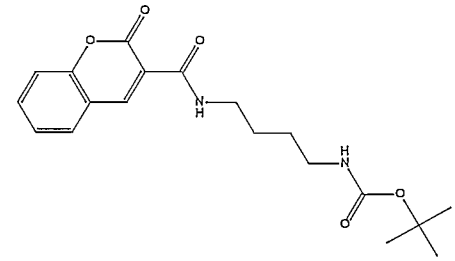
DW 9	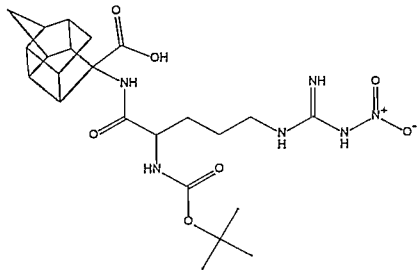	DW 10	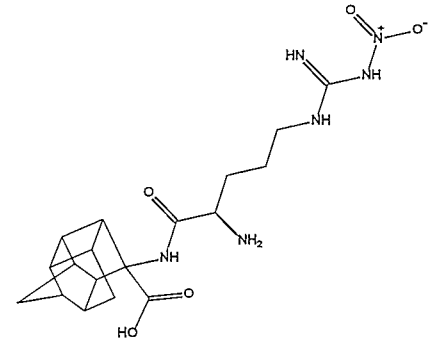
GT 3	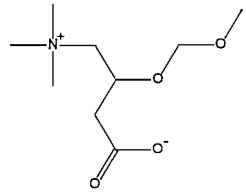	GT 4	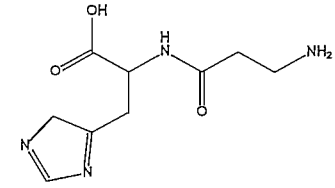

Table 3.2 (Continued): Hypothesis hits of calpain hypothesis

JB 13	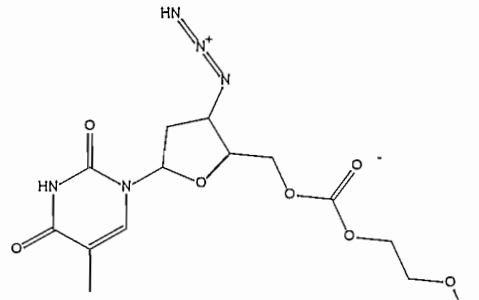
JB 14	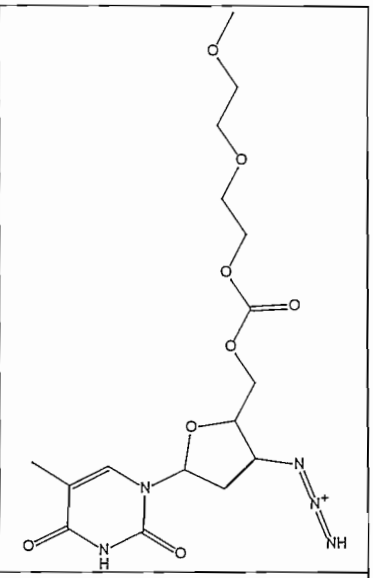
JB 15	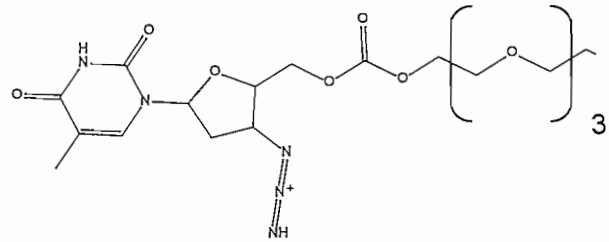
JB 16	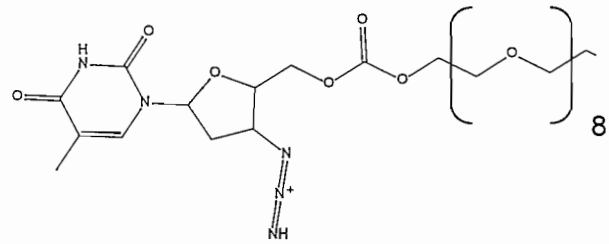
JB 17	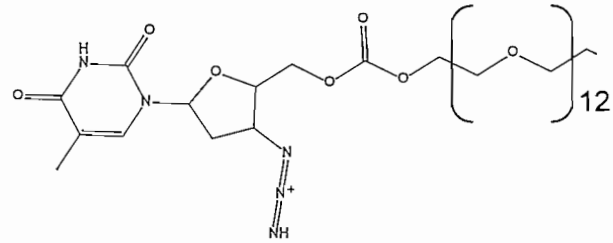

Table 3.2 (Continued): Hypothesis hits of calpain hypothesis

JB 18	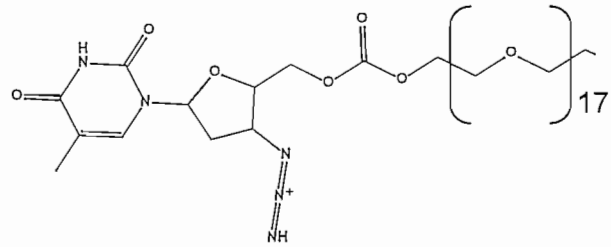
JB 41	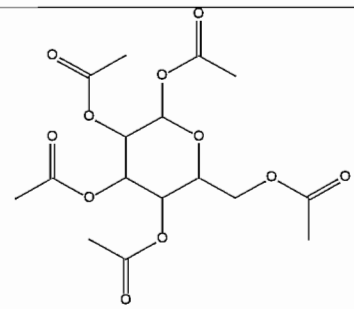
JB 50	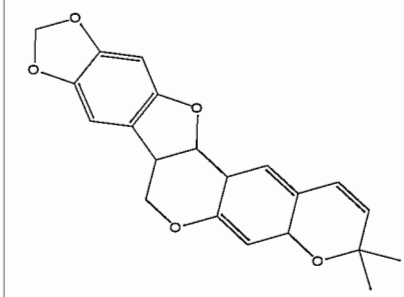
JB 51	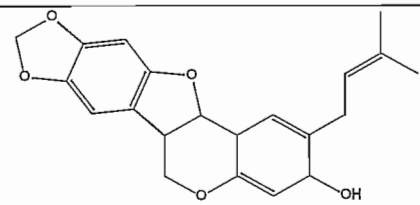
JB 52	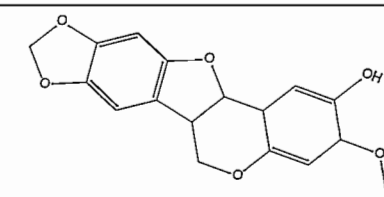
RL 1	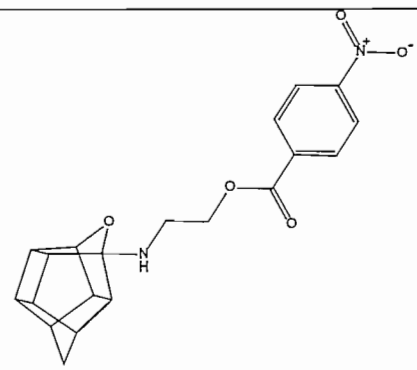
RL 5	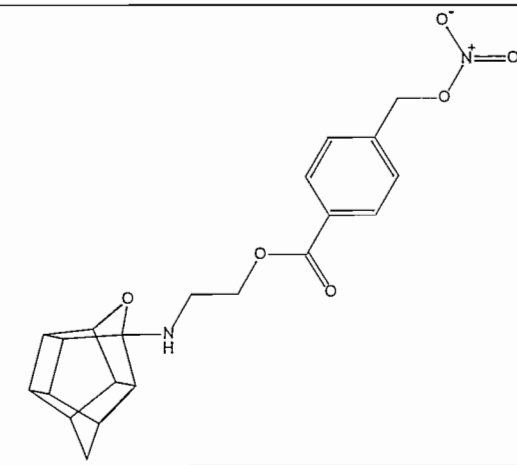
YG 1	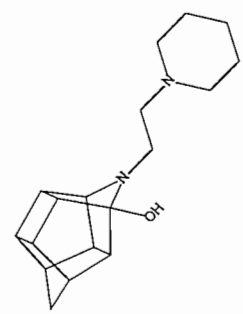
YG 2	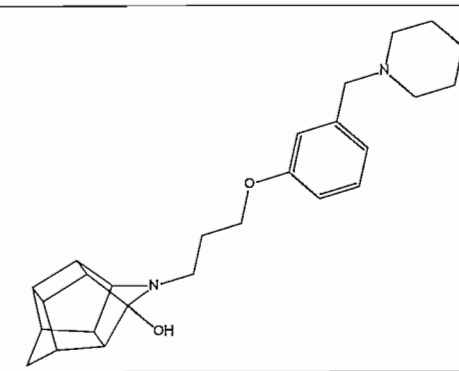

Table 3.2 (Continued): Hypothesis hits of calpain hypothesis

YG 3	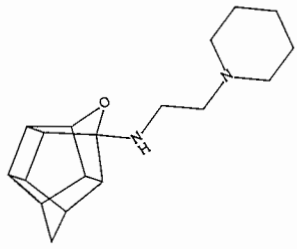	YG 6	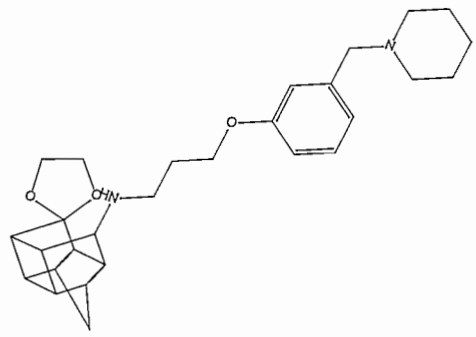

The compounds that were calpain hypothesis hits are structurally more diverse than the compounds that were CDK5/p25 hypothesis hits and no key moieties for activity could be identified. The hit compounds comprised of 11 distinct chemical classes.

3.4.2.3 Caspase 3

All the compounds in table 9 – 14 of the appendix were evaluated for compliance with the caspase 3 hypothesis. There were no hypothesis hits.

3.4.2.4 GSK3β

All the compounds in table 9 – 14 of the appendix were evaluated for compliance with the GSK3β hypothesis. The hypothesis hits are shown in table 3.3.

Table 3.3: Hypothesis hits of GSK3β hypothesis

Nr	Compound	Nr	Compound
JJ 13	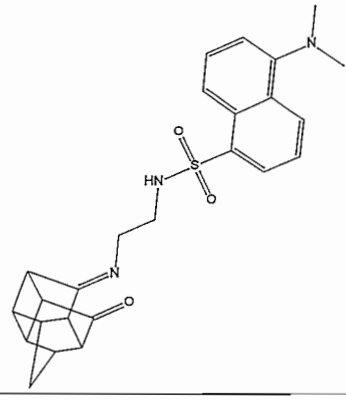	JB 7	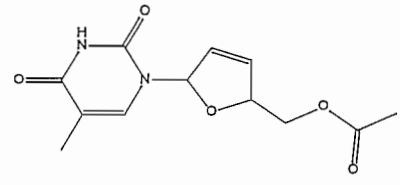

Table 3.3 (Continued): Hypothesis hits of GSK3β hypothesis

JB 8	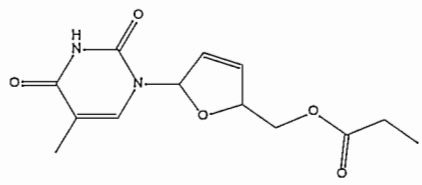	**JB 9**	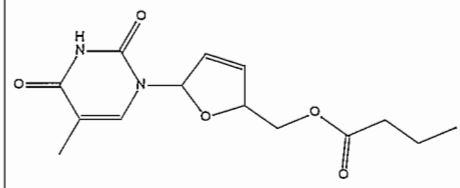
JB 10	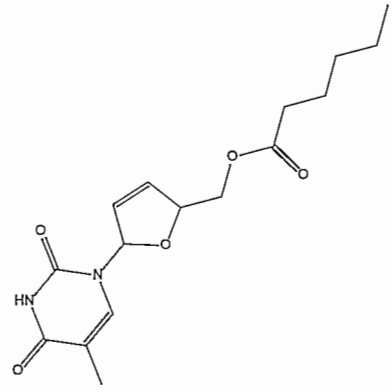	**JB 11**	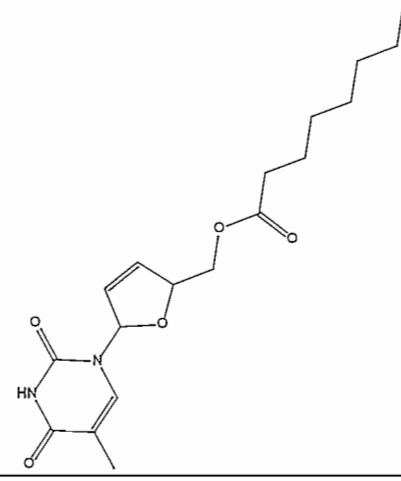
JB 12	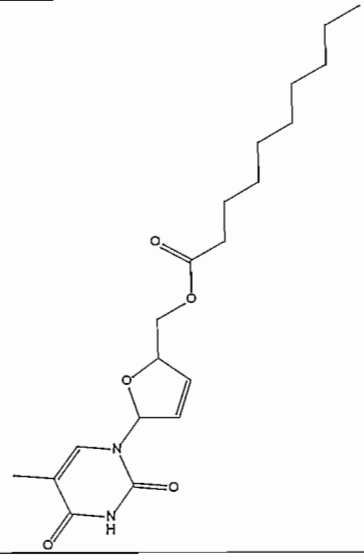	**JB 27**	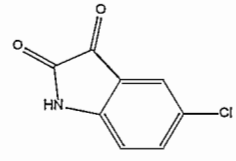
JB 35	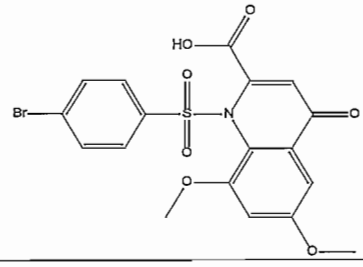		

All the compounds that were GSK3β hypothesis hits, contains at least two ring systems as well as hydrogen bond acceptors. The GSK3β hypothesis hits included four different chemical classes.

3.4.3 Conclusion

Except for caspase 3, various structurally divergent compounds were identified as possible hits with the potential to act as inhibitors of calpain, CDK5/p25 and GSK3β respectively. It may however be possible that when bulky and flexible molecules are tested on a hypothesis, they simply fold to fit into the hypothesis and will not necessarily adopt that specific conformation under natural circumstances. These hypotheses are therefore just predictions of where different types of chemical groups should be with respect to each other to possibly be enzyme inhibitors.

3.5 Docking studies

3.5.1 Background

As computational technology increases, molecular docking methods are developed to be more effective and can be applied during drug design and development (Tsai *et al.*, 2008). More 3D target structures are available now than ever before and it is necessary to understand the information represented by these structures (Schulz-Gasch & Stahl, 2003). Understanding molecular interactions are of critical importance to eventually control biological processes in living organisms (Koča *et al.*, 2000).

Docking can be described as the determination of the most energetically favourable binding interaction between a compound and the active site of an enzyme or receptor (Tsai *et al.*, 2008). Docking studies can prevent random experimental screening by identifying compounds in a database that show favourable electrostatic and steric interactions with the active site of the target receptor (Schulz-Gasch & Stahl, 2003).

3.5.2 Methods

The crystal structures utilised from the protein data bank (http://www.rcsb.org/) were all obtained by means of X-ray crystallography.

The crystal structure representing CDK5/p25 (figure 3.21) has a PDB code of 1UNL, a resolution of 2.2 Å and originates from *Homo sapiens*.

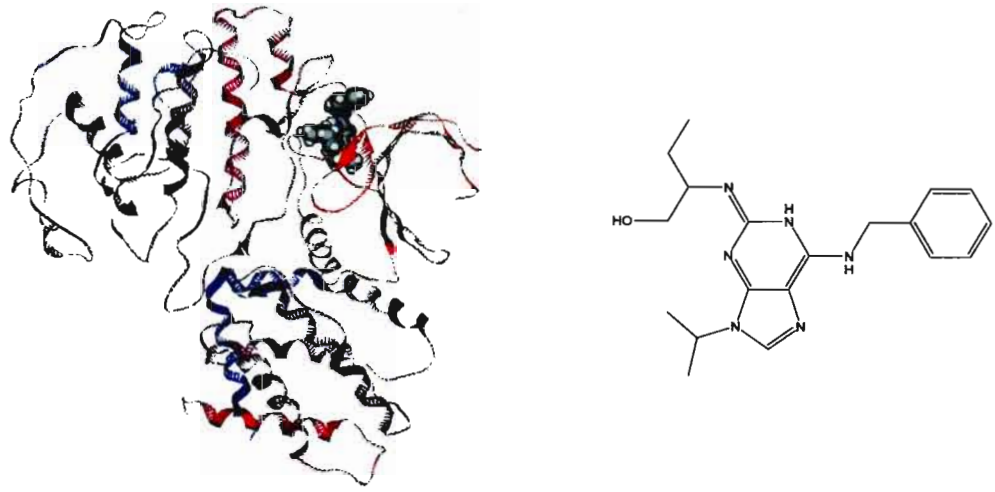

Figure 3.21: Crystal structure of CDK5/p25 (1UNL) with co-crystallised ligand. Ligand ((*R*)-roscovitine) is also shown next to the crystal structure.

The crystal structure representing calpain I (figure 3.22) has a PDB code of 1NXO, a resolution of 2.3 Å and originates from *Sus scrofa*.

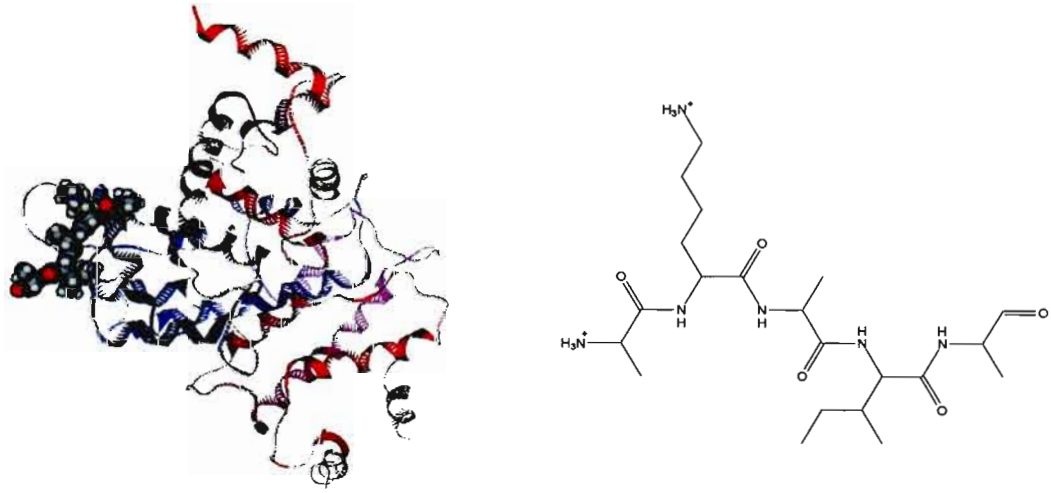

Figure 3.22: Crystal structure of calpain I (1NXO) with co-crystallised ligand. Ligand (calpastatin) is also shown next to the crystal structure.

The crystal structure representing caspase 3 (figure 3.23) has a resolution of 1.7 Å, a PDB code of 1NMS and originates from *Homo sapiens*.

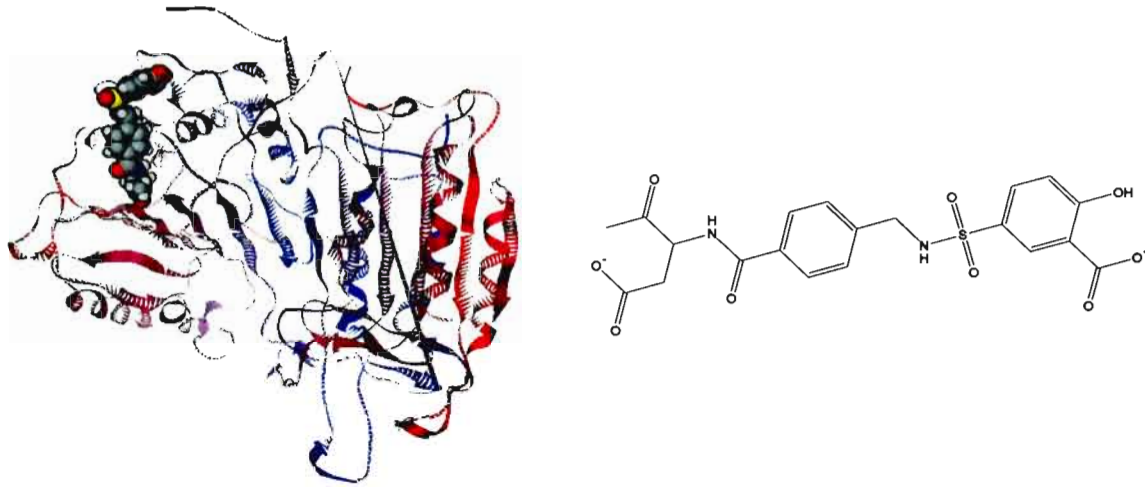

Figure 3.23: Crystal structure of caspase 3 (1NMS) with co-crystallised ligand. The ligand is also shown next to the crystal structure.

The crystal structure representing GSK3β (figure 3.24) has a PDB code of 1Q5K, a resolution of 1.94 Å and originates from *Homo sapiens*.

All the compounds in table 9 – 14 of the appendix were docked into the crystal structures of CDK5/p25, calpain I, caspase 3 and GSK3β respectively using molecular operating environment (MOE). The crystal structures were prepared for docking using the LigX application of MOE with the force field set to mmff94x. Default parameters and protocols were used for the docking process. Firstly the co-crystallised ligand was identified and the protein was protonated. The protein structure was then energy minimized with all the hydrogen atoms unconstrained and the heavy atoms tethered. All the unbound water molecules were deleted. The water molecules interacting with the active site were thus not deleted. The co-crystalised ligand was removed and docking was performed using the triangle matcher docking placement methodology. The original ligand was also docked into the structure to serve as reference for the dock scores.

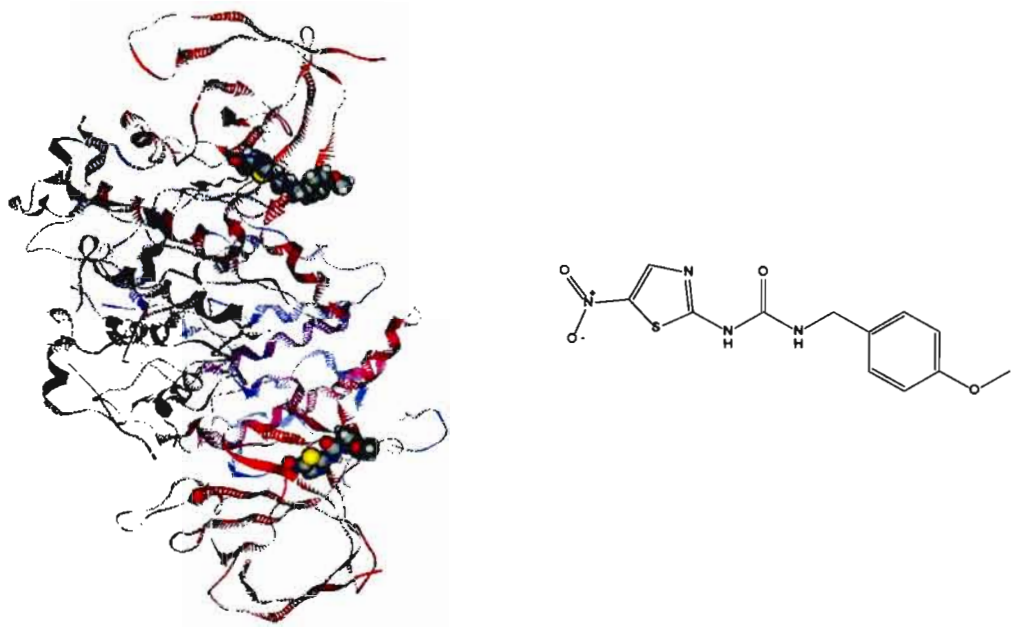

Figure 3.24: Crystal structure of GSK3β (1Q5K) with co-crystallised ligand. Ligand is also shown next to the crystal structure.

3.5.3 Results and discussion

The compounds that had better dock scores than the co-crystallised ligands are listed below in table 3.4 to table 3.7. The dock scores are given in kcal/mol. It should be noted that lower dock scores are deemed to be better than high dock scores. Only compounds with better dock scores than the respective co-crystallised ligands were selected. Compounds with dock scores in the same regions than the co-crystallised ligand were not selected because the aim was to identify only the most promising compounds.

3.5.3.1 CDK5/p25

The original co-crystallised ligand was docked into the CDK5/p25 active site cavity. The docked conformation was superposed onto the original conformation of the co-crystallised ligand in the CDK5/p25 active site. The RMSD value was 2.0071. The active site is situated in the catalytic cleft at the interface between the N and C lobes (Mapelli & Musacchio, 2003). A large number of compounds from diverse structural classes showed better dock scores than the co-crystallised ligand of CDK5/p25. Compound **JG4** had the best dock score.

Table 3.4: Dock scores of CDK5/p25 compounds (Structures of the compounds can be located in table 9 – 14 of the appendix)

Nr	Dock score	Nr	Dock score	Nr	Dock score	Nr	Dock score
JG4	-17.9304	**JG2**	-15.7214	**JG8**	-15.3117	**JB49**	-15.0880
JB14	-14.9231	**JP74**	-14.6651	**JG6**	-14.4808	**JB38**	-14.4109
RL2	-14.3233	**JG3**	-14.1726	**SD9**	-14.0723	**JB45**	-14.0124
JB52	-13.8807	**SD8**	-13.8678	**JB39**	-13.8609	**JB20**	-13.8603
SD10	-13.8514	**JB53**	-13.5682	**JB22**	-13.5590	**JB48**	-13.5566
JB21	-13.4233	**JB19**	-13.3991	**SD13**	-13.3113	**SD11**	-13.1468
DW4	-13.1241	**JB33**	-13.0613	**SD12**	-13.0575	**JB16**	-12.9972
JP17	-12.8930	**SM7**	-12.8923	**DW3**	-12.8666	**JJ18**	-12.8076
JP2	-12.7921	**JB13**	-12.7716	**DO29**	-12.7581	**SD27**	-12.7522
JB51	-12.7515	**JJ21**	-12.7230	**BR6**	-12.6952	**JP19**	-12.5176
JP50	-12.4823	**BR8**	-12.4778	**RL5**	-12.4298	**SD25**	-12.3845
JB23	-12.3711	**JB35**	-12.3567	**JJ8**	-12.3554	**JJ16**	-12.3500
JP69	-12.3335	**YG3**	-12.3196	**JG5**	-12.2940	**JJ15**	-12.2571
JB15	-12.2240	**JJ14**	-12.2149	**JP3**	-12.2085	**SM1**	-12.1775
JB34	-12.1714	**JB32**	-12.1653	**SD28**	-12.1569	**SD26**	-12.1434
JP5	-12.1405	**DW9**	-12.1217	**DW8**	-12.1216	**JP1**	-12.1059
DW10	-12.0786	**JB50**	-12.0533	**JJ13**	-12.0493	**JP4**	-12.0197
JP7	-11.9960	**SD16**	-11.9807	**SD24**	-11.9537	**JP72**	-11.9403
JJ17	-11.9363	**SD23**	-11.9238	**JP12**	-11.9151	**JP14**	-11.9103
JP31	-11.9092	**SD19**	-11.9013				

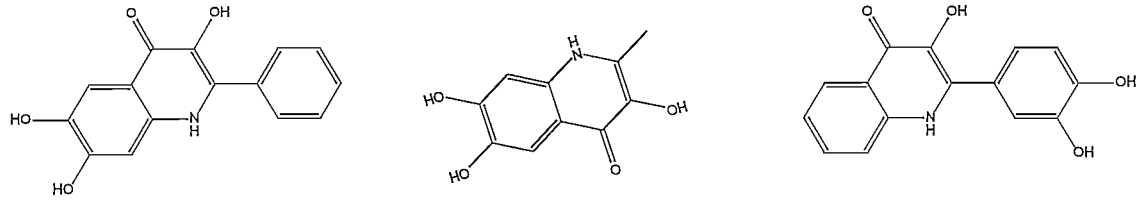

JG4 **JG2** **JG8**

Figure 3.25: Compounds with the best CDK5/p25 dock scores (**JG4**, **JG2** and **JG8**).

As shown in figure 3.26, the CDK5/p25 co-crystallised ligand interacts with the back bone of Gln130 (2.65 Å) and Cys83 (2.95 Å) by means of hydrogen bonds.

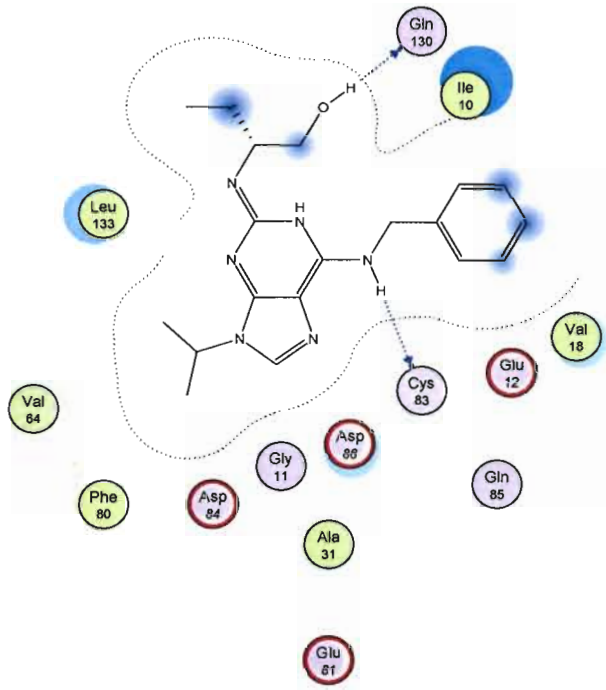

Figure 3.26: Interactions between the co-crystallised ligand and CDK5/p25.

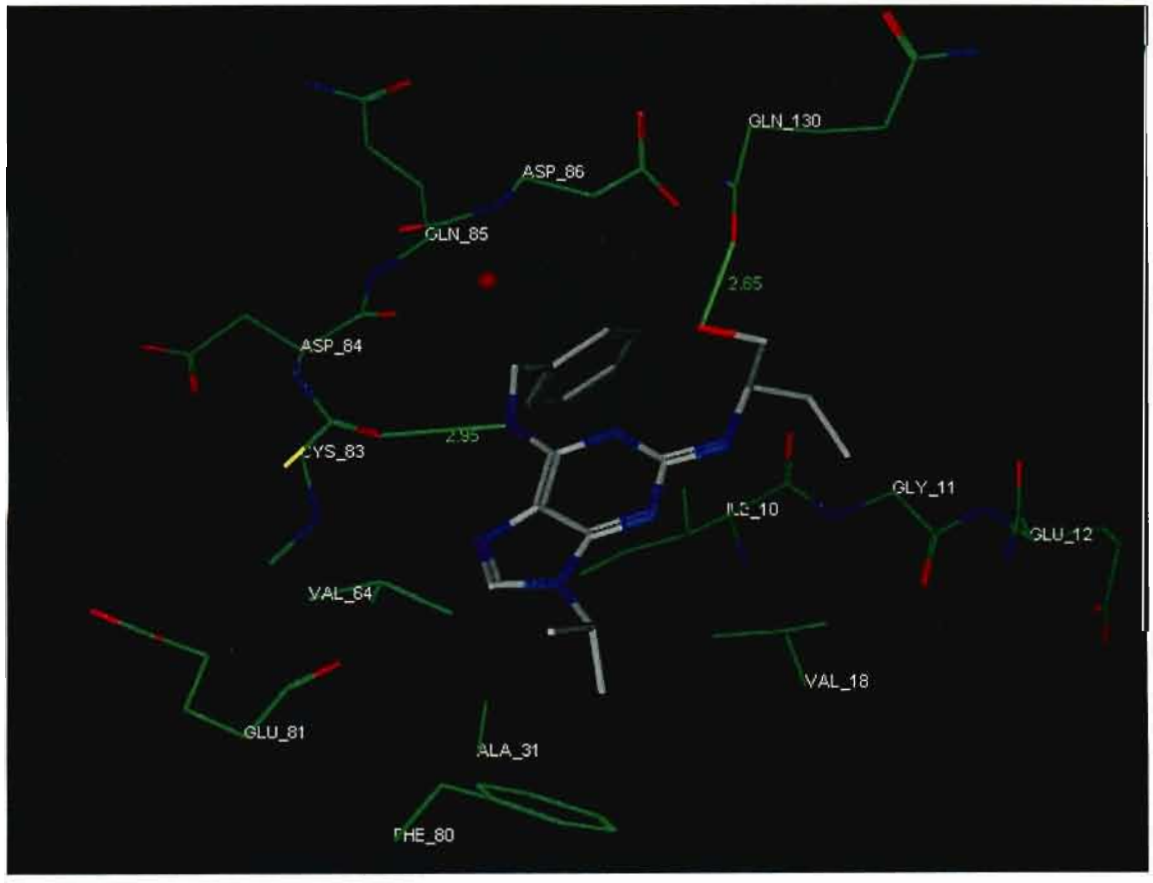

Figure 3.27: Interactions between the co-crystallised ligand and CDK5/p25.

JG4 interacts with CDK5/p25 (figure 3.28) via the back bone of Cys83 (3.08 Å) and the side chain of Asn144 (2.23 Å) by means of hydrogen bonds. A water bridge is formed between **JG4** and Glu51 and Lys33.

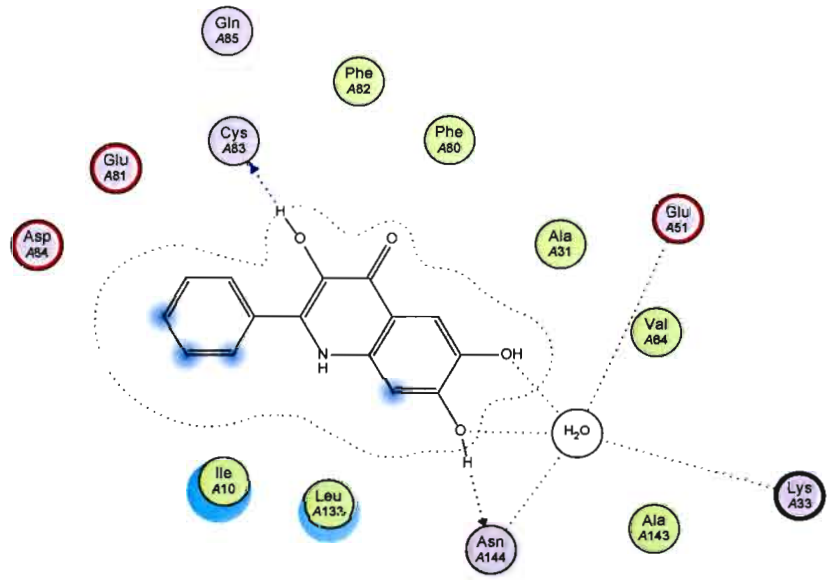

Figure 3.28: Interaction between compound with the best dock score (**JG4** of table 13 of the appendix) and CDK5/p25.

The CDK5/p25 ligand as well as compound **JG4** formed a hydrogen bond with Cys83 in the CDK5/p25 active site. This is an important interaction for CDK5/p25 inhibitory activity (Mapelli *et al.*, 2005; Ahn *et al.*, 2005) and indicated good probability of **JG4** being active on this system.

3.5.3.2 Calpain I

The original co-crystallised ligand was docked into the calpain I active site cavity. The docked conformation was superposed onto the original conformation of the co-crystallised ligand with an RMSD value of 2.8121.

The catalytic triad (Cys-His-Arg) of calpain I is located on domain II of the protein structure and form a catalytic active moiety only in the presence of calcium (Saez *et al.*, 2006).

Compounds from only two different structural classes had better dock scores than the co-crystallised ligand for calpain I and consists of fused ring systems.

Table 3.5: Dock scores of calpain I compounds

Nr	Dock score
JG4	-16.4452
JG3	-16.3226
JB52	-16.2944
JB50	-16.2501
JG2	-15.1563
JB51	-14.8698

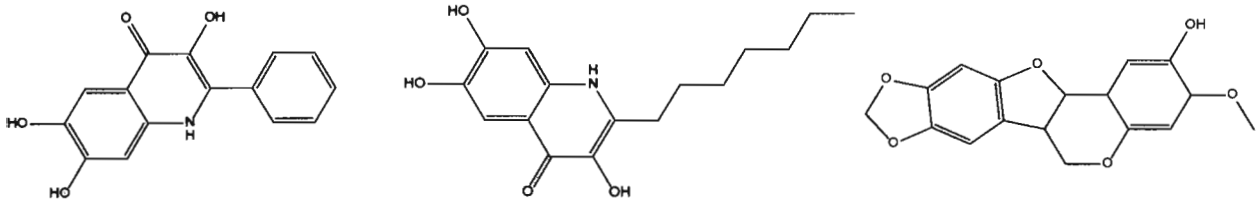

JG4 **JG3** **JB52**

Figure 3.29: Compounds with best dock scores (**JG4**, **JG3** and **JB52**).

The co-crystallised calpain I ligand interacts with calpain I by means of a hydrogen bond with the side chain of Asp235 (2.75 Å), as shown in figure 3.30.

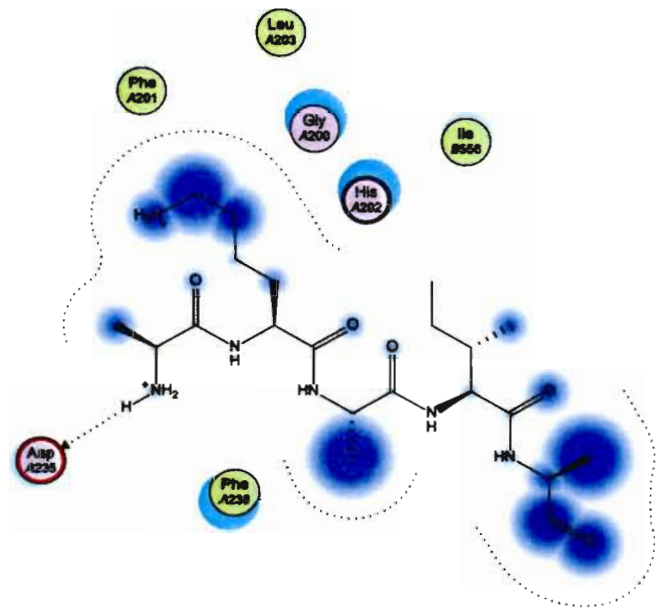

Figure 3.30: Interactions between the co-crystallised ligand and calpain I.

JG4 forms a hydrogen bond with the backbone of Ala199 (1.61 Å) and two hydrogen bonds with the side chains of Lys242 (2.61 Å and 2.78 Å). Two arene-arene interactions occur between **JG4** and Phe238 and Phe201 (figure 3.31).

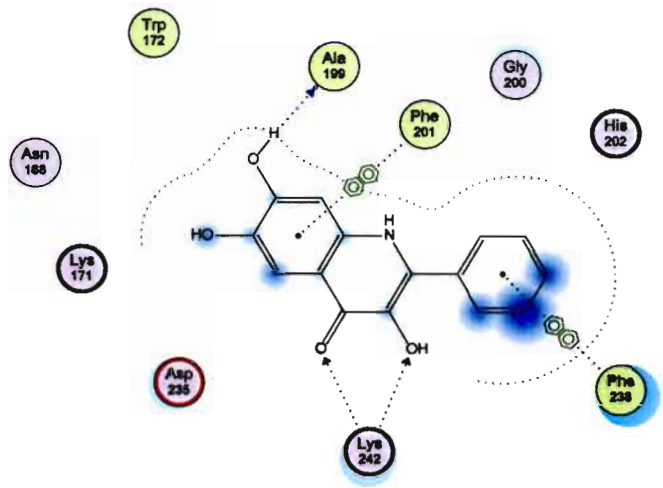

Figure 3.31: Interaction between compound **JG4** (table 13 of the appendix), with the best dock score, and calpain I.

The calpain I ligand and **JG4** did not show any interactions that were identical.

3.5.3.3 Caspase 3

The original co-crystallised ligand was docked into the caspase 3 active site cavity. The docked conformation was superposed onto the original conformation of the co-crystallised ligand with an RMSD value of 2.4148. Residues from both the p10 and p20 subunit from caspase 3 constitutes the active site and is located at the edge of the β sheet (Concha & Abdel-Meguid, 2002).

Only one compound had a better dock score than the co-crystallised ligand for caspase 3.

Table 3.6: Dock score of **JG8**

Nr	Compound	Dock score
JG8	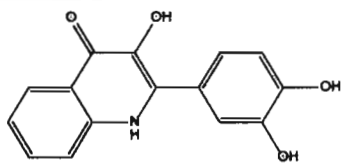	-16.4932

The co-crystallised caspase 3 ligand (figure 3.32) forms hydrogen bonds with the side chains of Asn208 (2.88 Å), Trp214 (3.04 Å), Gln161 (2.67 Å), Ser209 (2.86 Å) and two hydrogen

bonds with Arg64 (2.66 Å and 2.67 Å respectively). Arg207 is involved in three interactions with the ligand - two hydrogen bonds, one where the side chain (2.56 Å) is involved and the other where the back bone (2.73 Å) is involved and the third, an arene-cation interaction.

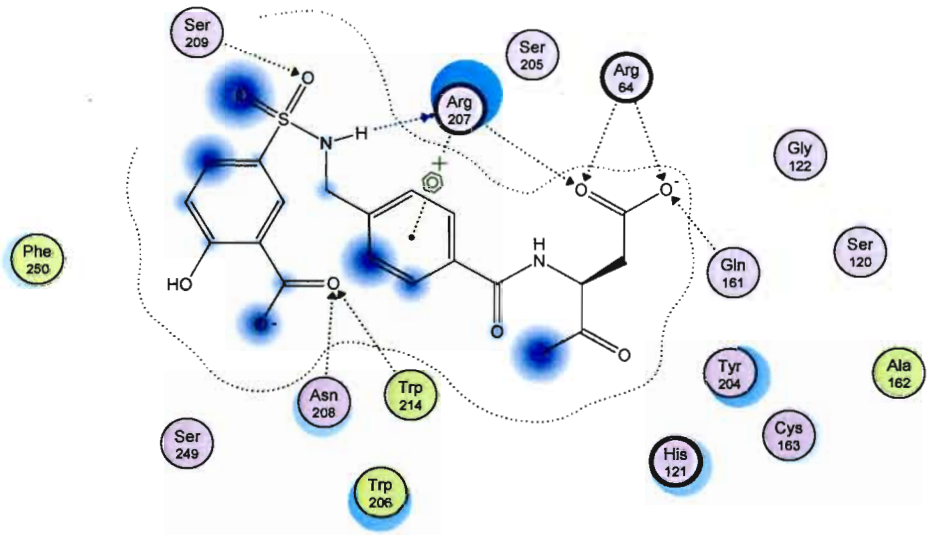

Figure 3.32: Interactions between the co-crystallised ligand and caspase 3.

JG8 interacts with caspase 3 (figure 3.33) by two hydrogen bonds with the back bone of Gly122 (2.61 Å) and Cys163 (2.86 Å). The compound also forms an arene-cation interaction with Arg207. A water bridge is formed between the compound and Glu123.

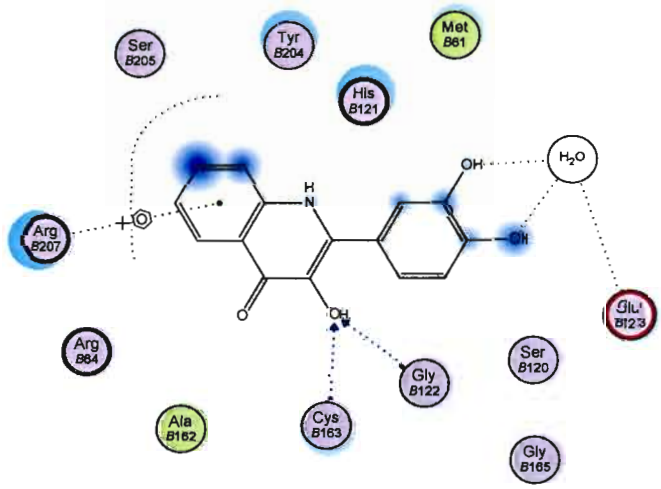

Figure 3.33: Interaction between compound with the best dock score (**JG8** of table 13 of the appendix) and caspase 3.

The only interaction exhibited by both the capase 3 ligand and **JG8** is an arene-arene interaction with Arg207.

3.5.3.4 GSK3β

The original co-crystallised ligand was docked into the GSK3β active site cavity. The docked conformation was superposed onto the original conformation of the co-crystallised ligand with an RMSD value of 1.5858.

At the interface of the N- and C- terminal domains, the following sites are formed: the ATP binding site, substrate binding site and the catalytic site. The active site channel consisting of these sites has an appropriate volume of 4290 $Å^3$ (Wagman *et al.*, 2004).

Diverse structural classes of compounds showed better dock scores than the co-crystallised ligand of GSK3β. Compound **JG3** had the best dock score.

Table 3.7: Dock scores of GSK3β compounds (Structures of the compounds can be located in table 9 – 14 of the appendix)

Nr	Dock score	Nr	Dock score	Nr	Dock score	Nr	Dock score
JG3	-16.1045	**JB18**	-15.6909	**JG8**	-15.5744	**JG4**	-15.5719
JB24	-15.5015	**JB17**	-15.4820	**JG2**	-15.0497	**JB23**	-14.9675
JB49	-14.8853	**RL5**	-14.7850	**SD9**	-14.7562	**JB16**	-14.6778
JG6	-14.6466	**JB45**	-14.4673	**JB38**	-14.4365	**SD8**	-14.3798
JB22	-14.2113	**JB20**	-13.8309	**SD10**	-13.7900	**JJ17**	-13.7871
JB12	-13.5542	**JB35**	-13.5120	**JB14**	-13.2835	**YG4**	-13.2700
JB15	-13.1793	**SD12**	-13.1387	**JJ16**	-13.1365	**JB39**	-13.0988
RL3	-13.0298	**JP9**	-13.0195	**DW4**	-12.9862	**JB13**	-12.9797
JJ18	-12.9504	**SD13**	-12.9374	**SD11**	-12.8551	**SD27**	-12.8421
RL1	-12.8394	**JB21**	-12.7983	**JJ15**	-12.6905	**JB51**	-12.6479
JB52	-12.6134	**JB34**	-12.5581	**JJ21**	-12.5535	**DW8**	-12.5384
JP74	-12.4706	**SD14**	-12.4538	**JB19**	-12.4432	**JB47**	-12.4401
JB53	-12.4251	**JP41**	-12.3474	**JB46**	-12.2848	**SM1**	-12.2481
JJ23	-12.2361	**JB50**	-12.2308	**SD20**	-12.2056	**JP2**	-12.2040
JB48	-12.1672	**JJ14**	-12.1330	**SD24**	-12.1174	**JB32**	-12.1034
SD21	-12.0615	**SD15**	-12.0305	**JJ22**	-11.9968	**JJ26**	-11.9595
SD17	-11.9017	**JP42**	-11.8526	**JB33**	-11.8461	**JP50**	-11.8322
SD26	-11.8115	**JP6**	-11.7937	**DW11**	-11.7935	**JJ13**	-11.7774
JP7	-11.7583	**JP73**	-11.7465	**JJ20**	-11.7135	**SD16**	-11.7052
JB7	-11.7039	**RL2**	-11.6975	**BR8**	-11.6735	**BR18**	-11.6666

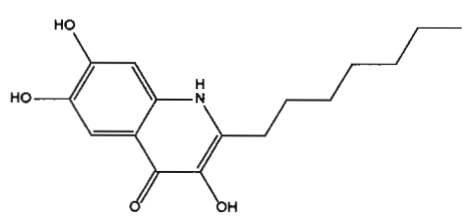

JG3

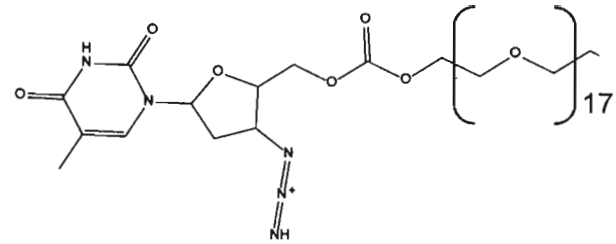

JB18

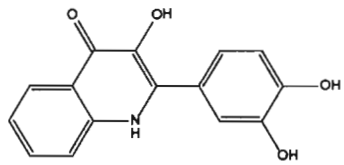

JG8

Figure 3.34: Compounds with the best GSK3β dock scores (**JG3**, **JB18** and **JG8**).

Two hydrogen bonds (figure 3.35) are formed between the back bone of Val135 (2.74 Å and 3.19 Å) and the GSK3β ligand. An arene-cation interaction takes place between the ligand and Arg141.

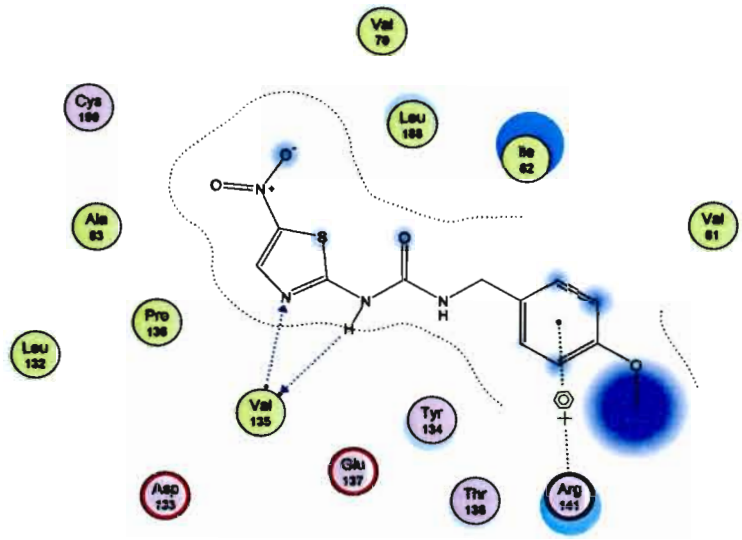

Figure 3.35: Interactions between the co-crystallised ligand and GSK3β.

For **JG3**, two hydrogen bonds are formed between the side chains of Lys85 (2.31 Å) and Asp200 (2.88 Å). Three water bridges are formed. One between water, Glu97, Phe201 and **JG3**, the other between water, Asp200, Val70, Asn186 and **JG3**. The final one is formed between water, Gln185 and **JG3** (figure 3.36).

Lys85 is a conserved and functionally important residue in kinase catalysis (Logé *et al.*, 2008). The interaction between **JG3** and Lys85 is thus an important interaction for the inhibition of GSK3β.

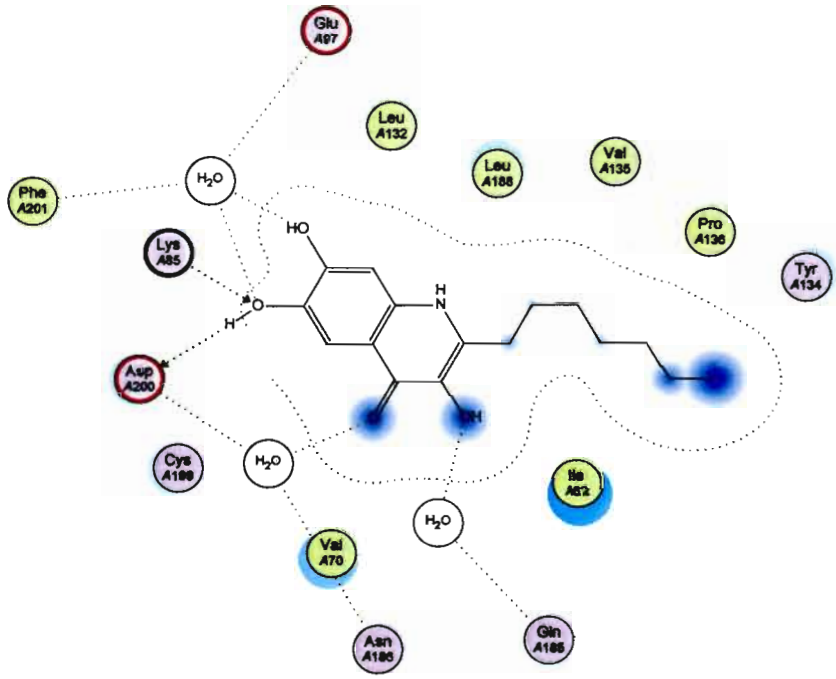

Figure 3.36: Interaction between compound with the best dock score (**JG3** of table 13 of the appendix) and GSK3β.

None of the interactions formed by the compound (**JG3**) with the best dock score, however correlate with the interactions formed by the co-crystallised ligand.

3.5.4 Conclusion

The interactions shown in the above figures will most probably be the prominent interactions needed for biological activity. The co-crystallised CDK5/p25 ligand and the compound with the best dock score for CDK5/p25 (**JG4**) both form a hydrogen bond with the back bone of Cys83. This interaction thus seems to be an important interaction for the inhibition of CDK5/p25. **JG4** (compound with best dock score for calpain I) does not form the same hydrogen bonds with calpain I as the co-crystallised ligand. It is possible that these compounds could inhibit calpain I via different interactions and/or mechanisms.

The co-crystallised ligand, as well as **JG8** (compound with the best dock score for caspase 3), form an arene-cation interaction with Arg207 and this may be a significant interaction for caspase 3 inhibition. With regards to GSK3β, the co-crystallised ligand and the compound

with the best dock score for GSK3β (**JG3**), did not have any interactions that were identical. Interaction with the highly conserved Lys85 may however indicate favourable interaction.

All the compounds with the best dock scores for the respective enzymes interacted with the actives sites at the hydroxyl moieties of the compounds. The presence of hydrogen bonding moieties in specific areas of a compound thus seems to be a prerequisite for interacting with these enzymes.

The docking studies thus determined if specific compounds would fit into the cavity of an enzyme and have the potential to interact with the enzyme.

4 Biological Assays

4.1 Background

In the molecular modelling chapters, the pharmacophore hypotheses combined with docking studies proved to be good indicators of possible activity. This was validated using known inhibitors and the subsequent screening of an in-house library identified structures with possible calpain I and/or GSK3β activity. As an experimental proof of concept and to test the model's predictive capabilities, the structures identified were subjected to a calpain I and GSK3β assay. Calpain I and GSK3β were selected for the experimental proof of concept in view of the validation performed in chapter 3.3 that illustrated these models had the best predictive capabilities.

4.1.1 Calpain

Calpain is a calcium-dependent cysteine protease (Lee *et al.*, 2000) requiring intracellular free Ca^{2+} for activation (Ray *et al.*, 2000). The most prominent role that calpain plays in neurodegeneration starts with its activation by calcium. Calpain then cleaves p35 directly to 25 (Kusakawa *et al.*, 2000) and p25 activates and deregulates CDK5, leading to apoptosis (Tsai *et al.*, 2004). Calpain can also lead to apoptosis by activating caspase 3 and 12 (Saez *et al.*, 2006) and treatment of AD mice with a calpain inhibitor showed improved synaptic and cognitive function (Kawamura *et al.*, 2005). It is thus clear that calpain plays a prominent role in the apoptotic processes and that it is a valuable target to explore in the prevention of neurodegenerative diseases.

There are two key isoforms of calpain found in the neuronal tissue, namely m-calpain and μ-calpain (calpain I) and they differ in the concentration of calcium needed for activation – 3 - 50 μM for half-maximal activity for μ-calpain and 0.2 - 1 mM for m-calpain (Lee *et al.*, 2000). Calpain I is prefered to perform assays because it is activated by lower levels of calcium and will thus be activated first during apoptotic processes because of increased calcium concentrations.

To determine the activity of possible calpain I inhibitors, a Calpain-Glo assay kit was purchased from Promega (Madison, USA). The assay is based on the measurement of luminescence, which is proportional to calpain I activity. Calpain I cleaves the substrate, Suc-LLVY-aminoluciferin, leading to the formation of Suc-LLVY and aminoluciferin. Aminoluciferin in turn is cleaved by luciferase, emitting a "glow-type" luminescent signal. The luciferase enzyme is isolated from the North American firefly *Photinus pyralis* and is believed by several sources to be the most effective bioluminescence system, with assays incorporating luciferase being sensitive, fast and reproducible (Branchini *et al.*, 2007).

4.1.2 GSK3β

GSK3 is a serine/threonine protein kinase that is widely expressed (Pap & Cooper, 1998). There are two GSK3 isoforms namely GSK3α and GSK3β (Moreno *et al.*, 1995). GSK3β has the ability to generate many phosphorylation sites on tau *in vitro* (Leroy *et al.*, 2007) and is therefore used to perform biological assays.

Neuronal apoptosis can be induced by the overexpression of GSK3 and small molecule inhibitors of GSK3 may potentially protect nerve cells from apoptosis (Cohen & Goedert, 2004). More specifically it has been shown that GSK3 can increase Aβ and inhibiting GSK3 would thus prevent this increase in Aβ (Cohen & Goedert, 2004). It also has the ability to hyperphosphorylate tau (Wagman *et al.*, 2004), accumulates in the cytoplasm of pre-tangle neurons and is thus associated with NFT (Engel *et al.*, 2006; Koh *et al.*, 2006). GSK3β might be a target in the treatment of AD and affective disorders based on the observation that lithium ions, used for the treatment of affective disorders, reduces Aβ by inhibiting GSK3β (Gurwitz & Eldar-Finkelman, 2001; Cohen & Goedert, 2004). GSK3β can also regulate activation of caspase 2 and caspase 8 (Lin *et al.*, 2007).

A Transcreener® ADP^2 FI assay kit donated by Bellbrook Labs (Madison, USA) was used to evaluate potential GSK3β inhibitors. The assay detects the amount of ADP generated by GSK3β by measuring fluorescence intensity.

GSK3β is used in solution with its substrate and ATP. ATP conversion takes place and ADP is formed. The Transcreener® ADP detection mixture consists of an ADP Alexa594 Tracer bound to the ADP^2 monoclonal antibody conjugated to an IRDye® QC-1 quencer. The ADP that is formed in the enzyme reaction displaces the tracer from the antibody and becomes unquenched. This in turn leads to a positive increase in fluorescence intensity and ADP production is proportional to an increase in fluorescence intensity. Thus, inhibitory activity of a compound is illustrated by a decrease in fluorescence intensity.

4.2 Methods

4.2.1 Calpain I

The compounds tested in the Calpain-Glo assay are shown in table 4.1. Compounds **JB50 – 52** were evaluated because they were hypothesis hits as well as showing better dock scores than the co-crystallised ligand in the calpain I enzyme used for the docking. **JJ13** and **JJ27** were hypothesis hits.

Table 4.1: Compounds evaluated in the calpain I assay

	Compound	Dock score (S) (kcal/mol)
JB52	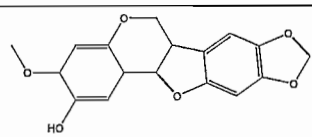	-16.2944
JB50	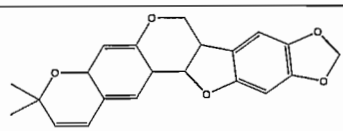	-16.2501
JB51	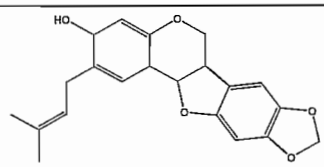	-14.8698
JJ13	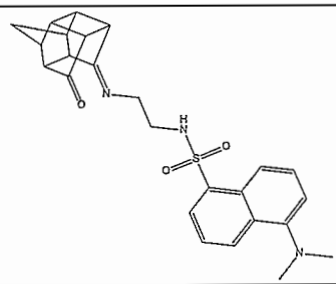	-11.5958
JJ27	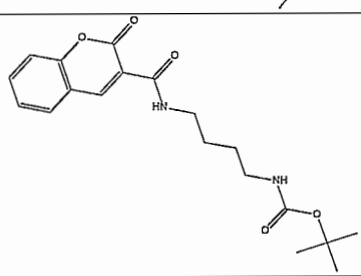	-11.2255

Inhibitor concentrations

In the first assay performed, all five compounds were evaluated at final concentrations of 10 nM, 100 nM, 1 µM, 10 µM and 100 µM in a final assay volume of 100 µl. A stock solution of 100 µM was prepared and diluted to obtain the necessary concentrations. In the second assay, compounds **JB50** and **JB51** were evaluated at final concentrations of 100 nM, 1 µM, 10 µM, 100 µM, 200 µM, 300 µM, 400 µM and 500 µM in a final assay volume of 100 µl. A stock solution of 500 µM was prepared and diluted to obtain the necessary concentrations.

Calpain buffer

The buffer for reconstitution of calpain I consists of the following:

Tris-HCl	20 mM, pH 7.5
Na-EDTA	1 mM
2-mercaptoethanol	5 mM

Assay procedure

The assay kit included buffer, substrate and luciferin detection reagent (LDR). The assay was performed using the following procedure and is also illustrated in figure 4.1.

1. The buffer and LDR were both thawed until it reached room temperature.
2. The bufffer (10 ml) was added to the LDR; it went into solution in approximately one minute.
3. The substrate was thawed and allowed to reach room temperature. It was thoroughly mixed by vortexing briefly.
4. Calpain-Glo Reagent (CGR) was formed by adding the substrate (100 µl) to the mixture in step 2. The above mentioned mixture was made by swirling and inverting. The substrate concentration was 80 µM in the reagent and 40 µM in the final assay. The apparent K_m for the substrate was 40 µM.
5. Calpain-Glo reagent was incubated at room temperature for 30 minutes prior to use.
6. 20 µl of a 1 M $CaCl_2$ was added to the Calpain-Glo reagent. The concentration of the $CaCl_2$ was 2 mM in the reagent and 1 mM in the final assay.
7. The following controls were necessary:

   Blank: Calpain-Glo reagent with $CaCl_2$ (50 µl), together with vehicle control for test sample (25 µl 10% DMSO solution) and 25 µl water.

   Positive control: Calpain-Glo reagent with $CaCl_2$ (50 µl), together with vehicle control (25 µl 10% DMSO solution) and 25 µl enzyme in buffer (final concentration was 50 nM).

   Negative control: Calpain-Glo reagent without $CaCl_2$ (50 µl) with vehicle control (25 µl 10% DMSO solution) and 25 µl enzyme in buffer.

8. For the testing of the compounds, a mixture of calpain I enzyme in buffer (25 µl) and sample (25 µl), in a white-walled multiwell plate was used. 50 µl of the Calpain-Glo reagent was added so that the final volume of the assay was 100 µl. The calpain I concentration in the final assay volume was 50 nM and the DMSO concentration was not more than 2.5%.
9. The contents were mixed at 300 - 500 rpm for 30 seconds and incubated at room temperature for 5 – 30 minutes. The maximal signal was reached within 5 - 15 minutes.
10. Luminescence was measured using a FL 600 Microplate Fluorescence\Luminescence Plate Reader (BIO-TEK Instruments, Neufarn, Germany) at 6, 10 and 15 minutes respectively.

40 nM compound in 25 µl
10% DMSO in 25 µl

200 nM calpain I in 25 µl

50 µl CGR

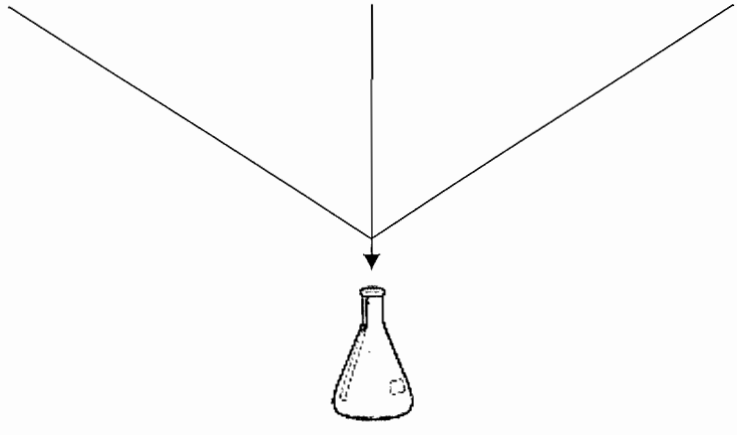

10 nM compound in 100 µl
2.5% DMSO in 100 µl
50 nM calpain I in 100 µl

Figure 4.1: Assay method using a final compound concentration of 10 nM.

Data calculations

For every luminescence measurement at time 6, 10 and 15 minutes, different blank values were obtained. The blank value was subtracted from all of the luminescence values at the specific times. The values were obtained in triplicate and did not differ significantly from each other. All the data points represent the average ± SEM of the luminescence values. The IC_{50}

values were calculated using the sigmoidal dose-response equation in Prism (Graphpad). The inhibition curves for all the compounds are shown at time 10 minutes. A period of 10 minutes was used because it is in the time range in which the assay achieves maximum sensitivity (5 – 15 minutes).

4.2.2 GSK3β

Reagents included in the assay kit are ADP[2] antibody IRDye QC-1 (antibody), ADP Alexa594 Tracer (tracer), Stop and detect buffer B (buffer B), ATP and ADP. All assays were performed in 384 well black Greiner microwell plates. Fluorescence was measured spectrophotometrically using the BioTek® Synergy HT microplate plate reader (BIO-TEK Instruments, Neufarn, Germany).

The compounds tested in this assay are shown in table 4.2. Compounds **JJ13** and **JB7** were hypothesis hits and had better dock scores than the co-crystallised ligand. Compound **JB27** was a hypothesis hit and compound **SD9** had a better dock score than the co-crystallised ligand. **SB216763**, was used as a positive control as it is reported to inhibit GSK3α with an IC_{50} value of 34 nM and was found to be equally effective against GSK3β in the same study (Coghlan *et al.*, 2000). In another study, the IC_{50} for **SB216763** against GSK3β was found to be 75 nM (Hu *et al.*, 2009). **LP11** was not a hypothesis hit and had a dock score slightly worse than the co-crystallised ligand.

Table 4.2: Compounds evaluated in GSK3β assay

Code	Structure	Dock score (S) (kcal/mol)
JJ13	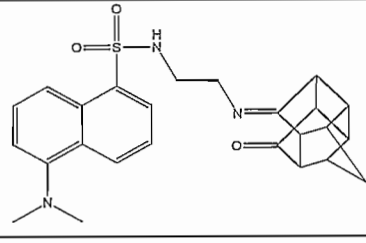	-11.7774
JB7	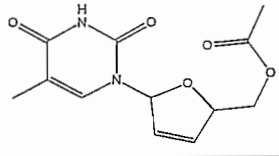	-11.7039
JB27	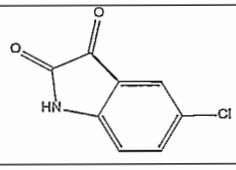	-11.5867

SD9	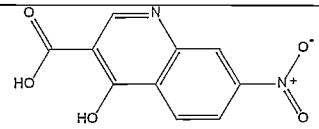	-14.7562
SB216763	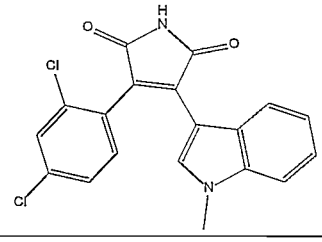	-12.3030
LP11	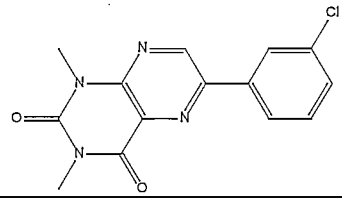	-10.9541

The consecutive steps used to perform the assay were as follows:

1) <u>Titrate tracer</u>

Optimal excitation is at 590 nM (10 nM bandwidth) and emission is at 617 nM (10 nM bandwidth). However, the instrument used could not measure at an exact emission of 617 nM. An emission of 645 nM (30 nM bandwidth) was subsequently used as advised by Bellbrook Labs.

The tracer was titrated in buffer B to determine if there was a linear response. A linear response is needed for the fluorescence values to be accurate. Concentrations of tracer tested were 1, 2, 3, 4, 5, 6, 7 and 8 nM in 0.5 X buffer B (buffer B is provided at a concentration of 10 X) with a final assay volume of 20 µl and all experiments were done in triplicate. The tracer was diluted to the above mentioned concentrations from an 8 nM stock solution.

A linear response was achieved with a R^2 value of 0.987, indicating that the the assay was accurate at an emission of 645 nM.

2) <u>Determining antibody concentration for the amount of ATP in the enzyme reaction</u>

The relationship between the ATP concentration and antibody concentration is linear for reactions that require between 0.1 and 100 µM ATP. 10 µM ATP was used in this assay and

the relationship was thus linear. The equation used is y = mx + c, where m=0.46 and c=0.3, as shown in figure 4.2.

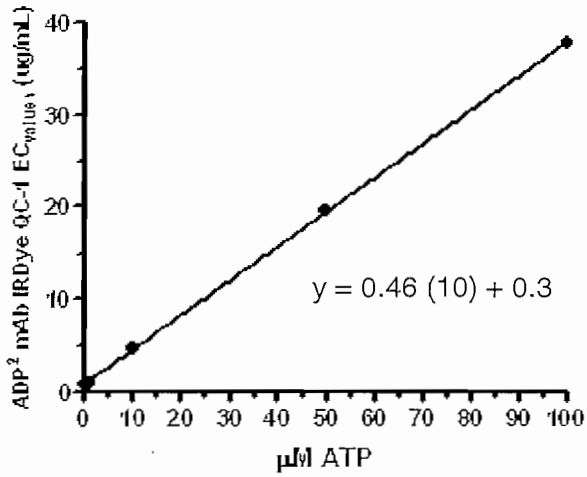

Figure 4.2: Graph to determine antibody concentration. The ATP concentration on the graph represents the concentration ATP in the 10 µl enzyme reaction prior to the addition of 10 µl ADP detection mixture. The antibody concentration is for the final 20 µl assay volume.

The ATP concentration was 10 µM in the GSK3β assay and thus the antibody concentration will be 4.9 µg/ml in the final 20 µl volume.

3) Instrument set-up

The maximum fluorescence window was defined by measuring the low (tracer and antibody) and high (free tracer) relative fluorescence units (RFU's).

a) Low RFU: 4.9 µg/ml ADP^2 Antibody IRDye QC-1 in 4 nM ADP Alexa594 Tracer/0.5 X stop & detect buffer B.
b) High RFU: 4 nM ADP Alexa594 Tracer/0.5 X stop & detect buffer B.

The difference between high and low RFU values gave the maximum assay window. However, the (high RFU)/(low RFU) ratio should be >5 for the assay results to be accurate. The ratio was determined to be 13 and the assay window was thus sufficient.

4) Enzyme buffer components

The enzyme buffer for dilution of GSK3β contains the following components:

- 50 mM Tris-HCl, pH 7.5
- 10 mM $MgCl_2$
- 0.1 mM EGTA

- 0.1 mM EDTA

5) Inhibitor concentrations

All the compounds, except **SB216763**, were evaluated at final concentrations of 10 nM, 100 nM, 1 µM, 10 µM, 100 µM, 250 µM, 500 µM and 1000 µM in a final assay volume of 20 µl. A stock solution of 1000 µM was prepared and diluted to obtain the necessary concentrations. **SB216763** was evaluated at final concentrations of 0.1 nM, 1 nM, 10 nM, 100 nM, 1 µM, and 10 µM in a final assay volume of 20 µl. A stock solution of 10 µM was prepared and diluted to obtain the necessary concentrations. No more than 2.5% DMSO is present in the 20 µl final assay volume, except for the 10 µM solution of **SB216763**, that had a final concentration of 5% DMSO. This was due to solubility challenges experienced for **SB216763**.

6) Detect ADP in an enzyme reaction

The final assay consisted of the enzyme reaction (10 µl) and the ADP detection mixture (10 µl). The enzyme reaction consisted of 50 nM enzyme, enzyme buffer and 30 µM substrate (2.5 µl) and test compounds (5 µl), which were mixed on a plate shaker before adding 10 µM ATP (2.5 µl). The components were mixed on a plate shaker again and then incubated at room temperature (20-25°C) for 60 minutes.

The ADP detection mixture consisted of ADP[2] antibody IRDye QC-1 (2*[4.9 µg/ml]), 8 nM ADP Alexa594 tracer and 1 X stop and detect buffer B. The ADP detection mixture was added to the enzyme reaction and mixed on a plate shaker. It was incubated at room temperature for 60 minutes and the fluorescence intensity was then measured. All assays were done in triplicate and average RFU values were used.

The following control assays were used:

- **0% ATP conversion control**

  ADP detection mixture (10 µl), enzyme reaction components without enzyme (2.5 µl), vehicle control (5 µl of a 10% DMSO solution) and 2.5 µl 100% ATP (0% ADP) defined the lower limit of the assay window.

- **100% ATP conversion control**

  ADP detection mixture (10 µl), enzyme reaction components without enzyme (2.5 µl), vehicle control (5 µl of a 10% DMSO solution) and 2.5 µl 100% ADP (0% ATP) defined the upper limit of the assay window.

- **Without antibody control**

  Contains tracer without antibody and it determines the maximum RFU.

- **Without tracer control**

  Contains antibody without tracer and is the sample blank.

- **ADP/ATP standard curve**

  A curve was plotted using the following ATP conversions: 0%, 2%, 4%, 6%, 8%, 10%, 20%, 30%, 40%, 60% and 100% (figure 4.3).

Table 4.3: Information for ADP/ATP standard curve

% ATP conversion	[ATP] (µM)	[ADP] (µM)	Volume of 40 µM ATP and ADP stock solutions for adenine concentration to remain constant at 10 µM
0	10	0	10 µl ATP and 0 µl ADP
2	9.8	0.2	9.8 µl ATP and 0.2 µl ADP
4	9.6	0.4	9.6 µl ATP and 0.4 µl ADP
6	9.4	0.6	9.4 µl ATP and 0.6 µl ADP
8	9.2	0.8	9.2 µl ATP and 0.8 µl ADP
10	9	1	9 µl ATP and 1 µl ADP
20	8	2	8 µl ATP and 2 µl ADP
30	7	3	7 µl ATP and 3 µl ADP
40	6	4	6 µl ATP and 4 µl ADP
60	4	6	4 µl ATP and 6 µl ADP
100	0	10	0 µl ATP and 10 µl ADP

For the ADP/ATP standard curve, 10 µl of the final assay volume (20 µl) contained ADP detection mixture. The other 10 µL contained enzyme buffer (2.5 µL), 2.5% DMSO (5 µL of a 10% DMSO solution) and ATP/ADP concentrations (2.5 µL) as shown in the last column of table 4.3.

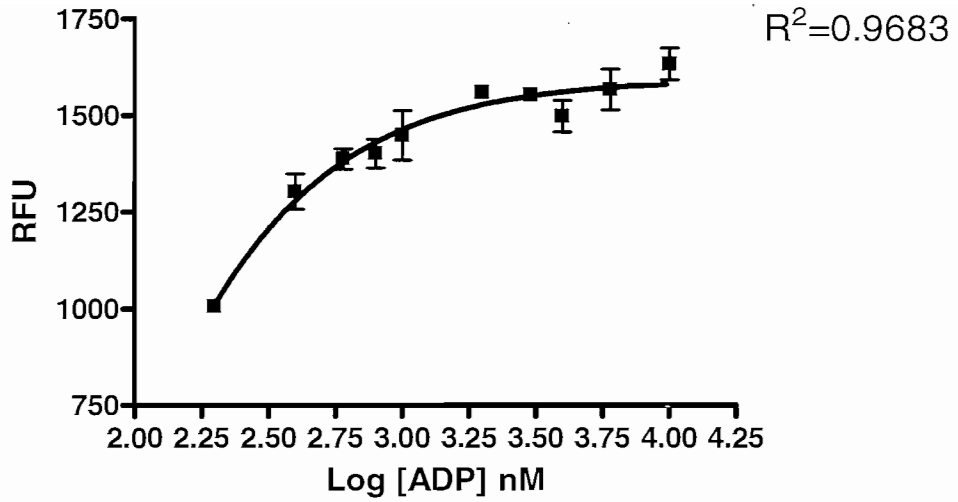

Figure 4.3: ADP/ATP standard curve.

7) **Data calculations**

The ADP/ATP standard curve is shown in figure 4.3. The fluorescence is proportional to the ADP production. The background fluorescence was determined from the 0% ATP conversion control and subtracted from the Relative Fluorescence Units (RFU) values. RFU values were converted to log [ADP] values by extrapolation of the ADP/ATP standard curve, only for RFU values smaller than 1006. IC_{50} values were then determined from the inhibition curves using the sigmoidal dose-response equation in Prism (Graphpad). RFU values are shown in table 20 of the appendix.

4.3 Results and discussion

4.3.1 Calpain I

The inhibition curves for all the compounds are shown at time 10 minutes (figures 4.4, 4.6, 4.8, 4.10 and 4.13). Relative Luminescence Units (RLU) are shown in table 19 of the appendix.

With compounds **JB50** and **JB51**, maximum inhibition of calpain I was obtained. **JB52** was not assayed at higher concentrations (limited number of assays in kit) but illustrated a similar inhibition curve (figure 4.4) to that of the structurally related **JB50** and **JB51** (figures 4.6 and 4.8). For compounds **JJ13** and **JJ27**, only partial inhibition was obtained at 100 µM (29.17% and 42.92% respectively).

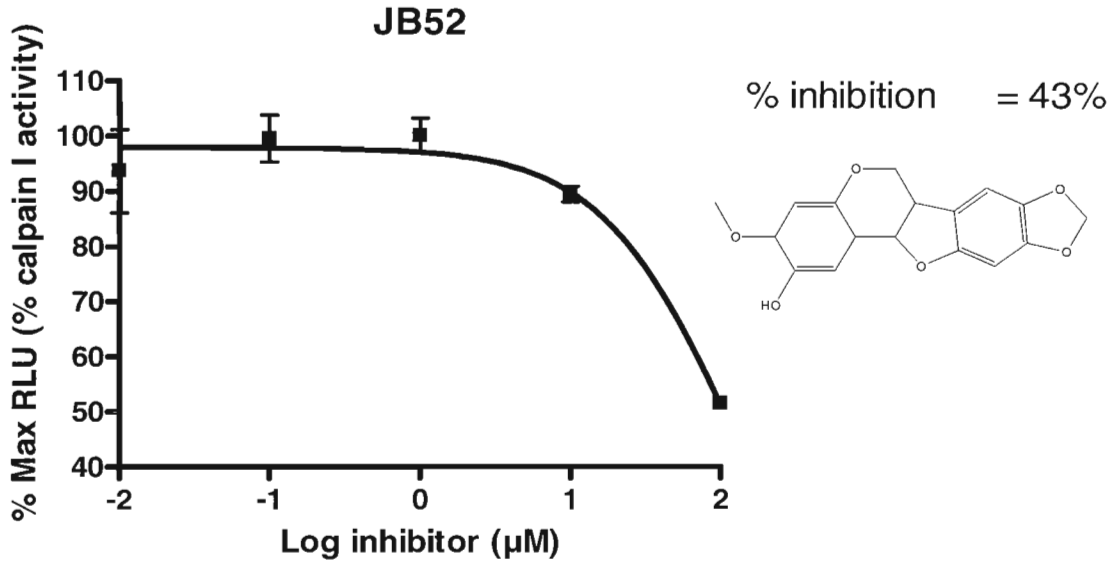

Figure 4.4: Dose-response curve for **JB52** at time 10 minutes. % Inhibition is 43% at 100 μM and R^2 = 0.9427.

Interactions between **JB52** and calpain I are shown in figure 4.5. The interaction diagrams (figures 4.5, 4.7, 4.9 and 4.11) were generated using Molecular Operating Environment (MOE). Three hydrogen bonds are formed with the side chains of the protein structure and the distance between **JB52** and Lys242, Asn168 and Lys171 is 2.89 Å, 3.16 Å and 2.36 Å respectively. There is also an arene-arene interaction between **JB52** and Phe201.

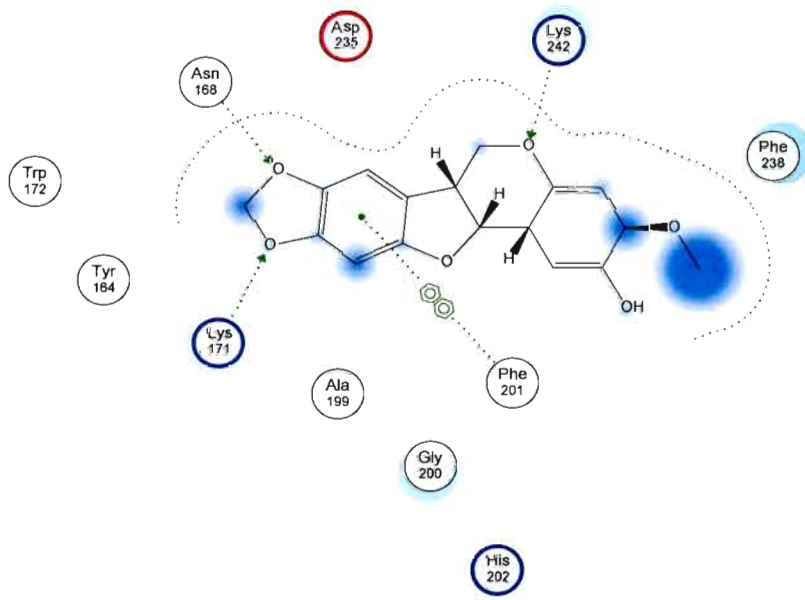

Figure 4.5: **JB52** interacting with the calpain I active site.

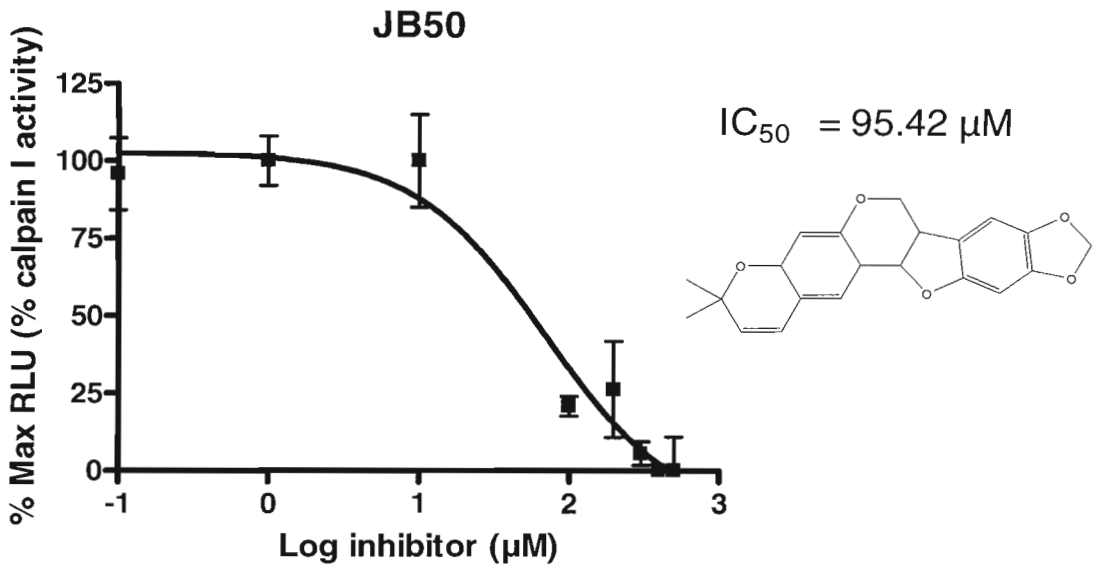

Figure 4.6: Dose-response curve for **JB50** at time 10 minutes. IC_{50} is 95.42 μM and R^2 = 0.9632.

Interactions between **JB50** and calpain I are shown in figure 4.7. Two hydrogen bonds are formed with the side chains of the protein structure and the distance between **JB50** and Lys242 and Lys171 is 2.92 Å and 2.46 Å respectively. There is also an arene-arene interaction between **JB50** and Phe201.

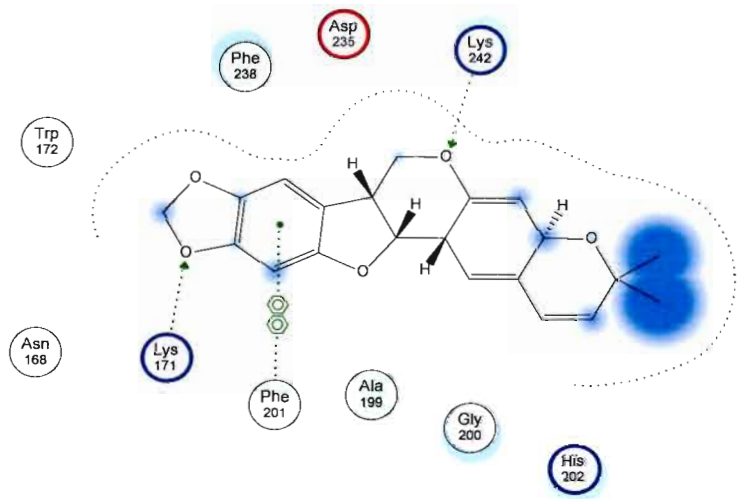

Figure 4.7: **JB50** interacting with the calpain I active site.

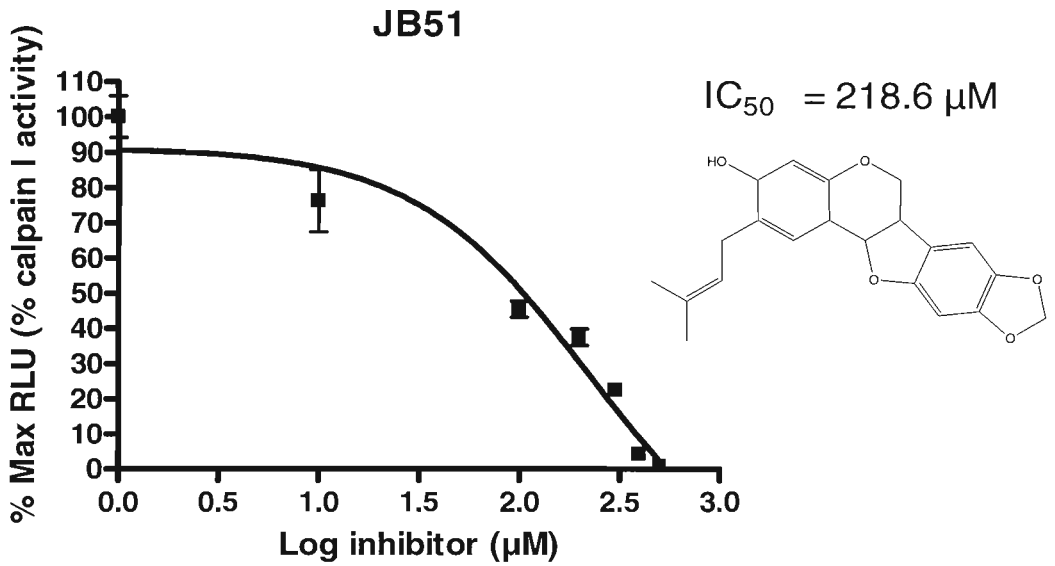

Figure 4.8: Dose-response curve for **JB51** at time 10 minutes. IC_{50} is 218.6 µM and R^2 = 0.9615.

Interactions between **JB51** and calpain I are shown in figure 4.9. Three hydrogen bonds are formed with the side chains of the protein structure and the distance between **JB51** and Lys242, Trp172 and Lys171 is 2.10 Å, 3.25 Å and 3.23 Å respectively. There is also an arene-arene interaction between **JB51** and Phe201.

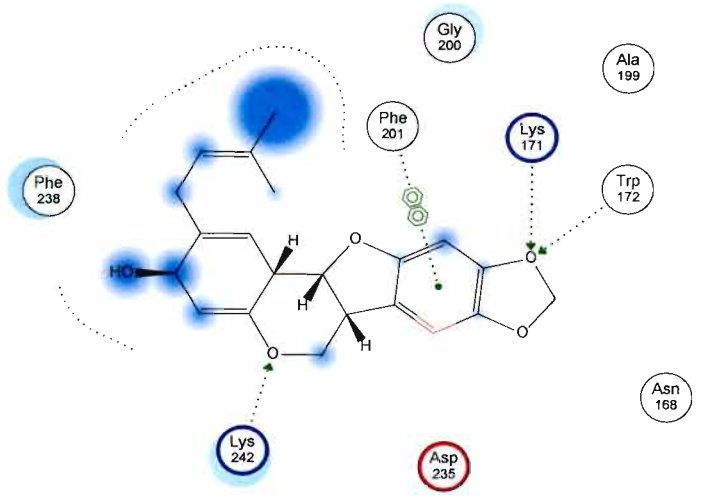

Figure 4.9: **JB51** interacting with the calpain I active site.

JB50, **JB51** and **JB52** all form hydrogen bonds with Lys242 and Lys171 as well as having an arene-arene interaction with Phe201.

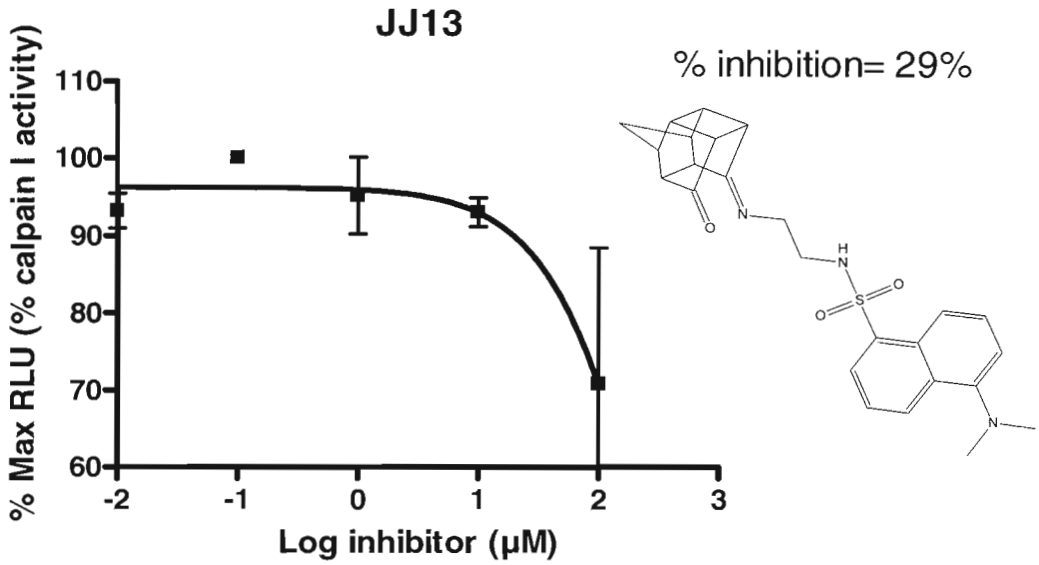

Figure 4.10: Dose-response curve for **JJ13** at time 10 minutes. % Inhibition is 29% at 100 µM and R^2 = 0.9528.

When investigating the conformation of **JJ13** on the calpain hypothesis (figure 4.12) as well as the interactions between **JJ13** and calpain I, it was found that only one point of the hypothesis (circled in figures 4.11 and 4.12) correlated with the part of **JJ13** that interacts with calpain I (figure 4.11).

A large part of **JJ13** that fits on the hypothesis does not interact with calpain I and does not even enter the active site cavity of calpain I completely (part of the compound surrounded by the dashed circle). This can explain why **JJ13** is not a potent inhibitor of calpain I although it was a hypothesis hit.

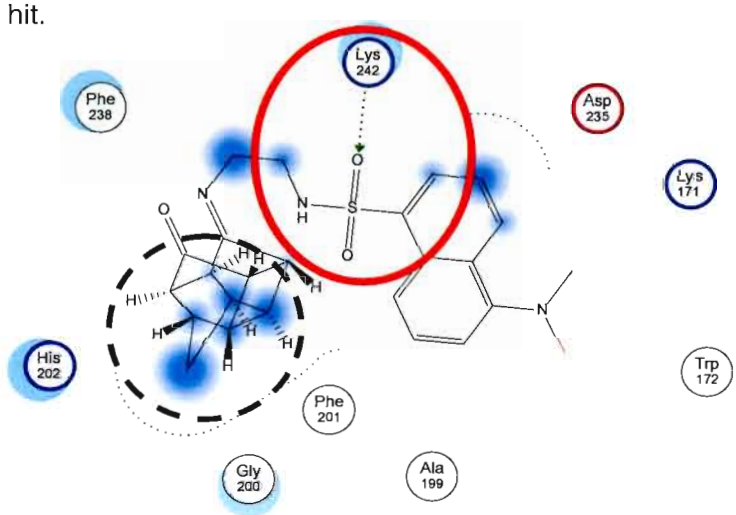

Figure 4.11: **JJ13** interacting with the calpain I active site.

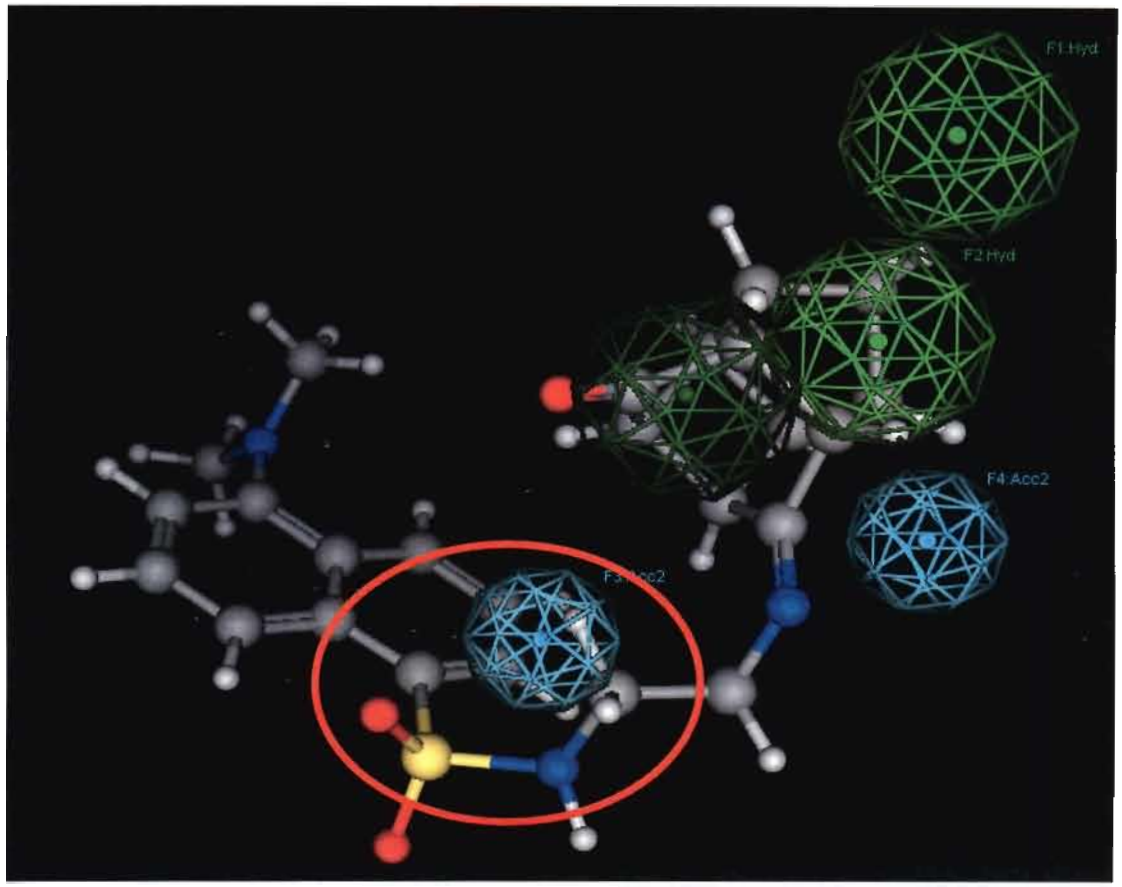

Figure 4.12: **JJ13** fitted on the calpain hypothesis.

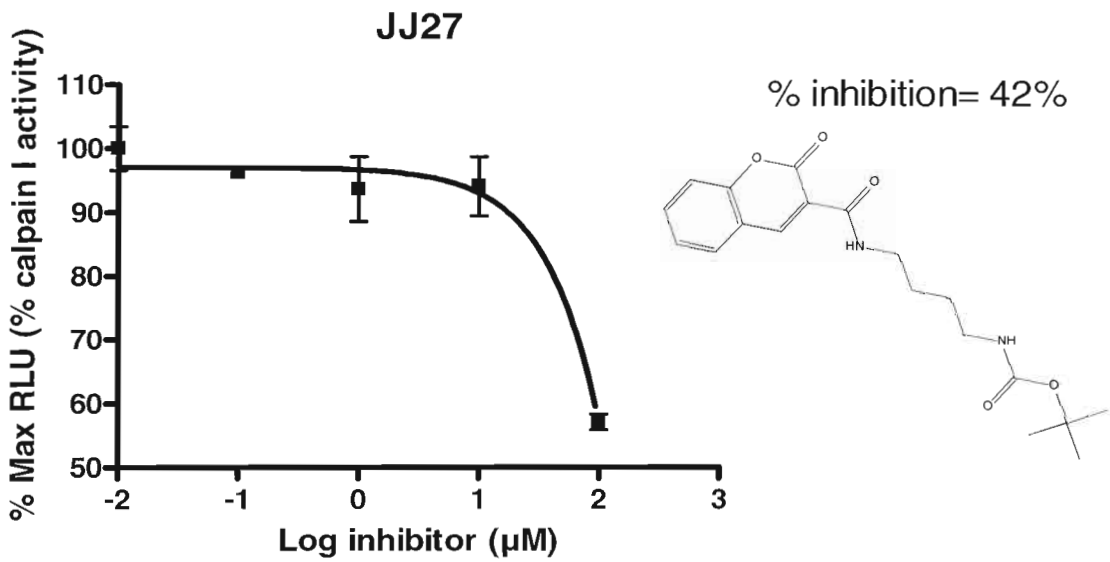

Figure 4.13: Dose-response curve for **JJ27** at time 10 minutes. % Inhibition is 42% at 100 µM and R^2= 0.9842.

A hydrogen bond is formed with the side chain of the calpain I protein structure and the distance between **JJ27** and Lys242 is 2.95 Å. There is also an arene-arene interaction between **JJ27** and Phe201.

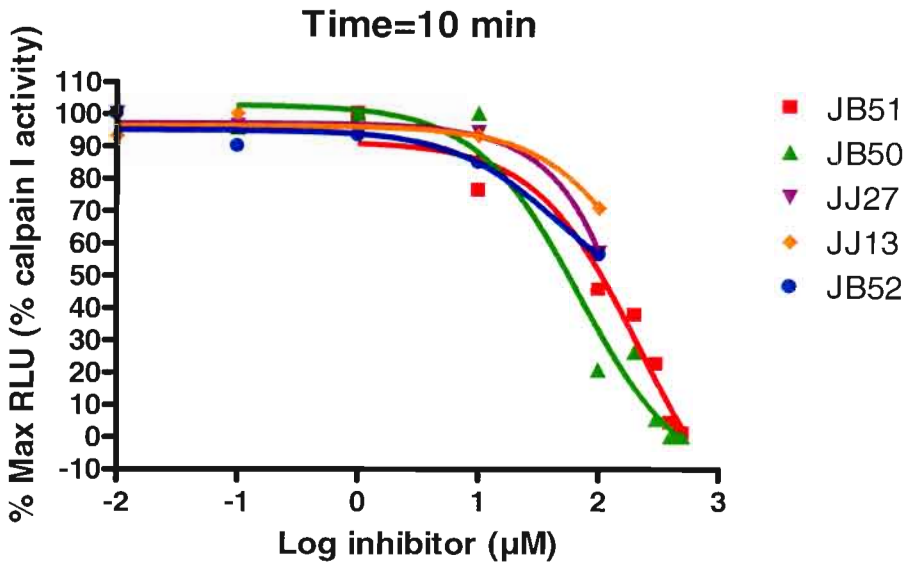

Figure 4.14: Dose-response curves of compounds in table 4.1 at time 10 minutes.

From figure 4.14 it is clear that only **JB50** and **JB51** exhibit maximal inhibition of calpain I.

To determine the K_i values for the compounds where 100% inhibition was obtained, the following equation was used:

$$K_i = \frac{IC_{50}}{1 + \frac{S}{K_m}}$$

(Cheng, 2001)

The IC_{50} is the concentration of the inhibitor producing a 50% inhibition of the enzyme, S is the substrate concentration and K_m is the Michaelis constant of the enzyme substrate (Cheng, 2001). For the calpain I assay, S was 40 µM and K_m was 40 µM as well. The K_i values determined for the inhibitors are shown in table 4.4.

Table 4.4: IC_{50} and K_i for compounds with 100% inhibition evaluated by the calpain I assay

Compound	IC_{50} (µM)	K_i from IC_{50} (µM)	% inhibition at 100 µM
JB50	95.42	47.71	54.47
JB51	218.6	109.3	79.27

4.3.2 GSK3β

100% inhibition of GSK3β was obtained at high concentrations (mM) for **JB7**, **JJ13** and **SD9** (figures 4.15, 4.17 and 4.19). **JB27** (figure 4.18) exhibited only partial inhibition at these concentrations. **LP11** (figure 4.22) and **SB216763** (figure 4.21), the positive control, showed solubility problems at higher concentrations. **JJ13** and **SD9** have similar inhibition curves, however **SD9** exhibits inhibitory activity at a lower concentration than **JJ13**. The area under the curve was the smallest for **JB7**, which was also the most active compound. **JB7** also illustrated inhibition at the lowest concentration, except when compared to **SB216763**. **LP11** only showed 45.59% inhibition of GSK3β at a concentration of 100 μM.

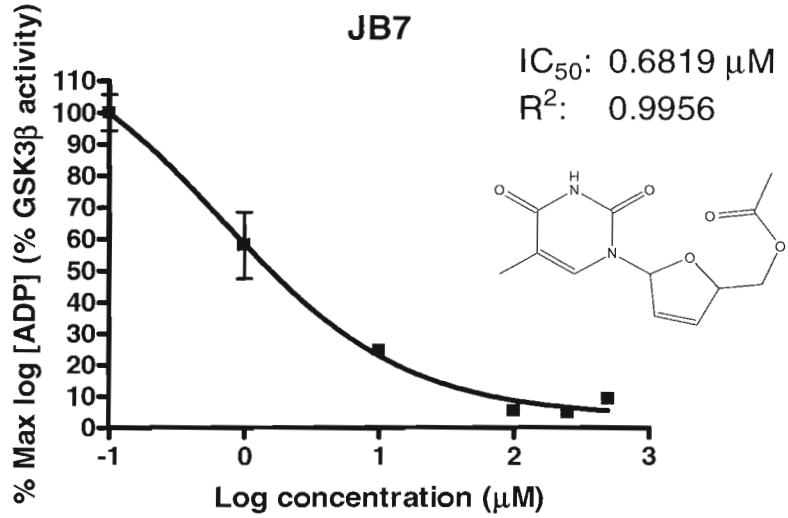

Figure 4.15: Dose-response curve for **JB7**.

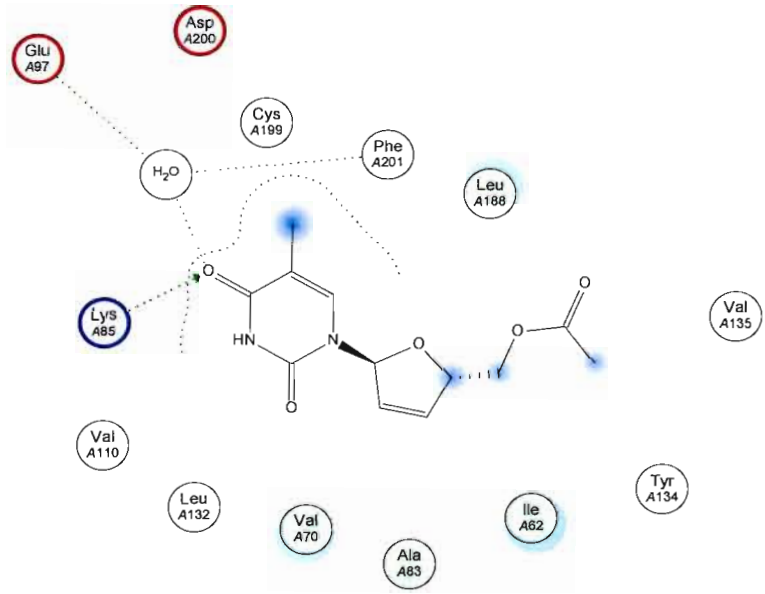

Figure 4.16: **JB7** interacting with the GSK3β active site.

Interactions between **JB7** and GSK3β are shown in figure 4.16. All interactions between the compounds and the GSK3β active site were calculated in MOE. A hydrogen bond is formed between **JB7** and the side chain of Lys85 with an interaction distance of 2.73 Å. There is also a water bridge between Glu97, Phe201, the water molecule and one of the carbonyl functions of **JB7**.

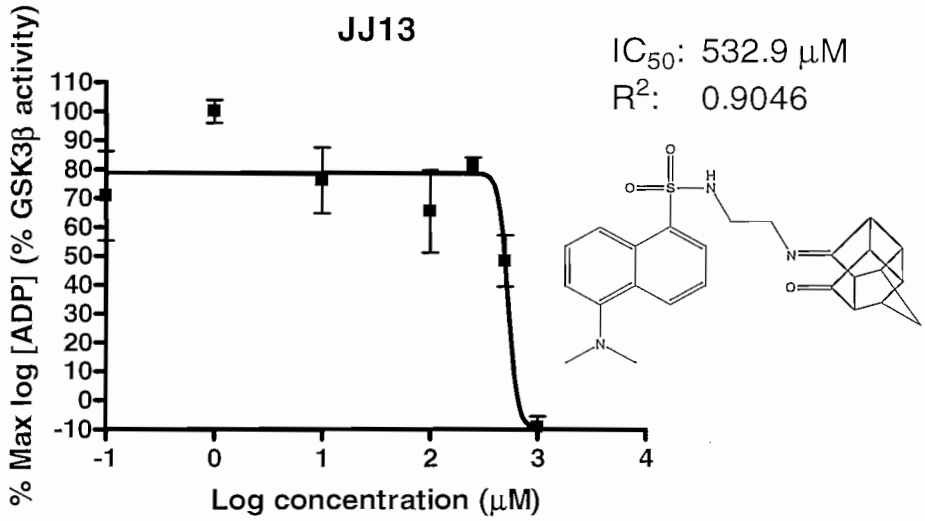

Figure 4.17: Dose-response curve for **JJ13.**

A hydrogen bond is formed between **JJ13** and the side chain of Lys183 of GSK3β. There is also a water bridge formed between the water molecule, Gln185 and **JJ13**. Significant inhibition of GSK3β is only obtained at concentrations greater than 100 µM (figure 4.17).

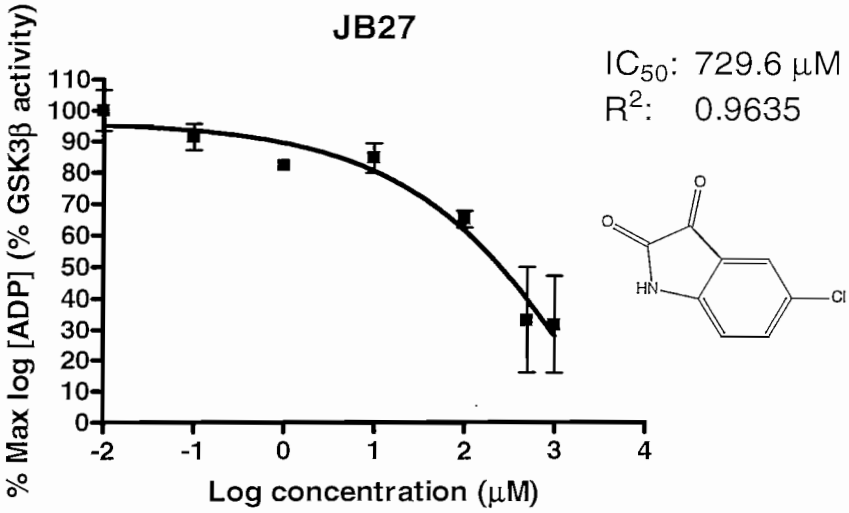

Figure 4.18: Dose-response curve for **JB27.**

A hydrogen bond is formed between **JB27** and the side chain of Lys85 with an interaction distance of 2.30 Å. There is also a water bridge between Glu97, Phe201, the water molecule and both of the carbonyl functions of **JB27**. **JB27** shows gradual inhibition of GSK3β (figure 4.18) and had the highest IC_{50} value of the compounds tested for calpain I inhibition.

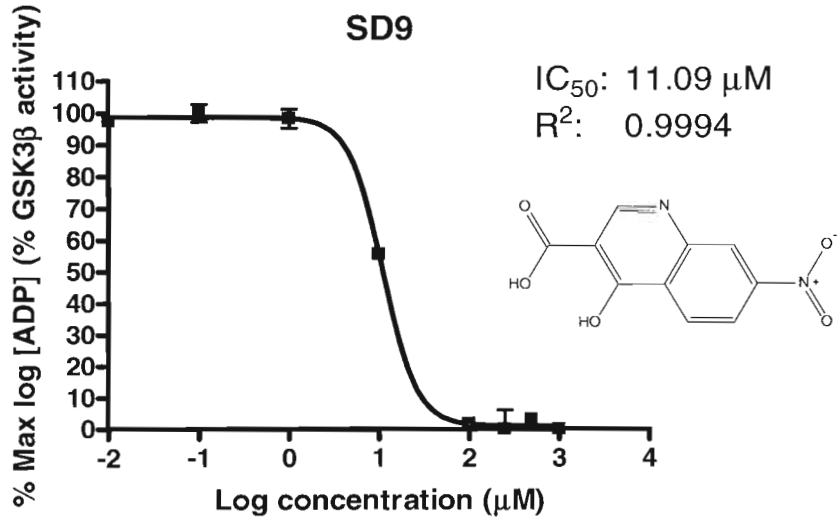

Figure 4.19: Dose-response curve for **SD9**.

The interactions between **SD9** and GSK3β are shown in figure 4.20. A hydrogen bond is formed between the carboxylic acid of **SD9** and the side chain of Lys85 with an interaction distance of 2.66 Å. This functional group also forms another hydrogen bond with the side chain of Asp200. There is also a water bridge between Asp200, Asn186, the water molecule and **SD9**. Maximal inhibition of GSK3β is already achieved at 100 µM (figure 4.19).

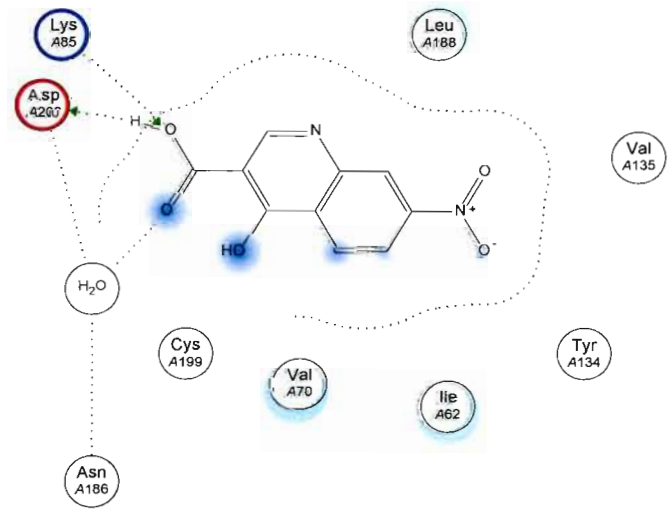

Figure 4.20: **SD9** interacting with the GSK3β active site.

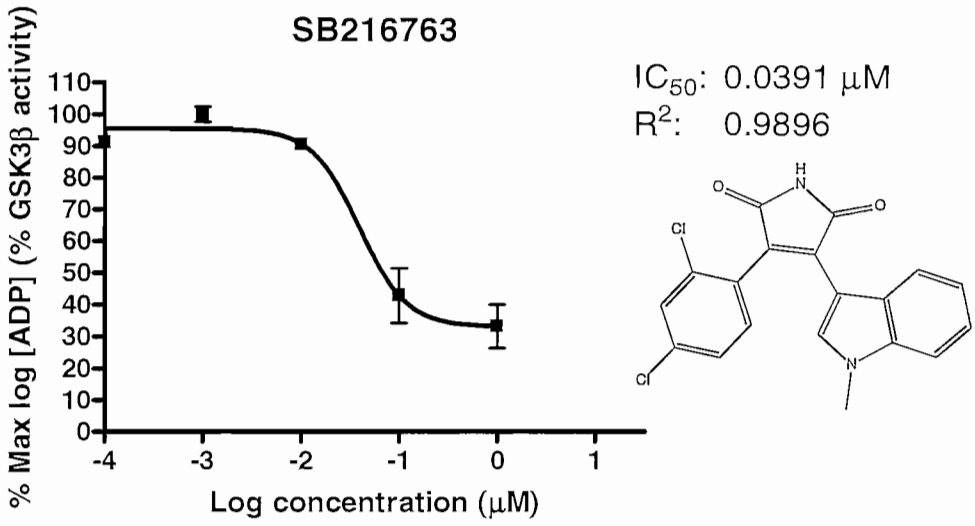

Figure 4.21: Dose-response curve for **SB216763.**

As indicated above, the solubility of the compound in the buffer limited the concentrations at which asays could be done. The calculated IC_{50} value does however correspond to that in literature (Coghlan *et al.*, 2000; Hu *et al.*, 2009). **SB216763** interacts with GSK3β by the formation of a water bridge with the water molecule and Gln185.

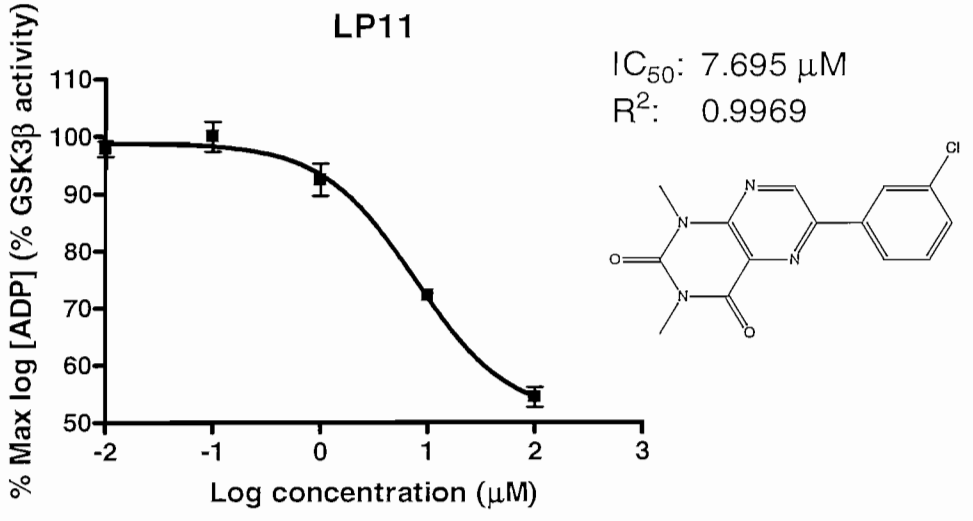

Figure 4.22: Dose-response curve for **LP11**.

LP11 also interacts with GSK3β by the formation of a water bridge with the water molecule and Gln185. 100% inhibition of GSK3β was not obtained due to solubility problems.

Table 4.5: IC_{50} values of compounds tested by GSK3β assay

Compound	IC_{50} (μM)
JB7	0.6819
JJ13	532.9
JB27	729.6[a]
SD9	11.09
SB216763	0.0391[b]
LP11	7.695[c]

[a]68.53% inhibition at 1 mM; [b]66.82% inhibition at 1 μM; [c]45.59% at 100 μM

JB7, **SD9** and **LP11** are partially structurally similar and were also the compounds with the lowest IC_{50} values, except for the positive control, **SB216763**.

4.4 Molecular dynamics studies

Molecular dynamics of the compounds tested in the biological assays were performed to obtain more insight into the interactions between the compounds and the enzymes and to possibly explain the activity of the compounds. It was also performed to determine if the conformers with the best dock scores had the lowest interaction potential.

4.4.1 Method

Molecular dynamic simulations were performed using Molecular Operating Environment (MOE) software. The 10 lowest energy conformations were used for each compound as calculated previously. The NVT ensemble was used for the molecular dynamics simulation and the Nosé-Poincaré-Anderson (NPA) algorithm was applied. In the NVT ensemble, the number of particles (N), volume (V) and temperature (T) is held constant. The temperature was held constant at 300 K and the pressure used was 101 kPa. The main simulation was done for 100 picoseconds with time steps of 0.0005 picoseconds. Water molecules and bond lengths of all bonds were constrained. The default values were used for the remainder of the parameters. The crystal structures of the enzymes (CDK5/p25, calpain, caspase 3 and GSK3β respectively) previously prepared for docking as described in chapter 3.4, were used as starting structures.

4.4.2 Results and discussion

4.4.2.1 Calpain I

The lowest and highest interaction potential between the compound and calpain I are listed in table 4.6 as well as the interaction potential energy of the conformer with the best dock score. Lower energies are seen as more favourable.

Table 4.6: Calpain I molecular dynamics results

Nr	Relative energy of conformer (kcal/mol)	Interaction potential energy between compound and calpain I (kcal/mol)	Conformer with best dock score
JB52	-13.8807	-312.6460	
	-13.1352	-337.7693	X
	-12.9768	-336.1552	
JB50	-12.0533	-326.7805	
	-11.1616	-320.4475	X
	-11.1108	-297.2298	
JB51	-12.1881	-326.2872	
	-11.6237	-325.4297	X
	-11.5073	-324.2066	
JJ13	0.2000	-368.3752	
	0.8074	-331.9472	X
	3.3192	-352.2480	
JJ27	1.000	-347.1309	
	2.5651	-338.8065	X
	3.2000	-363.0735	

Compound **JB51** and **JB52** had minimal variation between the interaction potential energy for the different energy conformers. Compound **JB50** showed only slight fluctuation between the interaction potential energy of the different energy conformers. It is interesting to note that these compounds illustrated the highest % inhibition at 100 μM.

For compound **JJ13**, the lowest energy conformer had the lowest interaction potential energy, but did not have the best dock score. This could indicate a limit in the docking procedure and the relatively large variations observed in the conformer energies would be an indication of the diverse structural conformations possible for this compound in solution.

For compound **JJ27**, the highest energy conformer had the lowest interaction potential energy. The energy necessary to obtain the optimal binding conformation could be part of the explanation for the lower activity of this compound. The conformation with the best dock score in this case however also had the highest interaction potential energy.

4.4.2.2 GSK3β

The lowest and highest interaction potential between the compound and GSK3β are shown in table 4.7 as well as the interaction potential of the conformer with the best dock score.

Table 4.7: GSK3β molecular dynamics results

Nr	Relative energy of conformer (kcal/mol)	Interaction potential energy between compound and GSK3β (kcal/mol)	Conformer with best dock score
JJ13	0.2000	-510.8900	
	1.0054	-475.5519	X
	2.6074	-495.6444	
JB7	-10.5251	-463.2505	
	-10.2387	-460.1468	X
JB27	-9.9474	-441.2477	X
	-9.4553	-442.1210	

Table 4.7 (Continued): GSK3β molecular dynamics results

SD9	0.0000	-465.5489	X
	0.8000	-458.8646	
SB216763	0.0000	-443.9855	X
	0.5441	-448.5951	
LP11	0.0000 (all conformers had identical energy)	-462.6825	X
	0.0000	-464.4275	

All of the compounds had minimal variation between the interaction potential energy of the different energy conformers. **JJ13** had the highest variation and the conformer with the best dock score did not have the lowest interaction potential energy and was also not the conformer with the lowest energy. This implicates that the lowest energy conformation is not the optimal conformation for docking.

4.5 Conclusion

From figures 4.5, 4.7 and 4.9 of the calpain I inhibitors, it is clear that hydrogen bonds between the compound and Lys171 and Lys242 of the calpain I active site as well as an arene-arene interaction with Phe201 are important for enzyme inhibition. The compounds that were hypothesis hits as well as having better dock scores than the co-crystallised ligand (**JB50** and **JB51**), also proved to be more potent experimentally than the compounds that were only hypothesis hits (**JJ13** and **JJ27**). The % inhibition at 100 μM for **JB52** and **JJ27** are similar as shown in table 4.4. **JB52**, **JB50** and **JB51** are structurally similar and are the most promising inhibitors of calpain I in this study. From the molecular dynamics investigation it was evident that the compounds (**JB50**, **JB51** and **JB52**) that exhibited the least variation between the interaction potential energy for the different energy conformers were also the most potent in the experimental study. **JJ13** and **JJ27** were less active and the lowest interaction potential energy conformers of each of these compounds were not the conformers with the best dock scores. Applying molecular dynamics for calpain I thus gave additional insight in the activity of the compounds tested as calpain I inhibitors.

From figures 4.16 and 4.20 it can be deduced that a hydrogen bond with the side chain of Lys85 and the formation of a water bridge are important interactions for the inhibition of GSK3β. The compounds (**JB7** and **JJ13**) that were hypothesis hits as well as having better dock scores than the co-crystallised ligand, were experimentally more potent than compound **JB27** which was only a hypothesis hit. Compound **SD9**, however, which was not a hypothesis hit but had a better dock score than the co-crystallised ligand, exhibited a lower IC_{50} value than **JJ13** and is thus a more potent inhibitor of GSK3β than **JJ13**. **LP11** was not a hypothesis hit but had a dock score in the same range as the co-crystallised ligand and was included in the biological assays due to its partial structural similarities to **JB7** and **SD9**. It showed a maximum inhibitory activity for GSK3β of 45.59% at 100 μM (insoluble at higher concentrations). The molecular dynamics studies of the GSK3β-inhibitor complexes of the different conformers of the compounds tested for GSK3β inhibitory activity gave little or no additional insight regarding the activity of the compounds.

SB216763 is a potent inhibitor of GSK3β and the IC_{50} value obtained in this study corresponds to that in literature (Coghlan *et al.*, 2000).

It is therefore clear from these investigations that by combining a pharmacophore hypothesis with docking studies, novel structures can successfully be investigated for their potential as inhibitors of the enzymes involved in apoptosis such as calpain I and GSK3β. Further investigation into the structures that showed promising inhibitory activity for these enzymes are indeed warranted. Refinement of these methods would however be essential.

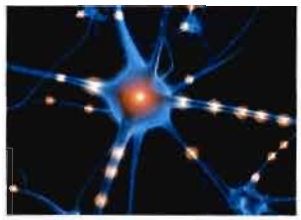

5 Conclusion

CDK5/p25, calpain I, caspase 3 and GSK3ß are some of the major enzymes that play a role in the apoptotic processes that lead to neurodegenerative diseases as discussed in detail in chapter 2. Calpain plays a prominent role in neurodegeneration, starting with its activation by calcium. Calpain then cleaves p35 directly to 25 (Kusakawa *et al.*, 2000) and p25 activates and deregulates CDK5, leading to apoptosis (Tsai *et al.*, 2004). Calpain can also lead to apoptosis by activating caspase 3 and 12 (Saez *et al.*, 2006). Neuronal apoptosis can further be induced by the over expression of GSK3ß (Cohen & Goedert, 2004) and It has been shown that GSK3ß increases Aß (Cohen & Goedert, 2004) and hyperphosphorylates tau (Wagman *et al.*, 2004).

In this study, small molecule pharmacophore hypotheses were formulated using training sets of structures obtained from various literature sources for the respective enzymes. In-house libraries were subsequently screened for molecules in compliance with the hypotheses. Docking studies were performed using the compounds in the in-house library. The compounds that illustrated the most promising results from the hypothesis compliance combined with the docking studies, were selected for the experimental proof of concept. This was performed by biological assays for calpain I and GSK3ß. Molecular dynamics of the enzyme-inhibitor complexes of the compounds used for the biological assays were performed.

The pharmacophore hypotheses for CDK5/p25, calpain, caspase 3 and GSK3ß all included features representing hydrogen bond donors and/or acceptors. This highlights the important role of the hydrogen bond interactions that are crucial for inhibitory activity for each of the enzymes. All four of the pharmacophore hypotheses also included hydrophobic regions. The pharmacophore hypotheses for both of the kinases, CDK5/p25 and GSK3ß, further included aromatic areas for key interactions.

From the validation of the model, in which a pharmacophore hypothesis was combined with docking studies, it was clear that this approach would not be sufficient to predict caspase 3 and CDK5/p25 activity accurately. The prediction potential for GSK3ß and calpain were 80% and 65% respectively and was thus used for the biological screening process.

The biological assays performed for calpain I and GSK3β to determine if the compounds that were theoretically identified as potential inhibitors (by using a pharmacophore hypothesis combined with docking studies), actually showed inhibition *in vitro*. The most potent inhibitor identified for calpain I (**JB50**), which was a hypothesis hit as well as having a higher dock score than the calpain I co-crystallised ligand, had an IC_{50} value of 95.42 μM. The most potent inhibitor identified for GSK3β (**JB7**), which was a hypothesis hit as well as having a higher dock score than the GSK3β co-crystallised ligand, had an IC_{50} value of 0.6819 μM.

Furthermore, the compounds that were calpain hypothesis hits as well as having better dock scores than the co-crystallised ligand (**JB50** and **JB51**), proved to be more potent experimentally than the compounds that were only hypothesis hits (**JJ13** and **JJ27**). The compounds (**JB7** and **JJ13**) that were GSK3β hypothesis hits as well as having better dock scores than the co-crystallised ligand, were experimentally also more potent than compound **JB27**, which was only a hypothesis hit.

From the molecular modelling done on the above structures, it is clear that hydrogen bonds between the inhibitor and Lys171 and Lys242 as well as an arene-arene interaction with Phe201 of the calpain I active site are essential for enzyme inhibition. The formation of a hydrogen bond with the side chain of Lys85 and the formation of a water bridge are important interactions between a compound and GSK3β for its inhibition.

Following from the molecular dynamics studies, it is evident that the compounds (**JB50**, **JB51** and **JB52**) that showed slight variation between the interaction potential energy for the different energy conformers, were the most active calpain I inhibitors *in vitro*. **JJ13** and **JJ27** were less active and the lowest interaction potential energy conformers of these compounds seemed not to be the conformers with the best conformation for enzyme binding. The molecular dynamics study for calpain I inhibitors thus gave some explanation regarding the activity of the compounds. For GSK3β, no explanation for the activity observed during the GSK3β biological assay could be obtained from the molecular dynamics runs.

From the above it can be concluded that the combination of a pharmacophore hypothesis and docking simulations proved to be valuable in identifying scaffolds and can be effectively applied during drug design of kinase and other enzyme inhibitors. The identified scaffolds could be further optimised as drug leads to design potent inhibitors during future studies. This optimisation can include refining the hypotheses and docking simulations as well as performing SAR and QSAR studies using the identified scaffolds.

References

ADLARD, P.A. & CUMMINGS B.J. 2004. Alzheimer's disease- a sum greater than its parts? *Neurobiology of aging*, 25(6):725-733.

AHN. J.S., RADHAKRISHNAN, M.L., MAPELLI, M., CHOI, S., TIDOR, B., CUNY, G.D., MUSACCHIO, A., YEH, L.A. & KOSIK, K.S. 2005. Defining cdk5 ligand chemical space with small molecule inhibitors of tau phosphorylation. *Chemistry & biology*, 12(7):811-823.

ALLEN. D.A., PHAM, P., CHOONG, I.C., FAHR, B., BURDETT, M.T., LEW, W., DELANO, W.L., GORDON, E.M., LAM, J.W., O'BRIEN, T. & LEE, D. 2003. Identification of potent and novel small-molecule inhibitors of caspase-3. *Bioorganic & medicinal chemistry letters*, 13(21):3651-3655.

ALVIRA, D., TAJES, M., VERDAGUER, E., ACUÑA-CASTROVIEJO, D., FOLCH, J., CAMINS, A. & PALLAS, M. 2006. Inhibition of the cdk5/p25 fragment formation may explain the antiapoptotic effects of melatonin in an experimental model of parkinson's disease. *Journal of pineal research*, 40(3):251-258.

BARZILAI, A. & MELAMED, E. 2003. Molecular mechanisms of selective dopaminergic neuronal death in Parkinson's disease. *Trends in molecular medicine*, 9(3):126-132.

BECKER, J.W., ROTONDA, J., SOISSON, S.M., ASPIOTIS, R., BAYLY, C., FRANCOEUR, S., GALLANT, M., GARCIA-CALVO, M., GIROUX, A., GRIMM, E., HAN, Y., MCKAY, D., NICHOLSON, D.W., PETERSON, E., RENAUD, J., ROY, S., THORNBERRY, N. & ZAMBONI, R. 2004. Reducing the peptidyl features of caspase-3 inhibitors: a structural analysis. *Journal of medicinal chemistry*, 47(10):2466-2474.

BIHOVSKY, R., TAO, M., MALLAMO, J.P. & WELLS, G.J. 2004. 1,2-Benzothiazine 1,1-dioxide α-ketoamide analogues as potent calpain I inhibitors. *Bioorganic & medicinal chemistry letters*, 14(4):1035-1038.

BRANCHINI, B.R., ABLAMSKY, D.M., MURTIASHAW, M.H., UZASCI, L., FRAGA, H. & SOUTHWORHT, T.L. 2007. Thermostable red and green light-producing firefly luciferase mutants for bioluminescent reporter applications. *Analytical biochemistry*, 361(2):253-262.

CARRAGHER, N.O. 2006. Calpain inhibition: a therapeutic strategy targeting multiple disease states. *Current pharmaceutical design*, 12(5):615-638.

CASTRO, A., ENCINAS, A., GIL, C., BRASE, S., PORCAL, W., PEREZ, C., MORENO, F.J. & MARTINEZ, A. 2008. Non-ATP competitive glycogen synthase kinase 3β (GSK-3β) inhibitors: study of structural requirements for thiadiazolidinone derivatives. *Bioorganic & medicinal chemistry*, 16(1):495-510.

CAVALLI, A., BOLOGNESI, M.L., MINARINI, A., TUMIATTI, V., RECANATINI, M. & MELCHIORRE, C. 2008. Multi-target-directed ligands to combat neurodegenerative diseases. *Journal of medicinal chemistry*, 51(3):347-372.

CHANG, C., EKINS, S., BAHADDURI, P. & SWAAN, P.W. 2006. Pharmacophore-based discovery of ligands for drug transporters. *Advanced drug delivery reviews*, 58(12-13):1431-1450.

CHATTERJEE. S., SENADHI, S., BOZYCZKO-COYNE, D., SIMAN, R. & MALLAMO, J.P. 1997. Nonpeptidic inhibitors of recombinant human calpain I. *Bioorganic & medicinal chemistry letters*, 7(3):287-290.

CHEN, Y.H., ZHANG, Y.H., ZHANG, H.J., LIU, D.Z., GU, M., LI, J.Y., WU, F., ZHU, X.Z., LI, J. & NAN, F.J. 2006. Design, synthesis and biological evaluation of isoquinoline-1,3,4-trione derivatives as potent caspase-3 inhibitors. *Journal of medicinal chemistry*, 49(5):1613-1623.

CHENG, H.C. 2001. The power issue: determination of K_B of K_i from IC_{50}. A closer look at the Cheng-Prusoff equation, the Schild plot and related power equations. *Journal of pharmacology and toxicological methods*, 46(2):61-71.

CHEUNG, Z.H. & IP, N.Y. 2004. Cdk5: mediator of neuronal death and survival. *Neuroscience letters*, 361(1-3):47-51.

CHICHARRO, R., ALONSO, M., ARAN, V.J. & HERRADON, B. 2008. Studies on calpain inhibitors. Synthesis of partially reduced isoquinoline-1-thione derivatives and conversion to functionalized 1-chloroisoquinolines. *Tetrahedron letters*, 49(14):2275-2279.

CHIN, P.C., MAJDZADEH, N. & D'MELLO, S.R. 2005. Inhibition of gsk3β is a common event in neuroprotection by different survival factors. *Molecular brain research*, 137(1-2):193-201.

CHU, W., ZHANG, J., ZENG, C., ROTHFUSS, J., TU, Z., CHU, Y., REICHERT, D.E., WELCH, M.J. & MACH, R.H. 2005. N-benzylisatin sulfonamide analogues as potent caspase-3 inhibitors: synthesis, in vitro activity, and molecular modeling studies. *Journal of medicinal chemistry*, 48(24):7637-7647.

CHURCHER, I. 2006. Tau therapeutic strategies for the treatment of alzheimer's disease. *Current topics in medicinal chemistry*, 6(6):579-595.

COGHLAN, M.P., CULBERT, A.A., CROSS, D.A.E., CORCORAN, S.L., YATES, J.W., PEARCE, N.J., RAUSCH, O.L., MURPHY, G.J., CARTER, P.S., COX, L.R., MILLS, D., BROWN, M.J., HAIGH, D., WARD, R.W., SMITH, D.G., MURRAY, K.J., REITH, A.D. & HOLDER, J.C. 2000. Selective small molecule inhibitors of glycogen synthase kinase-3 modulate glycogen metabolism and gene transcription. *Chemistry & biology*, 7(10):793-803.

COHEN, P. & GOEDERT, M. 2004. Gsk3 inhibitors: development and therapeutic potential. *Nature Reviews Drug Discovery,* 3(6):479-487.

COLANTONIO, P., LEBOFFE, L., BOLLI, A., MARINO, M., ASCENZI, P. & LUISI, G. 2008. Human caspase-3 inhibition by Z-*t*Leu-Asp-H: *t*Leu(P_2) counterbalances Asp(P_2) and Glu(P_3) specific inhibitor truncation. *Biochemical and biophysical research communications*, 377(3):757-762.

CONCHA, N.O. & ABDEL-MEGUID, S.S. 2002. Controlling apoptosis by inhibition of caspases. *Current medicinal chemistry*, 9(6):713-726.

CORTI, O., HAMPE, C., DARIOS, F., IBANEZ, P., RUBERG, M. & BRICE, A. 2005. Parkinson's disease: from causes to mechanisms. *Comptes rendus biologies*, 328(2):131-142.

CUERRIER, D., MOLDOVEANU, T., DAVIES, P.L. & CAMPBELL, R.L. 2006. Calpain inhibition by α-ketoamide and cyclic hemiacetal inhibitors revealed by x-ray crystallography. *Biochemistry*, 45(24):7446-7452.

DAI, Y. & GRANT, S. 2003. Cyclin-dependent kinase inhibitors. *Current opinion in pharmacology*, 3(4):362-370.

DHAVAN, R. & TSAI, L. 2001. A decade of cdk5. *Nature reviews molecular cell biology*, 2(10):749-759.

ENGEL, T., LUCAS, J.J., GÓMEZ-RAMOS, P., MORAN, M.A., ÁVILA, J. & HERNÁNDEZ, F. 2006. Cooexpression of FTDP-17 tau and GSK-3β in transgenic mice induce tau polymerisation and neurodegeneration. *Neurobiology of aging*, 27(9):1258-1268.

ENGLER, T.A., MALHOTRA, S., BURKHOLDER, T.P., HENRY, J.R., MENDEL, D., PORTER, W.J., FURNESS, K., DIEFENBACHER, C., MARQUART, A., REEL, J.K., LI, Y., CLAYTON, J., CUNNINGHAM, B., MCLEAN, J., O'TOOLE, J.C., BROZINICK, J., HAWKINS, E., MISENER, E., BRIERE, D., BRIER, R.A., WAGNER, J.R., CAMPBELL, R.M., ANDERSON, B.D., VAUGHN, R., BENNETT, D.B., MEIER, T.I. & COOK, J.A. 2005. The development of potent and selective bisarylmaleimide gsk3 inhibitors. *Bioorganic & medicinal chemistry letters*, 15(4):899-903.

FERNÁNDEZ-VIZARRA, P., FERNÁNDEZ, A.P., CASTRO-BLANCO, S., ENCINAS, J.M., SERRANO, J., BENTURA, M.L., MUÑOZ, P., MARTINEZ-MURILLO, R. & RODRIGO, J. 2004. Expression of nitric oxide system in clinically evaluated cases of Alzheimer's disease. *Neurobiology of disease*, 15(2):287-305.

GANESAN, R., MITTL, P.R.E., JELAKOVIC, S. & GRÜTTER, M.G. 2006. Extended substrate recognition in caspase-3 revealed by high resolution x-ray structure analysis. *Journal of molecular biology*, 359(5):1378-1388.

GERITS, N., KOSTENKO, S. & MOENS, U. 2006. In vivo functions of mitogen-activated protein kinases: conclusions from knock-in and knock-out mice. *Transgenic research*, 16(3):281-314.

GÓMEZ-RAMOS, A., DOMÍNGUEZ, J., ZAFRA, D., COROMINOLA, H., GOMIS, R., GUINOVART, J.J. & AVILA, J. 2006. Inhibition of gsk3 dependent tau phosphorylation by metals. *Current Alzheimer research*, 3(2):123-127.

GOODMAN, A.O.G., MURGATROYD, P.R., MEDINA-GOMEZ, G., WOOD, N.I., FINER, N., VIDAL-PUIG, A.J., MORTON, A.J. & BARKER R.A. 2008. The metabolic profile of early Huntington's disease- a combined human and transgenic mouse study. *Experimental neurology*, 210(2):691-698.

GRIMM, E.L., ROY, B., ASPIOTIS, R., BAYLY, C.I., NICHOLSON, D.W., RASPER, D.M., RENAUD, J., ROY, S., TAM, J., TAWA, P., VAILLANCOURT, J.P., XANTHOUDAKIS, S., ZAMBONI, R.J. 2004. Solid phase synthesis of selective caspase-3 peptide inhibitors. *Bioorganic & medicinal chemistry*, 12(5):845-851.

GURWITZ, D. & ELDAR-FINKELMAN, H. 2001. GSK-3 inhibitors: potential drugs for neurodegenerative disorders. *Drug discovery today*, 6(20):1072-1074.

HAGEMANN, C. & BLANK, J.L. 2001. The ups and downs of MEK kinase interactions. *Cellular signalling*, 13(12):863-875.

HAMANN, M., ALONSO, D., MARTIN-APARICIO, E., FUERTES, A., PEREZ-PUERTO, M.J., CASTRO, A., MORALES, S., NAVARRO, M.L., DEL MONTE-MILLAN, M., MEDINA, M., PENNAKA, H., BALAIAH, A., PENG, J., COOK, J., WAHYOUONO, S. & MARTINEZ, A. 2007. Glycogen synthase kinase-3 (GSK-3) inhibitory activity and structure-activity relationship (SAR) studies of the manzamine alkaloids. Potential for Alzheimer's disease. *Journal of natural products*, 70(9):1397-1405.

HAN, Y., GIROUX, A., GRIMM, E.L., ASPIOTIS, R., FRANCOEUR, S., BAYLY, C.I., MCKAY, D.J, ROY, S., XANTHOUDAKIS, S., VAILLANCOURT, J.P, RASPER, D.M., TAM, J., TAWA, P., THORNBERRY, N.A., PATERSON, E.P., GARCIA-CALVO, M., BECKER, J.W., ROTONDA, J., NICHOLSON, D.W. & ZAMBONI, R.J. 2004. Discovery of novel aspartyl ketone dipeptides as potent and selective caspase-3 inhibitors. *Bioorganic & medicinal chemistry letters*, 14(3):805-808.

HAN, Y., GIROUX, A., COLUCCI, J., BAYLY, C.I., MCKAY, D.J, ROY, S., XANTHOUDAKIS, S., VAILLANCOURT, J., RASPER, D.M., TAM, J., TAWA, P., NICHOLSON, D.W. & ZAMBONI, R.J. 2005. Novel pyrazinone mono-amides as potent and reversible caspase-3 inhibitors. *Bioorganic & medicinal chemistry letters*, 15(4):1173-1180.

HARISH, B.G., KRISHNA, V., SANTOSH KUMAR, H.S., KHADEER AHAMED, B.M., SHARATH, R. & KUMARA SWAMY, H.M. 2008. Wound healing activity and docking of glycogen-synthase-kinase-3-β-protein with isolated triterpenoid lupeol in rats. *Phytomedicine,* 15(9):763-767.

HEINER, M., KOCH, I. & WILL, J. 2004. Model validation of biological pathways using petri nets-demonstrated for apoptosis. *Biosystems*, 75(1-3):15-28.

HELAL, C.J., SANNER, M.A., COOPER, C.B., GANT, T., ADAM, M., LUCAS, J.C., KANG, Z., KUPCHINSKY, S., AHLIJANIAN, M.K., TATE, B., MENNITI, F.S., KELLY, K. & PETERSON, M. 2004. Discovery and SAR of 2-aminothiazole inhibitors of cyclin-dependent kinase 5/p25 as a potential treatment for alzheimer's disease. *Bioorganic & medicinal chemistry letters*, 14(22):5521-5525.

HERNANDEZ, A.A. & ROUSH, W.R. 2002. Recent advances in the synthesis, design and selection of cysteine protease inhibitors. *Current opinion in chemical biology*, 6(4):459-465.

HIGUCHI, M., IWATA, N. & SAIDO, T.C. 2005. Understanding molecular mechanisms of proteolysis in alzheimer's disease: progress toward therapeutic interventions. *Biochimica et biophysica acta*, 1751(1):60-7.

HÖLSCHER, C. 1998. Possible causes of alzheimer's disease: amyloid fragments, free radicals, and calcium homeostasis. *Neurobiology of diseases*, 5(3):129-141.

HOLZER, M., GÄRTNER, U., KLINZ, F.J., NARZ, F., HEUMANN, R. & ARENDT, T.H. 2001. Activation of mitogen-activated protein kinase cascade and phosphorylation of cytoskeletal proteins after neurone-specific activation of p21ras. I. Mitogen-activated protein kinase cascade. *Neuroscience*, 105(4):1031-1040.

HONMA, N., ASADA, A., TAKESHITA, S., ENOMOTO, M., YAMAKAWA, E., TSUTSUMI, K., SAITO, T., SATOH, T., ITOH, H., KAZIRO, Y., KISHIMOTO, T. & HISANAGA, S. 2003. Apoptosis-associated tyrosine kinase is a cdk5 activator p35 binding protein. *Biochemical and biophysical research communications*, 310(2):398-404.

HU, S., BEGUM, A.N., JONES, M.R., OH, M.S., BEECH, W.K., BEECH, B.H., YANG, F., CHEN, P., UBEDA, O.J., KIM, P.C., DAVIES, P., MA, Q., COLE, G.M. & FRAUTSCHY, S.A. 2009. GSK3 inhibitors show benefits in an Alzheimer's disease (AD) model of neurodegeneration but adverse effects in control animals. *Neurobiology of disease*, 33(2):193-206.

ISABEL, E., BLACK, W.C., BAYLY, C.I., GRIMM, E.L., JANES, M.K., MCKAY, D.J., NICHOLSON, D.W., RASPER, D.M., RENAUD, J., ROY, S., TAM, J., THORNBERRY, N.A., VAILLANCOURT, J.P., XANTHOUDAKIS, S. & ZAMBONI, R. 2003. Nicotinyl aspartyl ketones as inhibitors of caspase-3. *Bioorganic & medicinal chemistry letters*, 13(13):2137-2140.

ISABEL, E., ASPIOTIS, R., BLACK, W.C., COLUCCI, J., FORTIN, R., GIROUX, A., GRIMM, E.L., HAN, Y., MELLON, C., NICHOLSON, D.W., RASPER, D.M., RENAUD, J., ROY, S., TAM, J., TAWA, P., VAILLANCOURT, J.P., XANTHOUDAKIS, S. & ZAMBONI, R.J. 2007. Solid-phase analogue synthesis of caspase-3 inhibitors via palladium-catalyzed amination of 3-bromopyrazinones. *Bioorganic & medicinal chemistry letters*, 17(6):1671-1674.

JONES, M.A., MORTON, J.D., COXON, J.M., MCNABB, S.B., LEE, H.Y.Y., AITKEN, S.G., MEHRTENS, J.M., ROBERTSON, L.J.G., NEFFE, A.T., MIYAMOTO, S., BICKERSTAFFE, R., GATELY, K., WOOD, J.M. & ABELL, A.D. 2008. Synthesis, biological evaluation and molecular modelling of N-heterocyclic dipeptide aldehydes as selective calpain inhibitors. *Bioorganic & medicinal chemistry*, 16(14):6911-6923.

JOSEF, K.A., KAUER, F. & BIHOVSKY, R. 2001. Potent peptide α-ketohydroxamate inhibitors of recombinant human calpain I. *Bioorganic & medicinal chemistry letters*, 11(19):2615-2617.

JUSUF, A.A., SUSILOWATI, R., SAKAGAMI, H. & TERASIMA, T. 2002 Expression of ca^{2+}/calmodulin-dependent protein kinase (CaMK) Iβ2 in developing rat CNS. *Neuroscience*, 109(3):407-420.

KAWAMURA, M., NAKAJIMA, W., ISHIDA, A., OHMURA, A., MIURA, S. & TAKADA, G. 2005. Calpain inhibitor MDL 28170 protects hypoxic-ischemic brain injury in neonatal rats by inhibition of both apoptosis and necrosis. *Brain research*, 1037(1-2):59-69.

KIM, H.J., CHOO, H., CHO, Y.S., NO, K.T. & PAE, A.N. 2008. Novel GSK-3β inhibitors from sequential virtual screening. *Bioorganic & medicinal chemistry*, 16(2):636-643.

KNOCKAERT, M., GREENGARD, P. & MEIJER, L. 2002. Pharmacological inhibitors of cyclin-dependent kinases. *Trends in pharmacological sciences*, 23(9):417-425.

KOČA, J., LUDIN, M., PÉREZ, S. & IMBERTY, A. 2000. Single-coordinate-driving method for molecular docking: application to modeling of guest inclusion in cyclodextrin. *Journal of molecular graphics and modelling*, 18(2):108-118.

KOH, C.H.V., QI, R.Z., QU, D., MELENDEZ, A., MANIKANDAN, J., BAY, B.H., DUAN, W. & CHEUNG, N.S. 2006. U18666A-mediated apoptosis in cultured murine cortical neurons: role of caspases, calpains and kinases. *Cellular signalling*, 18(10):1572-1583.

KOIVUNEN, J., AALTONEN, V. & PELTONEN, J. 2006. Protein kinase C (PKC) family in cancer progression. *Cancer letters*, 235(1):1-10.

KOLCH, W. 2000. Meaningful relationships: the regulation of the ras/raf/MEK/ERK pathway by protein interactions. *Biochemical journal*, 351(2):289-305.

KORYAKOVA, A.G., RYZHOVA, E.A., BULANOVA E.A., KARAPETIAN, R.N., MIKITAS, O.V., KATRUKHA, E.A., KAZEY, V.I., OKUN, I., KRAVCHENKO, D.V., LAVROVSKY, Y.V., KORZINOV, O.M. & IVACHTCHENKO, A.V. 2007. Novel aryl and heteroaryl substituted N-[1-(4-phenylpiperazin-1-yl)propyl]-1,2,4-oxadiazole-5-carboxamides as selective GSK-3 inhibitors. *Bioorganic & medicinal chemistry letters*, 18(12):3661-3666.

KRAVCHENKO, D.V., KUZOVKOVA, J.A., KYSIL, V.M., TKACHENKO, S.E., MALIARCHOUK, S., OKUN, I.M. & IVACHTCHENKO, A.V. 2006. Pyrrolo[3,4-c]quinoline-1,3-diones as potent caspase-3 inhibitors: synthesis and SAR of 8-sulfamoyl-1,3-dioxo-2,3-dihydro-1H-pyrrolo[3,4-c]quinolines. *Letters in drug design and discovery*, 3(1):61-70.

[a]KRAVCHENKO, D.V., KYSIL, V.M., ILYN, A.P., TKACHENKO, S.E., MALIARCHOUK, S., OKUN, I.M. & IVACHTCHENKO, A.V. 2005. 1,3-Dioxo-4-methyl-2,3-dihydro-1H-pyrrolo[3,4-

c]quinolines as potent caspase-3 inhibitors. *Bioorganic & medicinal chemistry letters*, 15(7):1841-1845.

[b]KRAVCHENKO, D.V., KYSIL, V.M., TKACHENKO, S.E., MALIARCHOUK, S., OKUN, I.M. & IVACHTCHENKO, A.V. 2005. Pyrrolo[3,4-c]quinoline-1,3-diones as potent caspase-3 inhibitors. Synthesis and SAR of 2-substituted 4-methyl-8-(morpholine-4-sulfonyl)-pyrrolo[3,4-c]quinoline-1,3-diones. *European journal of medicinal chemistry*, 40(12):1377-1383.

KUO, G.H., PROUTY, C., DEANGELIS, A., SHEN, L., O'NEILL, D.J., SHAH, C., CONNOLLY, P.J., MURRAY, W.V., CONWAY, B.R., CHEUNG, P., WESTOVER, L., XU, J.Z., LOOK, R.A., DEMAREST, K.T., EMANUEL, S., MIDDLETON, S.A., JOLLIFFE, L., BEAVERS, M.P. & CHEN, X. 2003. Synthesis and discovery of macrocyclic polyoxygenated bis-7-azaindolylmaleimides as novel series of potent and highly selective glycogen synthase kinase-3β inhibitors. *Journal of medicinal chemistry*, 46(19):4021-4031.

KUSAKAWA, G., SAITO, T., ONUKI, R., ISHIGURO, K., KISHIMOTO, T. & HISANAGA, S. 2000. Calpain-dependent proteolytic cleavage of the p35 cyclin-dependent kinase 5 activator to p25. *The journal of biological chemistry*, 275(22):17166-17172.

LAFERLA, F.M. & ODDO, S. 2005. Alzheimer's disease: Aβ, tau and synaptic dysfunction. *Trends in molecular medicine*, 11(4):170-176.

LANGER, T. & WOLBER, G. 2004. Pharmacophore definition and 3D searches. *Drug discovery today: technologies*, 1(3):203-207.

LARSEN, S.D., STACHEW, C.F., CLARE, P.M., CUBBAGE, J.W. & LEACH, K.L. 2003. A catch-and-release strategy for the combinatorial synthesis of 4-acylamino-1,3-thiazoles as potential CDK5 inhibitors. *Bioorganic & medicinal chemistry letters*, 13(20):3491-3495.

LEE, M., KWON, Y.T., LI, M., PENG, J., FRIEDLANDER, R.M. & TSAI, L. 2000. Neurotoxicity induces cleavage of p35 to p25 by calpain. *Nature*, 405(6784):360-364.

LEE, K.Y., LEE, K.S., JIN, C. & LEE, Y.S. 2008. Design and synthesis of calpain inhibitory 6-pyridone 2-carboxamide derivatives. *European journal of medicinal chemistry,* 44(3):1331-1334.

LEE, K.S., SEO, S.H., LEE, Y.H., KIM, H.D., SON, M.H., CHUNG, B.Y., LEE, J.Y., JIN, C. & LEE, Y.S. 2005. Synthesis and biological evaluation of chromone carboxamides as calpain inhibitors. *Bioorganic & medicinal chemistry letters*, 15(11):2857-2860.

LEROY, K., YILMAZ, Z. & BRION, J.P. 2007. Increased level of active GSK-3β in Alzheimer's disease and accumulation in argyrophilic grains and in neurones at different stages of neurofibrillary degeneration. *Neuropathology and applied neurobiology*, 33(1):43-55.

LESCOP, C., HERZNER, H., SIENDT, H., BOLLIGER, R., HENNEBOHLE, M., WEYERMANN, P., BRIGUET, A., COURDIER-FRUH, I., ERB, M., FOSTER, M., MEIER, T., MAGYAR, J.P. & VON SPRECHER, A. 2005. Novel cell-penetrating α-keto-amide calpain inhibitors as potential treatment for muscular dystrophy. *Bioorganic & medicinal chemistry letters*, 15(23):5176-5181.

LEV, N., MELAMED, E. & OFFEN, D. 2003. Apoptosis and parkinson's disease. *Progress in neuro-psychopharmacology & biological psychiatry*, 27(2):245-250.

LI, B.S., ZHANG, L., TAKAHASHI, S., MA, W., JAFFE, H., KULKARNI, A.B. & PANT, H.C. 2002. Cyclin-dependent kinase 5 prevents neuronal apoptosis by negative regulation of c-jun n-terminal kinase 3. *The embo journal*, 21(3):324-333.

LI, J.Y., PLOMANN, M. & BRUNDIN, P. 2003. Huntington's disease: a synaptopathy? *Trends in molecular medicine*, 9(10):414-420.

LIN, C., CHEN, C., CHIANG, C., JAN, M., HUANG, W. & LIN, Y. 2007. GSK-3β acts downstream of PP2A and the PI 3-kinase akt pathway, and upstream of caspase-2 in ceramide-induced mitochondrial apoptosis. *Journal of cell sciences*, 120(16):2935-2943.

LOGÉ, C., TESTARD, A., THIÉRY, V., LOZACH, O., BLAIRVACQ, M., ROBERT, J.M., MEIJER, L. & BESSON, T. 2008. Novel 9-oxo-thiazolo[5,4-f]quinazoline-2-carbonitrile derivatives as dual cyclin-dependent kinase 1 (cdk1)/glycogen synthase kinase-3 (gsk-3) inhibitors: synthesis, biological evaluation and molecular modeling studies. *European journal of medicinal chemistry*, 43(7):1469-1477.

LOPEZ, O.L., BECKER, J.T., SWEET, R.A., MARTIN-SANCHEZ, F.J. & HAMILTON, R.L. 2006. Lewy bodies in the amygdala increase risk for major depression in subjects with Alzheimer disease. *Neurology*, 67(4):660-665.

LUBISCH, W., HOFMANN, H.P., TREIBER, H.J. & MÖLLER, A. 2000. Synthesis and biological evaluation of novel piperidine carboxamide derived calpain inhibitors. *Bioorganic & medicinal chemistry letters*, 10(19):2187-2191.

LUBISCH, W. & MÖLLER, A. 2002. Discovery of phenyl alanine derived ketoamides carrying benzoyl residues as novel calpain inhibitors. *Bioorganic & medicinal chemistry letters*, 12(10):1335-1338.

LUI, Y. & TEMPLETON, D.M. 2007. Cadmium activates CaMK-II and initiates CaMK-II-dependent apoptosis in mesangial cells. *FEBS letters*, 581(7):1481-1486.

LUM, C., KAHL, J., KESSLER, L., KUCHARSKI, J., LUNDSTROM, J., MILLER, S., NAKANISHI, H., PEI, Y., PRYOR, K., ROBERTS, E., SEBO, L., SULLIVAN, R., URBAN, J. & WANG, Z. 2008. 2,5-Diaminopyrimidines and 3,5-disubstituted azapurines as inhibitors of glycogen synthase kinase-3 (GSK-3). *Bioorganic & medicinal chemistry letters*, 18(12):3578-3581.

MAPELLI, M., MASSIMILIANO, L., CROVACE, C., SEELIGER, M.A., TSAI, L., MEIJER, L. & MUSACCHIO A. 2005. Mechanism of cdk5/p25 binding by cdk inhibitors. *Journal of medicinal chemistry*, 48(3):671-679.

MAPELLI, M. & MUSACCHIO, A. 2003. The structural perspective on cdk5. *Neurosignals*, 12(4-5):164-172.

MARTINEZ, A., ALONSO, M., CASTRO, A., PEREZ, C. & MORENO, F.J. 2002. First non-ATP competitive glycogen synthase kinase 3β (GSK-3β) inhibitors: thiadiazolidinones (TDZD) as potential drugs for the treatment of Alzheimer's. *Journal of medicinal chemistry*, 45(6):1292-1299.

MATTSON, M.P. 2001. Neuronal death and GSK-3β:a tau fetish? *Trends in neuroscience*, 24(5):255-256.

MCGINNIST, K.M., WHITTON, M.M., GNEGY, M.E. & WANG, K.K.W. 1998. Calcium/calmodulin-dependent protein kinase IV is cleaved by caspase-3 and calpain in SH-SY5Y human neuroblastoma cells undergoing apoptosis. *The journal of biological chemistry*, 273(32):19993-20000.

MEIJER, L., SKALTSOUNIS, A.L., MAGIATIS, P., POLYCHRONOPOULOS, P., KNOCKAERT, M., LEOST, M., RYAN, X.P., VONICA, C.A., BRIVANLOU, A., DAJANI, R., CROVACE, C., TARRICONE, C., MUSACCHIO, A., ROE, S.M., PEARL, L. & GREENGARD, P. 2003. GSK-3-selective inhibitors derived from tyrian purple inhibitors. *Chemistry & biology*, 10(12):1255-1266.

MELLON, C., ASPIOTIS, R., BLACK, C.W., BAYLY, C.I., GRIMM, E.L., GIROUX, A., HAN, Y., ISABEL, E., MCKAY, D.J, NICHOLSON, D.W., RASPER, D.M., ROY, S., TAM, J., THORNBERRY, N.A., VAILLANCOURT, J., XANTHOUDAKIS, S. & ZAMBONI, R. 2005. Lipophilic versus hydrogen-bonding effect in P_3 on potency and selectivity of valine aspartyl ketones as caspase 3 inhibitors. *Bioorganic & medicinal chemistry letters*, 15(17):3886-3890.

METTEY, Y., GOMPEL, M., THOMAS, V., GARNIER, M., LEOST, M., CEBALLOS-PICOT, I., NOBLE, M., ENDICOTT, J., VIERFOND, J. & MEIJER, L. 2003. Aloisines, a new family of cdk/gsk-3 inhibitors. SAR study, crystal structure in complex with cdk2, enzyme selectivity, and cellular effects. *Journal of medicinal chemistry*, 46(2):222-236.

MITCHELL, J.D. & BORASIO, G.D. 2007. Amyotrophic lateral sclerosis. *Lancet*, 369(9578):2031-2041.

MOLDOVEANU, T., CAMPBELL, R.T., CUERRIER, D. & DAVIES, P.L. 2004. Crystal structures of calpain-e64 and –leupeptin inhibitor complexes reveal mobile loops gating the active site. *Journal of molecular biology*, 343(5):1313-1326.

MONTERO, A., ALONSO, M., BENITO, E., CHANA, A., MANN, E., NAVAS, J.M. & HERRADON, B. 2004. Studies on aromatic compounds: inhibition of calpain I by biphenyl derivatives and peptide-biphenyl hybrids. *Bioorganic & medicinal chemistry letters*, 14(11):2753-2757.

MORENO, F.J., MEDINA, M., PÉREZ, M., DE GARCINI, E.M. & AVILA, J. 1995. Glycogen synthase kinase 3 phosphorylates recombinant human tau protein at serine-262 in the presence of heparin (or tubulin). *FEBS letters*, 372(1):65-68.

MYERS, R.H. 2004. Huntington's disease genetics. *NeuroRx®*, 1(2):255-262.

NAKAMURA, M. & INOUE, J. 2002. Exploration of peptidyl hydrazones as water-soluble calpain inhibitors. *Bioorganic & medicinal chemistry letters*, 12(12):1603-1606.

NAKAMURA, M., MIYASHITA, H., YAMAGUCHI, M., SHIRASAKI, Y., NAKAMURA, Y. & INOUE, J. 2003. Novel 6-hydroxy-3-morpholinones as cornea permeable calpain inhibitors. *Bioorganic & medicinal chemistry*, 11(24):5449-5460.

NAM, D. H., LEE, K.S., KIM, S.H., KIM, S.M., JUNG, S.Y., CHUNG, S.H., KIM, H.J., KIM, N.D., JIN, C. & LEE, Y.S. 2008. Design and synthesis of 4-quinolinone 2-carboxamides as calpain inhibitors. *Bioorganic & medicinal chemistry letters*, 18(1):205-209.

NEDEV, H.N., KLAIMAN, G., LEBLANC, A. & SARAGOVI, H.U. 2005. Synthesis and evaluation of novel dipeptidyl benzoyloxymethyl ketones as caspase inhibitors. *Biochemical and biophysical research communications*, 336(2):397-400.

OLESEN, P.H., SORENSEN, A.R., URSO, B., KURTZHALS, P., BOWLER, A.N., EHRBAR, U. & HANSEN B.F. 2003. Synthesis and in vitro characterization of 1-(4-aminofurazan-3-yl)-5-

dialkylaminomethyl-1H—[1,2,3]triazole-4-carboxylic acid derivatives. A new class of selective GSK-3 inhibitors. *Journal of medicinal chemistry*, 46(15):3333-3341.

OLNEY, J.W. 2003. Excitotoxicity, apoptosis and neuropsychiatric disorders. *Current opinion in pharmacology*, 3(1):101-109.

ORBA, Y., SUNDEN, Y., SUZUKI, T., NAGASHIMO, K., KIMURA, T., TANAKA, S. & SAWA, H. 2008. Pharmacological cdk inhibitor *R*-Roscovitine suppresses JC virus proliferation. *Virology*, 370(1):173-183.

PAP, M. & COOPER, G.M. 1998. Role of glycogen synthase kinase-3 in the phosphatidylinositol 3-kinase/akt cell survival pathway. *The journal of biological chemistry*, 273(32):19929-19932.

PATEL, D.S. & BHARATAM, P.V. 2008. Selectivity criterion for pyrazolo[3,4-b]pyrid[az]ine derivatives as GSK-3 inhibitors: CoMFA and molecular docking studies. *European journal of medicinal chemistry*, 43(5): 949-957.

PATRICK, G.N., ZUKERBERG, L., NIKOLIC, M., DE LA MONTE, S., DIKKES, P. & TSAI, L. 1999. Conversion of p35 to p25 deregulates cdk5 activity and promotes neurodegeneration. *Nature*, 402(6762):615-622.

PATZKE, H. & TSAI, L. 2002. Cdk5 sinks into ALS. *Trends in neurosciences*, 25(1):8-10.

PERRIN, B.J. & HUTTENLOCHER, A. 2002. Calpain. *The international journal of biochemistry & cell biology*, 34(7):722-725.

PHUKAN, J., PENDER, N.P. & HARDIMAN, O. 2007. Cognitive impairment in amyotrophic lateral sclerosis. *The lancet neurology*, 6(11):994-1003.

RAY, S.K., FIDAN, M., NOWAK, M.W., WILFORD, G.G., HOGAN, E.L. & BANIK, L. 2000. Oxidative stress and ca^{2+} influx upregulate calpain and induce apoptosis in PC12 cells. *Brain research*, 852(2):326-334.

ROCHAIS, C., DUC, N.V., LESCOT, E., DE- OLIVEIRA SANTOS, J.S., BUREAU, R., MEIJER, L., DALLEMAGNE, P. & RAULT, S. 2009. Synthesis of new dipyrrolo- and furopyrrolopyrazinones related to tripentones and their biological evaluation as potential kinases (CDKs1-5, GSK-3) inhibitors. *European journal of medicinal chemistry*, 44(2):708-716.

RZASA, R.M., KALLER, M.R., LIU, G., MAGAL, E., NGUYEN, T.T., OSSLUND, T.D., POWERS, D., SANTORA, V.J., VISWANADHAN, V.N., WANG, H.L., XIONG, X., ZHONG, W.

& NORMAN, M.H. 2007. Structure-activity relationships of 3,4-dihydro-1H-quinazolin-2-one derivatives as potential CDK5 inhibitors. *Bioorganic & medicinal chemistry*, 15(20):6574-6595.

SAEZ, M.E., RAMIREZ-LORCA, R., MORON, F.J. & RUIZ, A. 2006. The therapeutic potential of the calpain family: new aspects. *Drug discovery today*, 11(19-20):917-923.

SAKAI, J., YOSHIMORI, A., NOSE, Y., MIZOROKI, A., OKITA, N., TAKASAWA, R. & TANUMA, S. 2008. Structure-based discovery of a novel non-peptidic small molecular inhibitor of caspase-3. *Bioorganic and medicinal chemistry,* 16(9):4854-4859.

SAMII, A., NUTT, J.G. & RANSOM, B.R. 2004. Parkinson's disease. *Lancet*, 363(9423):1783-1793.

SCHULZ-GASH, T. & STAHL, M. 2003. Binding site characteristics in structure-based virtual screening: evaluation of current docking tools. *Journal of molecular modeling*, 9(1):47-57.

SCHULTZ, C., LINK, A., LEOST, M., ZAHAREVITZ, W., GUSSIO, R., SAUSVILLE, E.A., MEIJER, L. & KUNICK, C. 1999. Paullones, a series of cyclin-dependent kinase inhibitors: synthesis, evaluation of CDK1/cyclin B inhibition, and in vitro antitumor activity. *Journal of medicinal chemistry*, 42(15):2909-2919.

SENDEROWICZ, A.M. 2004. Targeting cell cycle and apoptosis for the treatment of human malignancies. *Current opinion in cell biology*, 16(6):670-678.

SHAH, M.A. & SCHWARTZ, G.K. 2006. Cyclin dependent kinases as targets for cancer therapy. *Update on cancer therapeutics*, 1(3):311-332.

SHARMA, M., MANCHATE, N.K., TYAGI, R.K. & SHARMA, P. 2007. Cyclin dependent kinase 5 (cdk5) mediated inhibition of the MAP kinase pathway results in CREB down regulation and apoptosis in PC12 cells. *Biochemical and biophysical research communications*, 358(2):379-384.

SHASTRY, B.S. 2001. Parkinson disease: etiology, pathogenesis and future of gene therapy. *Neuroscience research*, 41(1):5-12.

SHIRADKAR, M.R., AKULA, K.C., CASARI, V., BARU, V., CHININGIRI, B., GANDHI, S. & KAUR, R. 2007. Clubbed thiazoles by MAOS: a novel approach to cyclin-dependent kinase 5/p25 inhibitors as a potential treatment for alzheimer's disease. *Bioorganic & medicinal chemistry*, 15(7):2601-2610.

SHIRADKAR, M.S., PADHALINGAPPA, M.B., BHETALABHOTALA, S., AKULA, K.C., TUPE, A.D., PINNINTI, R.R. & THUMMANAGOTI, S. 2007. A novel approach to cyclin-dependent kinase 5/p25 inhibitors: a potential treatment for Alzheimer's disease. *Bioorganic & medicinal chemistry*, 15(19):6397-6406.

SIMPSON, C.L. & AL-CHALABI, A. 2006. Amyotrophic lateral sclerosis as a complex genetic disease. *Biochimica et biophysica acta*, 1762(11-12):973-985.

SINGH, S. & DIKSHIT, M. 2007. Apoptotic neuronal death in Parkinson's disease: involvement of nitric oxide. *Brain research reviews*, 54(2):233-250.

SMITH D.G., BUFFET, M., FENWICK, A.E., HAIGH, D., IFE, R.J., SAUNDERS, M., SLINGSBY, B.P., STACEY, R. & WARD, R.W. 2001. 3-Anilino-4-arylmaleimides: potent and selective inhibitors of glycogen synthase kinase-3 (GSK-3). *Bioorganic & medicinal chemistry letters*, 11(5):635-639.

STOICA, B.A., MOVSESYAN, V.A., LEA IV, P.M. & FADEN, A.I. 2003. Ceramide-induced neuronal apoptosis is associated with dephosphorylation of Akt, BAD, FKHR, GSK-3β, and induction of the mitochondrial-dependent intrinsic caspase pathway. *Molecular and cellular neuroscience*, 22(3):365-382.

SURMEIER, D.J. 2007. Calcium, ageing, and neuronal vulnerability in parkinson's disease. *The lancet neurology*, 6(10):933-938.

TER HAAR, E., COLL, J.T., AUSTEN, D.A., HSIAO, H., SWENSON, L. & JAIN, J. 2001. Structure of gsk3β reveals a primed phosphorylation mechanism. *Nature structural biology*, 8(7)593-596.

TRIPATHY, R., GU, Z.Q., DUNN, D., SENADHI, S.E., ATOR, M.A. & CHATTERJEE, S. 1998. P_2-proline-derived inhibitors of calpain I. *Bioorganic & medicinal chemistry letters*, 8(19):2647-2652.

TSAI, L., LEE, M. & CRUZ, J. 2004. Cdk5, a therapeutic target for alzheimer's disease? *Biochimica et biophysica acta*, 1697(1-2):137-142.

TSAI, K.C., WANG, S.H., HSIAO, N.W., LI, M., WANG, B. 2008. The effect of different electrostatic potential on docking accuracy: a case study using dock5.4. *Bioorganic & medicinal chemistry letters,* 18(12):3509-3512.

USSAT, S., WERNER, U. & ADAM-KLAGES, S. 2002. Species-specific differences in the usage of several caspase substrates. *Biochemical and biophysical research communications*, 297(5):1186-1190.

VICKERS, J.C., DICKSON, T.C, ADLARD, P.A., SAUNDERS, H.L., KING, C.E. & MCCORMACK, G. 2000. The cause of neuronal degeneration in Alzheimer's disease. *Progress in neurobiology*, 60(2):139-165.

WAGMAN, A.S., JOHNSON, K.W., BUSSIERE, D.E. 2004. Discovery and development of gsk3 inhibitors for the treatment of type 2 diabetes. *Current pharmaceutical design*, 10(10):1105-1137.

WANG, C.X., SONG, J.H., SONG, D.K., YONG, V.W., SHUAIB, A. & HAO, C. 2006. Cyclin-dependent kinase-5 prevents neuronal apoptosis through ERK-mediated upregulation of bcl-2. *Cell death and differentiation*, 13(7):1203-1212.

WANG, K.K.W., NATH, R., POSNER, A., RASER, K.J., BUROKER-KILGORE, M., HAJIMOHAMMADREZA, I., PROBERT JR., A.W., MARCOUX, F.W., YE, Q., TAKANO, E., HATANAKA, M., MAKI, M., CANER, H., COLLINS, J.L., FERGUS, A., LEE, K.S., LUNNEY, E.A., HAYS, S.J. & YUEN, P. 1996. An alpha-mercaptoacrylic acid derivative is a selective nonpeptide cell-permeable calpain inhibitor and is neuroprotective. *Proceedings of the national academy of sciences of the united states of america,* 93(13):6687-6692.

WANG, Y., JIA, S., TSENG, B., DREWE, J. CAI, S.X. 2007. Dipeptidyl aspartyl fluoromethylketones as potent caspase inhibitors: peptidomimetic replacement of the p_2 amino acid by 2-aminoaryl acids and other non-natural amino acids. *Bioorganic and medicinal chemistry letters*, 17(22):6178-6182.

WEI, Z., SONG, M.S., MACTAVISH, D., JHAMANDAS, J.H. & KAR, S. 2008. Role of calpain and caspase in β-amyloid-induced cell death in rat primary septal cultured neurons. *Neuropharmacology*, 54(4):721-733.

WEISHAUPT, J.H., KUSSMAUL, L., GRÖTSCH, P., HECKEL, A., ROHDE, G., ROMIG, H., BÄHR, M. & GILLARDON, F. 2003. Inhibition of CDK5 is protective in necrotic and apoptotic paradigms of neuronal cell death and prevents mitochondrial dysfunction. *Molecular and cellular neuroscience*, 24(2):489-502.

WELLS, G.J., TAO, M., JOSEF, K.A. & BIHOVSKY, R. 2001. 1,2-Benzothiazine 1,1-dioxide p_2-p_3 peptide mimetic aldehyde calpain I inhibitors. *Journal of medicinal chemistry*, 44(21):3488-3503.

[a]WITHERINGTON, J., BORDAS, V., GAIBA, A., GARTON, N.S., NAYLOR, A., RAWLINGS, A.D., SLINGSBY, B.P., SMITH, D.G., TAKLE, A.K. & WARD, R.W. 2003. 6-Aryl-pyrazolo[3,4-b]pyridines: potent inhibitors of glycogen synthase kinase-3 (GSK-3). *Bioorganic & medicinal chemistry letters*, 13(18):3055-3057.

[b]WITHERINGTON, J., BORDAS, V., GAIBA, A., GARTON, N.S., NAYLOR, A., RAWLINGS, A.D., SLINGSBY, B.P., SMITH, D.G., TAKLE, A.K. & WARD, R.W. 2003. 6-Heteroaryl-pyrazolo[3,4-b]pyridines: potent and selective inhibitors of glycogen synthase kinase-3 (GSK-3). *Bioorganic & medicinal chemistry letters*, 13(18):3059-3062.

[c]WITHERINGTON, J., BORDAS, V., GARLAND, S.L., HICKEY, D.M.B., IFE, R.J., LIDDLE, J., SAUNDERS, M., SMITH, D.G. & WARD, R.W. 2003. 5-Aryl-pyrazolo[3,4-b]pyridines: potent inhibitors of glycogen synthase kinase-3 (GSK-3). *Bioorganic & medicinal chemistry letters*, 13(9):1577-1580.

[d]WITHERINGTON, J., BORDAS, V., HAIGH, D., HICKEY, D.M.B., IFE, R.J., RAWLINGS, A.D., SLINGSBY, B.P., SMITH, D.G. & WARD, R.W. 2003. 5-Aryl-pyrazolo[3,4-b]pyridazines: potent inhibitors of glycogen synthase kinase-3 (GSK-3). *Bioorganic & medicinal chemistry letters*, 13(9):1581-1584.

WOODHOUSE, A., DICKSON, T.C., WEST, A.K., MCLEAN, C.A. & VICKERS, J.C. 2006. No difference in expression of apoptosis-related proteins and apoptotic morphology in control, pathologically aged and alzheimer's disease cases. *Neurobiology of diseases*, 22(2):323-333.

WOOD-KACZMAR, A., GANDHI, S. & WOOD, N.W. 2006. Understanding the molecular causes of parkinson's disease. *Trends in molecular medicine*, 12(11):521-528.

WRIGHT, M.H., FARQUHAR, M.J., ALETRARI, M., LADDS, G. & HODGKIN, M.N. 2008. Identification of caspase 3 motifs and critical residues in human phospholipase D1b and phospholipase D2a. *Biochemical and biophysical research communications*, 369(2):478-484.

ZENG, Y., LI, Q., HANZLIK, R.P. & AUBE, J. 2005. Synthesis of a small library of diketopiperazines as potential inhibitors of calpain. *Bioorganic & medicinal chemistry letters*, 15(12):3034-3038.

ZHANG, Y., JUNG, S.Y., JIN, C., KIM, N.D., GONG, P. & LEE, Y.S. 2009. Design and synthesis of 4-aryl-4-oxobutanoic acid amides as calpain inhibitors. *Bioorganic & medicinal chemistry letters*, 19(2):502-507.

ZHANG, J., KRISHNAMURTHY, P.K. & JOHNSON, G.V.W. 2002. Cdk5 phosphorylates p53 and regulates its activity. *Journal of neurochemistry*, 81(2):307-313.

ZHONG, W., LIU, H., KALLER, M.R., HENLEY, C., MAGAL, E., NGUYEN, T., OSSLUND, T.D., POWERS, D., RZASA, R.M., WANG, H.L., WANG, W., XIONG, X., ZHANG, J., NORMAN, M.H. 2007. Design and synthesis of quinolin-2(1H)-one derivatives as potent CDK5 inhibitors. *Bioorganic & medicinal chemistry letters*, 17(19):5384-5389.

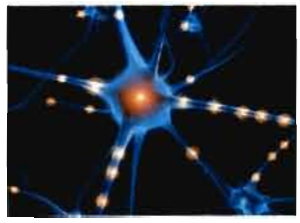

Appendix

Hypothesis generation for CDK5/p25

Table 1: Training set for CDK5/p25

	Compound	IC_{50} (nM)
i	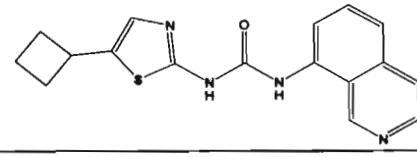	5
ii	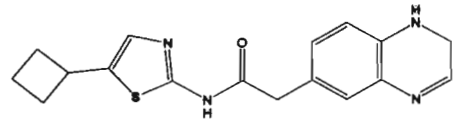	7
iii	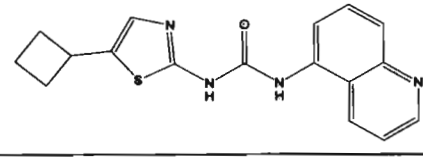	8
iv	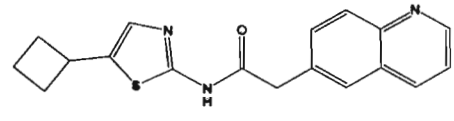	10
v	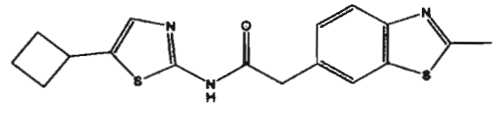	12
vi	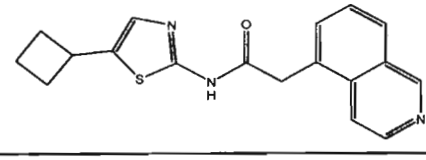	13
vii	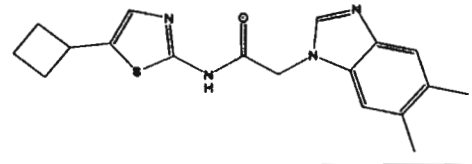	13

viii	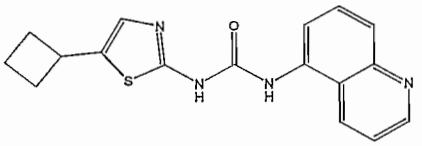	13
ix	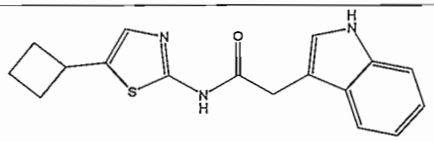	16
x	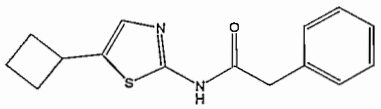	25
xi	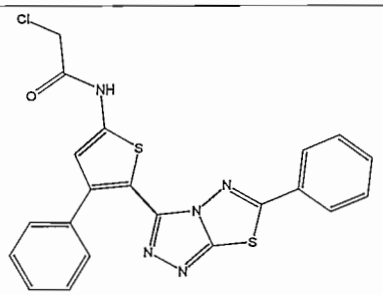	28
xii	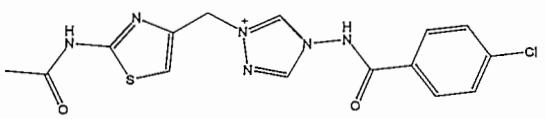	30
xiii	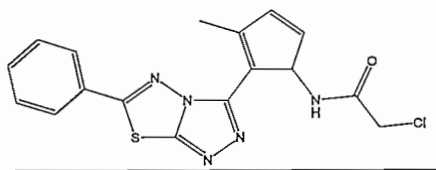	30
xiv	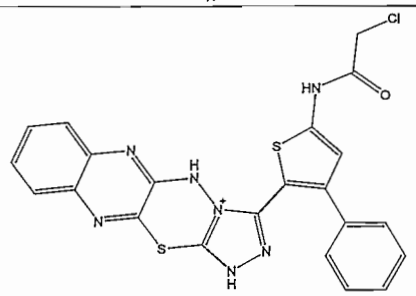	30
xv	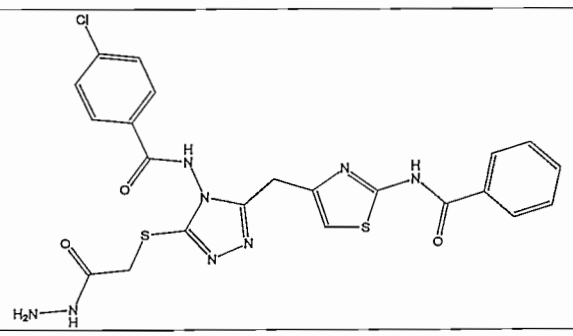	34

xvi	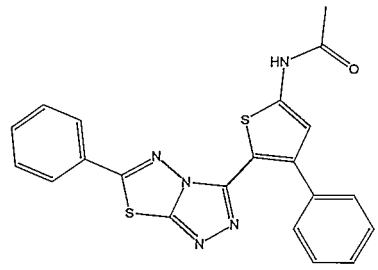	38
xvii	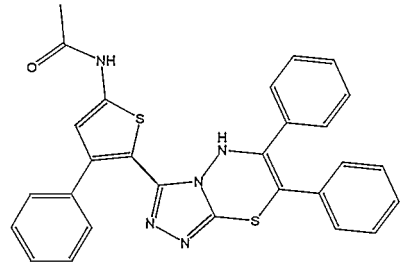	40
xviii	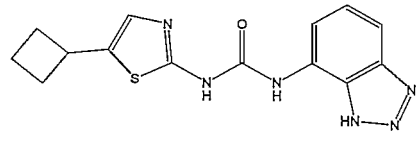	41
xix	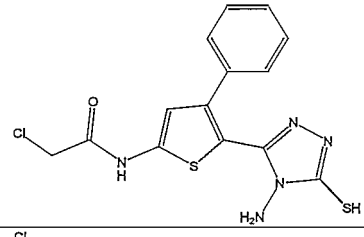	42
xx	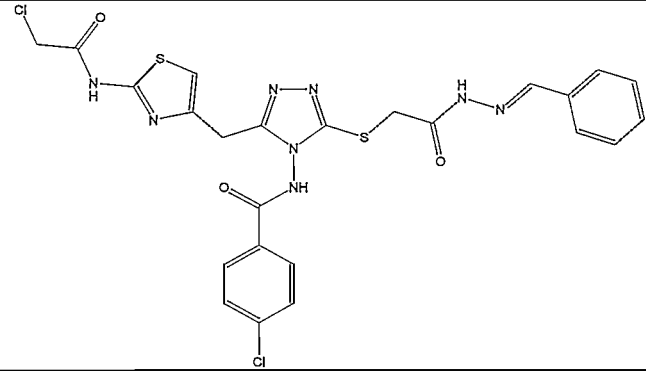	42
xxi	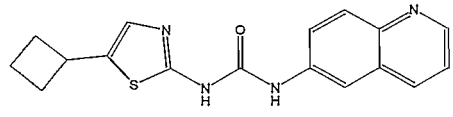	44
xxii	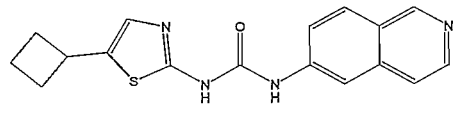	44

xxiii	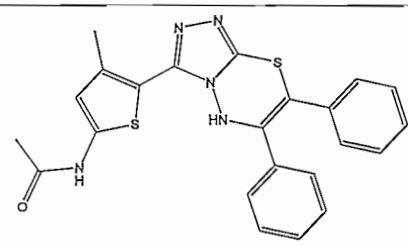	44
xxiv	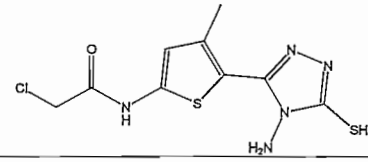	46
xxv	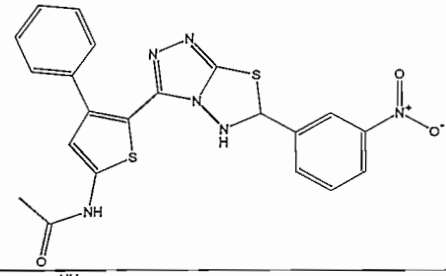	48
xxvi	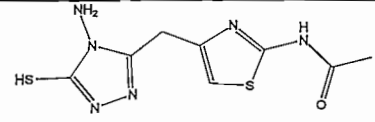	48
xxvii	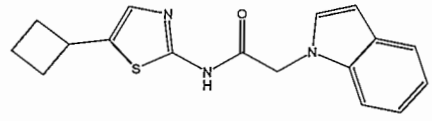	48
xxviii	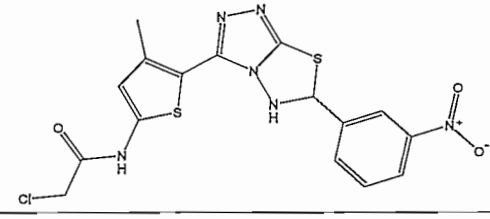	53

Table 2: Validation database for CDK5/p25

	Compound	IC_{50} (nM)
i	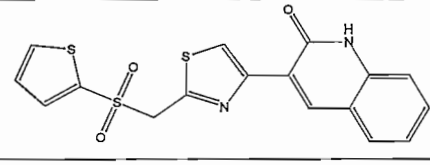	2.1

ii	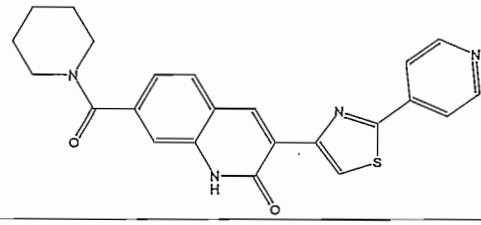	2.7
iii	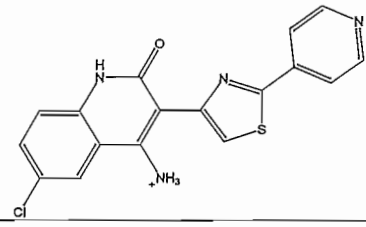	3.8
iv	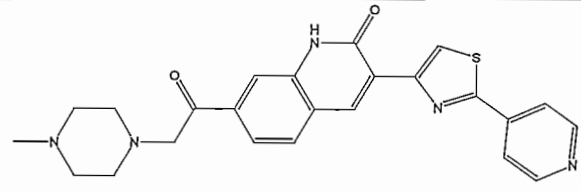	4.4
v	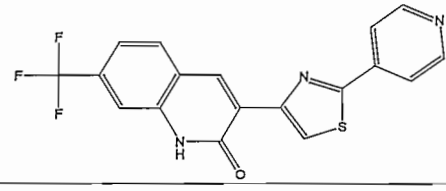	6.3
vi	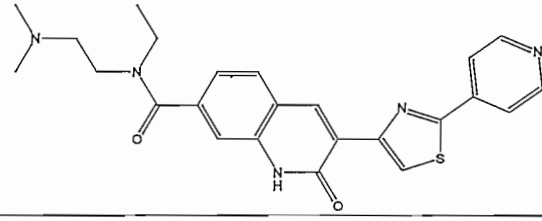	8.3
vii	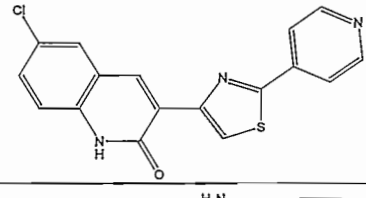	11
viii	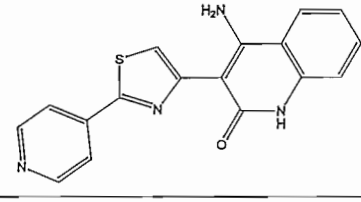	11
ix	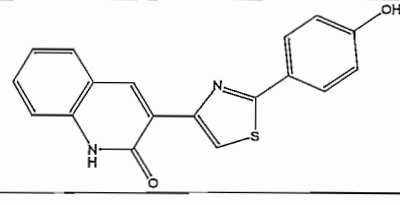	24

x	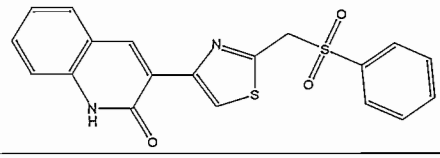	29
xi	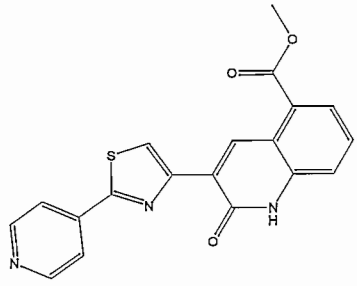	33
xii	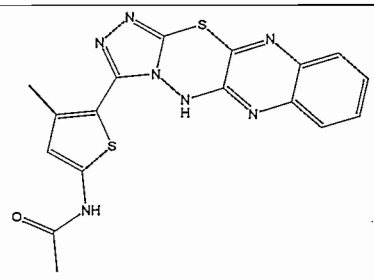	34
xiii	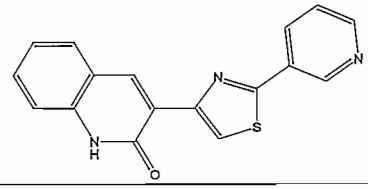	50
xiv	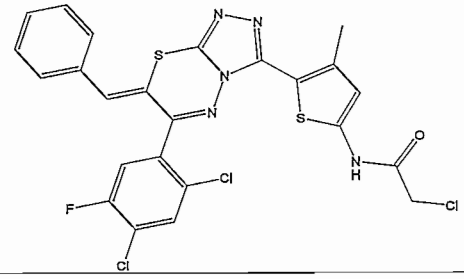	3420
xv	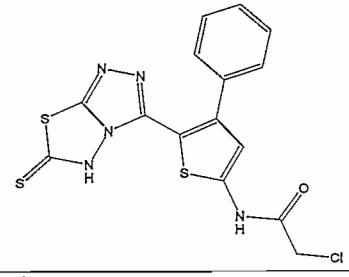	5896
xvi	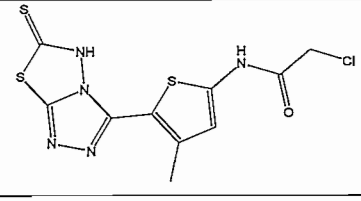	7480

xvii	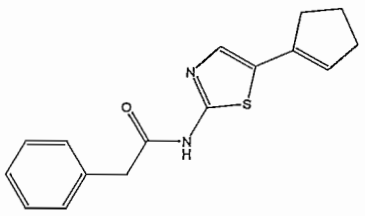	6530
xviii	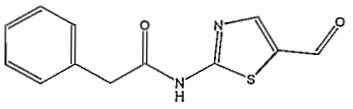	7670
xix	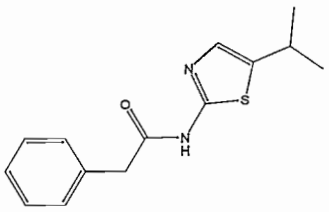	9770
xx	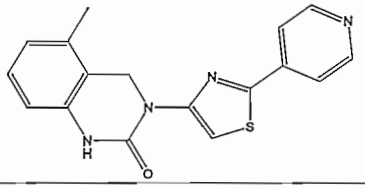	1260

Hypothesis generation for calpain

Table 3: Training set for calpain

	Compound	IC_{50} (nM)
i	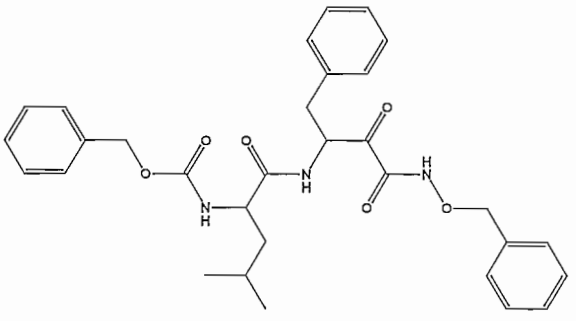	6

ii	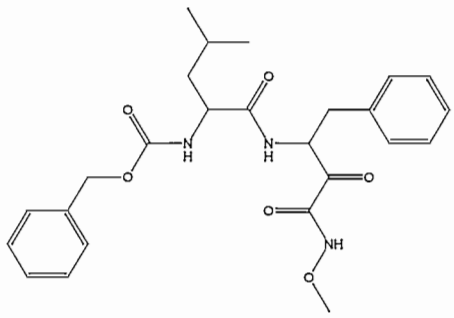	10
iii	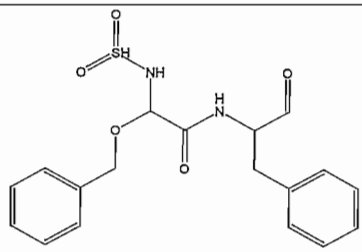	11
iv	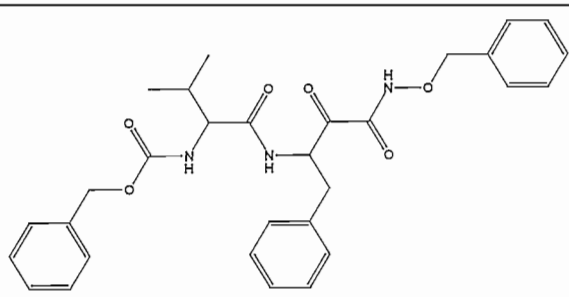	12
v	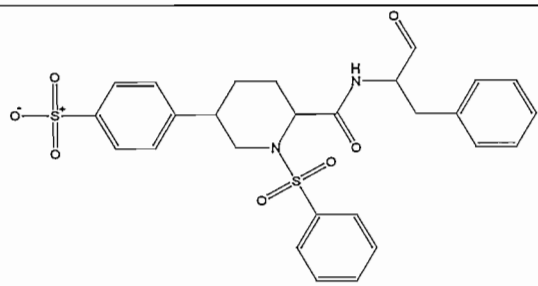	13
vi	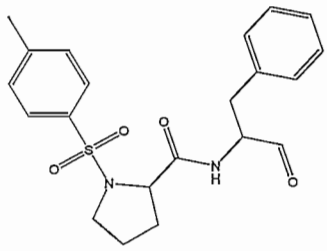	14
vii	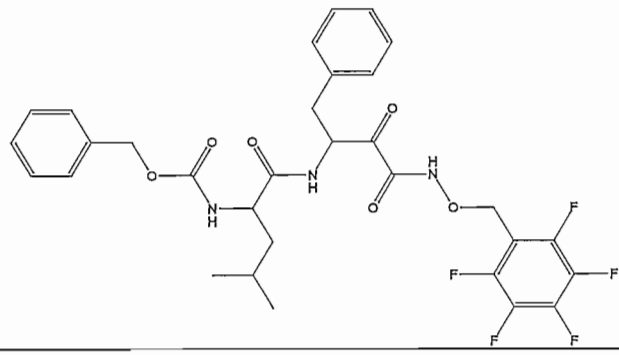	17

viii	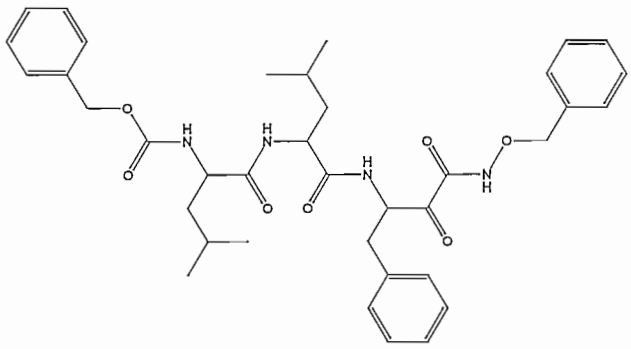	17
ix	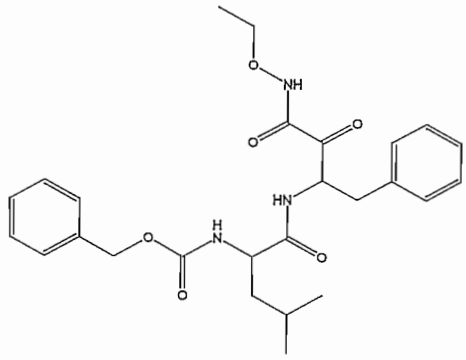	19
x	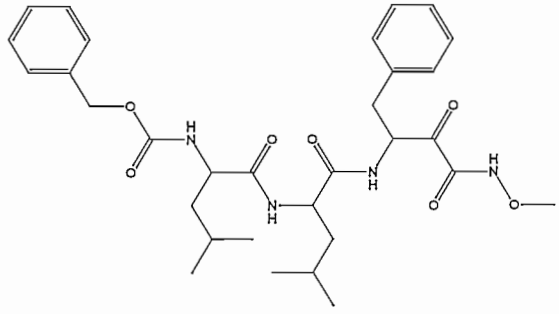	20
xi	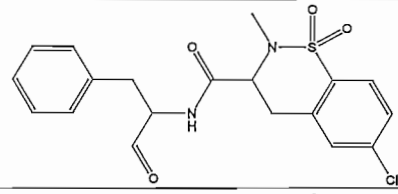	5
xii	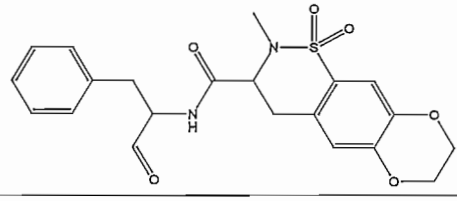	6
xiii	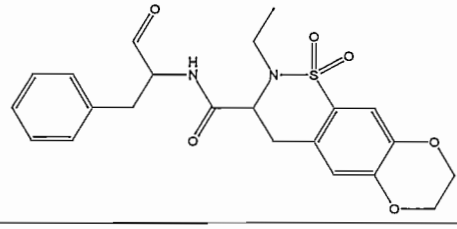	7

xiv	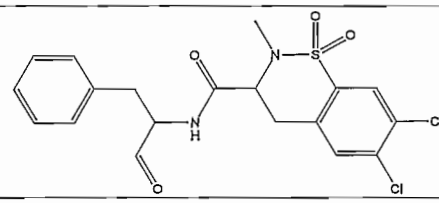	7
xv	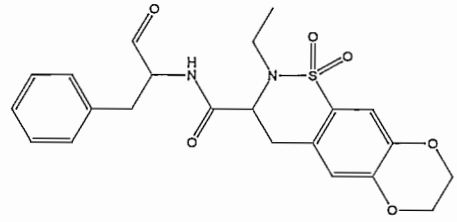	8
xvi	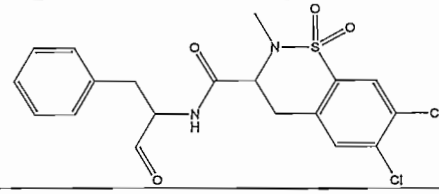	15
xvii	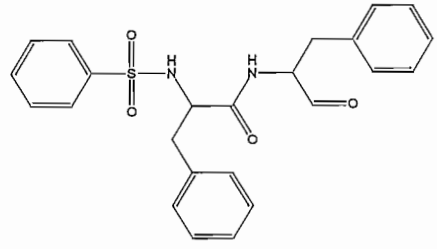	20
xviii	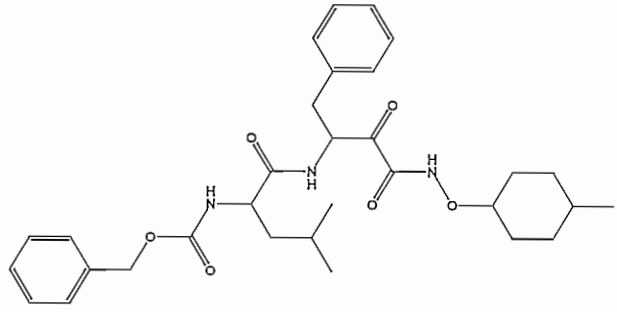	21
xix	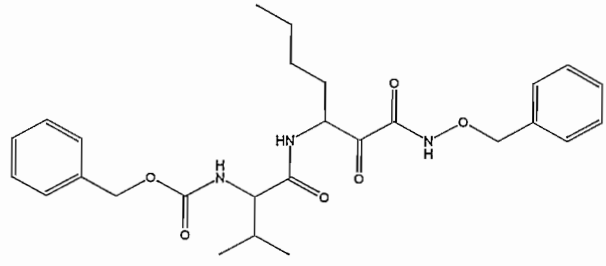	21
xx	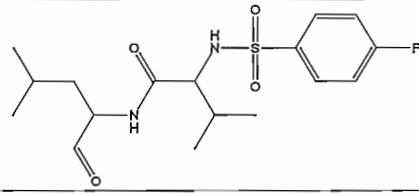	22

xxi	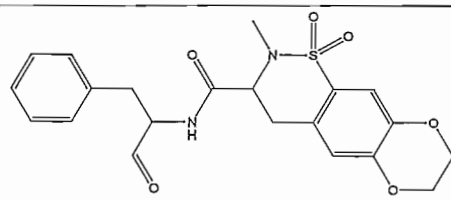	24
xxii	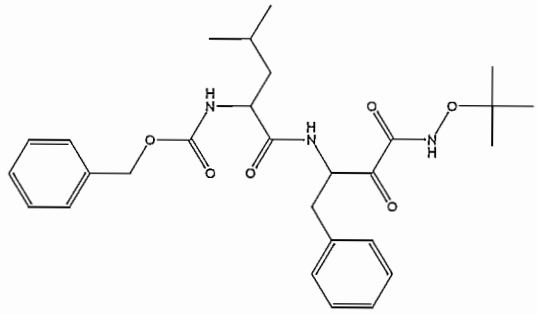	26
xxiii	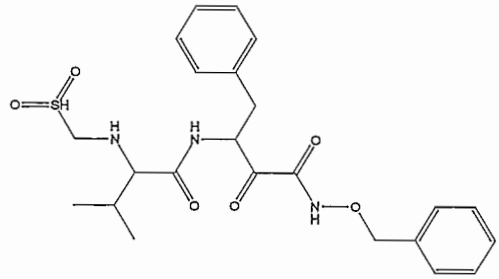	28
xxiv	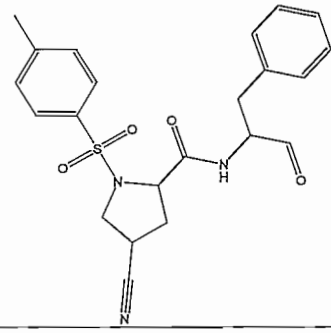	28
xxv	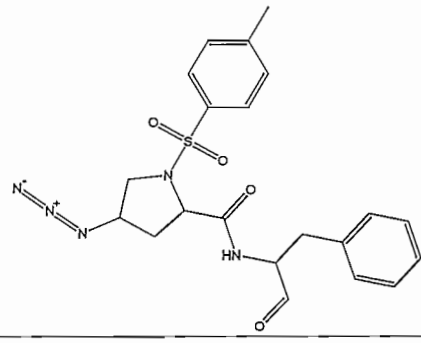	28

Table 4: Validation database for calpain

	Compound	IC_{50} (nM)
i	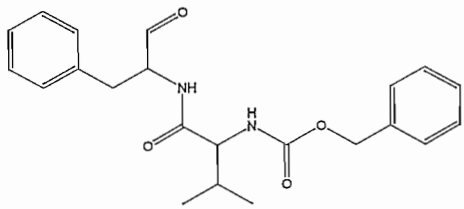	20
ii	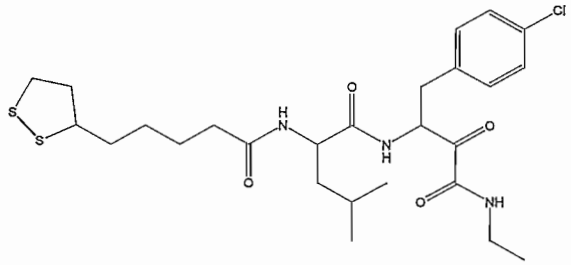	20
iii	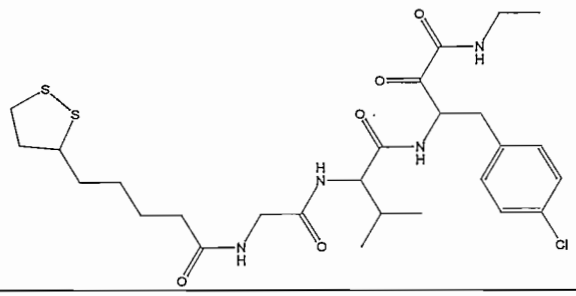	30
iv	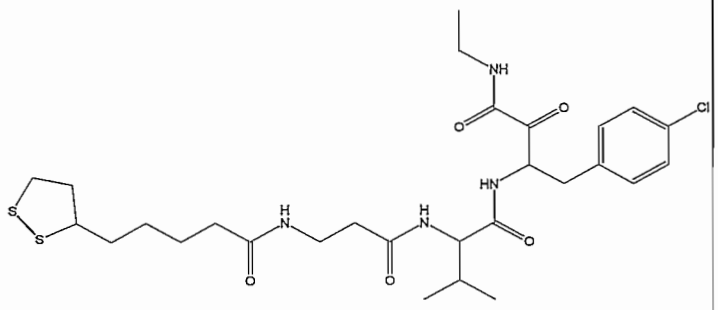	40
v	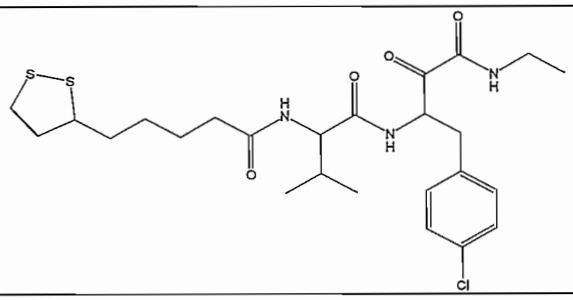	60

vi	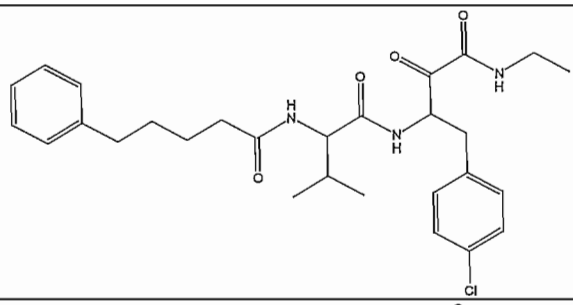	60
vii	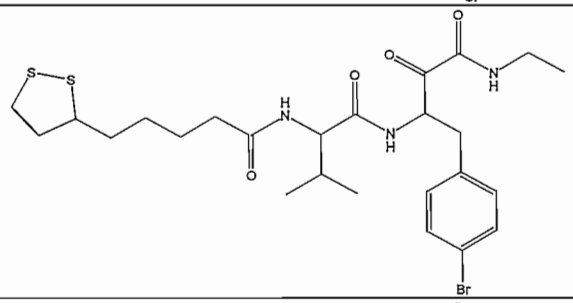	60
viii	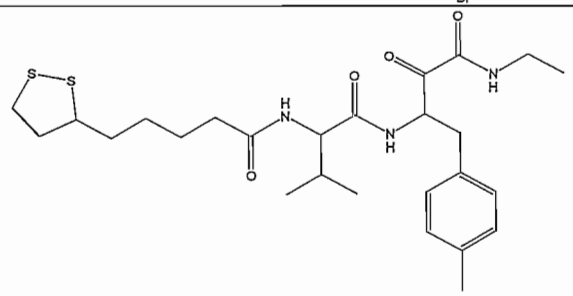	70
ix	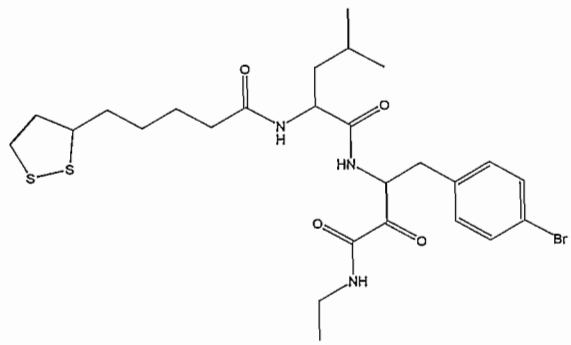	20
x	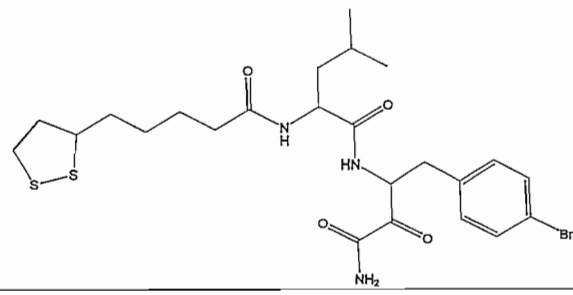	20

xi	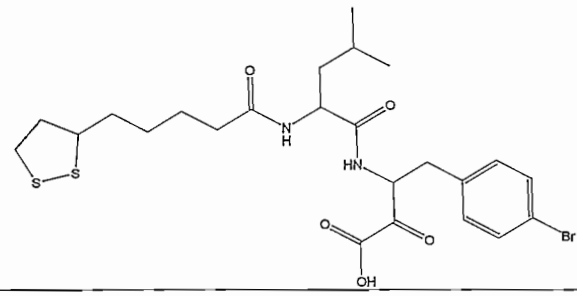	50
xii	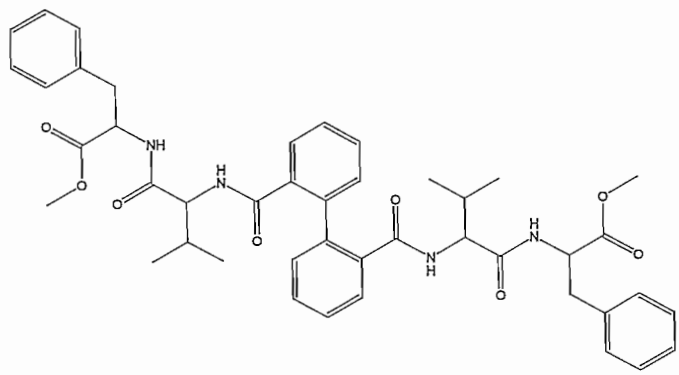	24
xiii	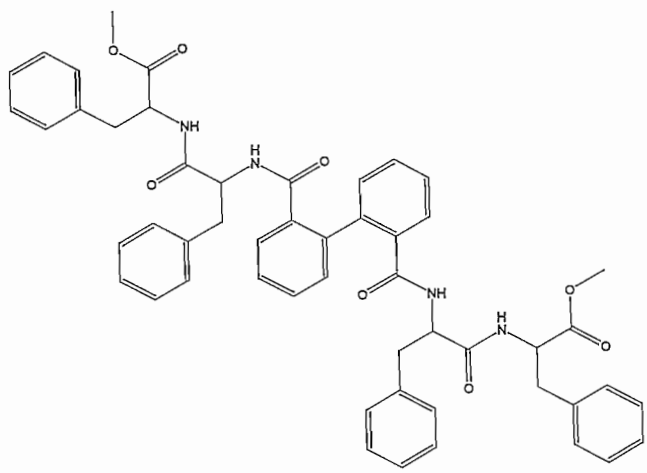	98
xiv	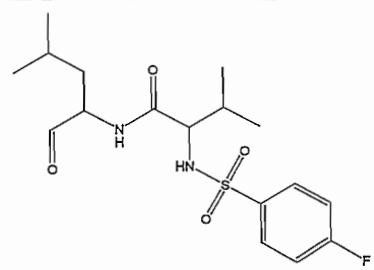	35
xv	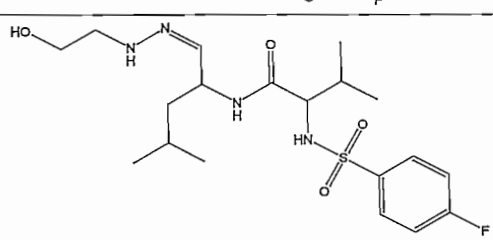	190

xvi	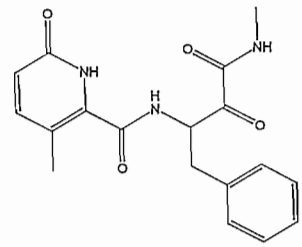	91420
xvii	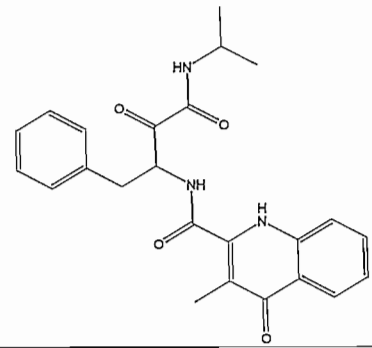	50000
xviii	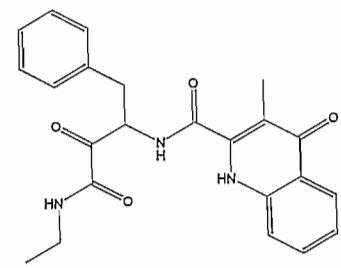	40170
xix	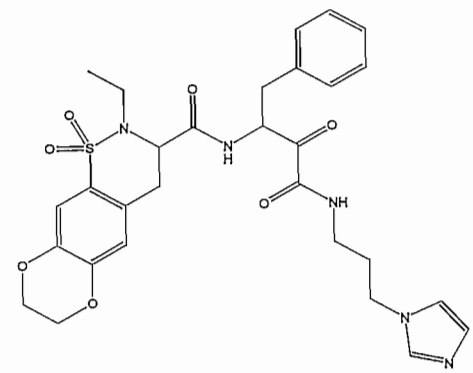	5000
xx	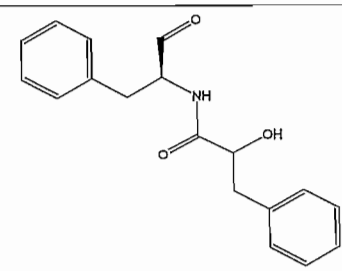	17000

xxi	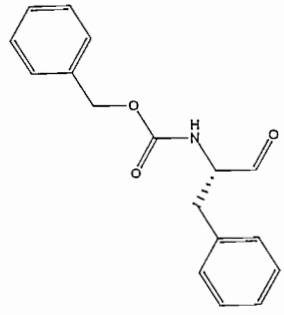	5500
xxii	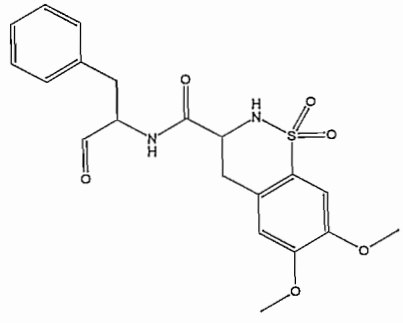	700
xxiii	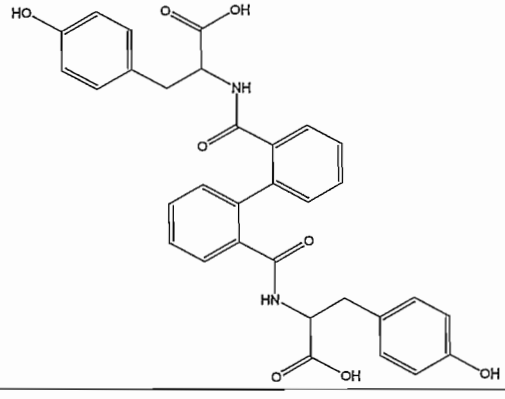	200000
xxiv	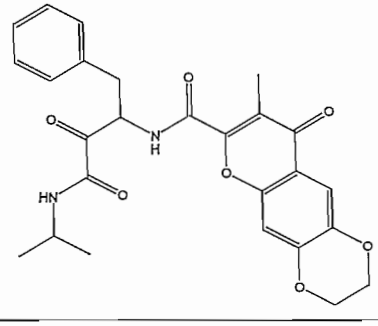	20000
xxv	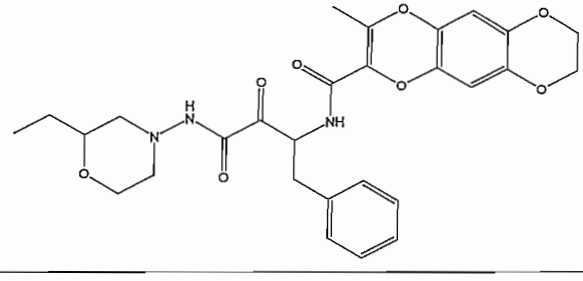	20000

Hypothesis generation for caspase 3

Table 5: Training set for caspase 3

	Compound	IC_{50} (nM)
i	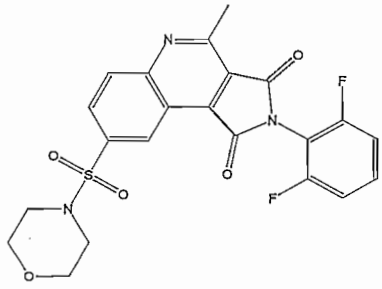	10
ii	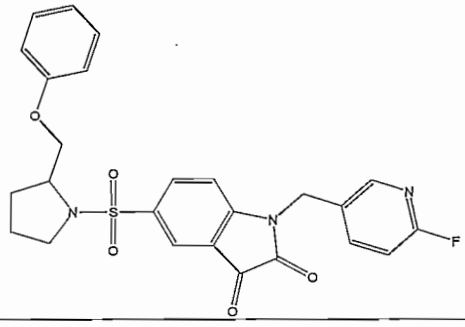	10.3
iii	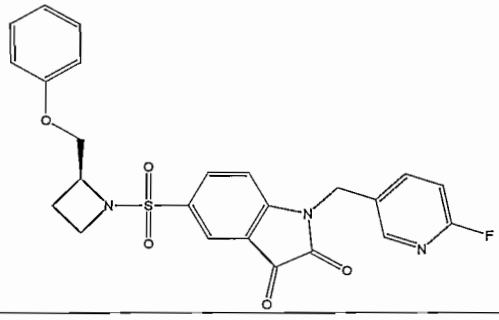	10.9
iv	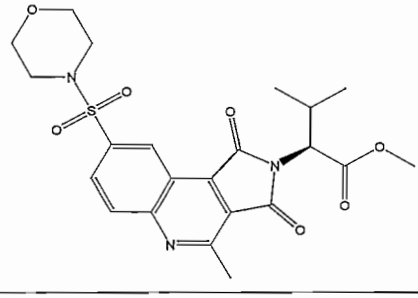	11

v	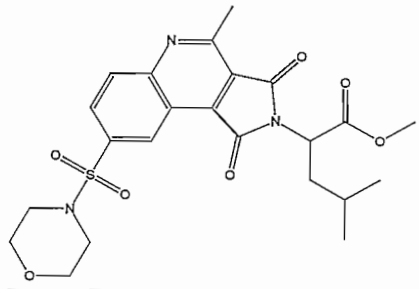	11
vi	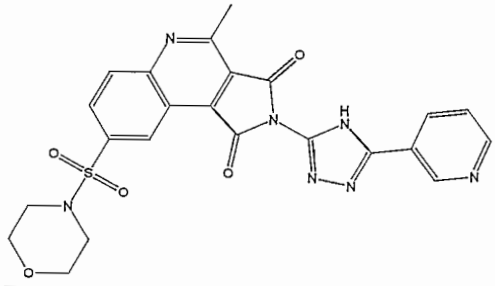	11
vii	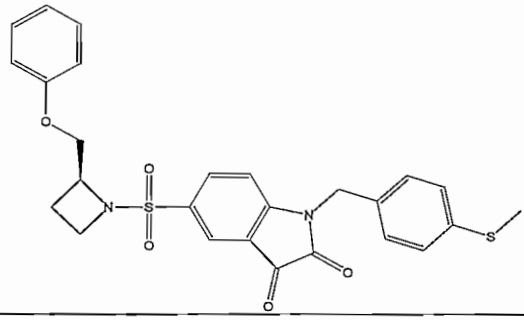	11.3
viii	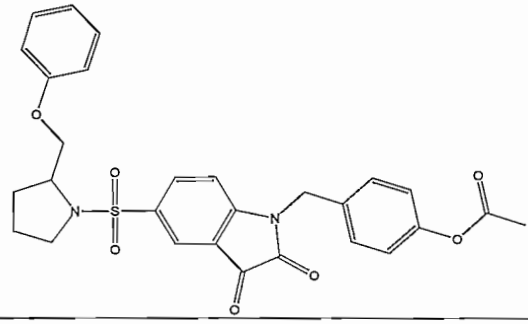	12
ix	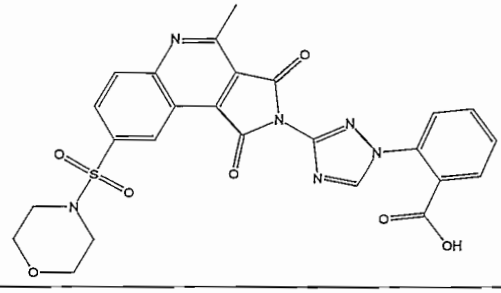	12

x	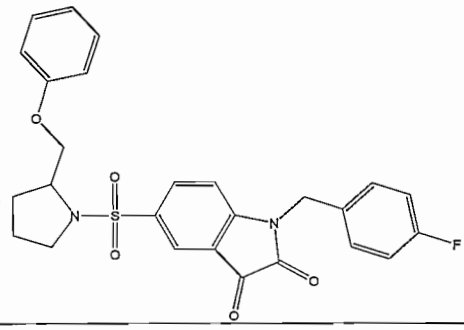	12.1
xi	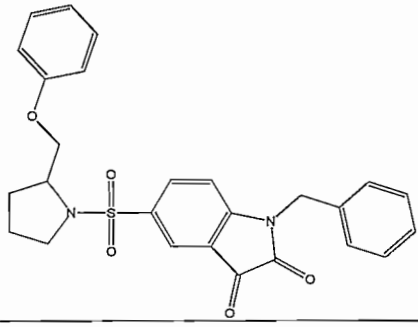	12.2
xii	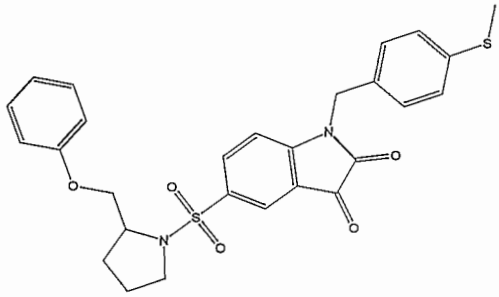	12.4
xiii	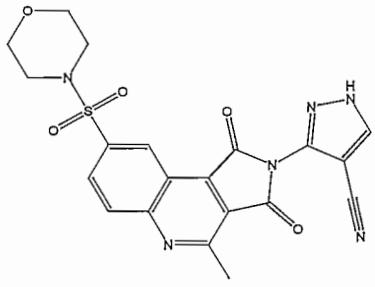	13
xiv	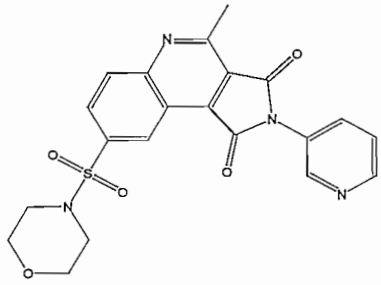	13

xv	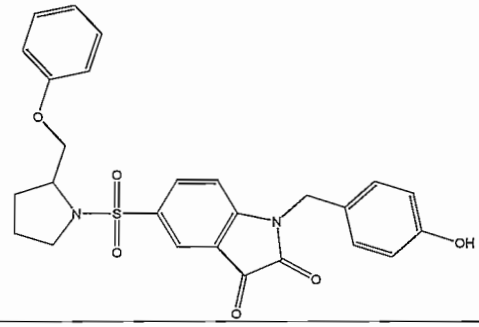	13.5
xvi	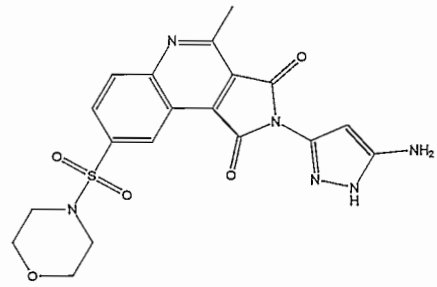	14
xvii	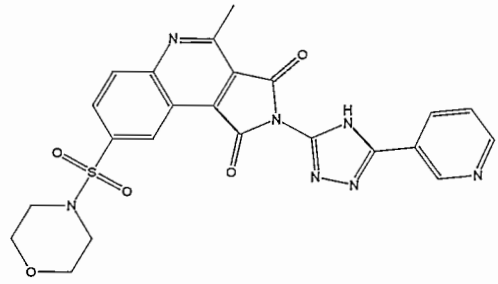	14
xviii	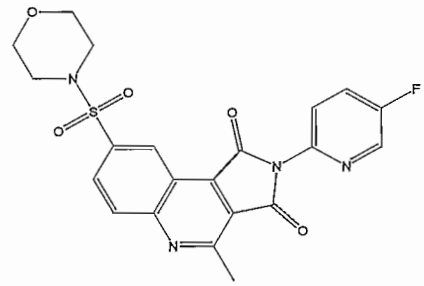	14
xix	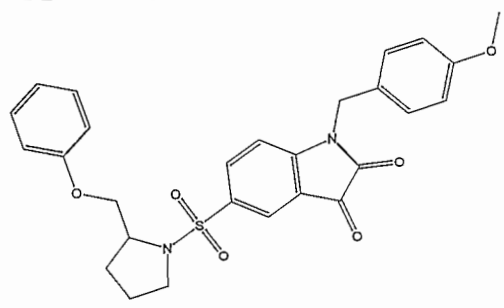	14.5

xx	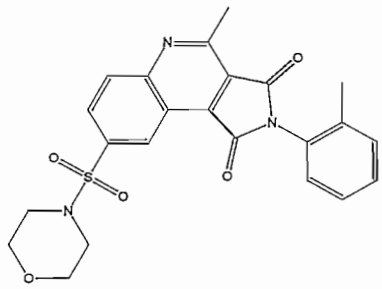	15
xxi	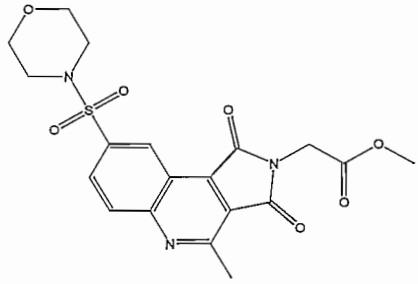	16
xxii	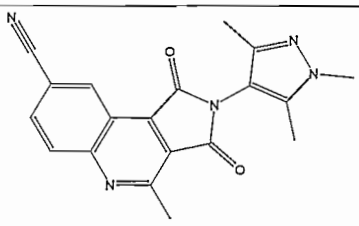	16
xxiii	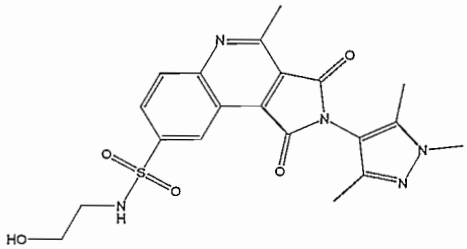	20
xxiv	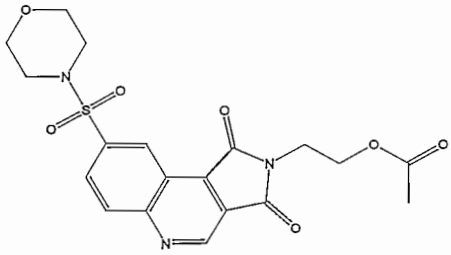	23
xxv	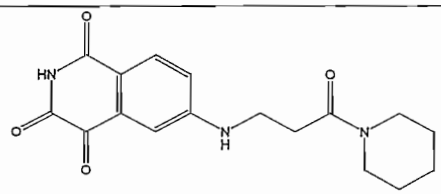	25

Table 6: Validation database for caspase 3

	Compound	IC_{50} (nM)
i	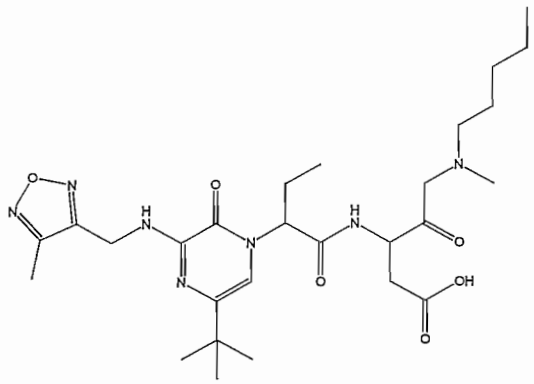	0.1
ii	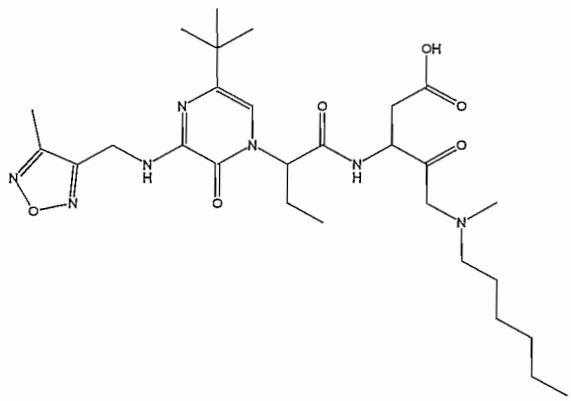	6
iii	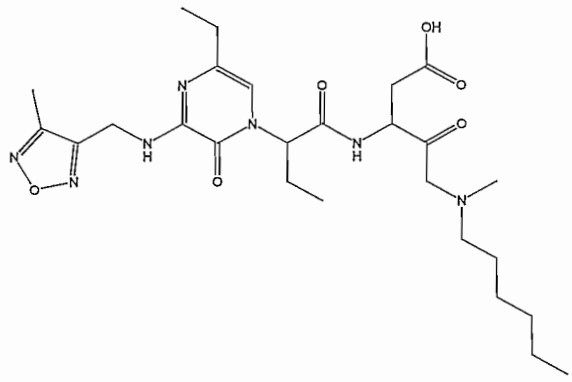	6
iv	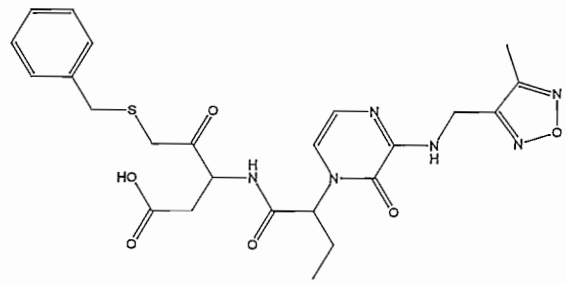	8

v	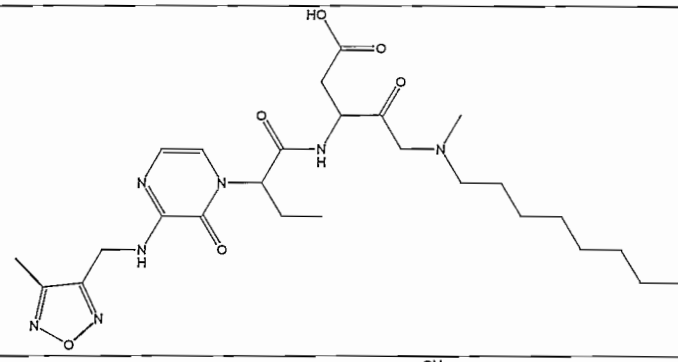	9
vi	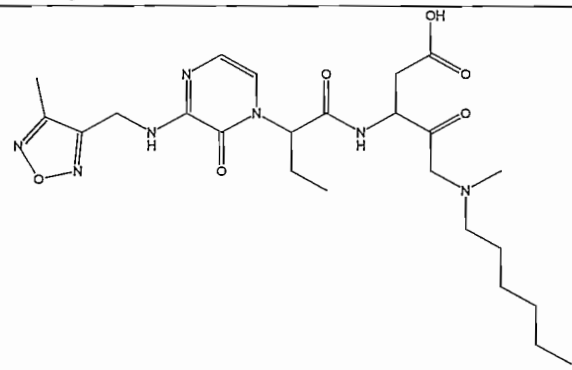	11
vii	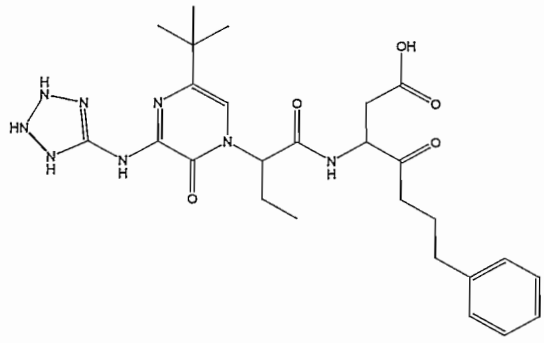	5
viii	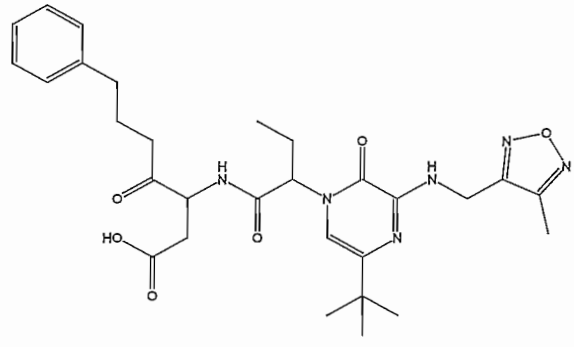	14
ix	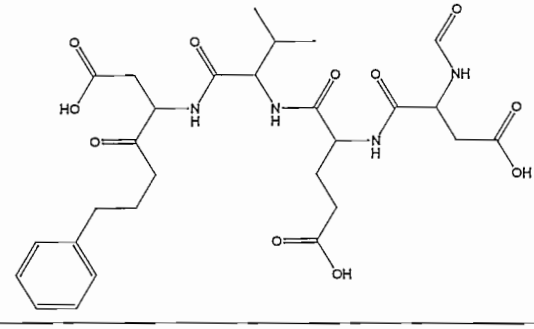	0.8

x	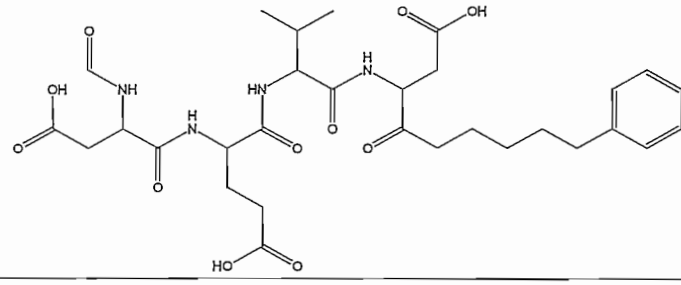	0.8
xi	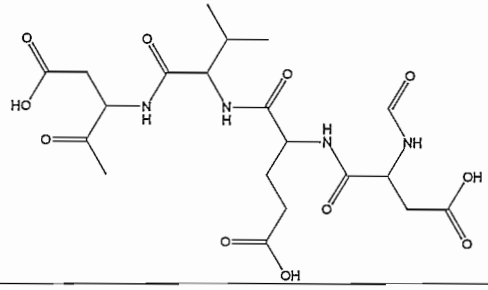	1.3
xii	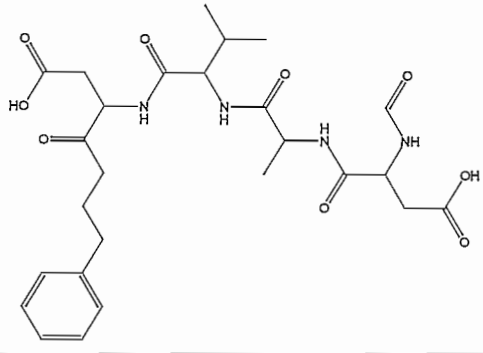	1.4
xiii	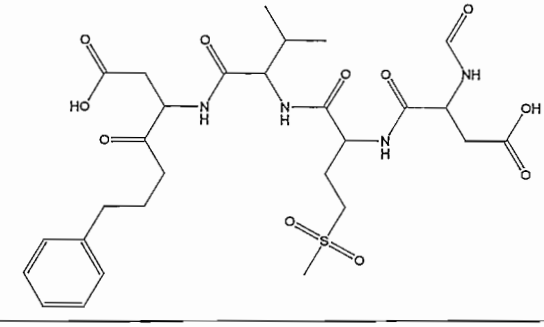	1.7
xiv	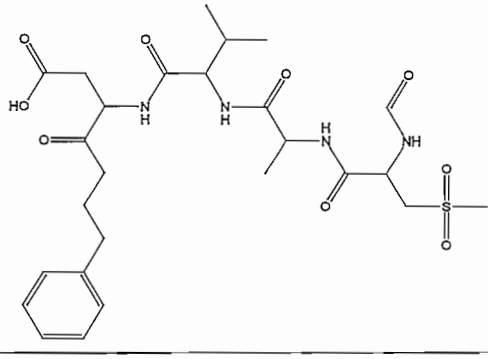	1.9

xv	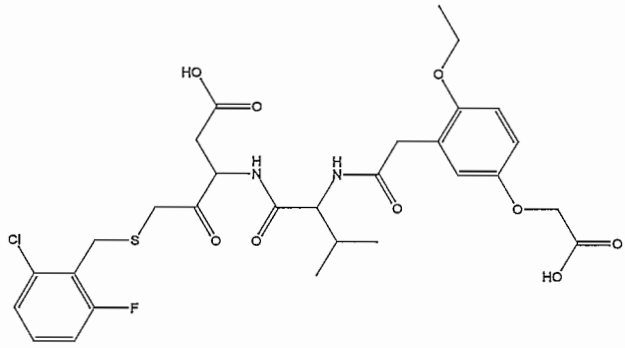	5
xvi	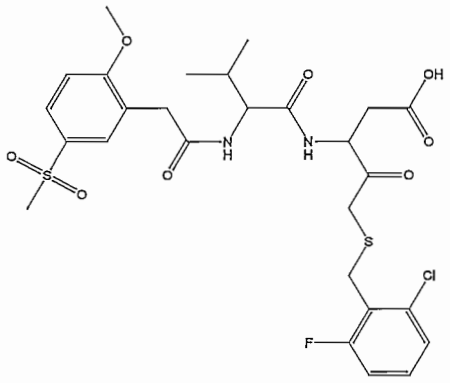	5
xvii	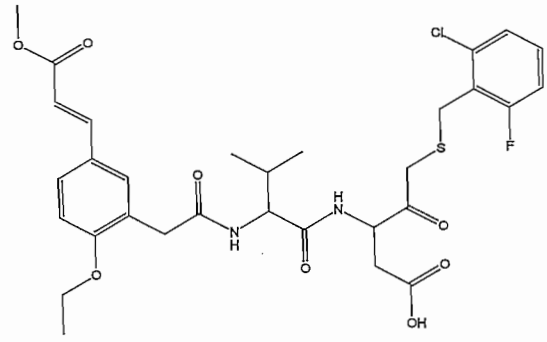	8
xviii	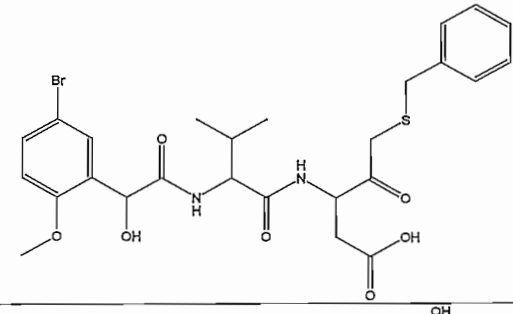	5
xix	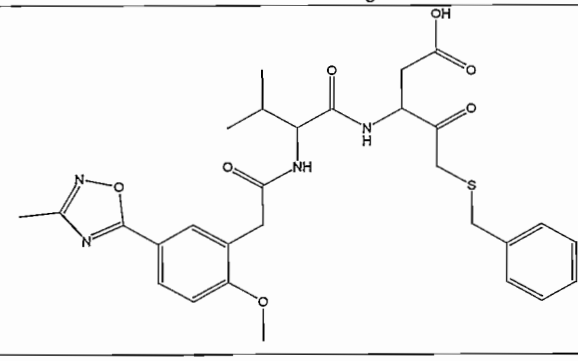	9

xx	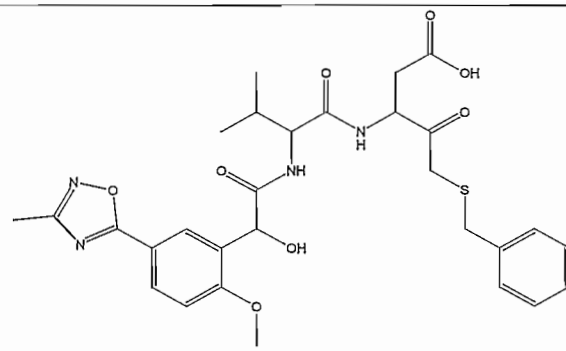	12
xxi	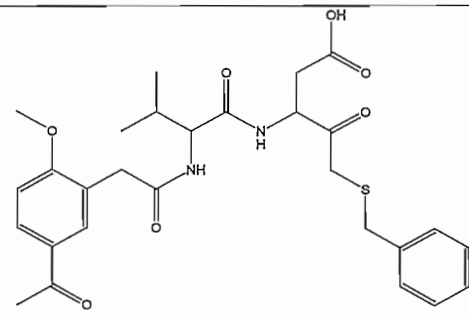	13
xxii	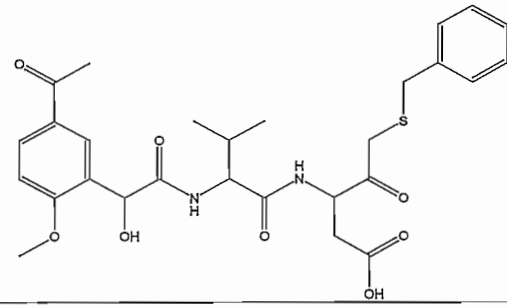	16
xxiii	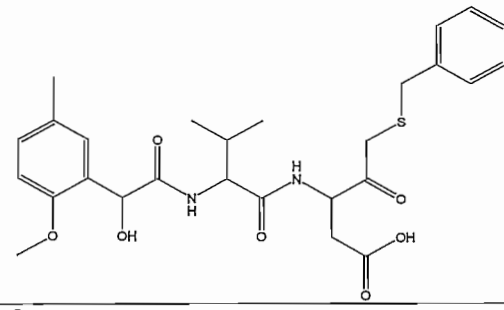	16
xxiv	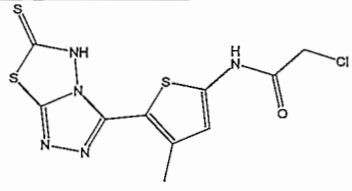	240
xxv	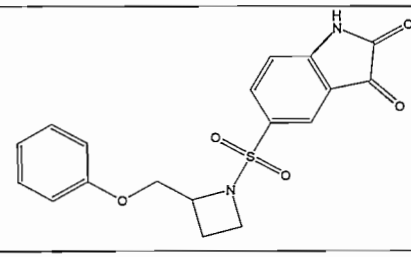	287

xxvi	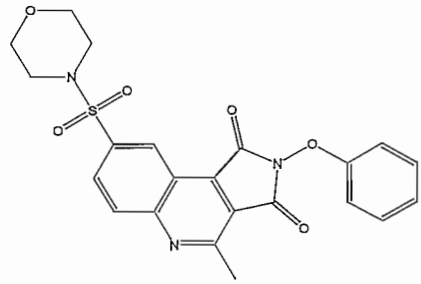	404
xxvii	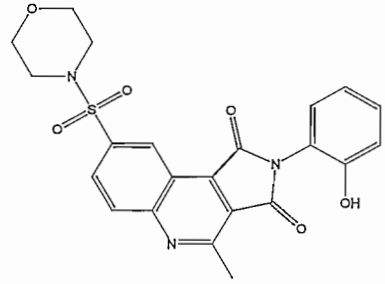	2300
xxviii	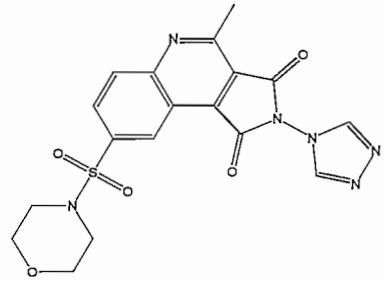	2980
xxix	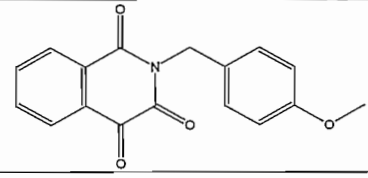	4630
xxx	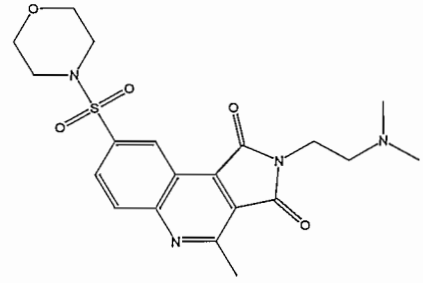	5500

Hypothesis generation for GSK3β

Table 7: Training set for GSK3β

	Compound	IC_{50} (nM)
i	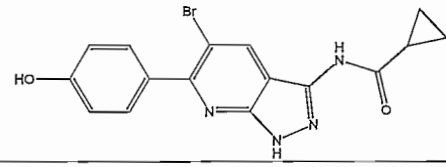	0.8
ii	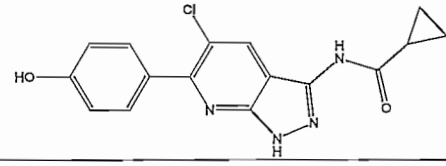	1
iii	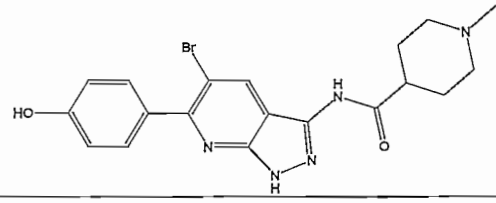	1
iv	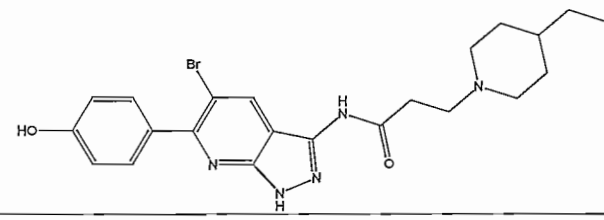	4
v	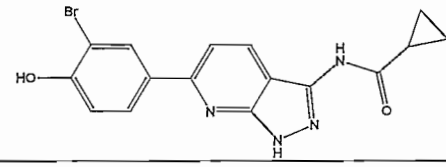	5
vi	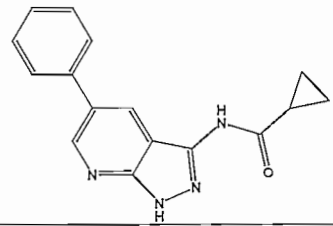	5
vii	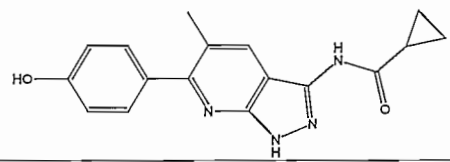	6
viii	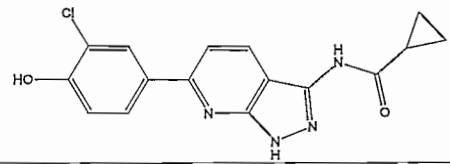	7

ix	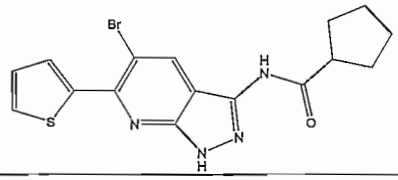	7
x	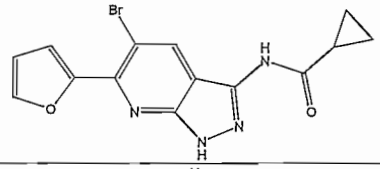	7
xi	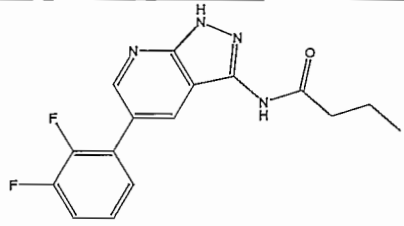	7
xii	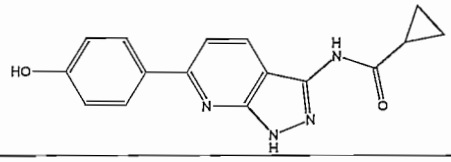	8
xiii	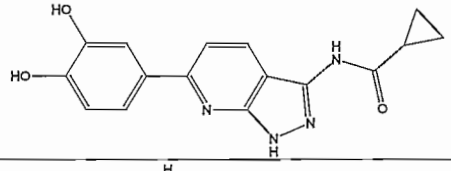	8
xiv	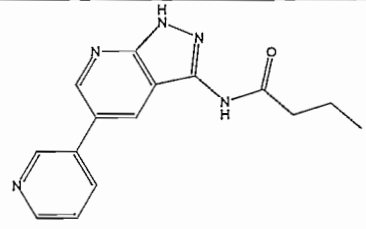	11
xv	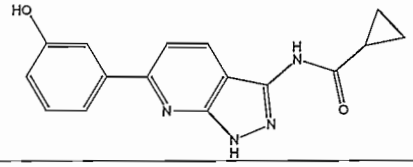	12
xvi	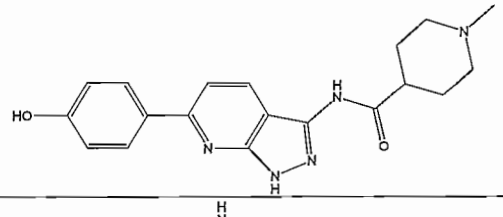	12
xvii	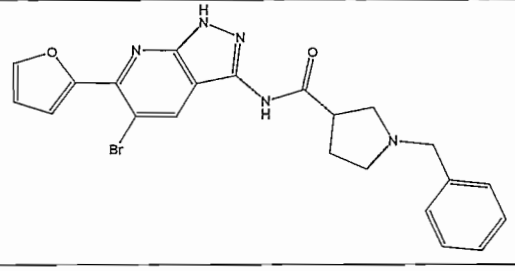	14

xviii	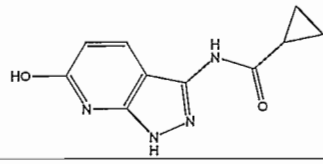	15
xix	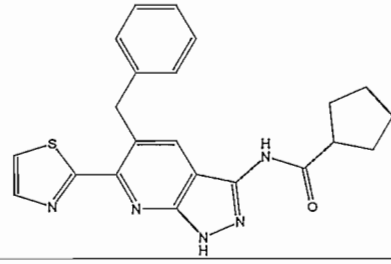	16
xx	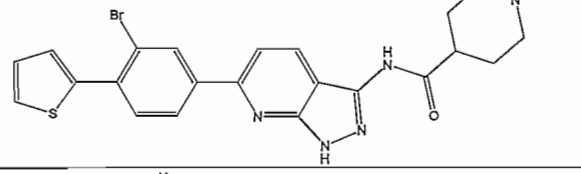	18
xxi	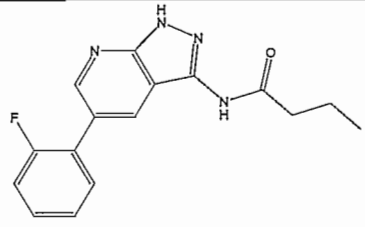	18
xxii	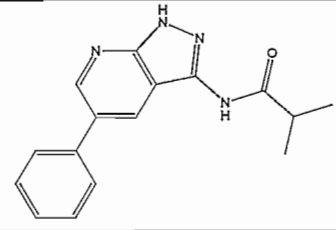	19
xxiii	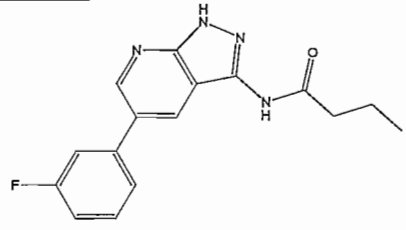	20
xxiv	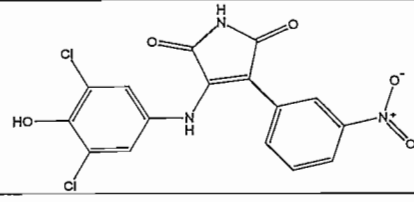	20
xxv	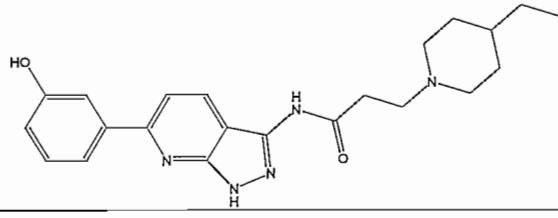	21

xxvi	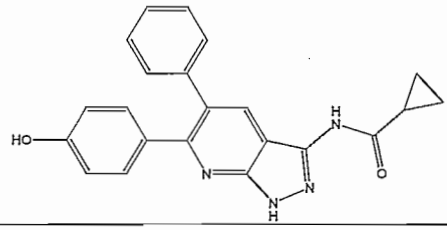	24
xxvii	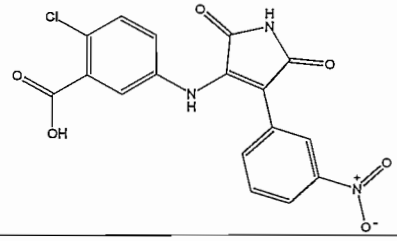	26
xxviii	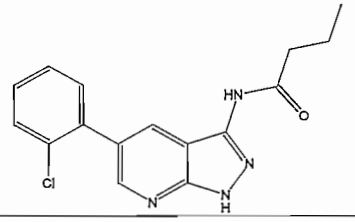	27
xxix	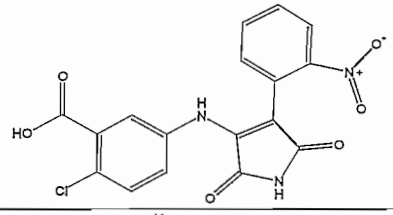	28
xxx	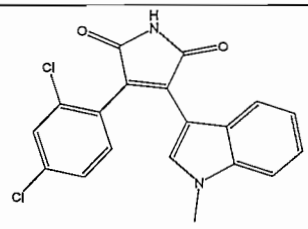	34
xxxi	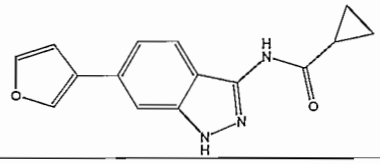	35
xxxii	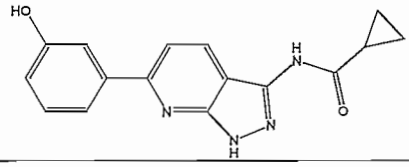	36
xxxiii	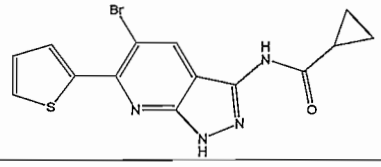	39

xxxiv	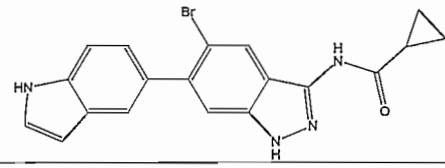	42
xxxv	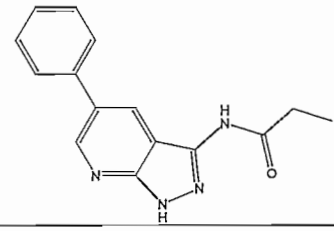	43
xxxvi	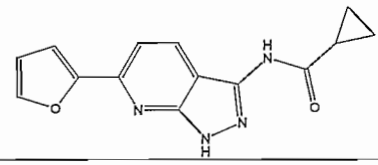	50
xxxvii	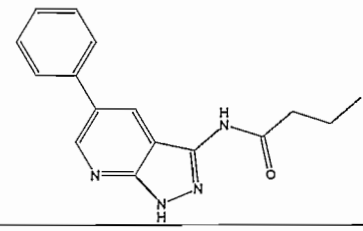	56
xxxviii	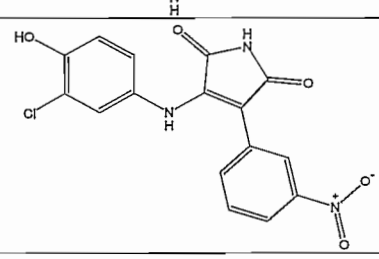	59
xxxix	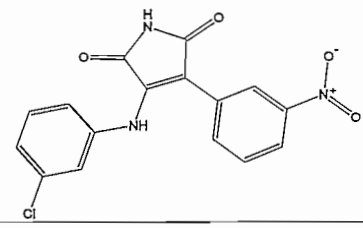	70
xl	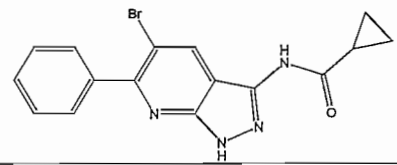	75
xli	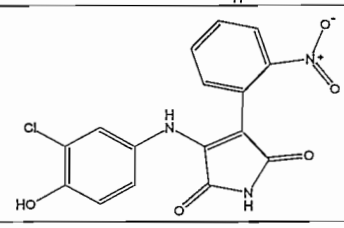	78

xlii	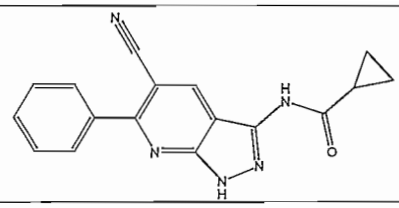	87
xliii	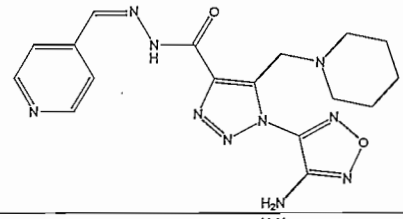	100
xliv	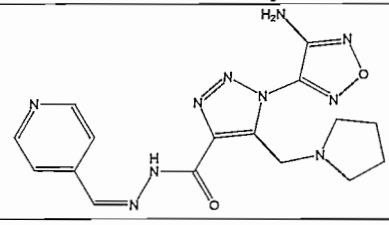	100

Table 8: Validation database for GSK3β

	Compound	IC_{50} (nM)
i	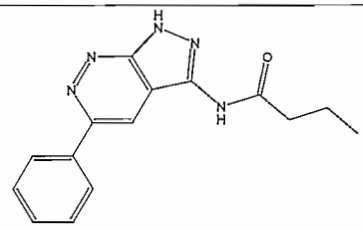	4
ii	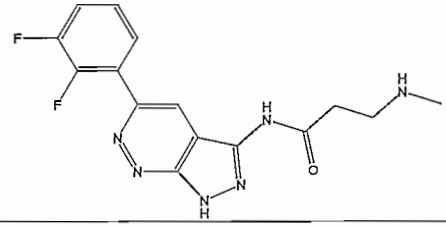	5
iii	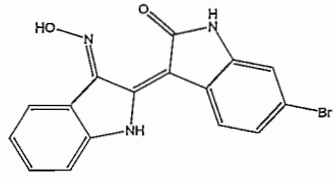	5
iv	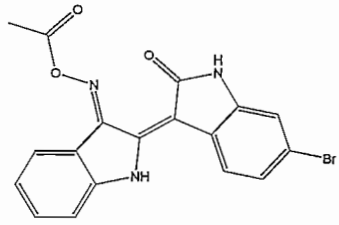	10

v	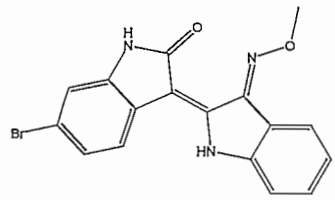	30
vi	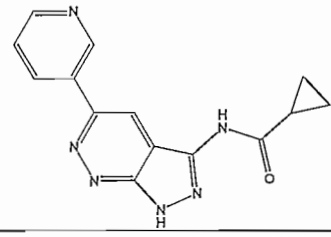	0.08
vii	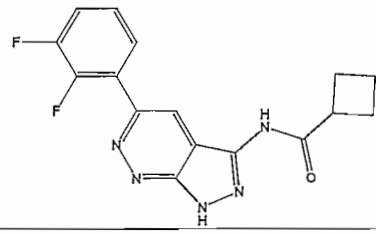	0.11
viii	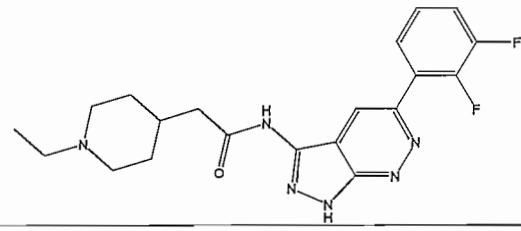	0.19
ix	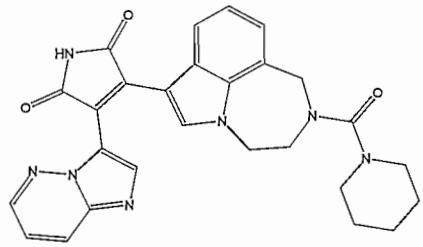	0.7
x	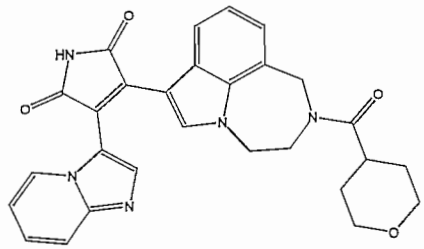	0.8
xi	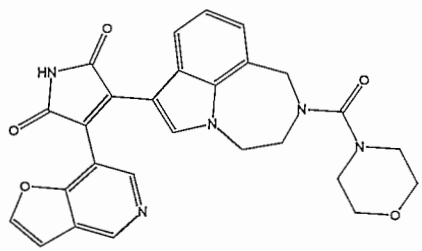	0.8

xii	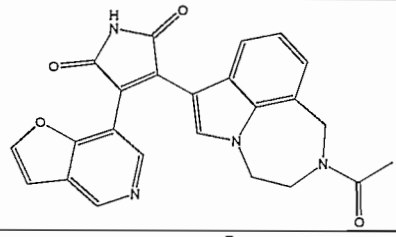	0.9
xiii	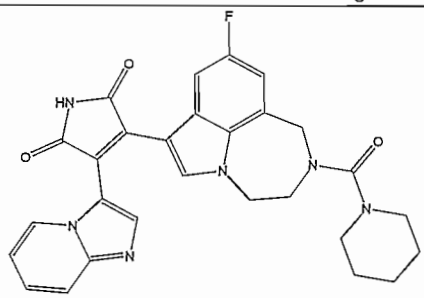	1.1
xiv	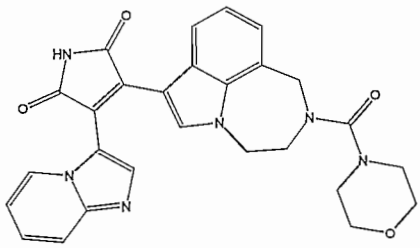	1.3
xv	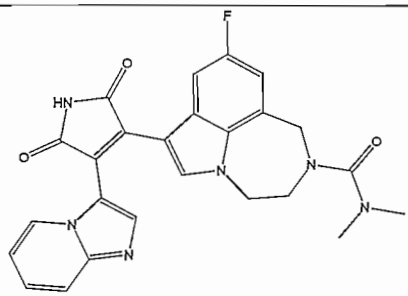	1.6
xvi	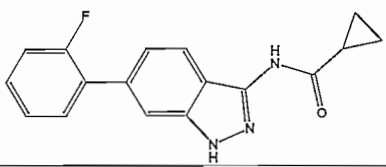	1000
xvii	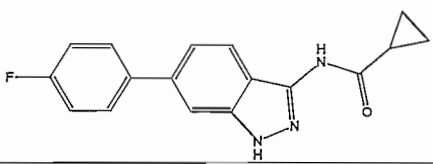	1000
xviii	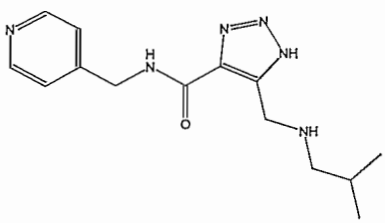	250000

xix	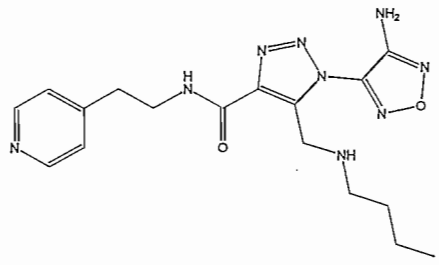	11700
xx	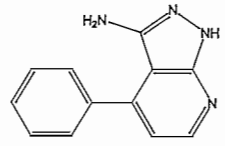	5000
xxi	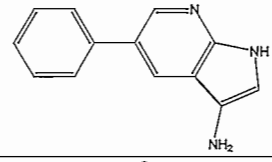	5000
xxii	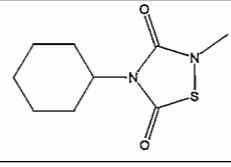	100000
xxiii	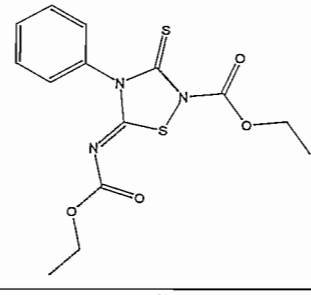	100000
xxiv	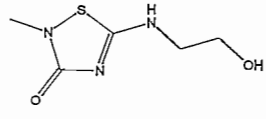	100000
xxv	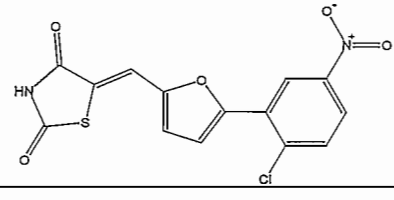	10000

Compounds used for screening of library and docking studies

Table 9: Library 1

Nr	Compound	Nr	Compound
QB1	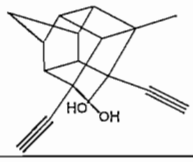	QB2	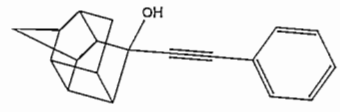
QB3	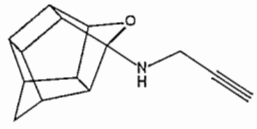	QB4	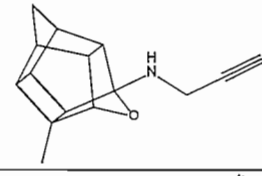
QB5	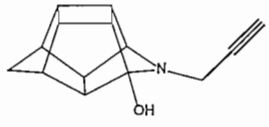	QB6	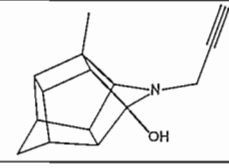
QB7	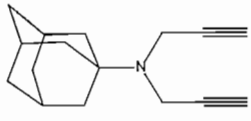	QB8	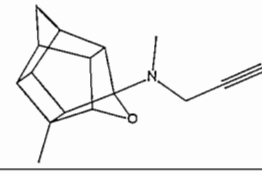
LP 1	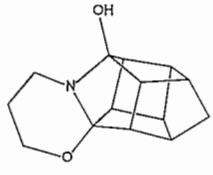	LP 2	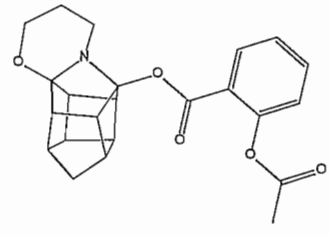
LP 3	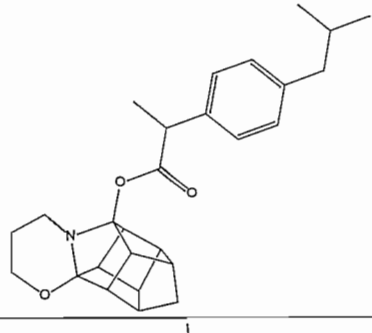	LP 4	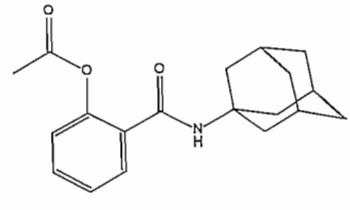
LP 5	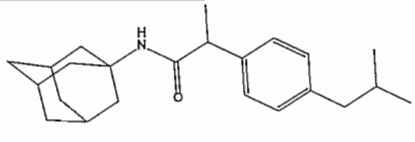	SM1	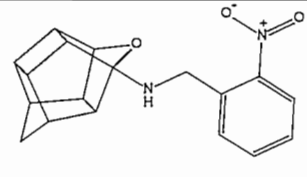

SM2	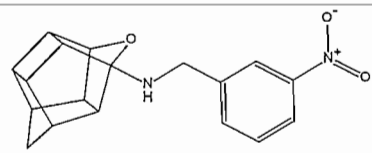	**SM3**	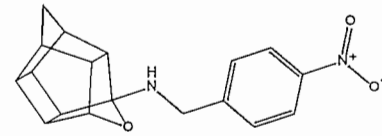
SM4	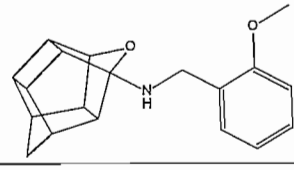	**SM5**	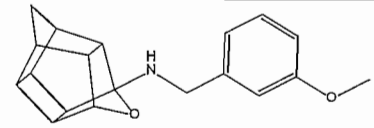
SM6	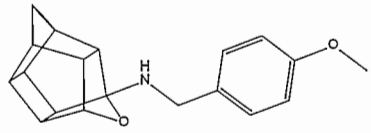	**SM7**	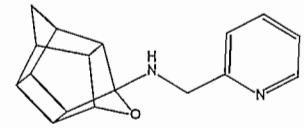
SM8	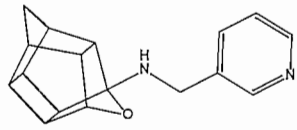	**SM9**	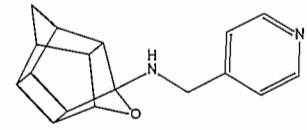
SM 10	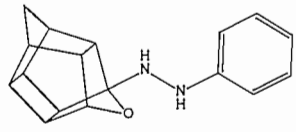	**SM 11**	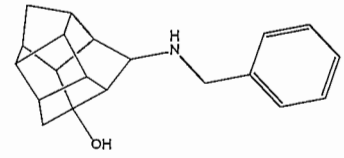
SM 12	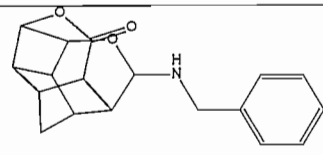	**SM 13**	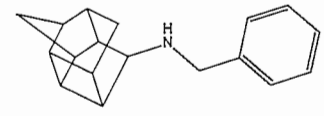
JJ 2	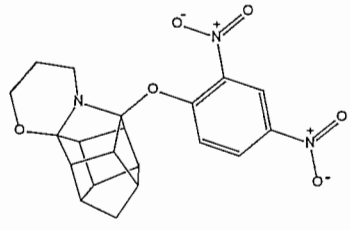	**JJ 3**	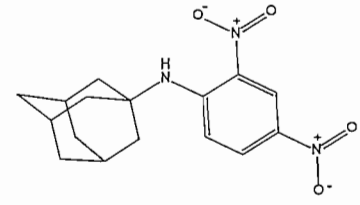
JJ 4	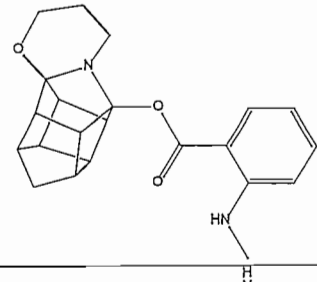	**JJ 5**	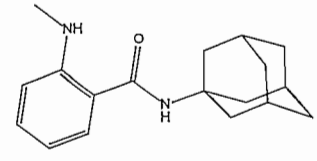
JJ 6	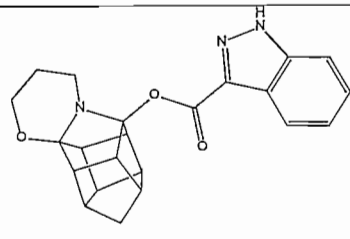	**JJ 7**	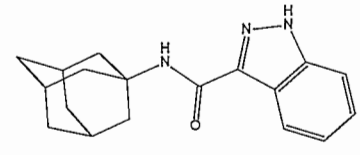

JJ 8	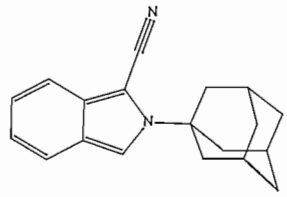	JJ 9	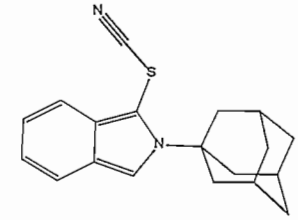
JJ 10	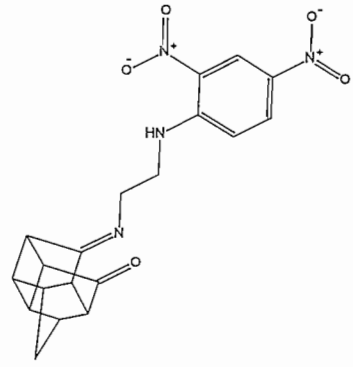	JJ 11	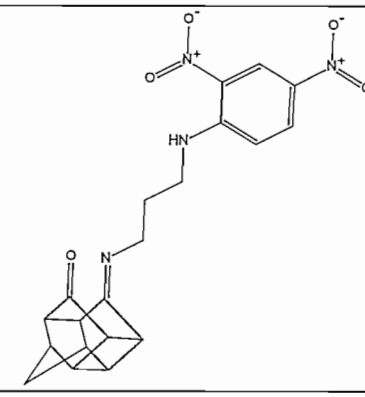
JJ 12	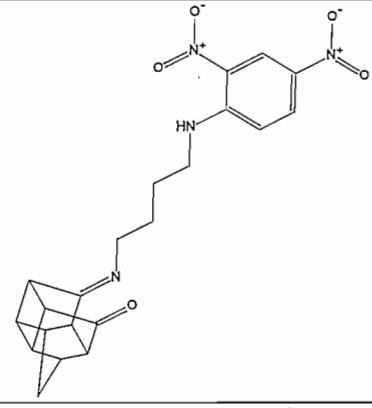	JJ 13	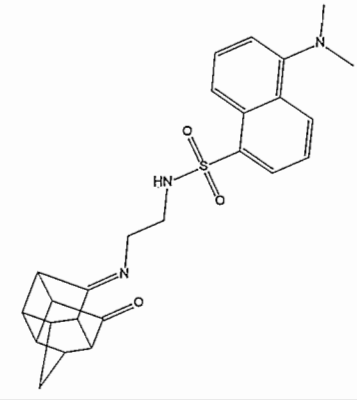
JJ 14	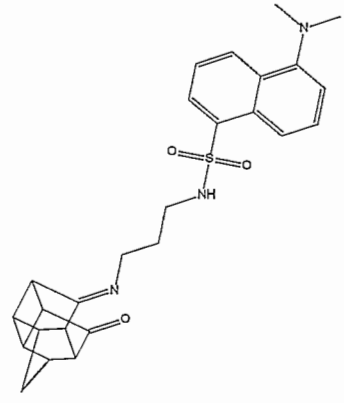	JJ 15	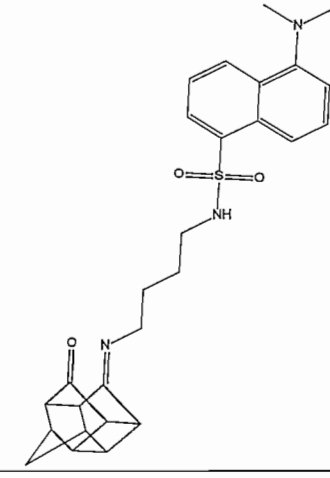
JJ 16	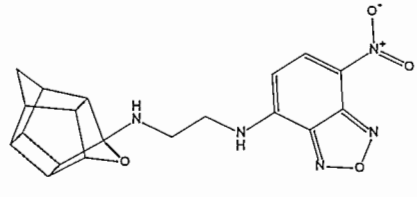	JJ 17	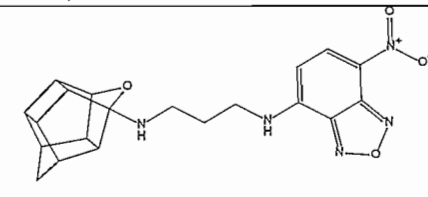

JJ 18	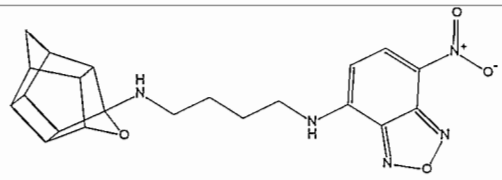	JJ 19	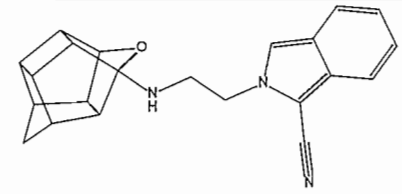
JJ 20	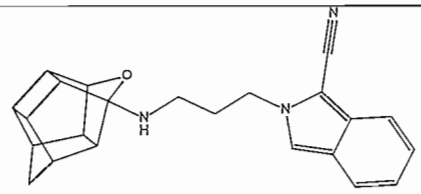	JJ 21	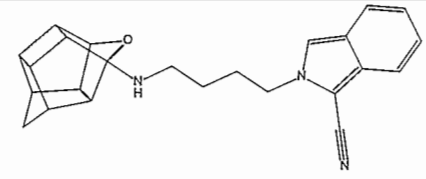
JJ 22	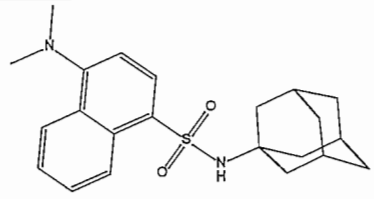	JJ 23	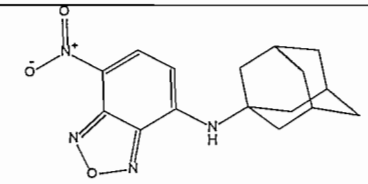
JJ 24	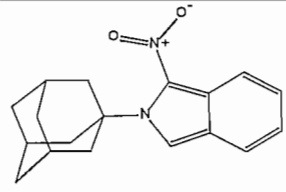	JJ 25	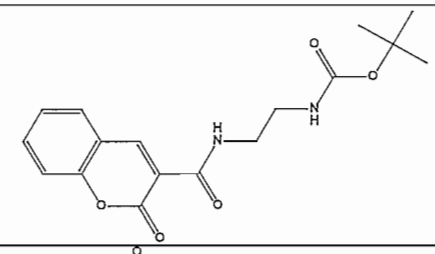
JJ 26	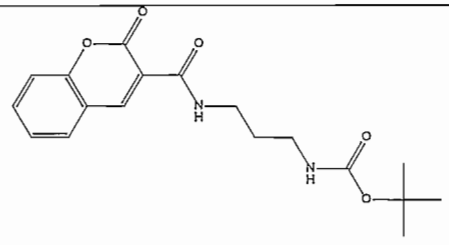	JJ 27	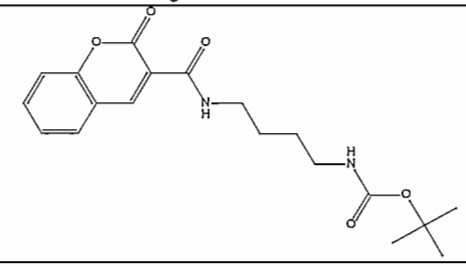
DW 1	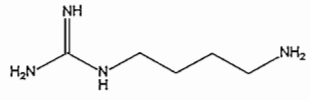	DW 2	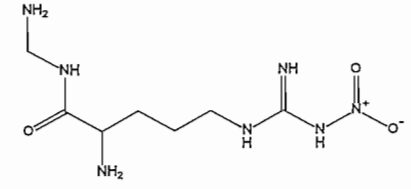

DW 3	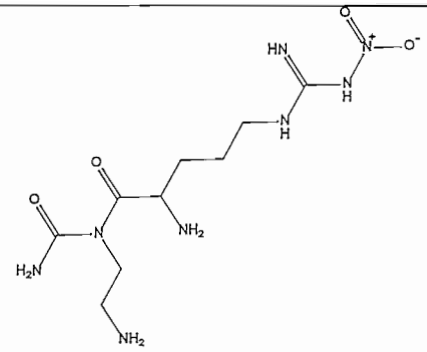	**DW 4**	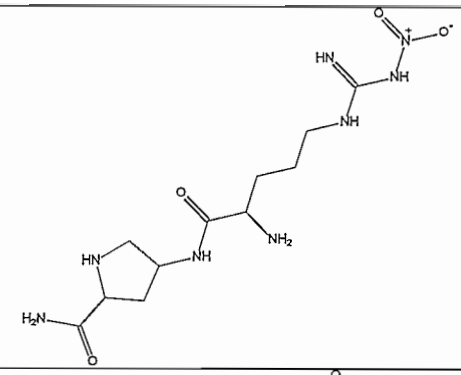
DW 5	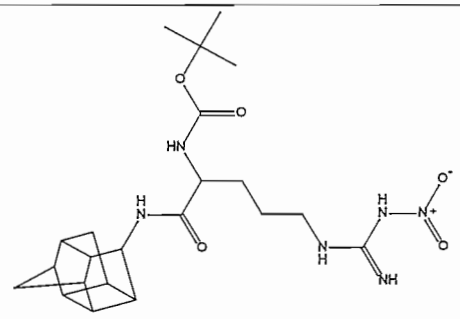	**DW 6**	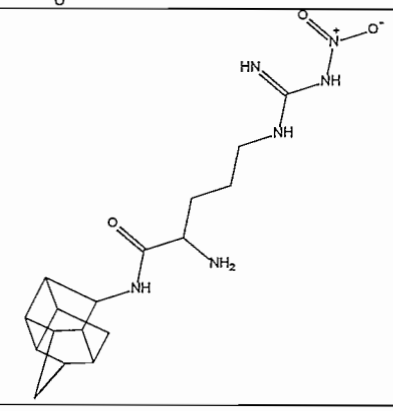
DW 7	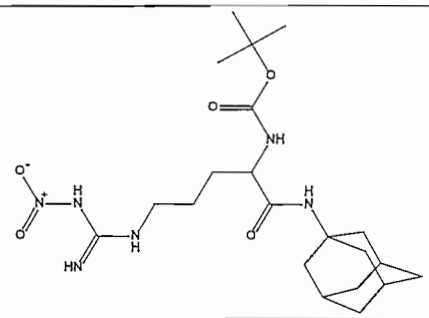	**DW 8**	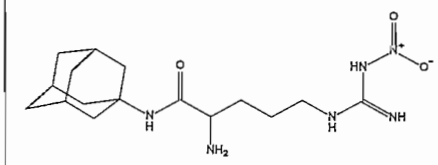
DW 9	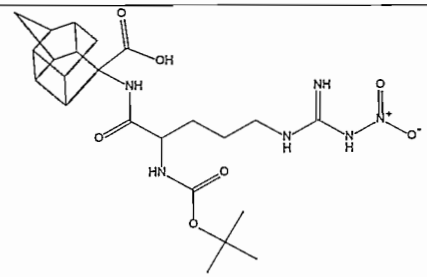	**DW 10**	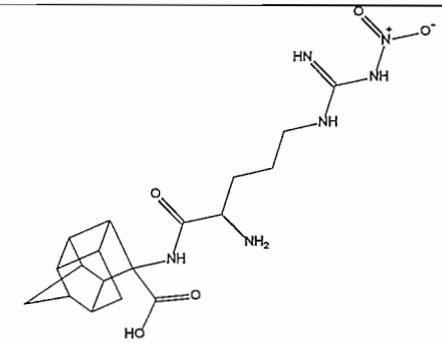
DW 11	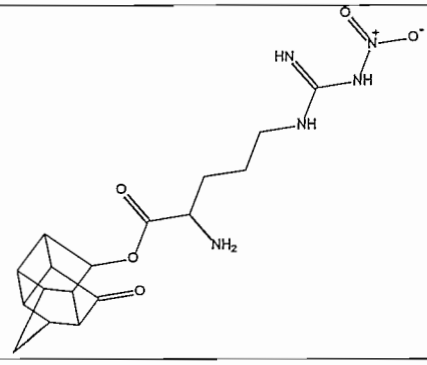	**DW 12**	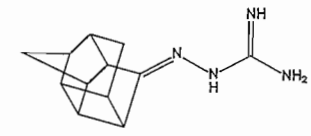

DW 13	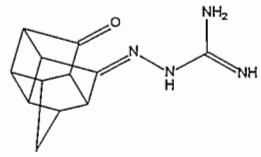	**DW 14**	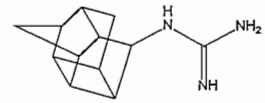
DW 15	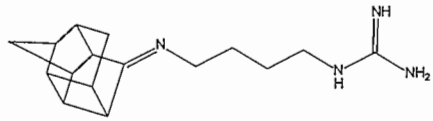		

Table 10: Library 2

Nr	Compound	Nr	Compound
OD1	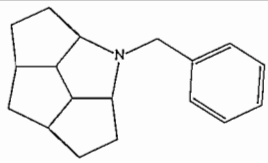	**OD2**	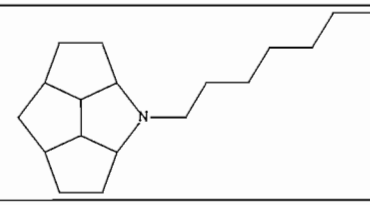
OD3	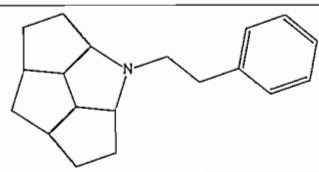	**OD4**	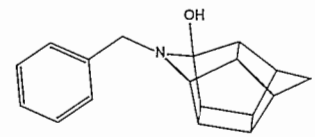
OD5	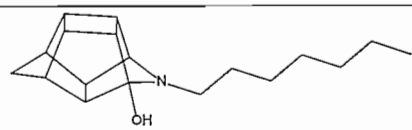	**OD6**	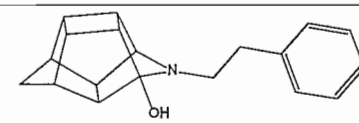
OD7	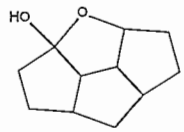	**RL 1**	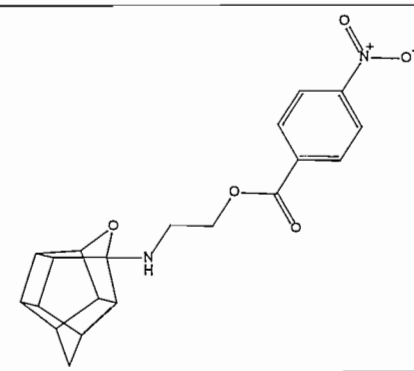

RL 2	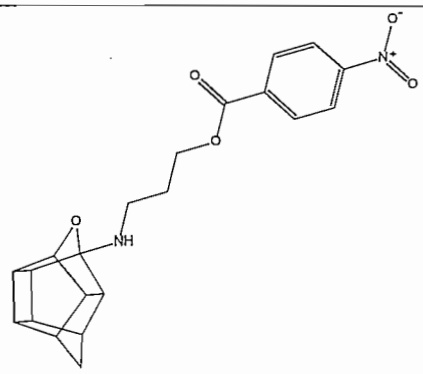	RL 3	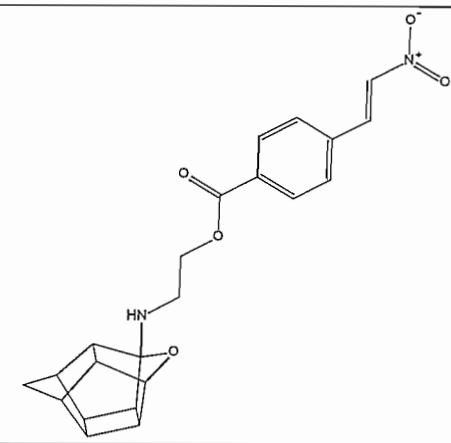
RL 4	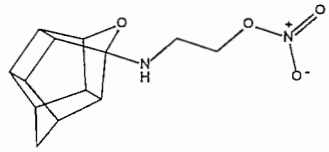	RL 5	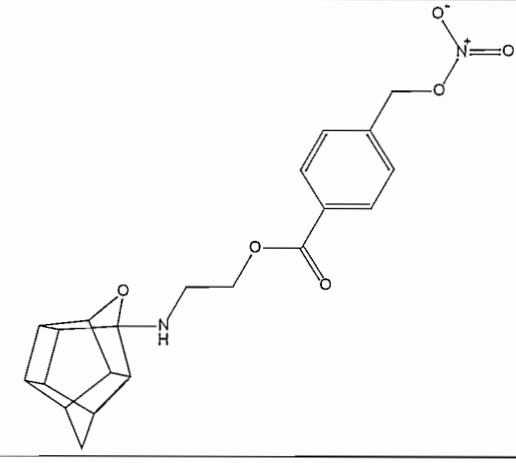
RL 6	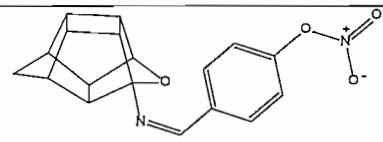	YG1	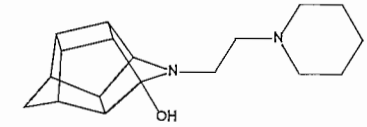
YG2	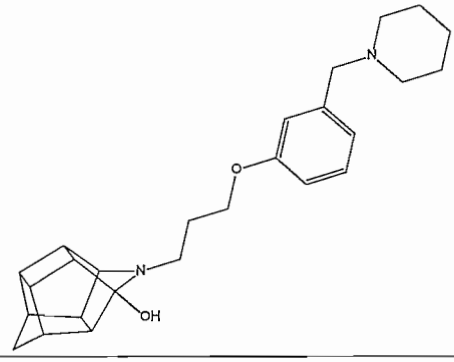	YG3	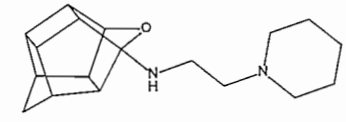

YG4	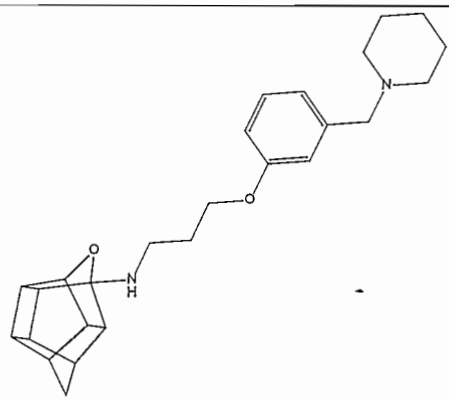	YG5	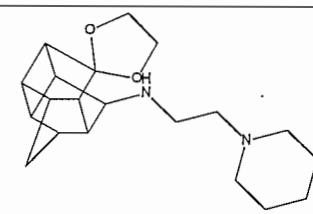
YG6	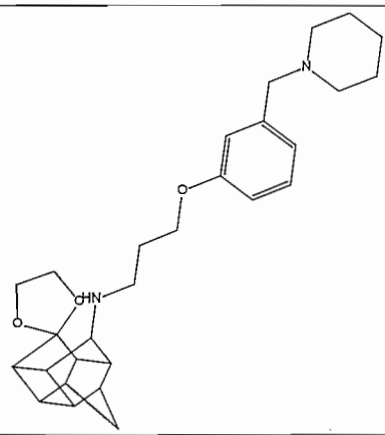	BR 6	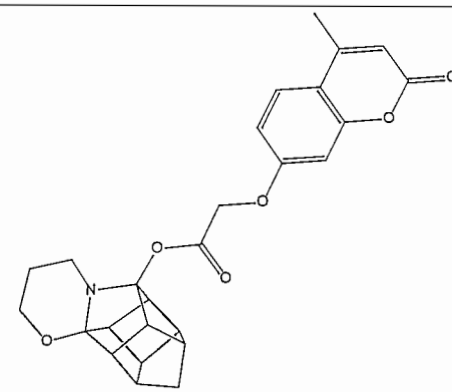

Table 11: Library 3

Nr	Compound	Nr	Compound
JP1	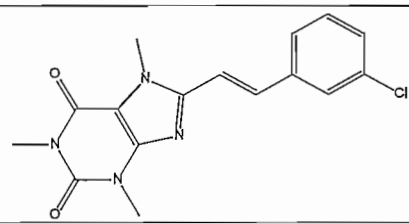	JP2	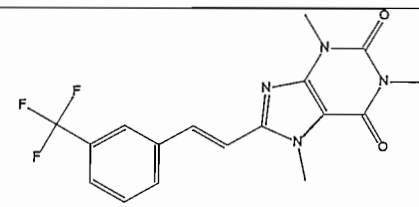
JP3	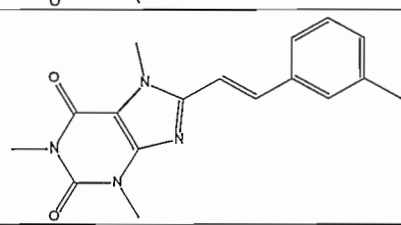	JP4	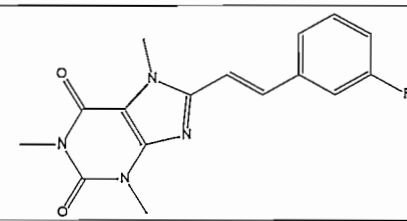
JP5	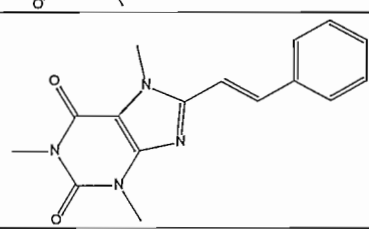	JP6	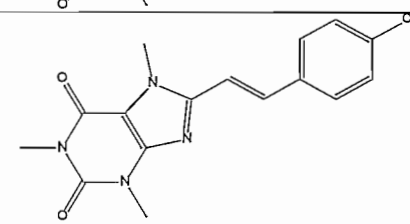

JP7	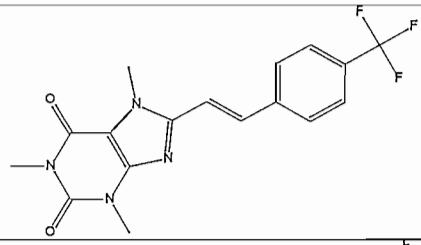	JP8	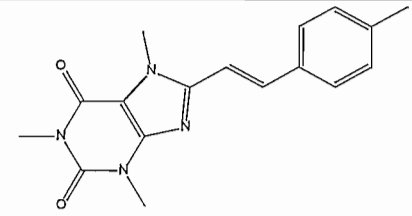
JP9	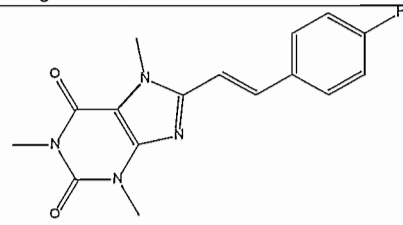	JP 10	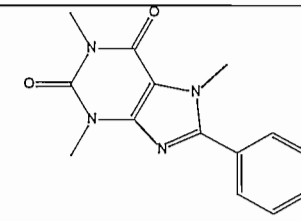
JP 11	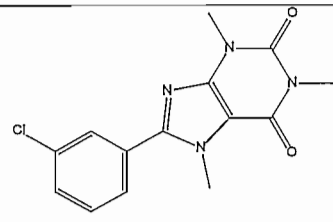	JP 12	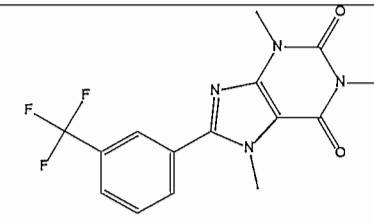
JP 13	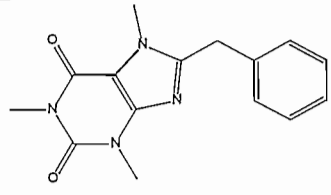	JP 14	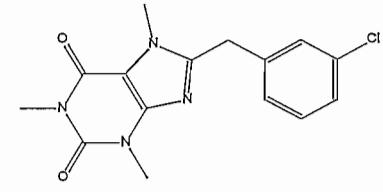
JP 15	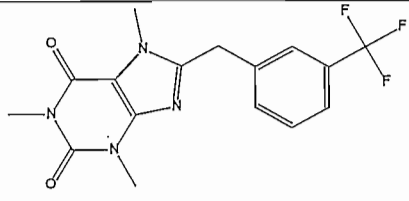	JP 16	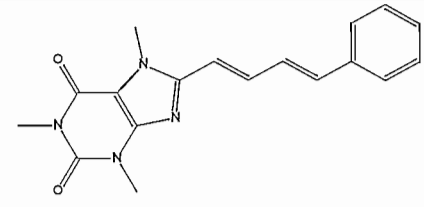
JP 17	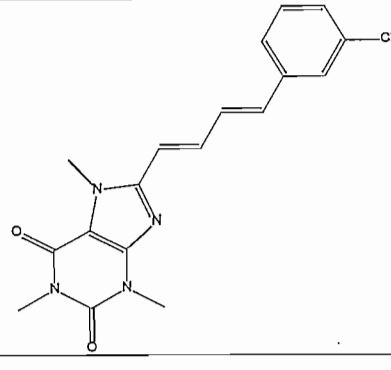	JP 18	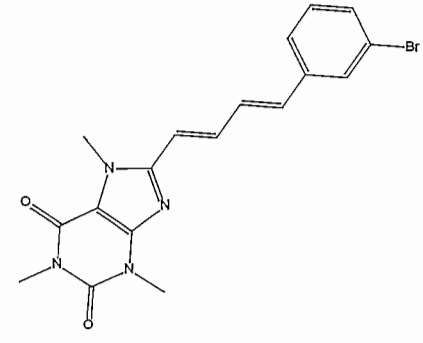

JP 19	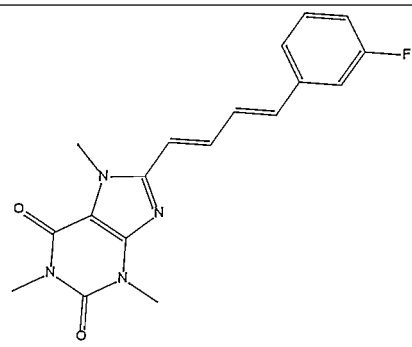	JP 20	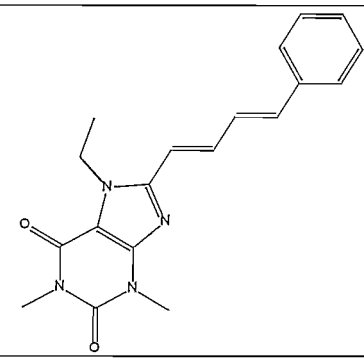
JP 21	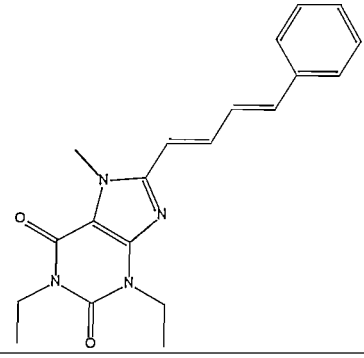	JP 22	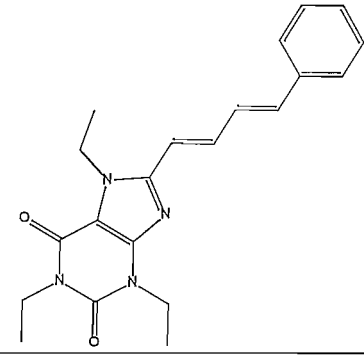
JP 23	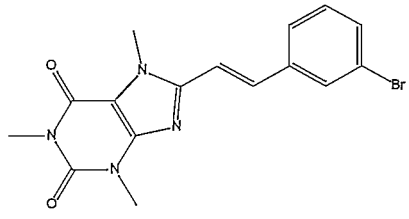	JP 24	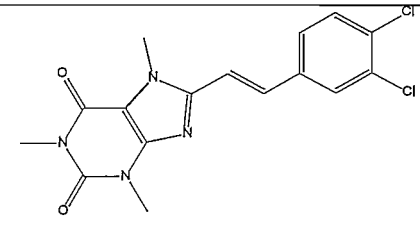
JP 25	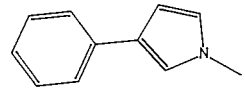	JP 26	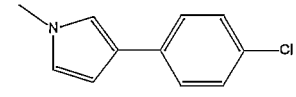
JP 27	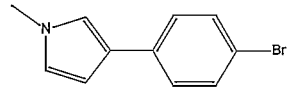	JP 28	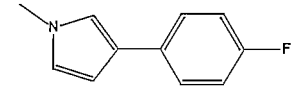
JP 29	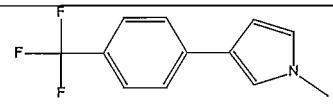	JP 30	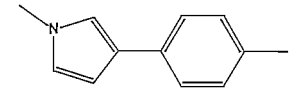
JP 31	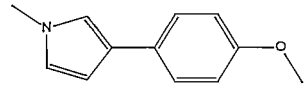	JP 32	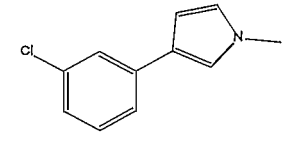
JP 33	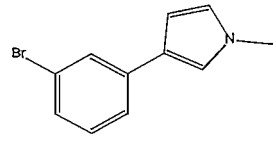	JP 34	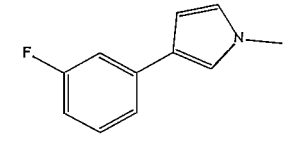

JP 35	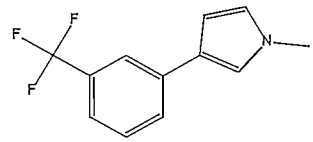	JP 36	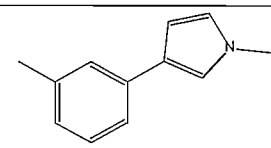
JP 37	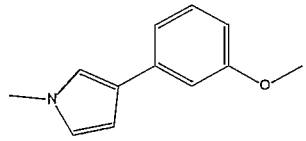	JP 38	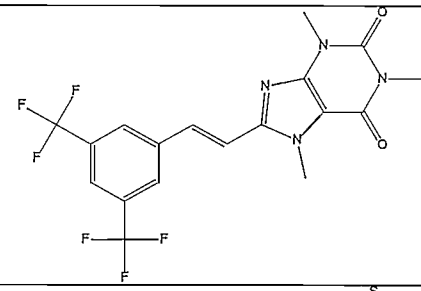
JP 39	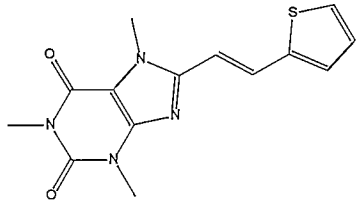	JP 40	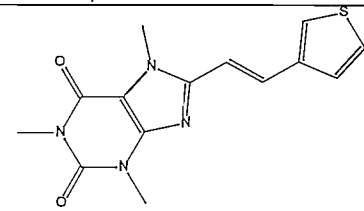
JP 41	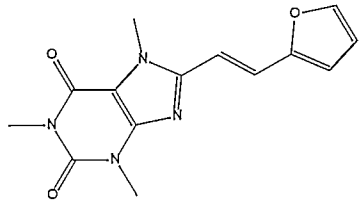	JP 42	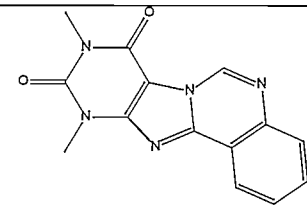
JP 43	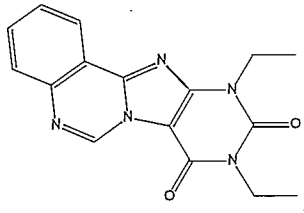	JP 44	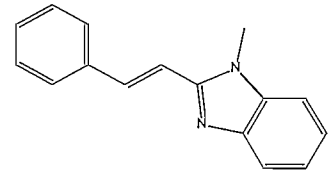
JP 45	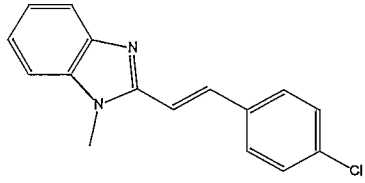	JP 46	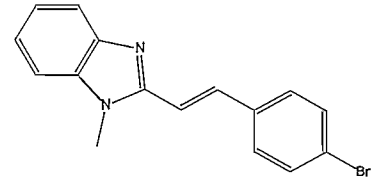
JP 47	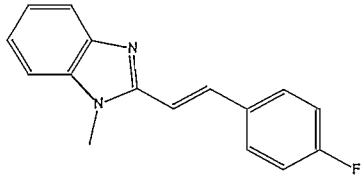	JP 48	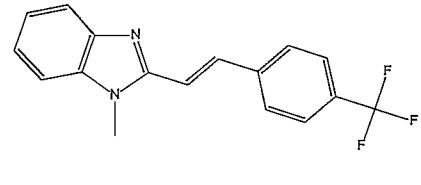

JP 49	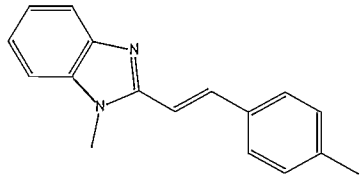	JP 50	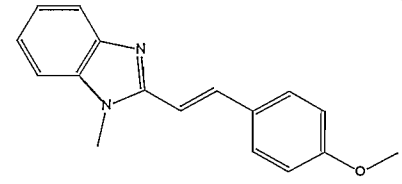
JP 51	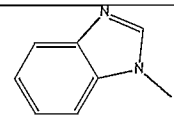	JP 52	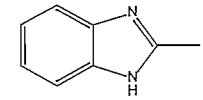
JP 53	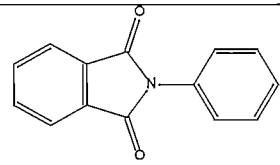	JP 54	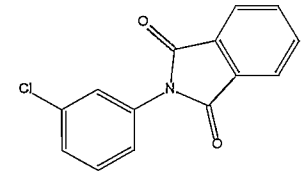
JP 55	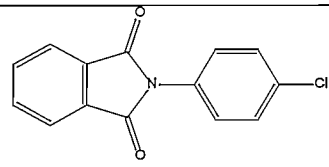	JP 56	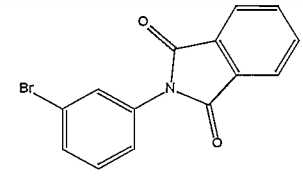
JP 57	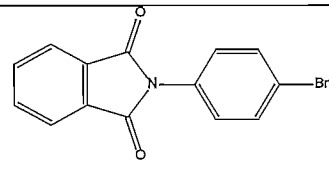	JP 58	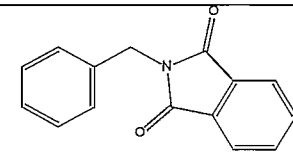
JP 59	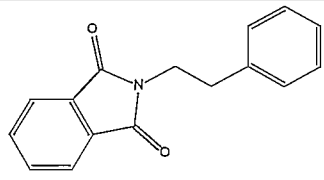	JP 60	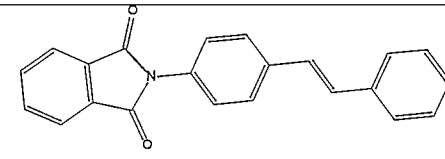
JP 61	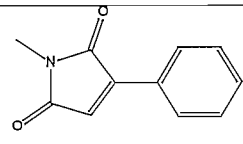	JP 62	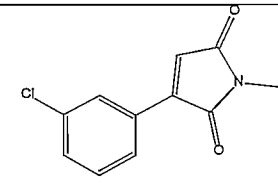

JP 63	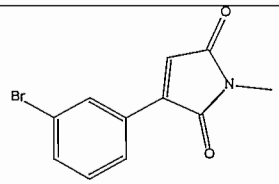	JP 64	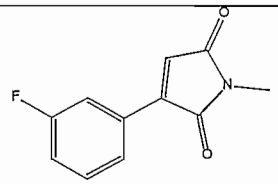
JP 65	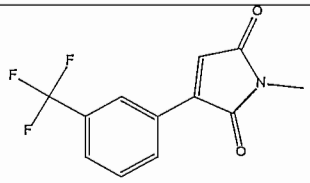	JP 66	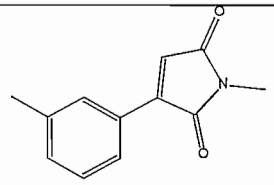
JP 67	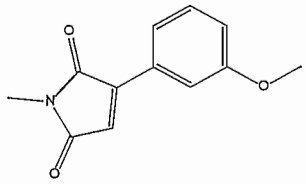	JP 68	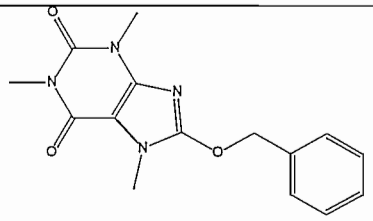
JP 69	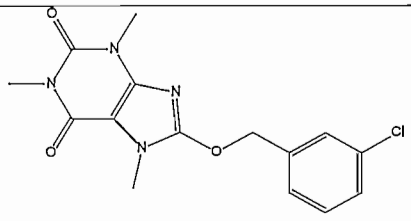	JP 70	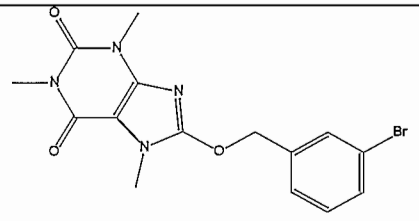
JP 71	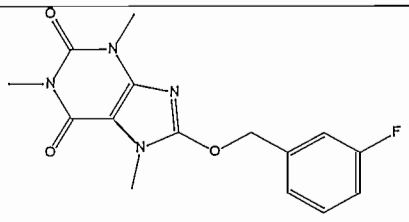	JP 72	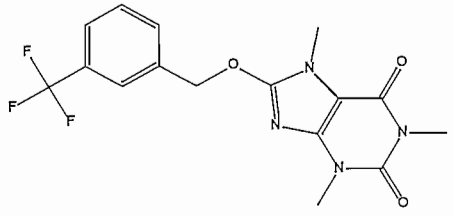
JP 73	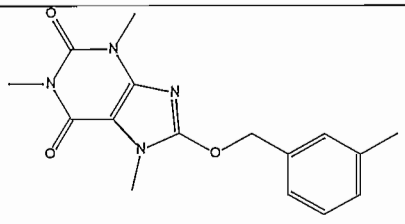	JP 74	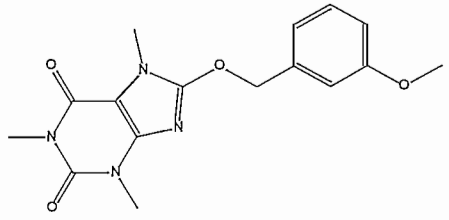
JP 75	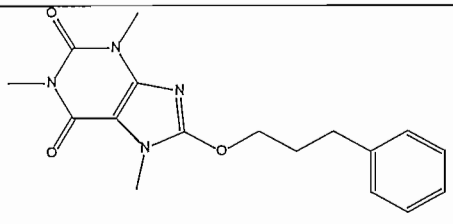	JP 76	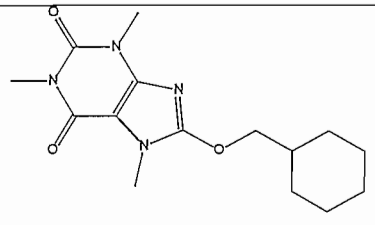

JP 77	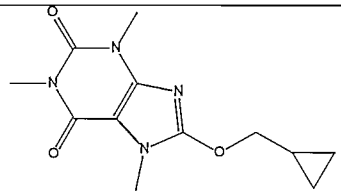	JP 78	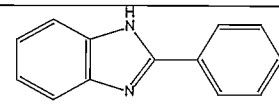
JP 79	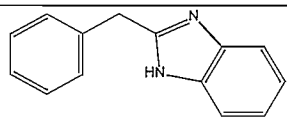	JP 80	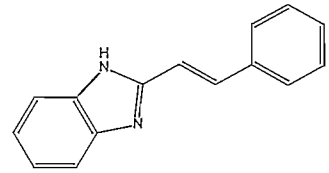
JP 81	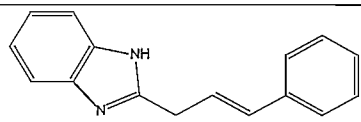	JP 82	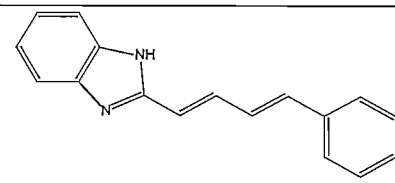
JP 83	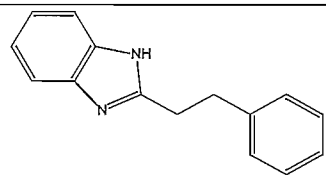	JP 84	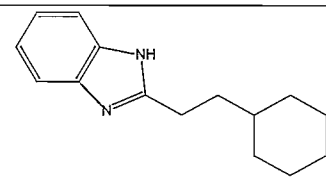
JP 85	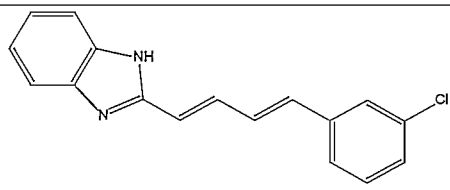	JP 86	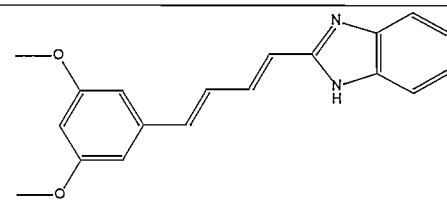

Table 12: Library 4

Nr	Compound	Nr	Compound
JB1	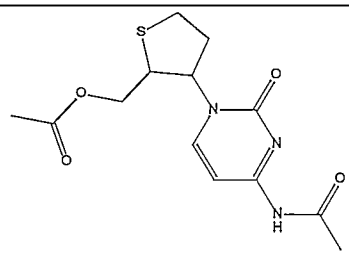	JB2	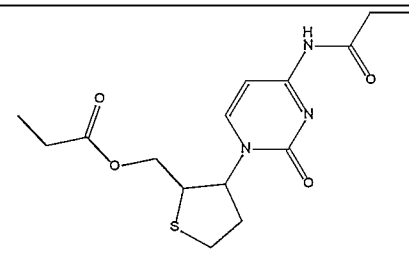

JB3	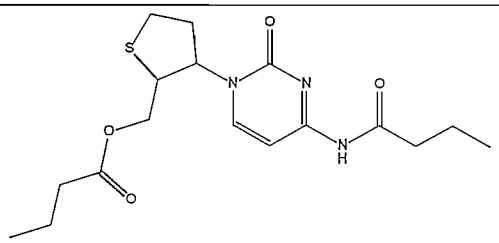	**JB4**	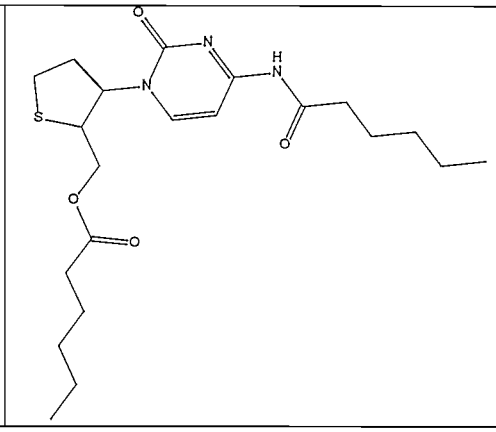
JB5	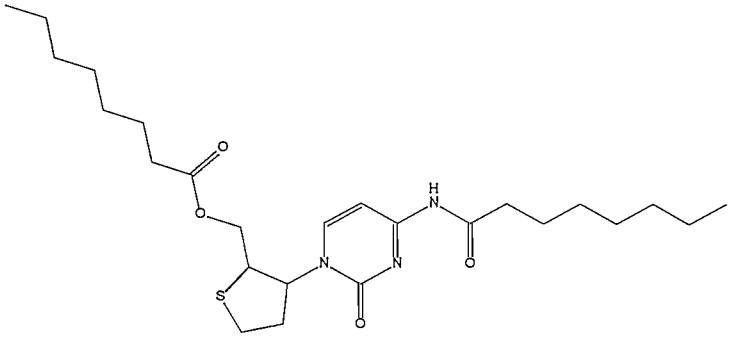		
JB6	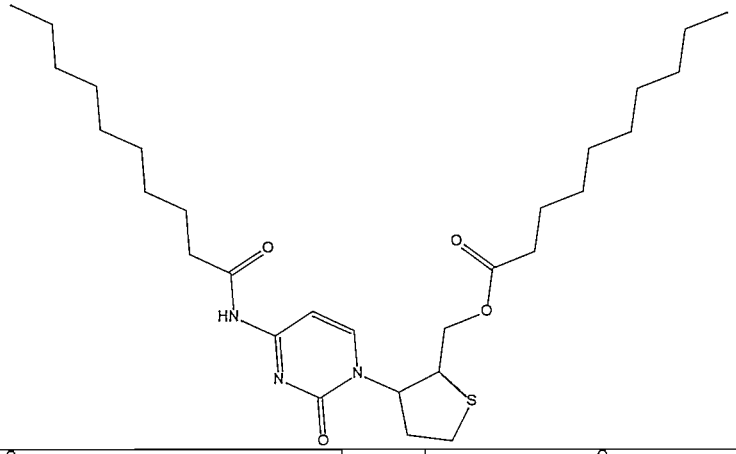		
JB7	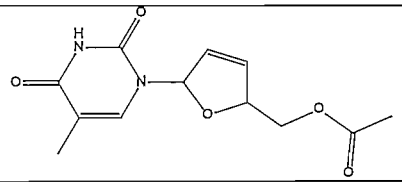	**JB8**	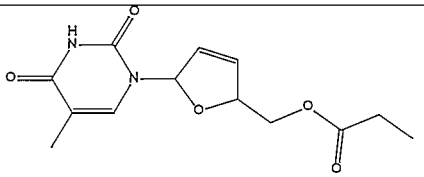
JB9	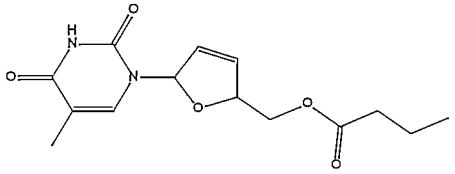	**JB 10**	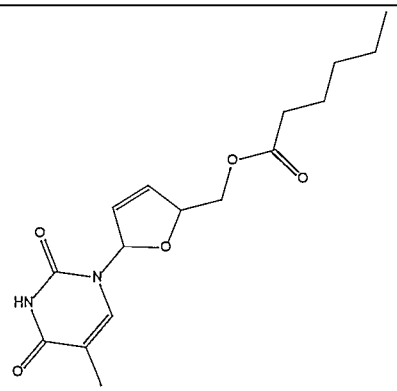

JB 11	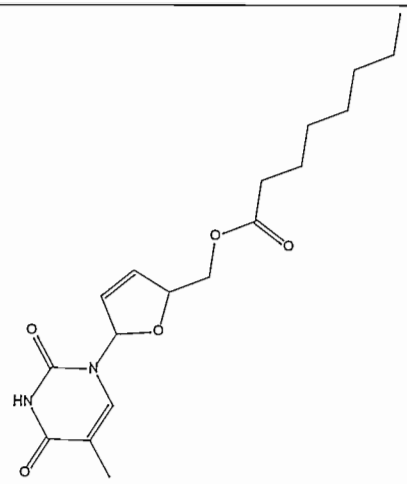
JB 12	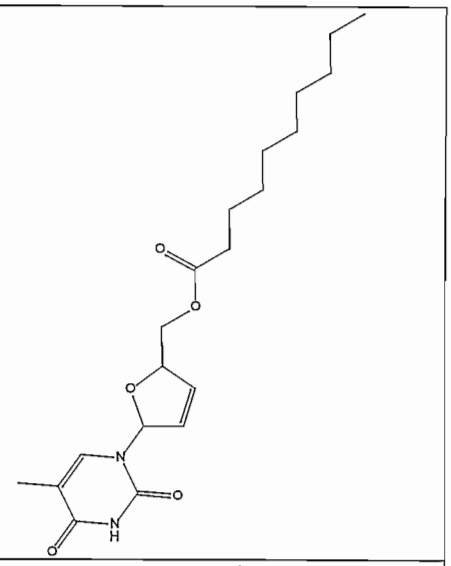
JB 13	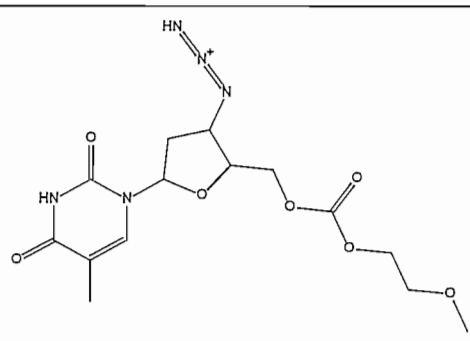
JB 14	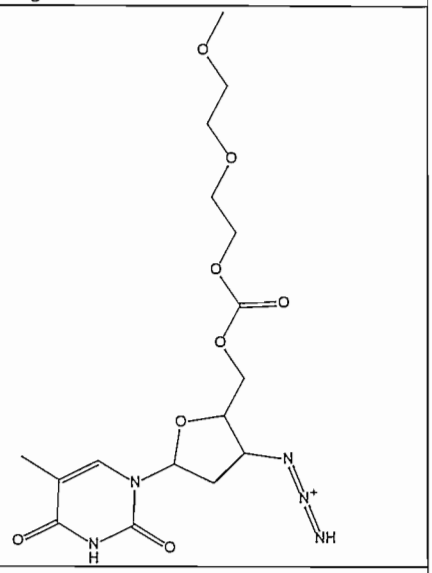
JB 15	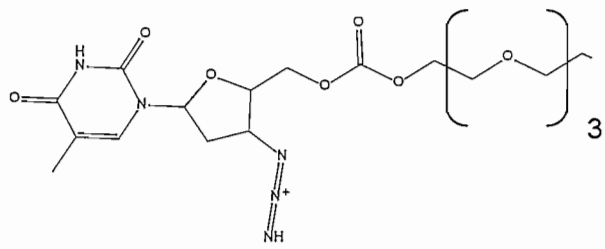
JB 16	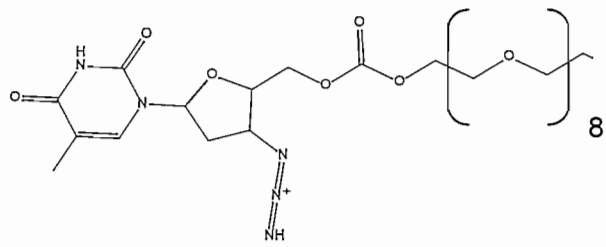

JB 17	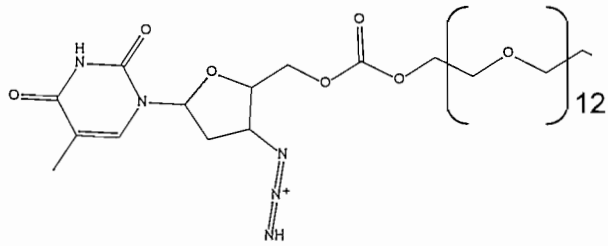
JB 18	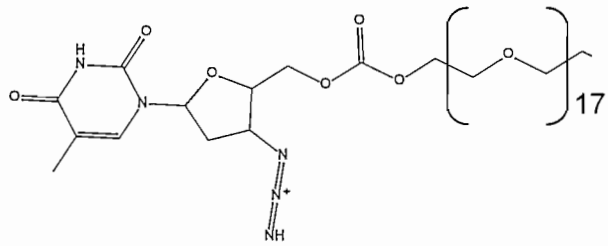
JB 19	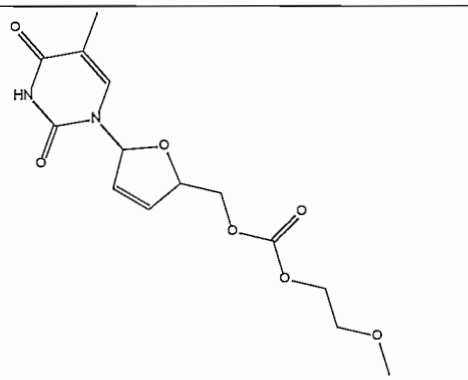
JB 20	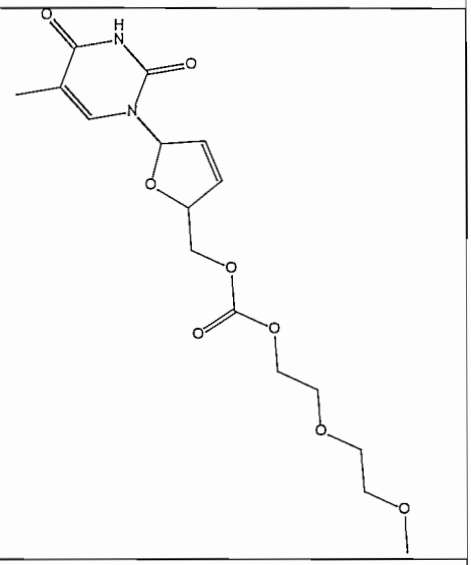
JB 21	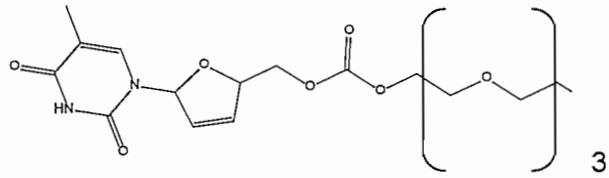
JB 22	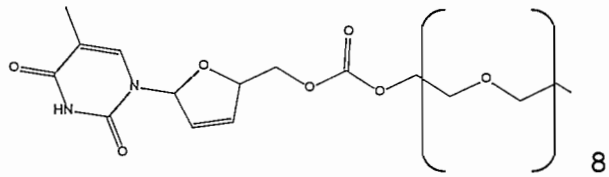
JB 23	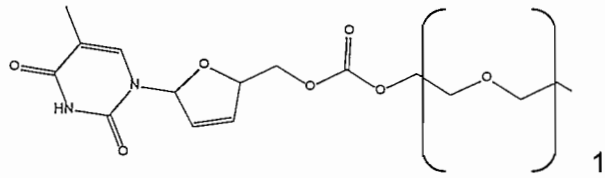

JB 24	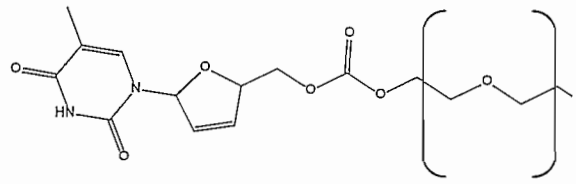 17		
JB 25	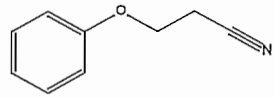	JB 26	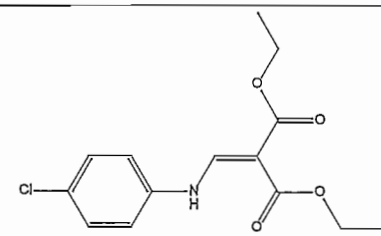
JB 27	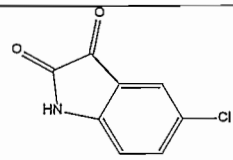	JB 28	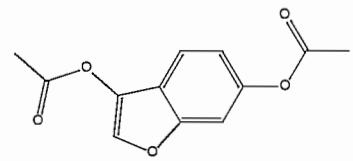
JB 29	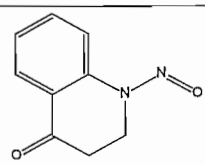	JB 30	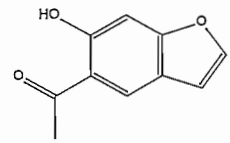
JB 31	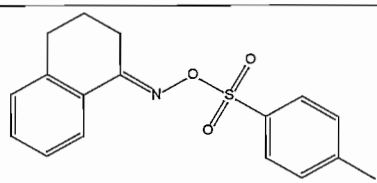	JB 32	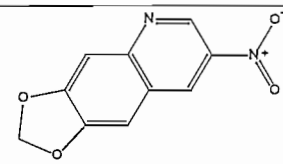
JB 33	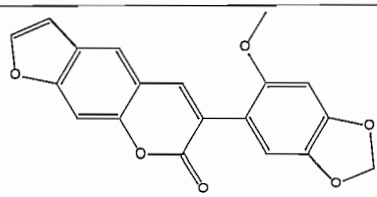	JB 34	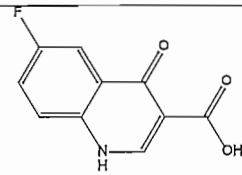
JB 35	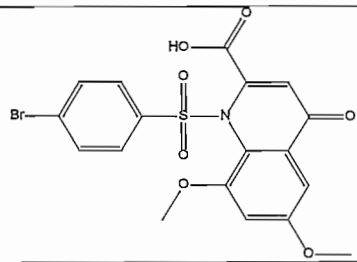	JB 36	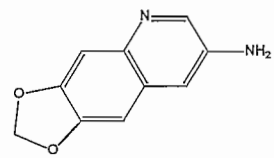

JB 37	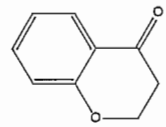	JB 38	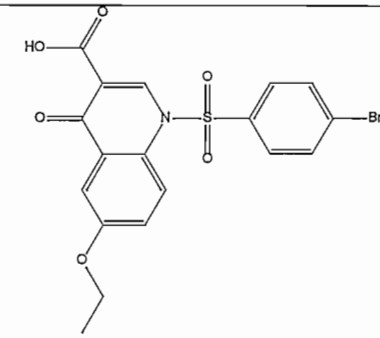
JB 39	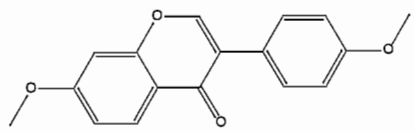	JB 40	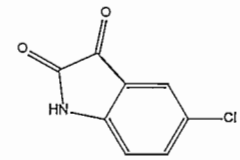
JB 41	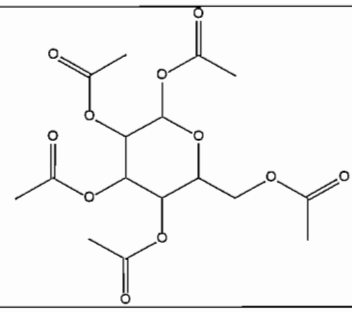	JB 42	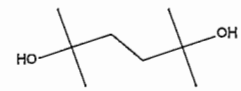
JB 43	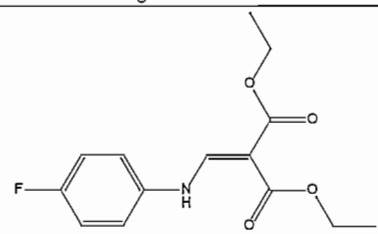	JB 44	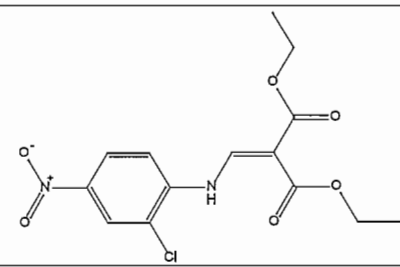
JB 45	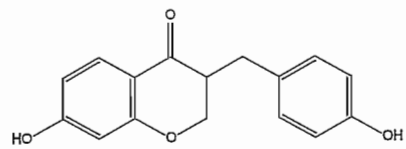	JB 46	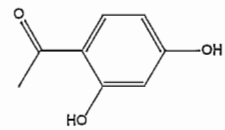
JB 47	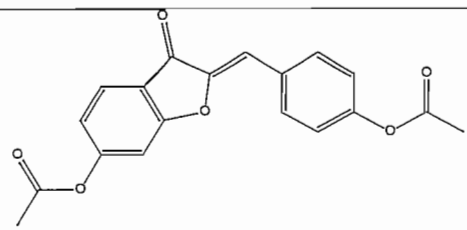	JB 48	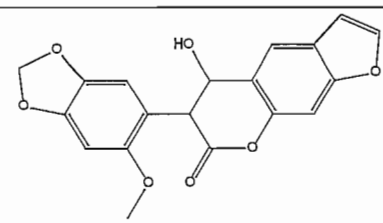

JB 49	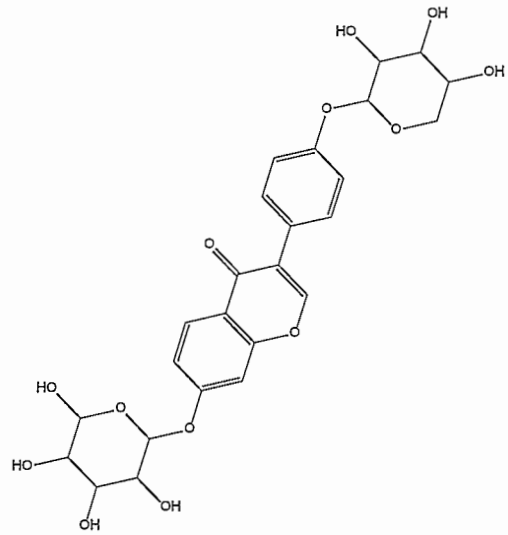	JB 50	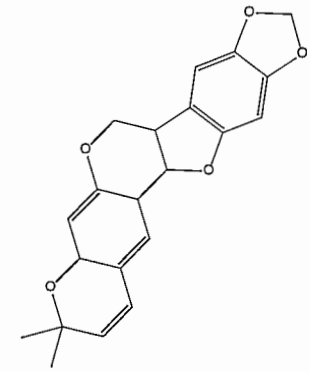
JB 51	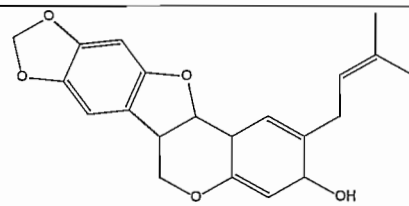	JB 52	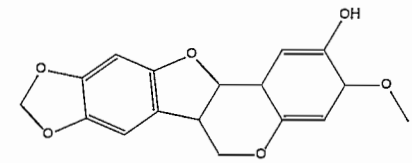
JB 53	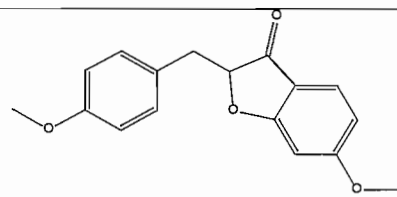		

Table 13: Library 5

Nr	Compound	Nr	Compound
JG 1	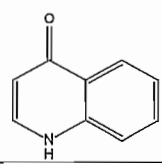	JG 2	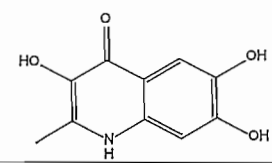
JG 3	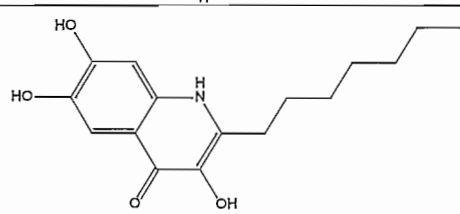	JG 4	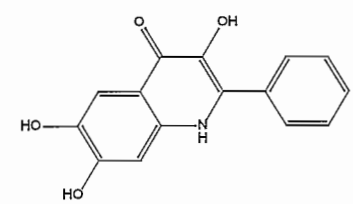

JG 5	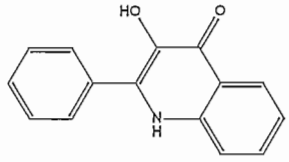	JG 6	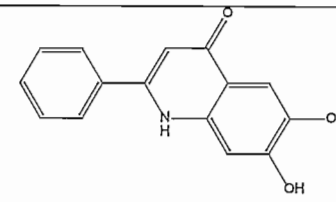
JG 7	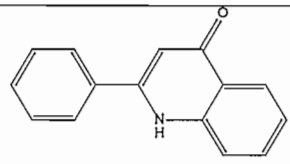	JG 8	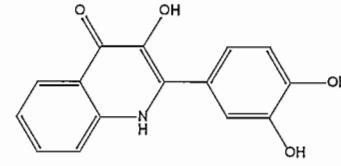
LP 6	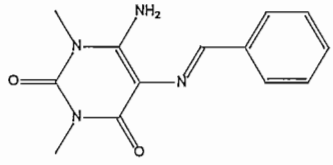	LP 7	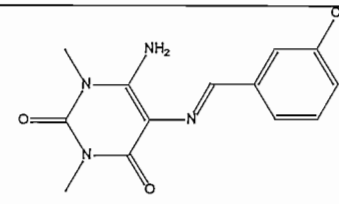
LP 8	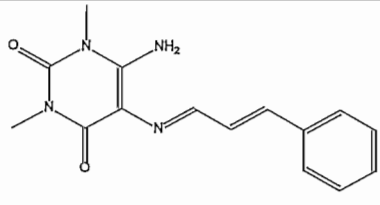	LP 9	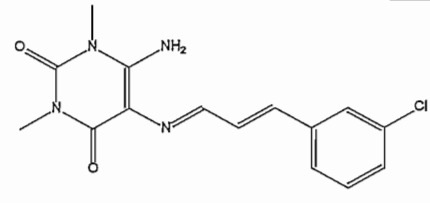
LP 10	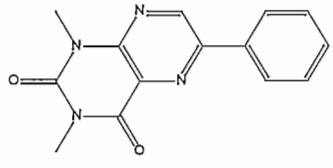	LP 11	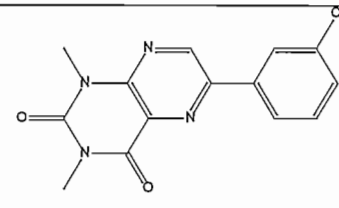
LP 12	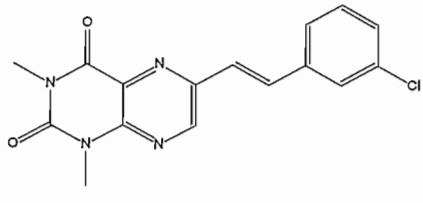	BR 1	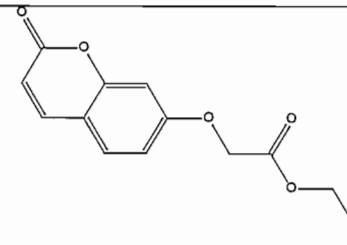

BR 2	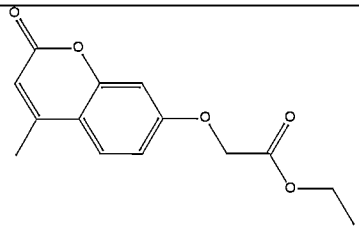	**BR 3**	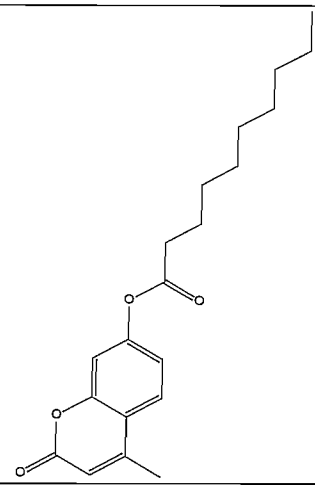
BR 4	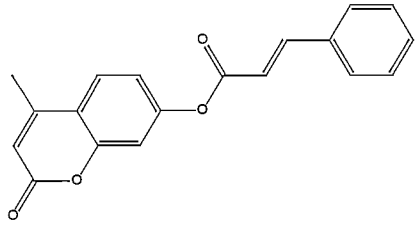	**BR 5**	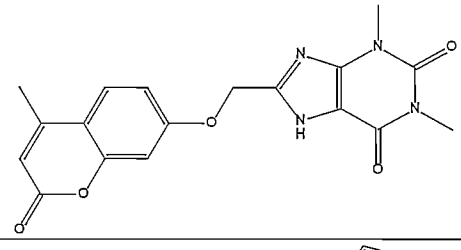
BR 7	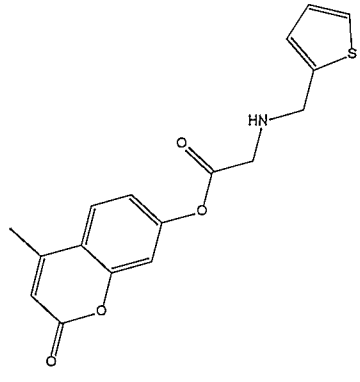	**BR 8**	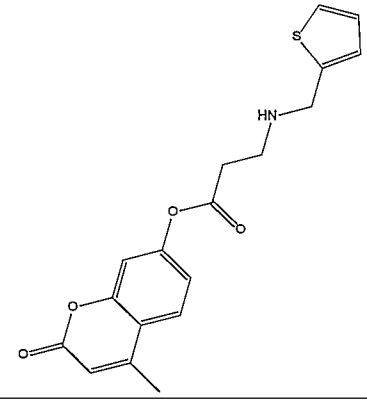
BR 9	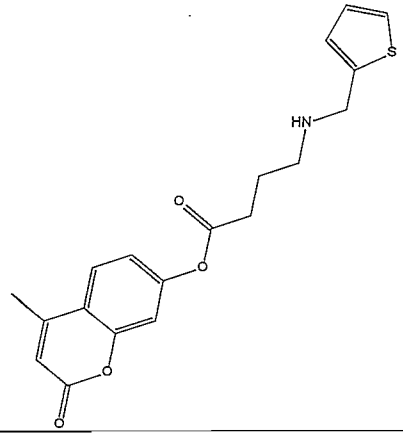	**BR 10**	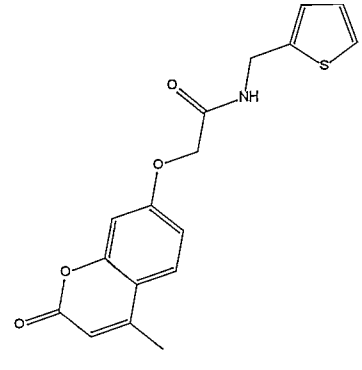

BR 11	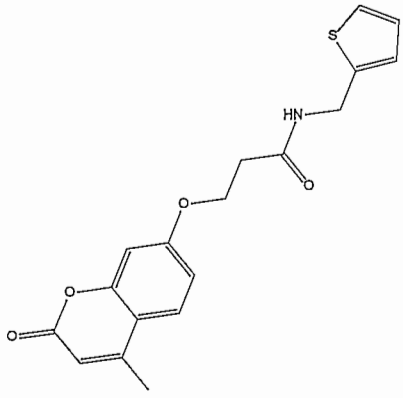	BR 12	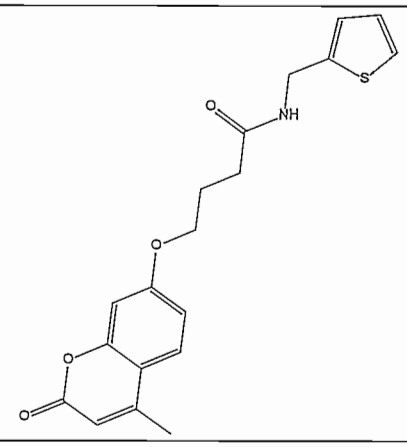
BR 13	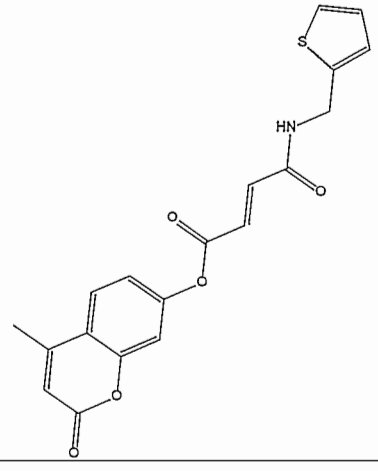	BR 14	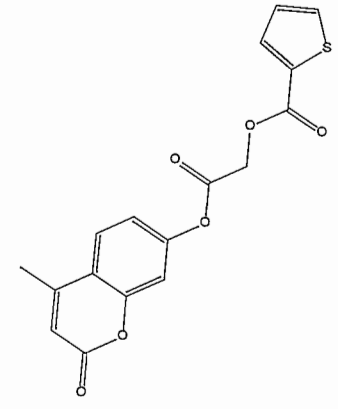
BR 15	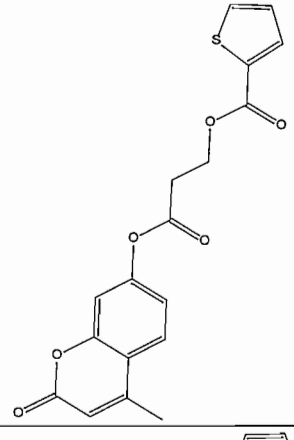	BR 16	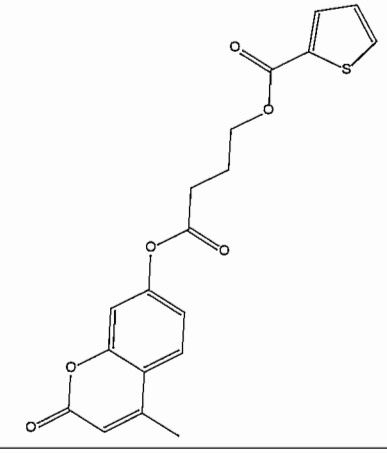
BR 17	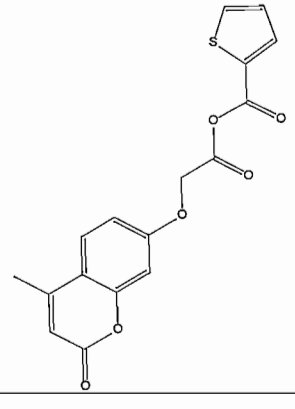	BR 18	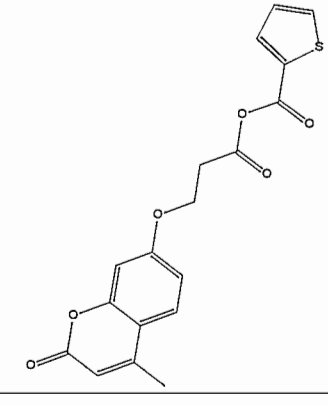

BR 19	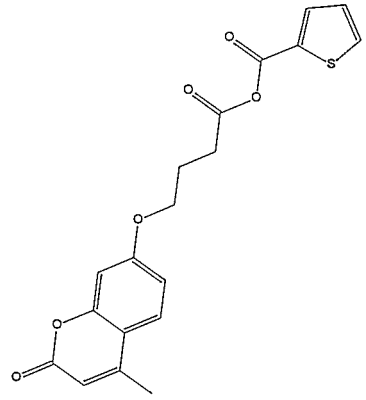	**BR 20**	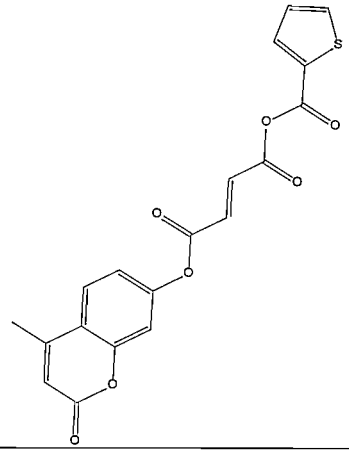
GT1	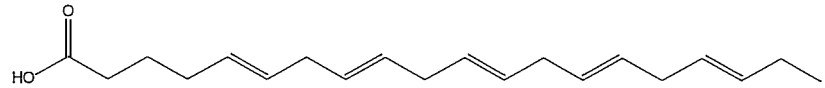		
GT2	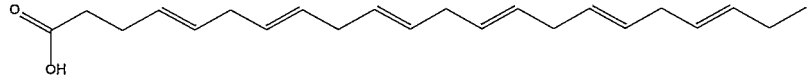		
GT3	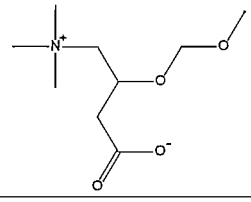	**GT4**	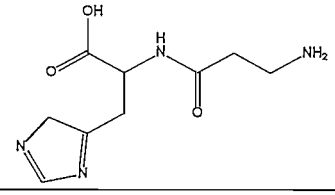
GT5	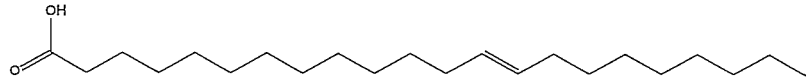		

Table 14: Library 6

Nr	Compound	Nr	Compound
HF1	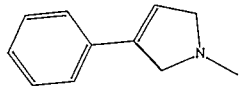	**HF2**	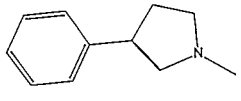
HF3	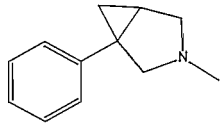	**HF4**	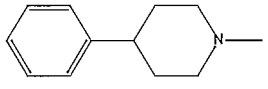

HF5	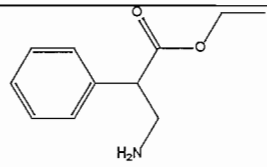	**HF6**	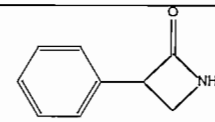
HF7	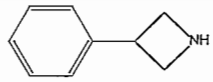	**HF8**	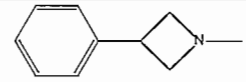
SD1	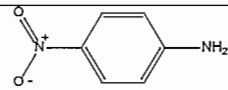	**SD2**	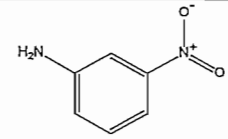
SD3	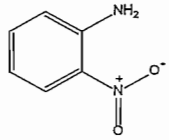	**SD4**	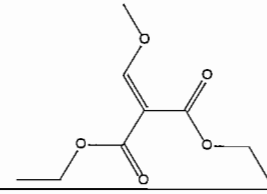
SD5	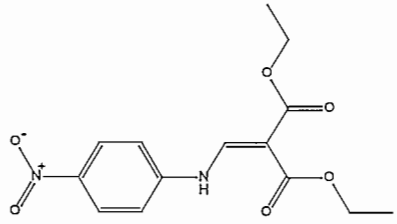	**SD6**	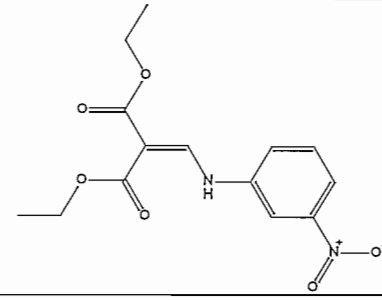
SD7	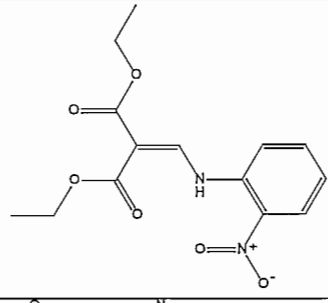	**SD8**	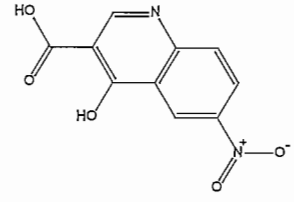
SD9	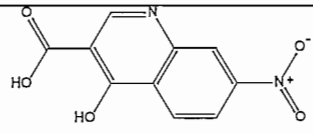	**SD10**	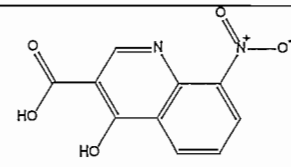
SD11	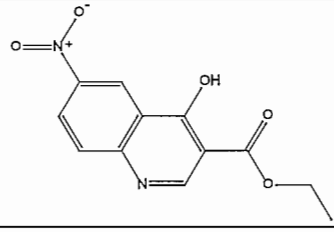	**SD12**	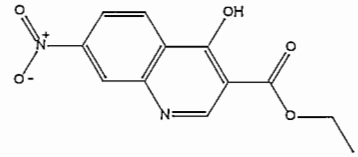

SD13	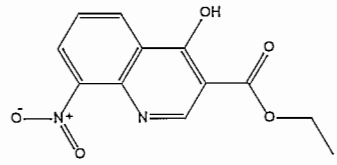	**SD14**	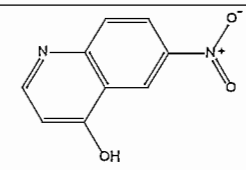
SD15	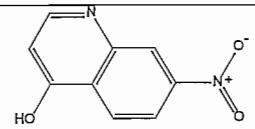	**SD16**	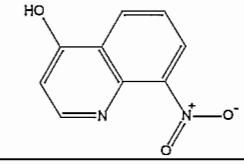
SD17	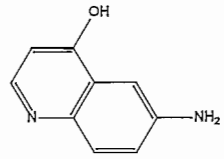	**SD18**	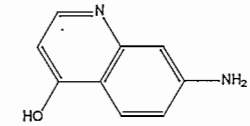
SD19	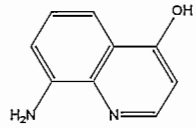	**SD20**	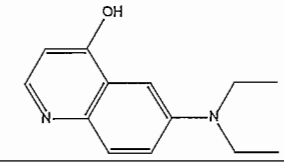
SD21	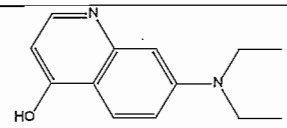	**SD22**	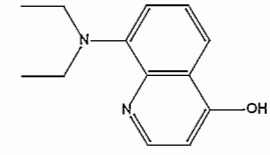
SD23	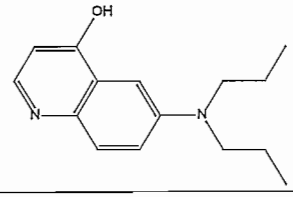	**SD24**	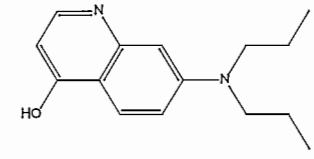
SD25	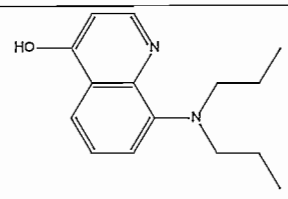	**SD26**	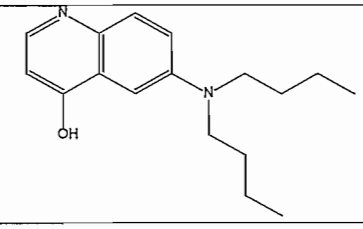
SD27	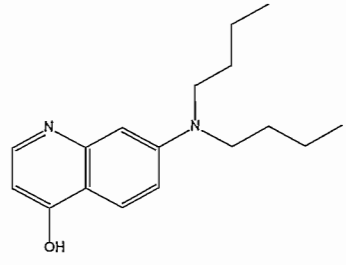	**SD28**	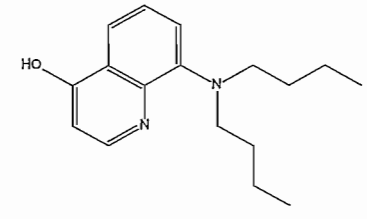

Compounds used for validation of hypotheses combined with docking studies

Table 15: Validation database for calpain

Nr	Compound	Experimental IC_{50} (nM)
i	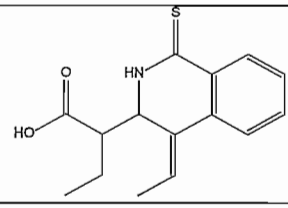	100 000
ii	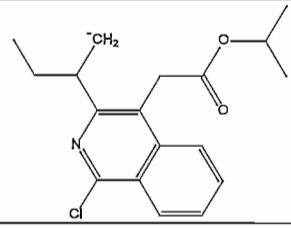	100 000
iii	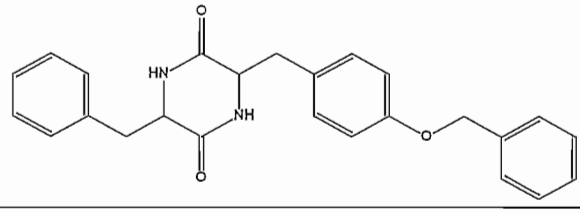	650 000
iv	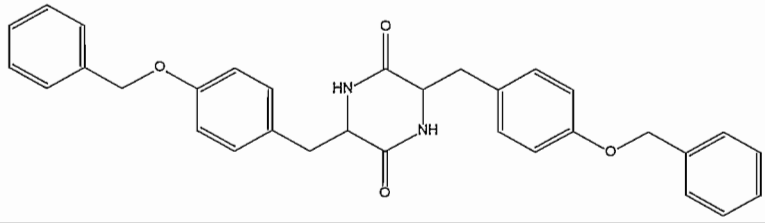	350 000
v	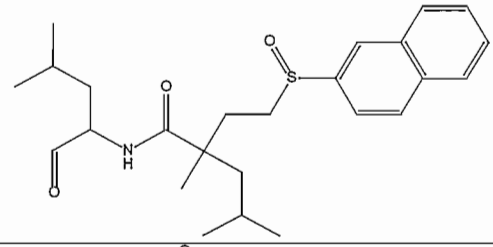	30
vi	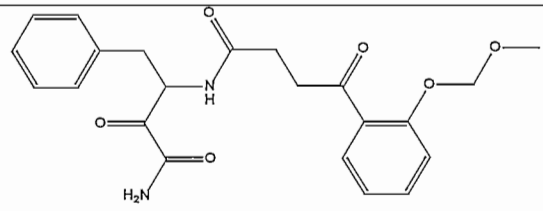	340

vii	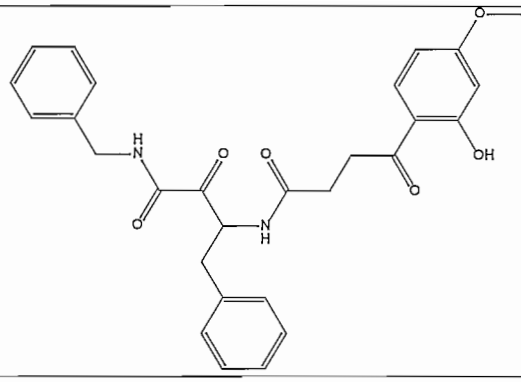	12 990
viii	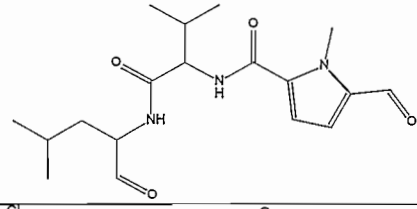	150
ix	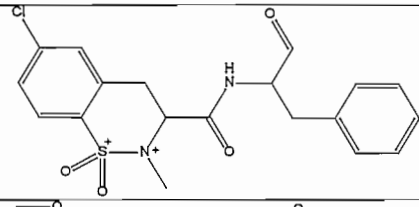	5
x	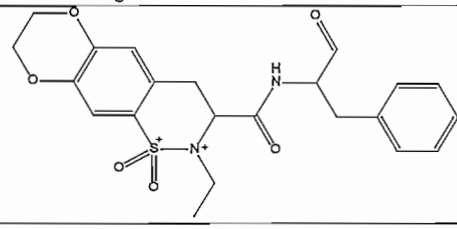	7

Table 16: Validation database for caspase 3

Nr	Compound	Experimental IC_{50} (nM)
i	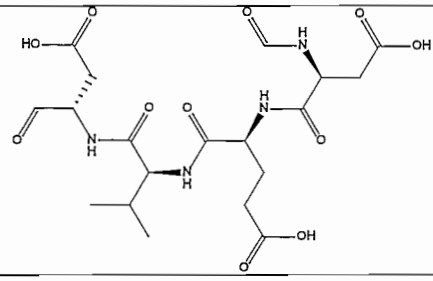	3.5

ii	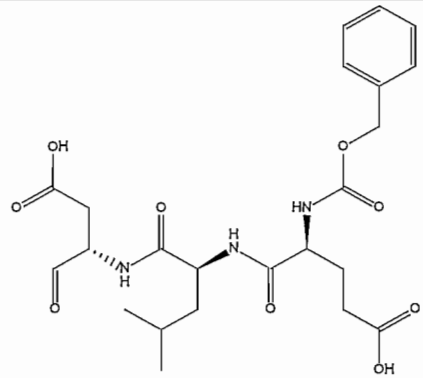	2.3
iii	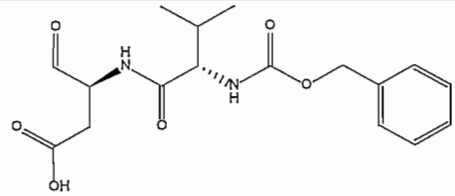	1750
iv	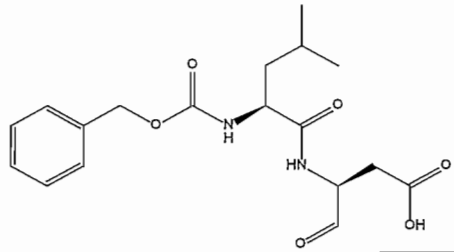	3470
v	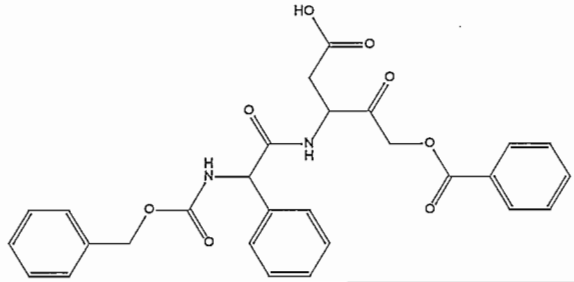	510
vi	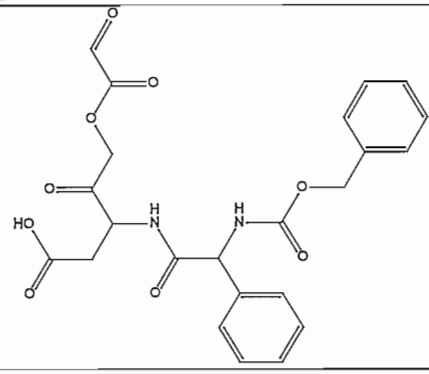	3790

vii	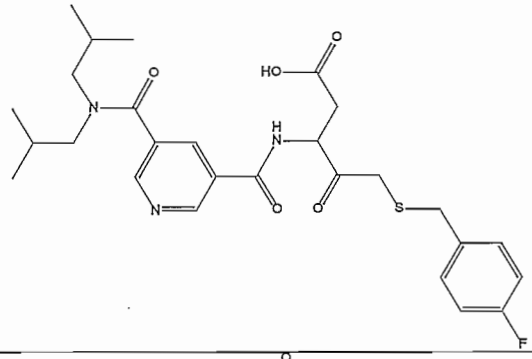	130
viii	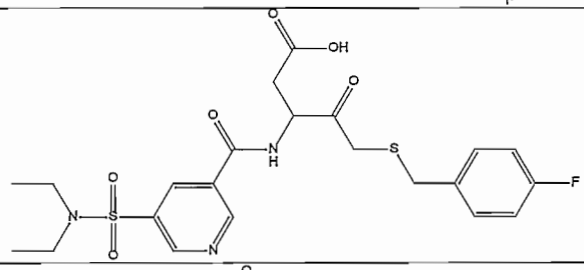	170
ix	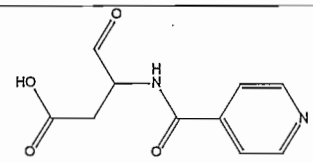	200 000
x	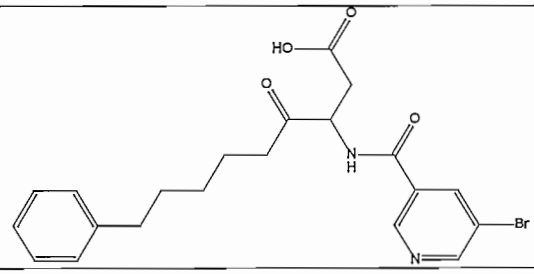	96 900

Table 17: Validation database for GSK3β

Nr	Compound	Experimental IC_{50} (nM)
i	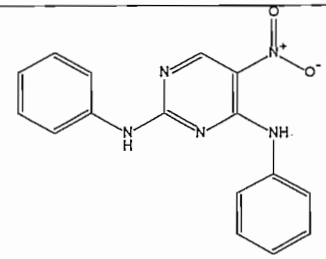	2 800
ii	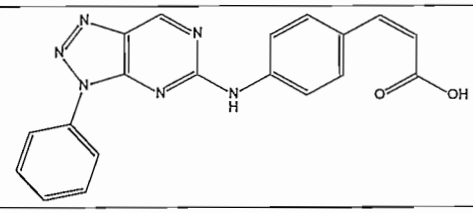	7

iii	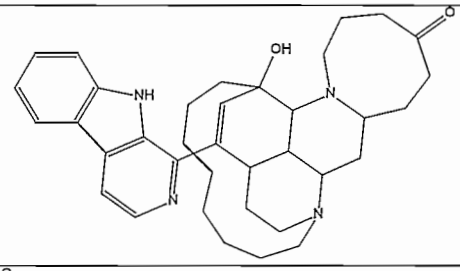	25 000
iv	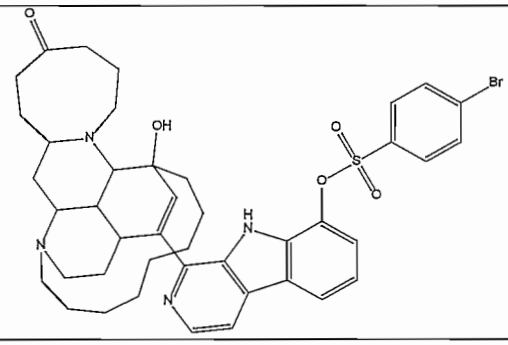	23 000
v	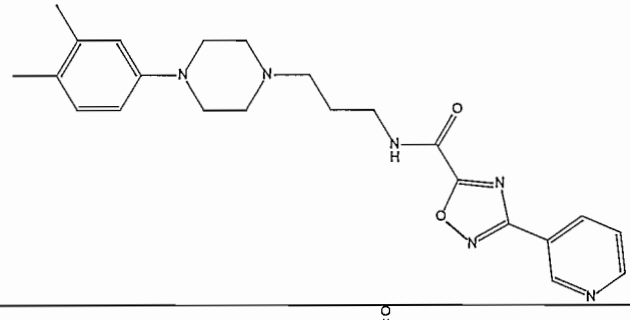	350
vi	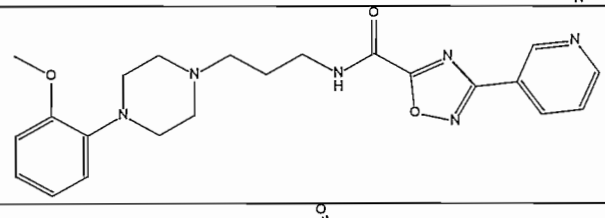	410
vii	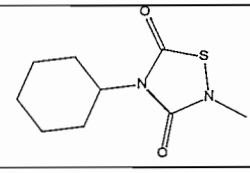	100 000
viii	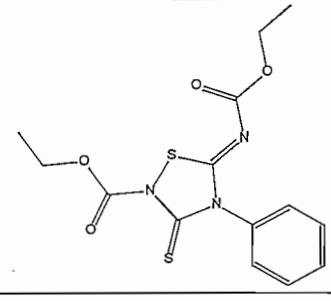	100 000

ix	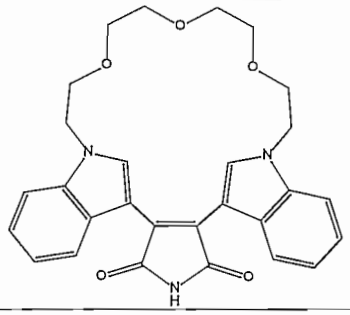	22
x	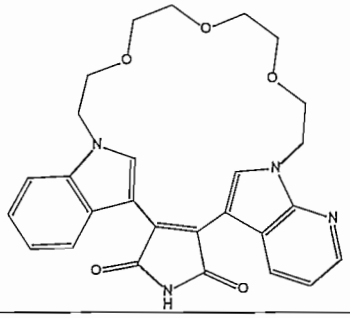	17

Table 18: Validation database for CDK5/p25

Nr	Compound	Experimental IC_{50} (nM)
i	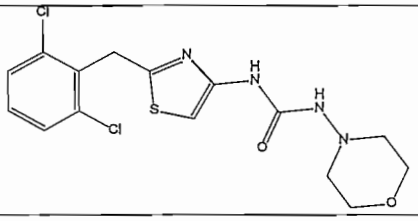	1000
ii	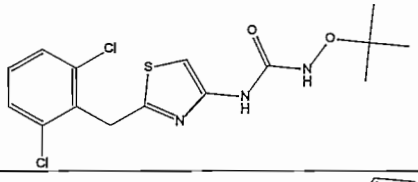	1000
iii	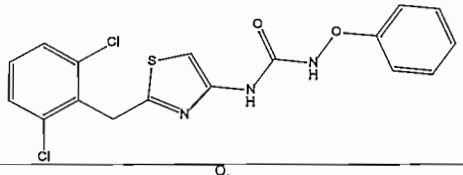	900
iv	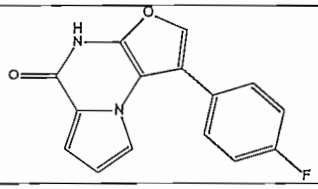	50 000

v	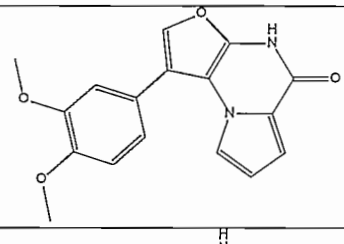	50 000
vi	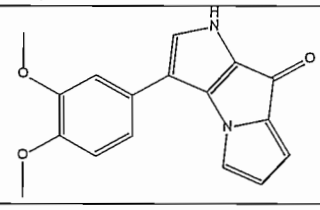	50 0000

Table 19: RLU values of compounds tested for calpain I inhibition

[JB51] µM	Log calpain inhibitor (µM)	RLU	Standard error	% Max RLU
1	0.00	984	58.506410	100.00
10	1.00	750	87.033200	76.22
100	2.00	448	22.430140	45.53
200	2.30	369	23.240290	37.50
300	2.48	221	20.406970	22.46
400	2.60	42	17.891650	4.27
500	2.70	9	16.522710	0.91

[JB50] µM	Log calpain inhibitor (µM)	RLU	Standard error	% Max RLU
0.1	-1.00	157	19.011690	95.73
1	0.00	164	13.076700	100.00
10	1.00	164	24.537950	100.00
100	2.00	34	5.291502	20.73
200	2.30	43	25.510350	26.22
300	2.48	9	6.244998	5.49
400	2.60	-24	4.000000	0.00
500	2.70	-13	17.854350	0.00

[JB52] µM	Log calpain inhibitor (µM)	RLU	Standard error	% Max RLU
0.01	-2	13347	1321.24	100.00
0.10	-1	12011	744.97	89.99
1.00	0	12453	558.37	93.30
10.00	1	11316	246.13	84.78
100.00	2	7530	95.75	56.42

[JJ27] µM	Log calpain inhibitor (µM)	RLU	Standard error	% Max RLU
0.01	-2	18330	623.052200	100.00
0.10	-1	17638	58.506410	96.22
1.00	0	17164	923.230300	93.64
10.00	1	17242	848.159100	94.06
100.00	2	10462	223.081500	57.08

[JJ13] µM	Log calpain inhibitor (µM)	RLU	Standard error	% Max RLU
0.01	-2	16448	391.963600	93.20
0.10	-1	17648	104.170300	100.00
1.00	0	16790	877.968600	95.14
10.00	1	16416	334.097800	93.02
100.00	2	12500	3104.939000	70.83

Table 20: RFU values of compounds tested for GSK3β inhibition

[JB7] µM	Log [JB7] µM	RFU	Standard error	[ADP] nM	Log [ADP] nM	% Max log [ADP]
0.1	-1	788.000	45.1774	135.1167	2.130709	100.00
1	0	700.000	82.5853	118.5089	2.073751	58.03
10	1	625.333	6.4377	106.7928	2.028542	24.72
100	2	580.000	8.7369	100.5164	2.002237	5.33
250	2.3979	578.667	8.6859	100.3407	2.001477	4.77
500	2.6989	589.333	4.9103	101.7551	2.007556	9.25
[JJ13] µM	**Log [JJ13] µM**	**RFU**	**Standard error**	**[ADP] nM**	**Log [ADP] nM**	**% Max log [ADP]**
0.1	-1	868.000	162.497200	153.7008	2.186676	70.86
1	0	970.000	41.004070	184.2897	2.265501	100.00
10	1	888.000	119.675900	158.9546	2.201273	76.26
100	2	848.000	149.617300	148.6521	2.172171	65.50
250	2.3979	905.667	31.248110	163.9434	2.214694	81.22
500	2.6989	780.667	93.734260	133.5836	2.125753	48.34
1000	3	523.000	37.527770	93.3781	1.970245	-9.15

[JB27] µM	Log [JB27] µM	RFU	Standard error	[ADP] nM	Log [ADP] nM	% Max log [ADP]
0.01	-2	731.333	48.3885	124.0089	2.093453	100.00
0.1	-1	698.000	31.2623	118.1661	2.072493	91.38
1	0	661.333	14.3333	112.2096	2.050030	82.13
10	1	671.000	35.0856	113.7376	2.055904	84.55
100	2	590.667	19.4708	101.9335	2.008317	64.97
500	2.6989	449.667	123.9816	85.2287	1.930586	32.98
1000	3	442.667	113.8425	84.3762	1.926922	31.47

[SD9] µM	Log [SD9] µM	RFU	Standard error	[ADP] nM	Log [ADP] nM	% Max log [ADP]
0.01	-2	679.6667	9.8150	115.1254	2.061171	97.38
0.1	-1	684.6667	19.0992	115.9338	2.064210	100.00
1	0	681.3333	20.6263	115.3942	2.062184	98.26
10	1	598.3333	3.5277	102.9641	2.012686	55.66
100	2	486.0000	12.8106	89.1368	1.950057	1.77
250	2.3979	429.0000	41.4501	83.1321	1.919769	0.00
500	2.6989	489.0000	14.7460	89.4685	1.951670	3.16
1000	3	436.6667	11.6667	83.9039	1.923782	0.00

[SB] µM	Log [SB] µM	RFU	Standard error	[ADP] nM	Log [ADP] nM	% Max log [ADP]
0.0001	-4	704.3333	15.3768	119.2548	2.076476	91.16
0.001	-3	724.0000	17.5784	122.6993	2.088842	100.00
0.01	-2	702.6667	11.2891	118.9674	2.075428	90.41
0.1	-1	591.6667	61.8852	102.0674	2.008887	42.82
1	0	568.0000	49.3288	98.9457	1.995397	33.18
10	1	587.3333	33.3283	101.4885	2.006417	41.06

[LP11] µM	Log [LP11] µM	RFU	Standard error	[ADP] nM	Log [ADP] nM	% Max log [ADP]
0.01	-2	663.0000	9.8150	112.4716	2.051043	68.90
0.1	-1	666.6667	19.0992	113.0501	2.053271	70.39
1	0	653.6667	20.6263	111.0123	2.045371	65.10
10	1	617.6667	3.5277	105.6900	2.024034	50.84
100	2	585.3333	12.8106	101.2225	2.005277	38.30
250	2.3979	647.3333	41.4501	110.0328	2.041522	62.53
500	2.6989	689.3333	14.7460	116.6933	2.067046	79.60
1000	3	737.6667	11.6667	125.1878	2.097562	100.00

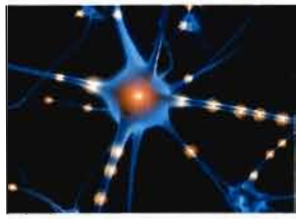

Acknowledgements

I want to thank the following persons/institutions:

My **Lord** and **Saviour** for His motivation, presence and unconditional love, especially during tough times.

My supervisor and co-supervisor, **Prof. Sarel Malan** and **Prof. Douglas Oliver**, for your insights and inspiration.

All the **staff** at the Department of Pharmaceutical Chemistry at the North-West University, Potchefstroom campus, for your assistance, support and agreeing to allow me to screen your compound libraries for theoretical activity.

Prof. Jaco Breytenbach, **Jacques Joubert, Prof. Sandra van Dyk** and **Louis Prins** for the use of your compounds during the biological assays.

The Department of Biochemistry at the North-West University, Potchefstroom campus, especially **Prof. Francois van der Westhuizen**, for the use of his facilities and equipment during the evaluation of compounds by biological assays.

Bellbrook Labs for the Transcreener® ADP^2 FI assay kit they donated for the GSK3ß assay and their support and advice during the performance of the assay.

My **family** and **friends**, your support and encouragement are highly appreciated.